Delivery of Cytomegalovirus T cell antigens for diagnostic and vaccination purposes

DISSERTATION ZUR ERLANGUNG DES
DOKTORGRADES DER NATURWISSENSCHAFTEN (DR. RER. NAT.)
DER FAKULTÄT FÜR BIOLOGIE UND VORKLINISCHE MEDIZIN
DER UNIVERSITÄT REGENSBURG

vorgelegt von
Richard Kiener
aus
Neustadt a.d. Waldnaab
im Jahr
2017

Das Promotionsgesuch wurde eingereicht am:

26.10.2017

Die Arbeit wurde angeleitet von:
Prof. Dr. Ralf Wagner

Unterschrift:

Richard Kiener

Content declaration:

The results section of this thesis comprises 3 chapters, the second and third of which have been submitted for peer-reviewed publication.

Chapter I: **"**Influence of posttranslational modifications on protein delivery to antigen-presenting cells**"** (not yet submitted, manuscript in preparation)

Chapter II: "Delivery of IE-1 **and pp65 by Adenovirus virus vectors" (submitted)**

Data from this chapter have been submitted for publication under the title: "New CMV vaccine candidates based on Adenovirus 19a/64 exhibit broad cellular tropism and efficiently induce antigen expression in dendritic cells"

Authors: Richard Kiener, Markus Fleischmann, Christiane Schwegler, Zsolt Ruzsics, Christian Thirion, Silke Schrödel, Benedikt Asbach, Ralf Wagner

Personal contribution: Richard Kiener (RK) collected parts of the data and supervised collection of the residual data by students. RK analyzed the data, prepared all figures and wrote the paper.

Chapter III**: "Delivery of** IE-1 and pp65 **by Sendai virus vectors"** (submitted)

Data from this chapter have been submitted for publication under the title: "Novel Sendai virus vectors efficiently transduce monocyte-derived dendritic cells and potently restimulate T cell responses *ex vivo*"

Authors: Richard Kiener, Markus Fleischmann, Marian Alexander Wiegand, Christiane Schwegler, Christine Kaufmann, Eva Felder, Hans-Helmut Niller, Benedikt Asbach, Ralf Wagner

Personal contribution: same as for chapter II

Contents

I. Abstract

Human Cytomegalovirus (CMV) is a highly prevalent β-herpesvirus that establishes life-long latency after primary infection. Congenital CMV infection is the most common viral complication in newborns, causing a number of late sequelae that range from impaired hearing to mental retardation. At the same time, managing CMV reactivation during immunosuppression remains a major hurdle in post-transplant care.

Since CMV-specific T cells are critical for controlling viral reactivation, monitoring of T cell responses is a promising strategy to identify patients at risk for symptomatic CMV disease. T cell responses are mostly quantified after antigen-specific restimulation, which requires presentation of pathogen-derived peptides by antigen-presenting cells (APCs). Here, it was tested if protein carbamoylation, a posttranslational modification of amino groups occurring *in vivo* during renal dysfunction or inflammation, impacts the uptake of recombinant proteins into APCs and, as a result, also T cell restimulation. The CMV proteins immediate-early 1 (IE-1) and pp65, which are the main targets of T cell-mediated immunity during CMV infection, as well as the Epstein-Barr virus (EBV) protein BZLF1 were chosen as model proteins and recombinantly produced for addressing this question. As a result of protein carbamoylation, antigen-specific restimulation of T cells was increased for pp65 (mean increase 39%, ranging from 6-112% for different blood donors) and BZLF1 (mean increase 80%, ranging from 5-161%), but decreased for IE-1. Mass spectrometry analysis revealed that lysine residues were almost completely modified (>90%), while arginine carbamoylation was negligible under the chosen conditions (0.3%). The removal of positive charges from amino groups as a result of carbamoylation was found to be important for the enhanced restimulation of pp65-specific T cells, since this effect could be reverted by addition of the polyanionic competitor fucoidan. In addition, protein maleylation, another posttranslational modification removing positive charges from amino groups, mediated a similar increase in the restimulation of pp65-specific T cells. T cell responses to carbamoylated pp65 were increased compared to the unmodified protein, irrespective of whether monocytes, macrophages or dendritic cells acted as APCs. Improved restimulation of pp65-specific T cells was shown to be the result of enhanced protein uptake into APCs, which increased both MHC-I and MHC-II presentation.

In summary, protein charges appear to have a major influence on uptake into antigen-presenting cells, which could be harnessed for improving current methods for T cell immunomonitoring and the design of novel vaccines.

In the second part of this thesis, new viral vectors delivering the T cell immunogens IE-1 and pp65 were evaluated with regard to suitability as future CMV vaccine candidates. The vectors were based on Adenovirus 19a/64 (Ad19a/64) or Sendai virus (SeV) and compared side-by-side to the well-established vector platforms Ad5 and Modified Vaccinia Ankara (MVA). All vectors were characterized virologically and immunologically in a series of *ex vivo* assays

with a focus on dendritic cells (DCs), which are the main population priming T cell responses *in vivo*.

It was found that unlike Ad5, Ad19a/64 vectors readily transduce a broad panel of immune cells, including monocytes, T cells, NK cells and monocyte-derived dendritic cells (moDCs). Both Ad19a/64- and MVA-transduced moDCs efficiently restimulated IE-1 or pp65-specific T cells, but MVA induced a higher amount of cytotoxicity in this cell type. Ad5 and Ad19 induced upregulation of the maturation markers CD86 and HLA-DR in moDCs whereas expression of CD80 and CD83 was largely unaltered. By contrast, MVA transduction led to downregulation of all markers.

To enhance the safety of SeV vectors, a replication-deficient strain (rdSeV) that infects target cells in a non-productive manner while retaining viral gene expression was used in this thesis. rdSeV was compared to the parental, replication-competent Sendai virus strain (rcSeV) as well as MVA. rcSeV was capable of replicating to high titers in DCs while rdSeV infected cells abortively. Due to the higher degree of attenuation, IE-1 and pp65 protein levels mediated by rdSeV after infection of DCs were markedly reduced compared to the parental rcSeV strains, but antigen-specific restimulation of T cell clones was not negatively affected by this. Importantly, rdSeV showed reduced cytotoxic effects compared to rcSeV and MVA and was capable of mediating DC maturation as well as secretion of Interferon α and Interleukin 6.

Taken together, these data demonstrate that both rdSeV and Ad19a/64 have great potential as novel vector systems for the delivery of CMV immunogens.

II. Zusammenfassung

Das humane Zytomegalievirus (CMV) weist weltweit hohe Seroprävalenz auf und etabliert nach der Primärinfektion lebenslange Latenz. Infektionen mit CMV sind die häufigste virale Komplikation bei Neugeborenen und verursachen eine Reihe von Spätfolgen wie Schwerhörigkeit oder geistige Behinderungen. Zusätzlich stellen CMV Reaktivierungen die bedeutendste pathogen-assoziierte Komplikation bei Transplantatempfängern dar.

Da T Zellen eine entscheidende Rolle bei der Kontrolle viraler Reaktivierungen einnehmen, stellt die Überwachung CMV-spezifischer T Zell Antworten eine vielversprechende Strategie zur frühzeitigen Identifikation von Patienten mit erhöhtem Risiko für symptomatische CMV Erkrankung dar. Derzeit werden pathogen-spezifische T Zellen hauptsächlich infolge von Restimulation mit entsprechenden Antigenen nachgewiesen und quantifiziert, was deren Prozessierung und Präsentation durch Antigen-Präsentierenden Zellen (APCs) voraussetzt. In dieser Arbeit wurde untersucht, ob Carbamoylierung (eine posttranslationale Modifikation die auch *in vivo* im Zuge von Niereninsuffizienz oder Entzündungen vorkommt) die Aufnahme rekombinanter Proteine in APCs und damit die Restimulation von T Zellen beeinflusst. Hierfür wurden die CMV Proteine *Immediate-early 1* (IE-1) und pp65, welche während CMV Infektionen die stärksten T Zell Antworten hervorrufen, sowie das Epstein-Barr virus (EBV) Protein BZLF1 rekombinant hergestellt. Carbamoylierung verbesserte die Restimulation pp65-spezifischer T Zellen im Durchschnitt um 39%, (6-112%, je nach individuellem Blutspender) und BZLF1-spezifischer T Zellen um 80% (5-161%), wohingegen die IE-1 Antworten stark verringert waren. Massenspektrometrische Analysen zeigten, dass unter den gewählten Reaktionsbedingungen Lysine quantitativ modifiziert wurden (>90%), wohingegen Arginin-Carbamoylierung kaum nachzuweisen war (0.3%). Es zeigte sich außerdem, dass das Entfernen positiver Ladungen infolge der Carbamoylierung notwendig für die verbesserte T Zell Restimulation ist, da sich der Effekt durch Zugabe des polyanionischen Kompetitors Fucoidan aufheben ließ. Zudem hatte Maleylierung, eine weitere posttranslationale Modifikation, welche das Entfernen positiver Ladungen von Aminogruppen zur Folge hat, einen ähnlichen Einfluss auf die Restimulierung pp65-spezifischer T Zellen. Die Verbesserung der T Zell Stimulation durch carbamoyliertes pp65 war unabhängig davon ob Monozyten, Makrophagen oder dendritische Zellen als APCs fungierten. Der Grund hierfür scheint eine generell erhöhte Aufnahme in Antigen-präsentierende Zellen zu sein, wobei sowohl MHC-I, als auch MHC-II Präsentation verbessert waren.

Zusammenfassend lässt sich festhalten, dass die Ladung von Proteinen die Aufnahme in APCs stark beeinflusst, was beispielsweise in die Verbesserung aktueller T Zell Diagnostika oder die Herstellung neuartiger Impfstoffe einfließen könnte.

Im zweiten Teil dieser Arbeit wurden neuartige virale Vektoren für die Verabreichung der T Zell Immunogene IE-1 und pp65 hinsichtlich ihrer Eignung als CMV Impfstoffkandidaten evaluiert. Die Vektoren basieren auf dem Adenovirus Subtyp 19a/64 (Ad19a/64), sowie Sendai Virus (SeV) und wurden direkt mit den etablierten Vektoren Adenovirus Subtyp 5

(Ad5) und *Modified Vaccinia Ankara* (MVA) verglichen. Alle Vektoren wurden in einer Reihe von *ex vivo* Studien hinsichtlich verschiedener virologischer und immunologischer Parameter charakterisiert. Hierbei lag ein besonderer Fokus auf dendritischen Zellen (DCs), da diese *in vivo* hauptsächlich für das *Priming* naiver T Zellen verantwortlich sind.

Hierbei zeigte sich, dass Ad19a/64 Vektoren im Gegensatz zu Ad5 in der Lage sind, ein breites *Panel* an Immunzellen, bestehend aus Monozyten, T Zellen, NK Zellen und *monocyte-derived dendritic cells* (moDCs), zu transduzieren. Sowohl Ad19a/64, als auch MVA waren in der Lage, moDCs effizient zu transduzieren und die Restimulation IE-1- und pp65-spezifischer T Zell Klone zu vermitteln. Allerdings induzierte MVA in einem deutlich stärkeren Ausmaß als Ad19a/64 Zytotoxizität in DCs. Infolge der Transduktion mit Ad5 und Ad19a/64 wurden die Maturationsmarker CD86 und HLA-DR hochreguliert, wobei das Expressionsniveau der Marker CD80 und CD83 unverändert blieb. Im Gegensatz dazu wurde die Expression aller Maturationsmarker infolge der Transduktion mit MVA herabreguliert.

Um die Sicherheit SeV-basierter Vektoren zu erhöhen, wurde in dieser Arbeit ein replikationsdefizienter Virusstamm (rdSeV) eingesetzt, der die Expression viraler Gene in Zielzellen induziert, wobei die Bildung neuer Viruspartikel unterbleibt. rdSeV wurde sowohl mit dem parentalen, replikationskompetenten SeV Stamm (rcSeV), als auch mit MVA verglichen. Es zeigte sich, dass rcSeV effizient in humanen DCs repliziert, wohingegen Infektion mit rdSeV abortiv abläuft. Mit dem erhöhten Grad an Attenuierung von rdSeV ging, verglichen mit rcSeV, zugleich ein vermindertes Expressionsniveau von IE-1 und pp65 einher, jedoch war die Restimulation antigenspezifischer T Zellen hiervon nicht negativ beeinflusst. Es ist zudem hervorzuheben, dass rdSeV auch geringere Zytotoxizität im Vergleich mit rcSeV und MVA aufwies und die Maturation von DCs, sowie die Sezernierung von Interferon α und Interleukin 6 induzierte.

Insgesamt zeigen diese Daten, dass sowohl rdSeV, als auch Ad19a/64 vielversprechende neue Vektorsysteme für die Verabreichung von CMV Immunogenen darstellen.

III. Introduction

III.1. Human Cytomegalovirus

The family *Herpesviridae* comprises more than 100 known individual virus species that are capable of infecting a wide variety of mammals, birds and reptiles[1]. They share a common virion architecture that is characterized by the presence of an icosahedral nucleocapsid containing a linear, double-stranded DNA genome. The capsid is surrounded by an amorphous layer termed the tegument and further enveloped by a host cell-derived lipid bilayer with viral glycoproteins (Figure 1)[2]. Nine herpesviruses, which are classified into three subfamilies, have humans as their primary host: α-herpesviruses (herpes-simplex virus type 1 and 2, varicella-zoster virus), β-herpesviruses (human cytomegalovirus, human herpesvirus types 6A and 6B) and γ-herpesviruses (Epstein-Barr virus, human herpesvirus type 7, Kaposi's sarcoma-associated herpesvirus).

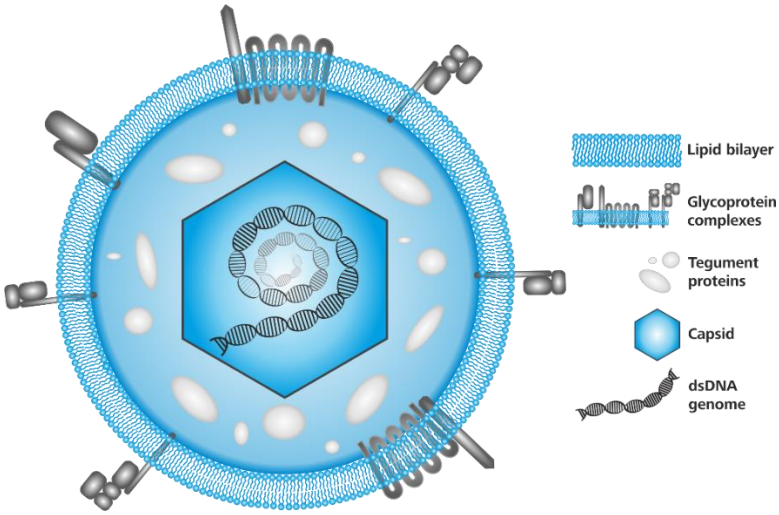

Figure 1 – Structural features of herpesvirus particles
Herpesviruses exhibit a characteristic virion architecture that includes an icosahedral capsid containing a double-stranded DNA (dsDNA) genome. The nucleocapsid is surrounded by a lipid envelope, which holds different types of glycoprotein spikes that are involved in adhesion and membrane fusion. Capsid and envelope are separated by an unstructured layer referred to as the tegument, which contains viral and host cell-derived proteins. Figure adapted from Gardner and Tortorella[3].

Human cytomegalovirus (CMV, HHV-5), which owes its name to the characteristic enlargement of infected cells ("cytomegaly") during lytic replication, is considered the prototype of β-herpesviruses[4]. CMV is distributed globally and infects the majority of the human population. Seroprevalence rates range, depending on the geographic region, from 30% to 100%, but generally increase with age[5–7]. Like all herpesviruses, CMV establishes life-long latency with periodic reactivations after primary infection[8]. Horizontal transmission can occur through close contact with persons who excrete the virus in their body fluids, for example by kissing, sexual contact or breastfeeding. Blood transfusion, solid-organ transplantation (SOT) or hematopoietic stem cell transplantation (HSCT) constitute additional routes of CMV transmission[9]. At the same time, vertical transmission from mother to child can occur pre- or perinatally as a result of primary infection or viral reactivation during pregnancy[10]. Given that persistently infected individuals are not protected from reinfection despite virus-specific cellular and humoral immunity, superinfection with an additional CMV strain can also increase the risk of mother-to-child transmission[11,12].

III.2. Virion composition and replication

CMV, which is among the most complex human-pathogenic viruses known, displays a virion architecture that is characteristic of all herpesviruses (Figure 1). With approximately 235 kilobase pairs (kb), CMV has the largest genome of all herpesviruses known to cause disease in humans[13]. The exact number of genes encoded by CMV is still a matter of debate and varies, depending on the annotation criteria, strongly from about 150 to more than 230[14–16]. Next to an undefined number of protein-coding genes, CMV also encodes several long noncoding- and micro-RNAs[1,17]. The genome is flanked by terminal repeat (TR) sequences and divided by internal repeats (IR) into two individual genomic regions that are referred to as unique long (UL, upstream of IRs) and unique short (US, downstream of IRs; Figure 2). Accordingly, CMV genes are named by a prefix indicating the unique region in which they are found and numbered sequentially[18,19]. The genome is enclosed by an icosahedral protein capsid made up of 162 capsomers. It is formed by 4 capsid proteins termed major capsid protein (MCP, UL86), triplex 1 (TRI1, UL46), triplex 2 (TRI2, UL85) and smallest capsid protein (SCP, UL48A)[20].

Figure 2 – Schematic representation of the Cytomegalovirus genome
The genome of CMV is flanked by repeat sequences referred to as terminal repeat long (TRL) and terminal repeat short (TRS). Additional repeat sequences, termed internal repeat long (IRL) and internal repeat short (IRS), divide the genome into two individual sections which contain protein-coding genes: unique long (UL) and unique short (US).

The capsid is surrounded by the viral tegument, an unstructured layer that contains a high number of viral proteins. In fact, more than half of the 71 viral proteins that are found within CMV particles are located in the tegument, along with numerous host cell-derived proteins[21]. During viral replication, tegument proteins are involved in a number of key steps such as capsid delivery to the nucleus (UL47 and UL48[21]), gene regulation (UL82[22]) and assembly of newly generated virions (UL99[23]), yet the function of many tegument components remains elusive. Evasion of innate and adaptive immune responses, which is critical for viral replication, is also carried out in part by tegument proteins. For instance, the phosphoprotein pp65 (UL83), which is the most abundant protein both in the tegument as well as in the entire virion[15], protects infected cells from innate immunity by inhibiting natural killer (NK) cell cytotoxicity through interaction with the NKp30 activating receptor[24]. In addition, pp65 also counteracts adaptive immune responses by mediating the accumulation of HLA class II molecules in lysosomes and inducing the degradation of the HLA-DR α-chain in this compartment[25].

Capsid and tegument are encased by a host-derived lipid envelope containing various glycoprotein complexes (GCs) that are necessary for entry into different cell types (Figure 3). These complexes comprise oligomers of gB (GC I; encoded by UL55), the gM/gN dimer (GC

II; UL100/ UL73), the gH/gL/gO trimer (GCIII; UL75/UL115/UL74) and the pentameric complex (PC) consisting of gH/gL and UL128/UL130/UL131a. The core fusion machinery consists of the proteins gB, gH and gL, which are conserved throughout the herpesvirus family[26]. Entry into fibroblasts takes place by macropinocytosis, followed by the fusion of viral and cellular membranes. This process is mediated by GC I and GC III and requires no changes in pH[27,28]. By contrast, entry into epithelial, endothelial, dendritic cells and monocytes requires virion uptake via endocytosis or macropinocytosis and a fusion event that relies on vesicle acidification. This entry pathway is mediated by GC I, GC III and PC[29–33]. The function of GC II in these processes is still not fully understood, but it is presumed to induce initial tethering of virus particles to target cells through interaction with heparan sulfate proteoglycans[34].

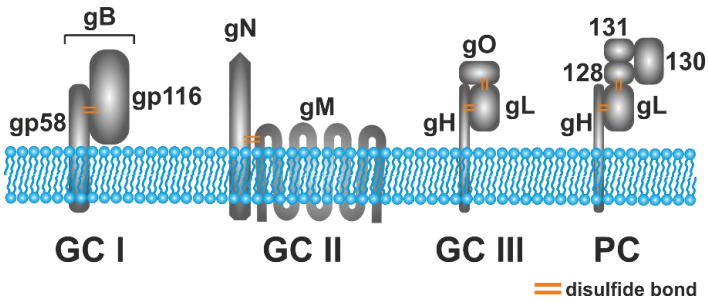

Figure 3 – Quaternary structure and topology of glycoprotein complexes
Glycoproteins (gp) on CMV virions are present in several glycoprotein complexes (GCs). These complexes include GC I (gB, which consists of gp58 and gp116), GC II (gM and gN), GC III (gH, gO, gL) and the pentameric complex (PC, gH/gL and UL128/130/131a). Orange lines indicate subunits that are held together by disulfide bonds. Figure adapted from Gardner and Tortorella[3].

Upon entry, the capsid is released into the host cell cytoplasm and transported along microtubules to the nuclear membrane, where viral DNA is inserted through nuclear pores[35]. Expression of CMV genes occurs in three sequential phases termed immediate-early (IE), early (E) and late (L). Immediate-early genes are the first to be transcribed and their proteins mediate the transcription of early gene products which are, among others, responsible for the replication of viral DNA[36,37]. In turn, the presence of early-phase proteins is a prerequisite for transition into the late phase, where structural components for the assembly of progeny virions are mainly synthesized[38].

Expression of IE genes occurs immediately upon nuclear entry of CMV DNA and does not require *de novo* synthesis of viral proteins. IE genes in the UL region comprise the IE-A (major immediate early) and IE-B locus as well as UL115-119. Additional IE genes located in the US region include US3 and the TRS1/IRS1 genes[36]. From the major immediate-early locus, multiple proteins are being produced by alternative splicing, with the 72 kDa IE-1 (UL123) and the 86 kDa IE-2 (UL122) being the most abundant and important ones[39]. IE-2 is the principal activator of early genes and its presence is indispensable for viral replication[40]. IE-1 is also capable of mediating early gene expression, but under certain *in vitro* conditions like infection at high multiplicities of infection (MOIs), viral replication can also be completed in the absence of this protein[41]. In addition to viral genes, IE proteins also modulate a number of host genes[36]. IE-1 and IE-2 further contribute to viral immune evasion by various mechanisms, for instance by blocking apoptosis[42] or dampening cytokine release from infected cells by interfering with JAK-STAT and NFκB-signalling[43–45]. Moreover, IE-1

also antagonizes host immunity by promoting the disassembly of PML nuclear bodies, which are key mediators of innate immune responses within the cell nucleus[46–48].

Early genes mostly function in one of two ways: One subset of gene products is directly involved in viral DNA synthesis, cleavage and packing of the viral genome. The other subset creates a cellular environment that is ideal for viral replication, for example by modulating factors that are involved in control of cellular DNA synthesis or by contributing to the evasion of immune responses[37]. Viral DNA synthesis occurs in the host cell nucleus from a genomic region termed *ori*Lyt and requires, next to some cellular factors, a variety of viral proteins including the helicase-primase complex (UL105, UL70 and UL102[49]), the viral DNA polymerase (UL54)[50] as well as its accessory protein (UL44)[51] and the single-stranded DNA binding protein (UL57)[52]. Replication of the viral genome is an essential activation event for the expression of late genes which are required for virus assembly and egress[38]. Capsid assembly and DNA packaging occur in the nucleus, followed by translocation of DNA-containing capsids into the cytoplasm, which is mediated by the virally encoded nuclear egress complex (NEC, UL50 and UL53)[53,54]. During nuclear egress, capsids obtain a primary envelope derived from the inner nuclear membrane, which is subsequently lost by fusion with the outer nuclear membrane[55,56]. Further maturation steps, during which capsids obtain their final tegument layer, then take place in the cytoplasm[57]. CMV virions obtain their secondary envelope, including viral glycoproteins, by budding into vesicles of the trans-Golgi network. Finally, mature virions are released by fusion of the vesicle membrane with the plasma membrane of the host cell[58].

In some cell types, transcription of IE genes is suppressed, a scenario in which CMV is capable of switching from lytic replication to a latent phase[59]. During latency, no progeny virus is produced and only a small set of latency-associated genes is transcribed[60]. Cells from the myeloid lineage like $CD34^+$ progenitor cells, monocyte precursors and monocytes have been proposed as a site of latency for CMV[61–64]. Reactivation of lytic replication presumably occurs as a result of terminal monocyte differentiation, for example to dendritic cells[65,66].

III.3. Immune responses to CMV

Upon infection, CMV triggers a multitude of innate and adaptive host immune responses. Although the virus cannot be eliminated entirely as soon as latent reservoirs are established, CMV reactivation events are efficiently confined in immunocompetent individuals, thereby inhibiting systemic virus spread and symptomatic CMV disease. This life-long interaction with the immune system leaves a profound imprint on various effector cell populations, particularly on T cells, B cells and NK cells.

As a first line of defense, CMV is subject to innate sensing by Toll-like receptors (TLRs) and other pattern-recognition receptors[13]. This is exemplified by the activation of TLR3 and TLR9 during infection with murine cytomegalovirus (MCMV)[67,68], or the interaction of gB/gH from

human cytomegalovirus with TLR2[69,70]. Toll-like receptor engagement leads to the production of inflammatory cytokines, ultimately resulting in the activation of effector cell subsets, such as NK cells.

An important role for NK cells in controlling CMV infection has been firmly established from studies demonstrating their involvement in the clearance of experimental MCMV infection[71,72]. Moreover, the adoptive transfer of NK cells can provide protection from MCMV infection in mice[73], and in humans, CMV infection can occasionally be controlled by NK cells, even in the absence of additional T cell responses[74]. Natural killer cells are a highly diverse group of lymphocytes that are capable of eliminating pathogen-infected or cancerous cells through the secretion of cytolytic effector molecules[38]. They are divided into various subsets, based on the expression of characteristic combinations of activating and inhibitory cell surface receptors. NK cell activation is regulated by a fine-tuned integration of signals from those invariant, germline-encoded receptors[75]. It was recently demonstrated that infection with Cytomegalovirus induces the clonal expansion of NK cells expressing the activating receptor NKG2C[76]. While NKG2C$^+$ cells normally make up only a minority of NK cells in peripheral blood, their frequency was found to be markedly increased upon acute CMV infection[77]. Such expansion of NKG2C$^+$ cells has also been described for other viral infections such as HIV and HBV, but was only observed in CMV seropositive individuals[78]. This implies that initial 'priming' by CMV is required for secondary expansion of this NK subset in response to other viral infections. Nevertheless, the initial activation of NKG2C$^+$ NK cells is likely not a result of direct recognition of CMV, but rather by differences in the expression of MHC-I molecules on infected cells, especially upregulation of HLA-E[79]. Along with selective expansion, NKG2C$^+$ cells from CMV seropositive donors were also found to produce more IFN-γ upon stimulation, compared to the identical NK subset from CMV seronegative donors[80]. These findings, which imply immune memory-like properties, are further underlined by profound epigenetic alterations in NKG2C$^+$ NK cells as a result of CMV infection[81]. Such results challenge the traditional view of innate immune cells as being short-lived and incapable of retaining any form of memory and blur the lines between innate and adaptive immunity[82].

Next to NK cell mediated immunity, CMV infection also triggers antibody responses against the various glycoprotein complexes that are located on the virion surface (Figure 3)[83]. The contribution of antibody responses to protection from Cytomegalovirus infection is controversial, in part due to the fact that seropositive individuals can get superinfected with another CMV strain even despite detectable antibody responses. However, there is substantial evidence supporting a role for humoral immunity in restricting viral dissemination and limiting the severity of CMV disease[13,84,85]. During natural CMV infection, detectable antibody responses are mostly directed against gB, gH/gL and Pentameric complex (PC)[86,87]. Of those, PC-specific antibody responses appear to have the highest neutralizing capacity and vaccines that are based on this complex elicit strong and broadly neutralizing responses in different animal models[88–91]. PC-specific antibodies are also 100- to 1000-fold more potent

in inhibiting epithelial and endothelial cell infection compared with those targeting gB or gH/gL/gO[92]. Consequently, such antibody responses may be superior in preventing the infection of placental cytotrophoblasts, which adopt an endothelial phenotype during gestation (Figure 4)[83]. Although many molecular determinants of intrauterine CMV infection are still unclear, infection of this cell type is thought to be a critical event during CMV transmission to fetuses[93,94]. This is supported by studies that found a reduced risk of fetal transmission when primary CMV infection during pregnancy was concomitant with early development of PC-specific antibodies[95,96]. As a result, the PC is a central component of many current vaccine concepts that aim at the induction of antibody responses for the prevention of mother-to-child transmission[97].

Despite an undisputable contribution of NK- and B cells, T cell-mediated immunity is still considered the predominant mechanism by which latent CMV infection is controlled *in vivo*[13]. CMV infection induces profound changes in the T cell memory compartment and an extraordinarily large proportion of T cells is often dedicated solely to this pathogen. Dominant responses to single epitopes regularly reach 5-10% of total $CD8^+$ T cells in peripheral blood and up to 30% of the overall cytotoxic T cell (CTL) responses are sometimes CMV-specific in healthy adults[98,99]. However, there is considerable variation in magnitude and breadth of T cell responses between individuals, a phenomenon that is still not fully understood[100]. Typically, T cell responses to CMV tend to increase with age, display an effector memory (T_{EM}) phenotype and lack markers of T cell exhaustion[99,101,102]. The gradual expansion and long-term maintenance of CMV-specific T cell populations after initial infection is often referred to as 'memory inflation', although this term has not been formally defined and was originally introduced in the context of MCMV infection[103]. It is remarkable that large numbers of CMV-specific T cells are sustained over many years without diminished effector functions, given that in other chronic viral infections such as HIV, HBV or HCV, virus-specific T cells typically decrease in number and show signs of exhaustion over time[104,105]. It has been hypothesized that this is due to differences in the antigenic burden, since the aforementioned viruses typically replicate continuously and to high titers *in vivo*. This results in constant stimulation of virus-specific T cells, a condition that favors functional exhaustion over time. By contrast, CMV reactivation from latency seems to occur sporadically and on a smaller scale, therefore avoiding permanent restimulation of T cells[106,107]. However, it is still unclear if the extraordinarily high number of CMV-specific T cells in some individuals is a requirement for protection or simply the result of gradual, life-long expansion of an initial pool of effector cells that is driven by periodic reactivation events[108]. Due to its profound and long-lasting impact on the immune system, CMV is also suspected of accelerating immune senescence, but it is currently not clear if this has clinical implications[109,110].

Although many questions about the nature of the CMV-specific T cell pool are still unaddressed, their potency in controlling CMV infection is well established. For instance, antibody-mediated depletion of $CD8^+$ T cells in rhesus monkeys leads to reactivation of

rhCMV[111]. Depletion of lymphocytes in mice also results in reactivation of MCMV replication, which can be suppressed by adoptive transfer of T cells[112,113]. Similarly, CMV-specific T cell responses and subsequent control of viral replication, could be restored in immunocompromised patients through adoptive T cell transfer[114–116]. T cell responses are directed against a high number of CMV proteins: Using overlapping 15-mer peptides comprising 213 CMV genes for the stimulation of T cells from 33 seropositive adults, Sylwester *et al.* found that a total of 151 open-reading frames (70%) were immunogenic[98]. Most individuals recognize 5-10 proteins in each T cell subset, with IE-1, IE-2 and pp65 generally inducing the strongest CTL responses and gB, pp65, UL16 and TRL14 dominating the $CD4^+$ T cell compartment[13,108].

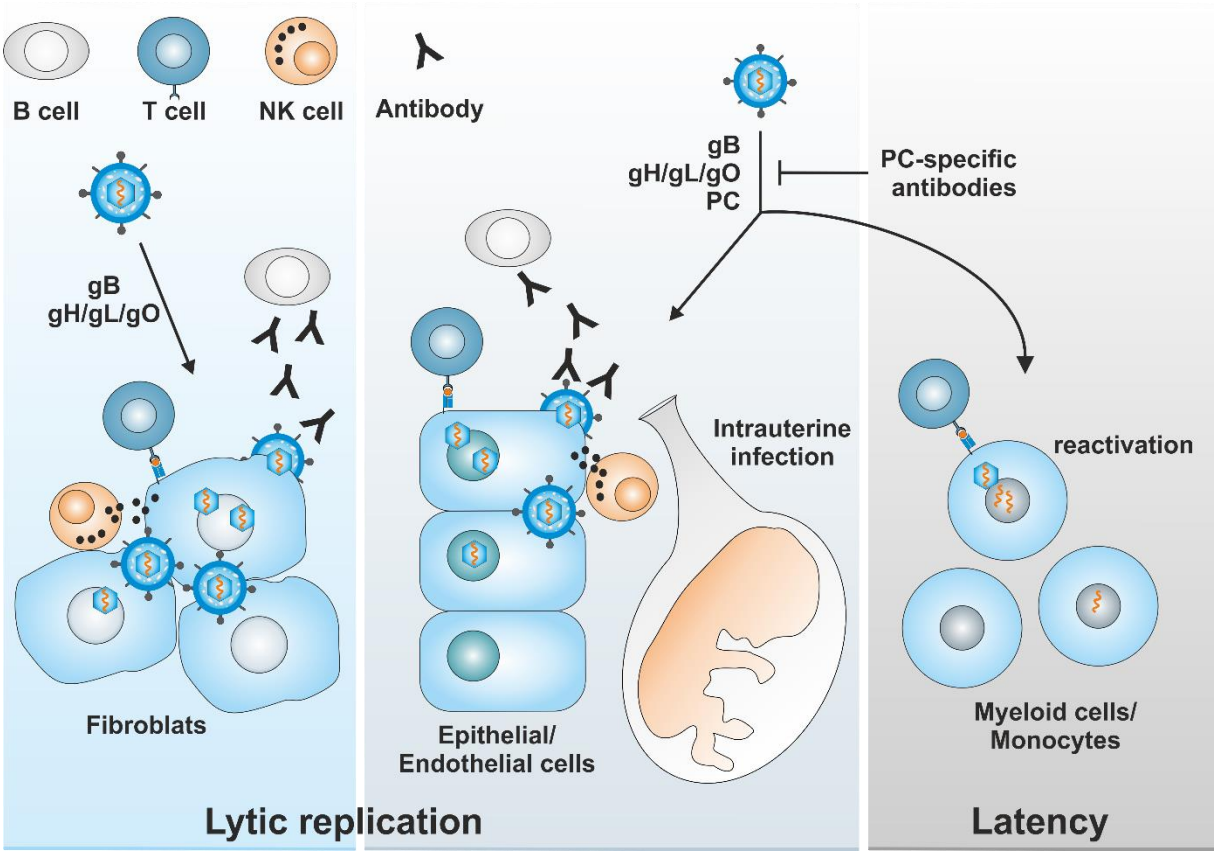

Figure 4 – Immune responses to CMV
CMV is capable of infecting a wide variety of cells ranging from fibroblasts to epithelial cells, endothelial cells and myeloid cells (e.g. monocytes and precursors thereof). Fibroblast infection is mediated by the glycoprotein complexes gB (GC I) and gH/gL/gO (GC III), while for the infection of the residual cell types, the pentameric complex (PC) is required in addition to GC I and GC III. Lytic replication is confined (among others) by T cell, B cell and NK cell mediated antibody responses. Antibodies that are directed against the pentameric complex are particularly potent in inhibiting endothelial/epithelial cell infection and might therefore be superior in preventing intrauterine infection. During latency, which is established in certain cells from the myeloid lineage, only a small set of latency-associated genes is expressed. Viral reactivation from latently infected cells (for example as a result of monocyte differentiation) is controlled predominantly by T cell mediated immunity.

III.4. Clinical implications

In healthy individuals, primary infection is mostly asymptomatic or merely accompanied by mild symptoms resembling those of an infectious mononucleosis[117]. However, CMV causes

considerable morbidity and even life-threatening complications in immunocompromised individuals such as transplant recipients and AIDS patients[118–120]. Cytomegalovirus particles can infect a remarkably broad range of cells and spread to virtually every organ within its host[121]. As a result, CMV disease can result in a variety of clinical manifestations such as colitis, pneumonitis, encephalitis, hepatitis and retinitis[122,123].

Human cytomegalovirus also represents one of the most common congenital infections worldwide with an estimated prevalence of 0.64% at birth and is a leading cause of disability in children (Figure 5)[124,125]. The risk for intrauterine transmission is highest (30-35%) if a seronegative mother becomes infected with CMV during pregnancy[125]. By contrast, viral reactivation in a seropositive mother less frequently results in fetal infection (1.2-1.4%)[7,126]. Neonatal symptoms of congenital CMV infection include microcephaly, hepatosplenomegaly, petechiae, jaundice, chorioretinitis, thrombocytopenia and anemia[127]. The mortality rate among infants with symptomatic CMV disease at birth is 10–30% and only about 10% fully recover, while the remaining children will have long-term sequelae ranging from sensorineural hearing loss and delayed neural development to mental retardation[128,129]. However, even children with congenital CMV infection that show no symptoms at birth may develop late sequelae, albeit with lower frequency (8-15%)[130,131]. Early infection of the fetus, particularly in the first trimester, is generally associated with an increased likelihood of severe complications[132].

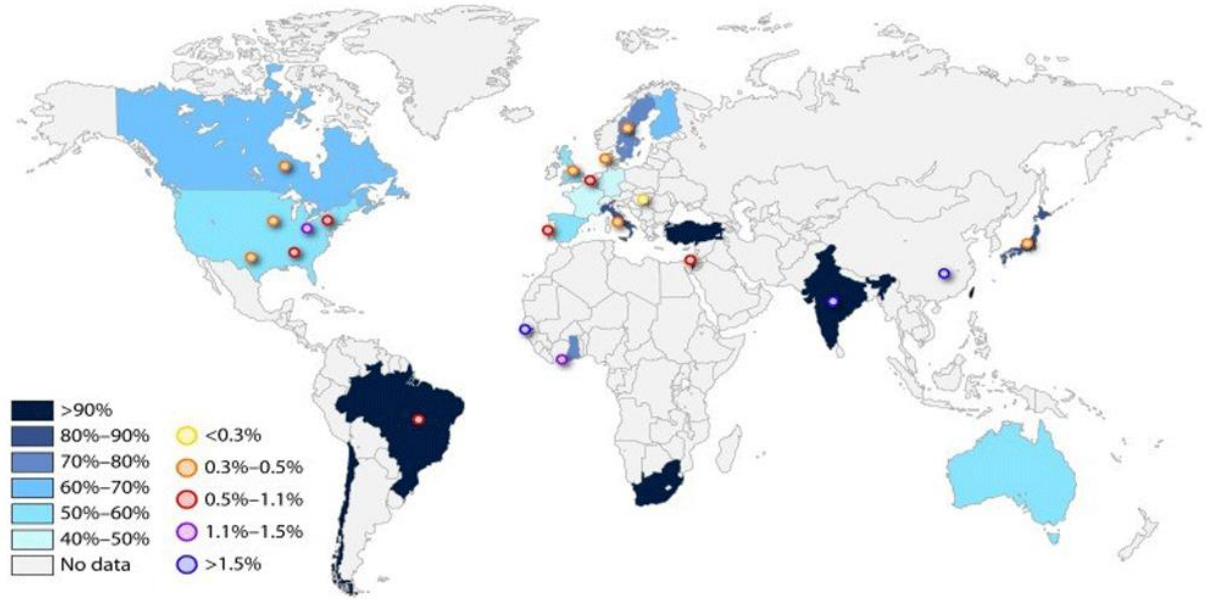

Figure 5 - Global CMV seroprevalence levels and incidence of congenital CMV infection
Cytomegalovirus seroprevalence rates among women of reproductive age (reproduced from Manicklal et al.[124]) are displayed in different shades of color, and congenital CMV birth prevalence rates are shown by the circles. Figure from Emery and Lazzarotto[132].

CMV is considered an opportunistic pathogen, mostly causing severe disease as a result of inadequate immune responses. Besides congenital infections, where the virus often encounters an immune system that is not fully developed yet, this is also the case during innate or

acquired immunodeficiency. Accordingly, an increased risk for CMV disease has been described in numerous innate immunodeficiency syndromes like Fanconi anemia, severe combined immunodeficiency (SCID) or common variable immunodeficiency (CVID)[133–135]. Acquired immunodeficiency, mainly due to HIV infection, also predisposes for symptomatic CMV disease. The broad application of combined antiretroviral therapy (ART) has reduced the incidence of CMV disease from being the most significant opportunistic infection to a rarity during treatment[122,136,137]. However, given that a high proportion of HIV positive individuals is still without access to ART, CMV remains a significant co-morbidity in patients suffering from AIDS.

Because the number of solid-organ and haematopoietic stem cell transplantations has been increasing in recent years, transplant recipients are another steadily growing group with a high incidence of CMV disease. New potent immunosuppressive agents contribute to decreasing the incidence of graft rejection, but at the same time, patients are left highly susceptible to opportunistic infections[138]. Although various pathogens frequently cause disease in transplant recipients (e.g. EBV, Adenoviruses, mycobacteria or fungi), CMV is still the most common infection[139–142]. The risk for severe complications is generally greatest if a CMV seronegative donor receives a graft from a seropositive donor (D+/R-)[143]. However, a multitude of additional factors such as the age of the transplant recipient, the state of immunosuppression, genetic predispositions or the type of organ graft influence the clinical outcome as well: For example, lung, small intestine and pancreas transplant recipients are at higher risk for severe complications than kidney or liver transplant recipients[118,144].

Antiviral agents such as Ganciclovir, Valganciclovir, Foscarnet and Cidofovir are available for the treatment of CMV disease and capable of reducing the incidence of CMV reactivation after transplantation[145–147]. However, renal toxicity and interactions with other drugs, as well as the emergence of resistant virus strains, limit their therapeutic potential[148–150]. Thus, to avoid unnecessary administration of antivirals, preemptive therapy is often applied instead of universal prophylaxis for the management of CMV reactivation after transplantation[151,152]. As part of this strategy, antiviral therapy is only initiated if a predefined threshold level of viral DNA copy number in blood is surpassed, because viremia usually precedes symptomatic CMV disease[136,153]. Although preemptive therapy is useful for reducing drug-related toxicities, there is still controversy about whether it is preferable to universal prophylaxis, especially in high risk constellations (D+/R-)[152,154]. Next to small molecule drugs interfering with viral replication, CMV reactivation can also be controlled by adjusting the level of immunosuppression or through adoptive transfer of virus-specific T cells, but early identification of patients at risk for viral relapse is critical for the success of all these interventions[155–157].

III.5. Monitoring of CMV-specific immune responses

Due to the key role of T cell mediated immune responses in controlling CMV replication, there is a strong correlation between loss of CMV-specific T cells and viral reactivation. As

early as 1991, Reusser *et al.* reported that in a cohort of bone marrow transplant recipients, none of the patients with detectable CMV-specific T cells developed CMV disease. At the same time, more than half of patients lacking CMV-specific T cell responses died of CMV pneumonia[158]. Since then, a plethora of studies was published highlighting the diagnostic value of virus-specific T cells for the prediction of CMV reactivation[159–162]. For example, more recent work from Espigado *et al.* showed that after hematopoietic stem cell transplantation, early reconstitution of CMV-specific T cell responses (≤ 6 weeks), is associated with less incidence of CMV replication, reduced viral loads and better overall survival, compared to patients with delayed immune reconstitution[163]. Collectively, these results indicate that monitoring of virus-specific T cells is a promising approach for the early identification of patients that are at risk for CMV disease (Figure 6).

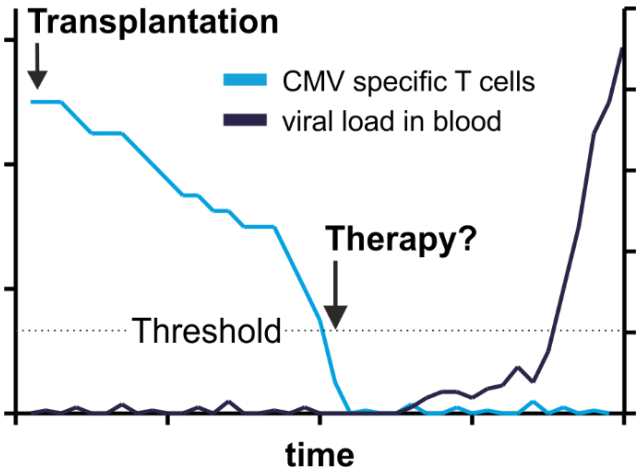

Figure 6 – Immune monitoring for the identification of patients at risk for CMV disease
Following transplantation, the quantity or function of T cells may decline as a result of drug-induced immunosuppression. Loss of CMV-specific T cell responses can result in re-activation of lytic CMV replication, concomitant with viremia and symptomatic disease. Quantification of CMV-specific T cells could help to identify patients with an elevated risk for CMV disease prior to viremia (which is the current criterion for initiating the administration of antivirals during preemptive therapy).

Various methods are currently available for assessing pathogen-specific T-cell immunity[164]. Such techniques are either based on direct detection of cells, for example after staining with MHC-multimers[165], or the quantification of activation markers such as Interferon γ (IFNγ) after stimulation with pathogen-derived antigens[166]. These markers can then be detected by intracellular cytokine staining (ICS), followed by flow cytometry analysis, or via Enzyme-linked immunosorbent (ELISA) or Enzyme-linked immunospot (ELISpot) methods.
Next to the detection method, various types of antigens are also available for stimulation, including viral lysates, peptide pools and recombinant proteins. IE-1 and pp65 are the preferred antigens for CMV in most assays, since they are the main targets of $CD8^+$ T cells[13,167]. Currently, there is no consensus on the ideal method for monitoring of CMV-specific T cells and proposed threshold levels still lack extensive validation[156]. Nevertheless, there is accumulating evidence that in the future, monitoring T cell immunity could become a cornerstone in the management of Cytomegalovirus in transplant recipients.

III.6. Current Status of CMV vaccine development

In 2000, a committee from the US national institutes of health tasked with prioritizing efforts for the development of novel vaccines assigned the highest level of priority to the

implementation of a CMV vaccine[168]. Taking the impact of CMV on morbidity and mortality into consideration, the committee estimated that if a vaccine with 100% efficacy was administered to the entire population, a total of 70.000 quality-adjusted life years (QALY) could be gained per year in the United States. In addition, the annual health care costs saved would be an estimated 4 billion per year in the US alone (assuming that the vaccine would cost 50$ per course). However, although the first vaccine efforts date back to the 1970s and a multitude of candidates has been developed since, a protective or therapeutic CMV vaccine has still not been licensed (Figure 7)[169]. An efficacious Cytomegalovirus vaccine is urgently needed, given that treatment options with antiviral agents are limited due to side effects and the emergence of resistant virus strains[170–172]. In addition, there is currently no therapy available for inhibiting intrauterine infection during pregnancy, although at least some concepts are undergoing clinical trials[132,173].

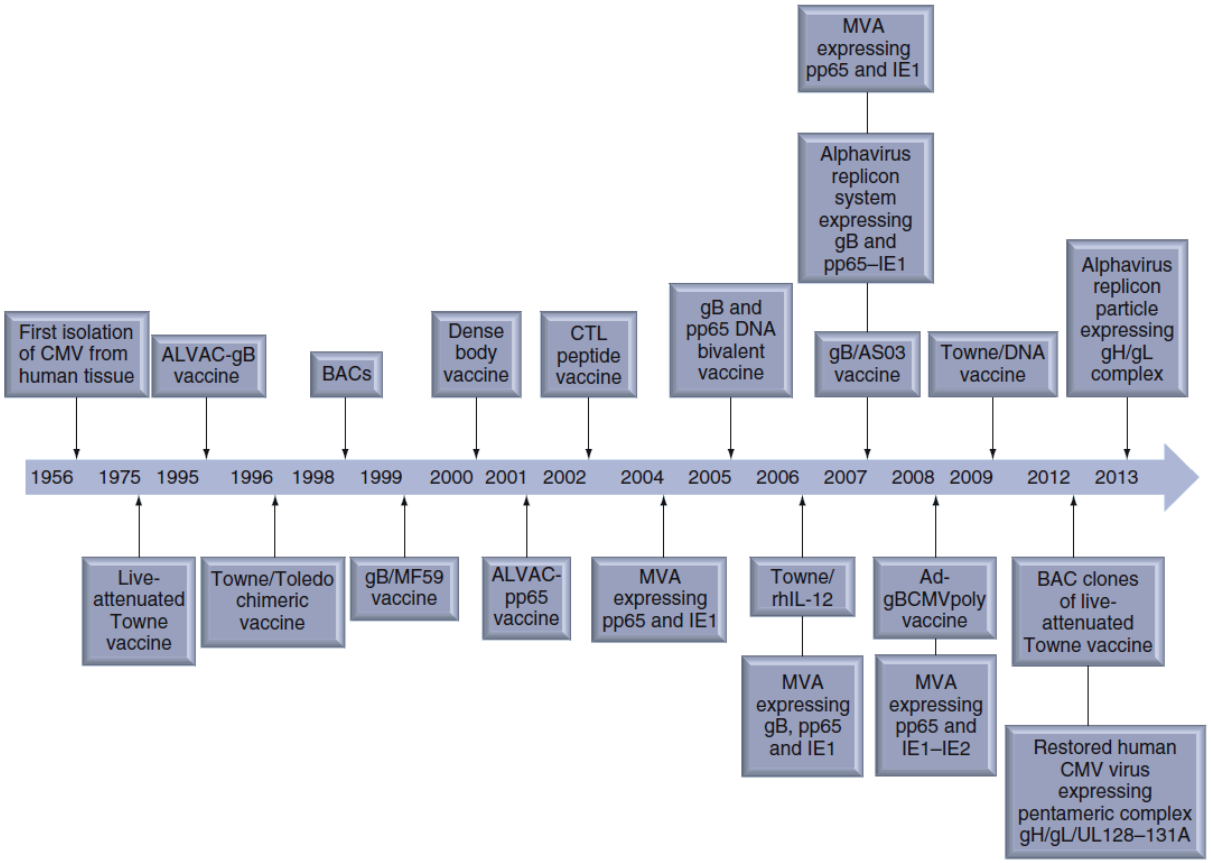

Figure 7 – History of CMV vaccine development
Summary of selected candidate vaccines that were evaluated in preclinical and clinical trials. Glycoprotein B (gB), pp65 and IE1 were mainly tested as potential targets, delivered by various platforms including the attenuated CMV Towne isolate[174], recombinant viral vectors encoding full-length antigens and epitopes[175,176], DNA[177], dense body (DB)[178] and subunit[179] vaccines. BAC: Bacterial artificial chromosome; CTL: Cytotoxic T-lymphocyte; MVA: Modified vaccinia Ankara. Figure from Dasari *et al.*[180]

Of the numerous candidate vaccines that were developed over the last decades, only few made it past the early stages of clinical trials[136]. However, modest efficacies have previously been reported in phase II studies for both prophylactic as well as therapeutic approaches

(e.g. 50% efficacy for gB protein with adjuvant MF59)[181,182]. While these results are encouraging and imply that the development of a CMV vaccine is feasible, it also underlines the necessity to explore novel, alternative vaccine concepts.

Since clear immunological correlates of protection from CMV infection have not been defined yet, vaccine candidates should ideally induce both humoral and cell-mediated immune responses[180,183]. As described above (section III.2), several different glycoproteins are expressed on the virion surface, all of which are targets for humoral immunity. Until recently, subunit vaccines designed for the induction of protective antibody responses mostly focused on the fusion protein gB. The rediscovery of the pentameric complex in 2005 as a crucial component for the infection of epithelial and endothelial cells revealed a new target for such vaccine concepts[184]. Indeed, inclusion of the pentameric complex into subunit vaccines or attenuated virus led to promising results in animal models[185,186].

At the same time, cell-mediated immunity plays a crucial role in controlling viral latency and limiting virus spread. T cell responses are directed against a variety of viral antigens, with the tegument protein pp65 and the transcriptional regulator IE-1 representing major targets[98,187]. Interestingly, expression of CMV antigens is frequently detected in glioblastoma cells[188,189], and as a result, therapeutic vaccination concepts that aim at expanding CMV-specific T cells for enhancing antitumor immunity are currently being tested in clinical studies[190].

Viral vectors are a favored tool for the delivery of heterologous antigens, in part due to their capability to efficiently prime T cell responses during vaccination[191]. Several such vectors, like the poxvirus strain Modified Vaccinia Ankara (MVA) are currently being evaluated as therapeutic vaccine candidates in clinical trials, although their efficacy has yet to be demonstrated[192,193]. However, repeated administration of an antigen by a given vector is impeded by the development of immunity to its backbone, which can be avoided by heterologous prime/boost immunizations. Hence, novel vectors should still be developed and assessed for their capacity to deliver CMV immunogens. Three different viral vector classes that were used in this work (MVA, AdV and SeV) are introduced in the following sections.

III.6.1. Modified Vaccinia Ankara (MVA)

Poxviruses containing foreign genes are a well-established platform for the development of novel vaccines and therapeutics in biomedical research. Advantages of poxvirus vectors include large packaging capacity for heterologous DNA, exclusive replication in the cytoplasm (minimizing the risk of genomic integration) and lack of persistence in the host, as well as high immunogenicity[194,195]. Most poxvirus vectors are based on the strain Vaccinia, which was originally used for the eradication of smallpox[196]. Vaccinia was long presumed to be derived from a strain of cowpox, but more recent analysis indicates that it likely originated from a strain of rodent or equine origin[197]. Although vaccinia exhibits strongly reduced virulence in humans, there are multiple well-documented cases of vaccination complications

as well as laboratory infections[198,199]. Hence, several highly attenuated, Vaccinia-derived virus strains were generated for usage as immunogen delivery vectors, including New York Vaccinia Virus (NYVAC)[200] and Modified Vaccinia Ankara (MVA)[201]. MVA was generated from the vaccinia virus strain Ankara, which was used at the vaccine institute in Ankara for smallpox vaccine production[194]. Serial passaging of this strain on chicken embryo fibroblast (CEF) cells led to the loss of approximately 15% of the viral genome over more than 500 passages[202,203]. The resulting MVA strain displays enhanced attenuation, as illustrated by its inability to replicate in human cell lines[204]. MVA is currently licensed as a vaccine against smallpox. Moreover, it is one of the most broadly used viral vectors for the delivery of antigens from various pathogens.

III.6.2. Adenovirus vectors

Human adenoviruses (AdVs) comprise a large family (>70 serotype) of non-enveloped, double-stranded DNA viruses that are subdivided into seven species termed A-G[1,205,206]. Depending on the serotype, AdV infection can affect the respiratory, gastrointestinal or urinary tract as well as the eye, occasionally causing severe disease. Nonetheless, natural infections with these ubiquitous viruses are mostly asymptomatic or merely accompanied by mild symptoms[207]. Recombinant, replication-defective adenoviruses are extensively utilized as vectors for vaccination, cancer treatment or the delivery of therapeutic genes. Reasons for the popularity of AdVs as vaccine vectors include high packing capacity and immunogenicity, combined with an excellent safety profile and the capability to infect both dividing and non-dividing cells[208–211]. Simple and inexpensive methods for vector construction and purification of high titer viral stocks from cell culture further contribute to making the AdV vector platform versatile in use.

Historically, most studies on basic aspects of Adenovirus biology were carried out using AdV type 5 (Ad5, a member of subgroup C), and as a consequence, recombinant vectors were almost exclusively based on Ad5 for many years[212]. However, broad usage of these vectors is limited by preexisting immunity to Ad5 in humans with the presence of neutralizing antibodies (NAbs) reaching up to 90% in some regions[213]. Efficient transduction by Ad5 is also confined to cells expressing the Coxsackie virus and Adenovirus receptor (CAR)[214]. Direct binding to erythrocytes, liver sequestration of virions and hepatotoxicity after intravenous administration constitute additional disadvantages of Ad5-based vectors counteracting broad clinical application[215–217].

In order to exploit the natural diversity of Adenoviruses and to overcome the limitations of Ad5-based vectors, an increasing number of AdVs from different subgroups have been vectorized in recent years[218]. Vector alternatives like Ad6 (NAb frequency ≈ 68%[213]), Ad26 (NAb frequency ≈ 43-68%[219]) or Ad35 (NAb frequency ≈ 5-18%[219]) were demonstrated to be immunogenic and well tolerated in animal models and humans[220–223]. Beyond that, chimpanzee Adenoviruses (chAdVs) like chAd3 and chAd63 are also emerging as a new vector

class, although preexisting immunity in humans (up to 33% NAb frequency for chAd63[224]) has been reported as well[225–227]. While the aforementioned AdV-based vaccine candidates mostly gave promising results in clinical trials, it has also become evident that repeated administration of the same vector is hampered by the induction of neutralizing antibodies[228]. This underlines that novel AdV vectors should still be established to meet an increasing demand for safe and efficacious delivery systems in gene therapy and vaccination[229].
Previously, an E1/E3-deleted gene therapy vector based on Adenovirus 19a (recently renamed to Ad64[230], NAb frequency ≈16-19%[231,232]), a member of subgroup D that causes epidemic keratoconjunctivitis in humans, has been described[233,234]. AdVs from this subgroup display a particularly broad host cell tropism since they bind to ubiquitously expressed sialic acids rather than CAR and might therefore be a promising alternative to Ad5-based vectors[235,236].

III.6.3. Sendaivirus vectors

Sendai virus (SeV) is a non-segmented, negative strand RNA virus that belongs to the family *Paramyxoviridae* and causes respiratory infections in mice[237]. A number of advantageous features have led to broad usage of SeV as a viral vector including exclusive replication in the host cell cytoplasm[238], efficient transduction of both dividing and non-dividing cells[239], broad target cell tropism[240,241] and replication to high titers in cell culture[242]. Importantly, it is also considered non-pathogenic in humans[243,244]. Sendai virus is currently tested as a Jennerian vaccine for human parainfluenza virus and as a viral vector for the delivery of human respiratory syncytial virus antigens[245–247]. In appreciation of its many favorable characteristics, SeV is also emerging as a vector for the delivery of immunogens from unrelated pathogens such as HIV-1 Gag[222,248].

III.7. Objective of this thesis

The quantification of virus-specific T cell responses is a promising method for assessing cell-mediated immunity to CMV in general and to predict viral reactivation from latency. Most methods for the identification of such T cells are based on the detection of activation markers like IFNγ upon antigen recognition via the T cell receptor complex (TCR). A prerequisite for TCR recognition of pathogen-derived peptides is their presentation by antigen-presenting cells (APCs) and accordingly, the efficiency with which antigens are delivered to these cells has a major impact on assay sensitivity (Figure 8). Thus, one main focus of this work was to increase the uptake of proteins into APCs to improve currently available methods for the measurement of cell-mediated immunity to CMV.

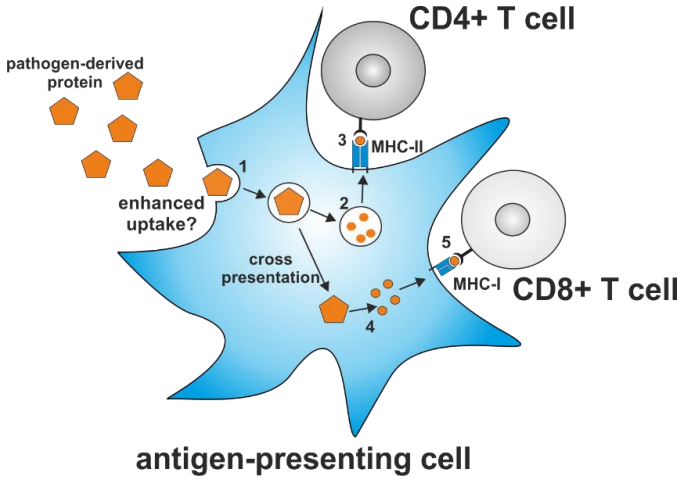

Figure 8 – Protein uptake and processing by antigen-presenting cells
Proteins are taken up from the extracellular space (1), degraded in endolysosomes (2), loaded onto MHC-II molecules and transported to the cell surface where they can interact with $CD4^+$ T cells (3). Alternatively, in a process termed cross-presentation, proteins escape endosomes and enter the cytoplasm, followed by proteasomal degradation (4). Peptides are then transferred to the endoplasmic reticulum, loaded onto MHC-I molecules and transported to the cell surface where they are recognized by antigen-specific $CD8^+$ T cells (5). Enhanced protein uptake might increase the overall amount of MHC presentation and, as a consequence, also T cell stimulation.

Previously, it was reported by Barabas *et al.* that storage of the Epstein-Barr virus (EBV) protein BZLF1 in high molar urea solutions prior to stimulation of immune cells enhances the restimulation of antigen-specific T cells[249]. Since this is a simple and inexpensive method for increasing T cell reactivation rates, the molecular mechanism underlying this phenomenon should be elucidated in order to evaluate whether this technique can be applied to a broader panel of antigens, comprising the CMV proteins IE-1 and pp65 besides EBV's BZLF1. As storage in urea induces protein carbamoylation, the main hypothesis to be tested here was that this posttranslational modification alters antigen uptake and T cell restimulation rates.

Beyond *ex vivo* applications, CMV proteins that are modified for enhanced uptake into APCs might also be used for the priming of adaptive immune responses during vaccination. Further, in order to influence magnitude and quality of the induced immune responses, a combination of various delivery methods in heterologous prime/boost immunizations might be required. Of the many conceivable delivery systems, live attenuated viral vectors are particularly interesting tools due to their inherent immunogenicity. Hence, another main focus of this work was the generation and preclinical characterization of novel virus vectors deliver-

ing CMV antigens. Two adenoviruses strains (Ad5 and Ad19a/64), the poxvirus strain Modified Vaccinia Ankara (MVA) as well as Sendai virus (SeV, a murine RNA virus) were chosen and recombinants expressing IE-1 or pp65 were generated. Since immunological information on SeV and Ad19a/64 is still limited, basic aspects of vector biology should be explored prior to *in vivo* studies to exclude possible immune evasion mechanisms like interference with antigen processing. Here, the vectors should be compared in a series of *ex vivo* assays to the well-established vector platforms Ad5 and MVA regarding parameters such as target cell tropism, cytotoxicity as well as antigen expression and presentation (Figure 9). Most parameters should be measured after transduction of dendritic cells (DCs), partly because they are the most potent APCs *in vivo*. In addition, DCs that are pulsed *ex vivo* with CMV antigens might be readily applied as a therapeutic vaccine, a strategy which is currently being employed with some success in clinical studies for the treatment of glioblastomas expressing CMV antigens[190,250].

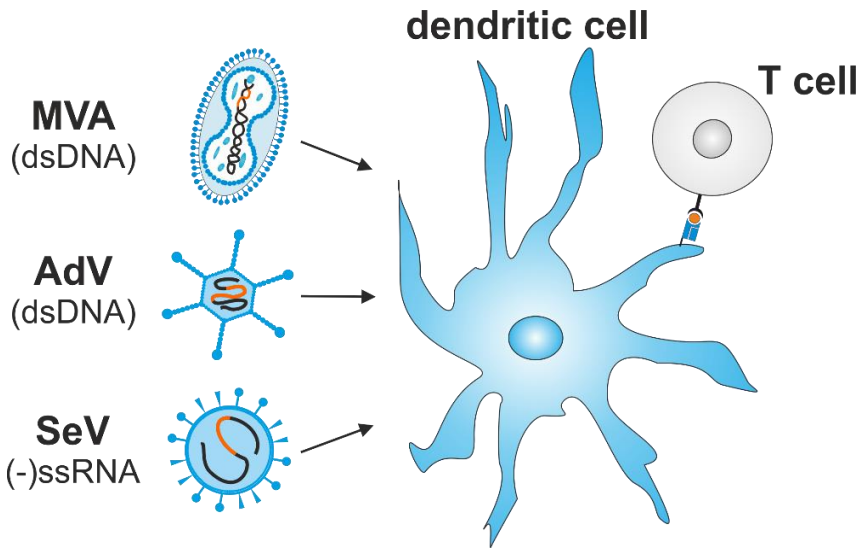

Figure 9 – Transduction of dendritic cells by viral vectors
The CMV antigens IE-1 or pp65 were inserted into the genomes of Modified Vaccinia Ankara (MVA), Adenovirus (AdV) and Sendai virus (SeV). After *ex vivo* transduction of human dendritic cells, various parameters like transduction rates, antigen expression and presentation, cytotoxicity and maturation of dendritic cells should be assessed.

IV. Results

IV.1. Influence of posttranslational modifications on protein delivery to antigen-presenting cells

Adaptive immune responses require priming of naïve lymphocytes, a function that is carried out mainly by professional antigen-presenting cells (APCs) like dendritic cells (DCs) and macrophages. These cells specialize in taking up proteins from the extracellular space, which are subsequently processed and presented on major histocompatibility (MHC) complexes. A defining property of professional antigen-presenting cells is the co-expression of MHC class one (MHC-I) and class two (MHC-II) complexes, which allows presentation of peptides to both CD4 and CD8 positive cells, respectively (most cell types express MHC-I only). In addition, professional APCs express a number of costimulatory molecules that activate T cells, thereby engaging multiple independent pathways in parallel and lowering the threshold signal required for T cell priming. Due to these properties, professional APCs hold a unique and central role in the initiation of immune responses and interaction with T cells. As a consequence, techniques that mediate efficient delivery of antigens to these cells have great potential both for the development of novel vaccine candidates (*in vivo*) as well as monitoring of antigen-specific effector cells (*ex vivo*).

It was previously reported that storage of the EBV protein BZLF1 in high molar (4 M) urea-solution results in increased stimulation of $CD4^+$ and $CD8^+$ T cells compared to urea-non-treated protein (Figure 10). It was further demonstrated that the urea-treated protein is taken up via clathrin-mediated endocytosis into a number of APCs, including monocyte-derived dendritic cells (moDCs), B cells and monocytes[249].

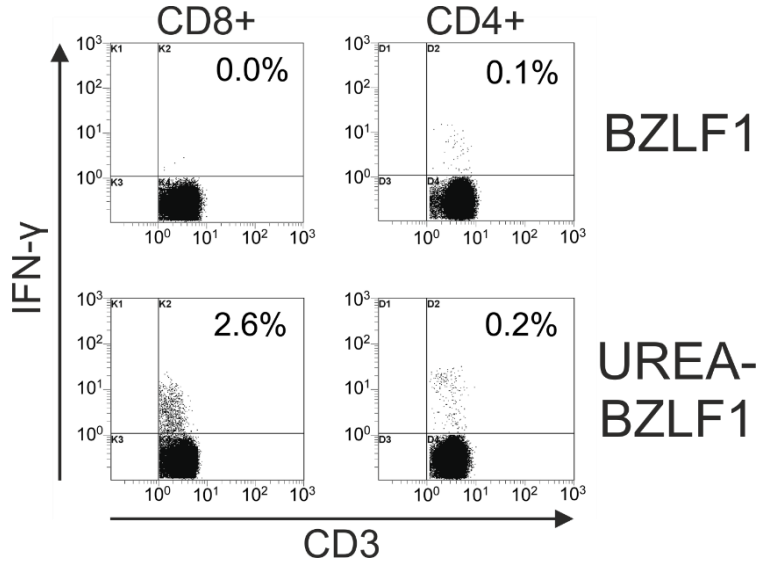

Figure 10 - Urea treatment increases the restimulation of BZLF1-specific T cells
Whole blood from an EBV-seropositive donor was stimulated with BZLF1 or urea-treated BZLF1 (10 µg/ml each) for 7 hours with Brefeldin A (BFA, 10 µg/ml) present during the last 4 hours. Cells were stained for CD3, CD4, CD8 and intracellular IFN-γ, followed by flow cytometry analysis. Shown is the percentage of $CD3^+CD8^+$ or $CD3^+CD4^+$ cells expressing IFN-γ from a representative stimulation of eight independent experiments using a total of 4 different donors. Plots show log fluorescence intensity. Modified from Barabas et al. (2008)[249].

Although protein storage in urea might be a simple and cost-effective method for increasing uptake into APCs in general, it is unclear if this treatment will have a similar effect when

applied to other candidate proteins. Moreover, the molecular mechanism by which UREA-treatment of the stimulating protein leads to increased T cell restimulation is not known.

In aqueous solution, urea is present in an equilibrium with cyanic acid and ammonium favoring urea (>99%)[251,252]. Tautomerization of cyanate leads to the formation of isocyanic acid, which in turn reacts with primary amino groups in a process termed carbamoylation. Protein carbamoylation is an irreversible, posttranslational modification that affects the α-amino group at the N-terminus as well as ε-amino groups of lysine and arginine side chains (Figure 11). While *in vitro*, carbamoylation is often an undesired side effect of protein storage in urea buffers[253], it has become evident that this modification also occurs *in vivo* where it has impact on a number of pathophysiological processes. For instance, it is considered a hallmark of ageing as well as a biomarker for renal dysfunction and uremia[254–257]. Carbamoylation has also been associated (among others) with the development of atherosclerosis, various immune system dysfunctions and the formation of anti-carbamoylated protein antibodies (reviewed in detail by Delanghe et al[258]). There are two main pathways by which cyanate formation and subsequent protein carbamoylation take place *in vivo*: i) Spontaneous dissociation of urea, a mechanism that leads to increased carbamoylation of serum proteins in uremic patients as a result of chronic kidney disease. ii) Formation of cyanate from the oxidation of thiocyanate, a reaction that is catalyzed by the enzyme myeloperoxidase (MPO) in the presence of hydrogen peroxide. MPO is released from neutrophils and macrophages during inflammation, thus inducing a local increase in protein carbamoylation at inflammatory sites[259].

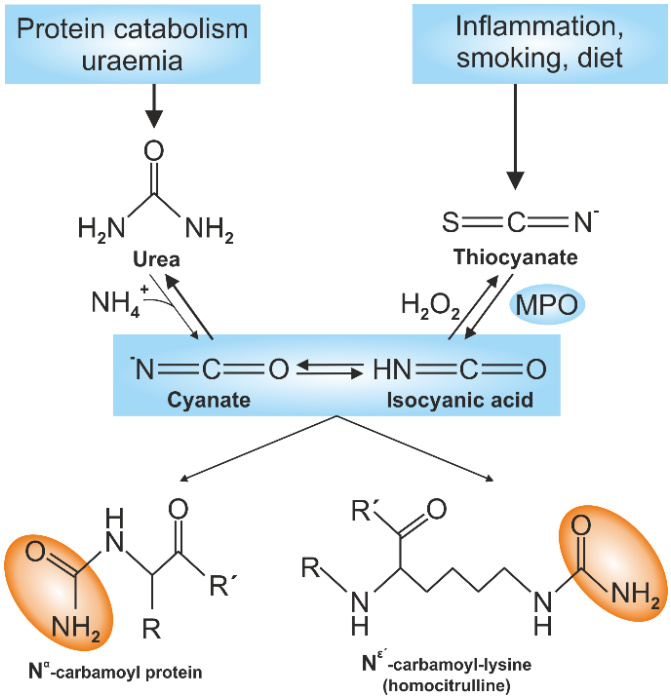

Figure 11 – Mechanisms of protein carbamoylation
The reaction of isocyanic acid (a tautomer of cyanate) with primary amino groups is termed carbamoylation. *In vivo*, carbamoylation occurs following the spontaneous dissociation of urea into cyanate and ammonium (NH_4^+). Protein carbamoylation as a result of this pathway is increased during renal dysfunction concomitant with uremia. Alternatively, cyanate can be formed by the enzymatic oxidation of thiocyanate in the presence of hydrogen peroxide (H_2O_2). This is catalyzed by myeloperoxidase (MPO), an enzyme stored mainly in the azurophilic granules of neutrophils that is released during inflammation. Smoking or certain dietary choices can lead to elevated levels of thiocyanate in blood, ultimately resulting in increased protein carbamoylation during inflammation. Figure adapted with permission from Elsevier © Verbrugge et al.[252], license number 4194070497430.

Since the immune system has evolved to distinguish self and altered-self components, and recognition of carbamoylated low-density lipoprotein (LDL) by monocytes had been reported before[260], it was intriguing to test if this modification might be responsible for the increased uptake of urea-treated proteins into antigen-presenting cells.

IV.1.1. Impact of protein carbamoylation on T cell restimulation

To assess a putative impact of carbamoylation on protein uptake into APCs and the subsequent restimulation of antigen-specific T cells, the CMV proteins IE-1 and pp65 as well as the EBV protein BZLF1 were chosen as model antigens. Besides carbamoylation, treatment with high molar urea also induces protein denaturation, which might influence the interaction with antigen-presenting cells as well. Furthermore, if urea is not removed from the protein after the treatment, low amounts will be present during stimulation, possibly impacting cellular homeostasis by changing the osmolarity of the culture medium. Thus, to separate a possible contribution of carbamoylation to T cell stimulation from any other influences urea might have, cyanic acid was used instead of urea to induce this posttranslational modification. For sensitive and antigen-specific stimulation of primary T cells, stimulator proteins have to meet certain quality criteria regarding purity and absence of bacterial contaminations such as lipopolysaccharide (LPS). Since there was no commercial source for full-length IE-1, pp65 and BZLF1 fulfilling those criteria, a suitable expression system first had to be determined, followed by establishment of a purification method under urea-free, native conditions. All proteins were fused C-terminally with a 6xHistidine tag, followed by a Strep tag (Figure 12A), thus allowing affinity purification using either nickel or Strep-Tactin beads[261]. For removal of the tandem affinity tag after purification, protein and tag were further separated by a short amino acid sequence recognized by the 3C protease of human rhinovirus[262]. To identify a suitable expression system, transient transfection of human HEK293F cells grown in suspension culture, inducible expression in *E. coli* cells as well as infection of insect cells with a recombinant baculovirus strain were evaluated. While yields were generally rather poor with HEK293F cells (below 50µg per l) and LPS contaminations proved challenging to avoid using *E. coli*, the best results regarding purity and yield were obtained with insect cells using the Bac-to-Bac expression system[263,264] (data not shown). While there was some variation between the different proteins and individual purification batches, yields ranging from several hundred micrograms to milligrams per liter of cell culture could be readily obtained, all of which were sufficiently pure and contained undetectable or very low (<5 EU/mg) levels of LPS.

Purification of pp65 from crude cell lysates was performed under native conditions using Ni-IDA beads (Figure 12B, section VI.3.2), followed by cleavage of the tag with Glutathione S-transferase (GST) tagged PreScission™ protease (section VI.3.2). To remove cleaved tag and protease, the eluate was incubated with an excess amount of Strep-Tactin Sepharose (binding the removed tag as well as uncleaved protein) and Glutathione Sepharose (binding

the protease). Quantitative cleavage and removal of undesired components were verified by Western blot analysis (Figure 12C) while purity of the final product was further assessed by silver staining of proteins after SDS PAGE (Figure 12D). Silver staining revealed that pp65 was sufficiently pure and only few contaminations were visible in the final product. However, even though the respective bands were not detected in Western blot analysis, they could also represent C-terminal degradation products in which the recognized epitopes were removed.

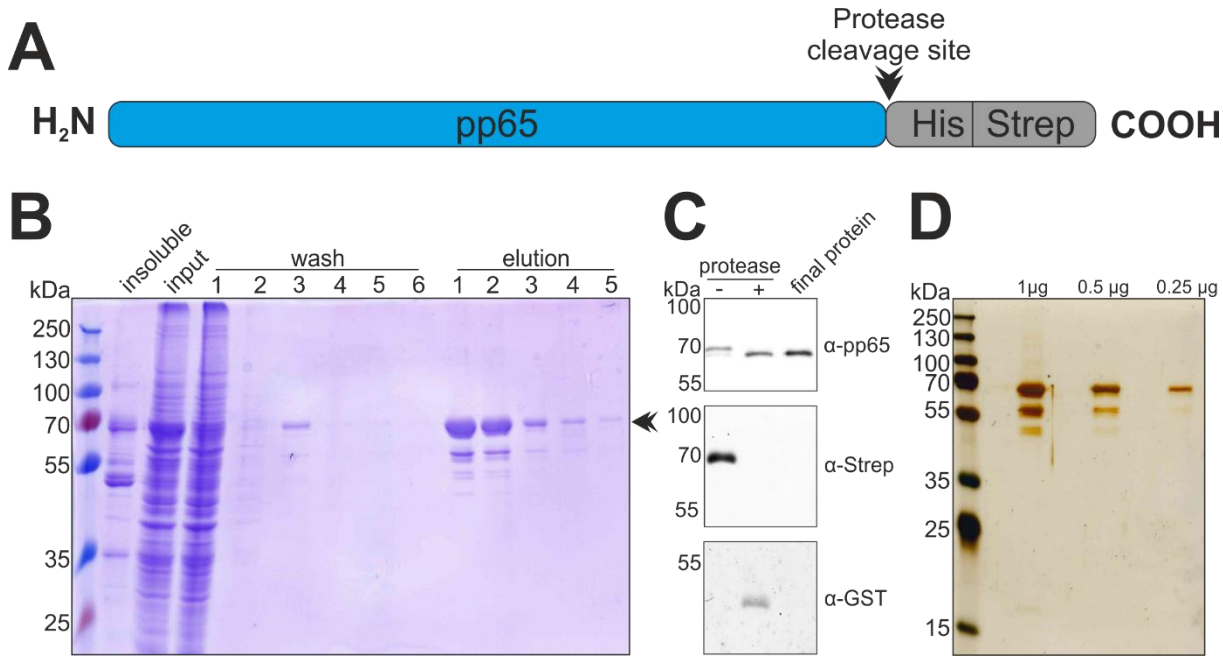

Figure 12 - Purification of pp65 from insect cells
(A) pp65 (65kDa) was fused C-terminally with a His/Strep tandem tag for affinity purification. Tag and protein are separated by the recognition sequence of the 3C protease of human rhinovirus, allowing removal of the tag by proteolytic cleavage using PreScission™ protease after purification. (B) pp65 was purified from Baculovirus-infected High Five cells using Ni-IDA beads. During purification, Aliquots were collected from the insoluble fraction that was pelletized after cell lysis, the cell lysate (input), the washing steps as well as the elution fractions. Samples were subjected to SDS-PAGE and Coomassie-staining. (C) Proteolytic cleavage was performed for removing the His/Strep tandem affinity tag after purification of pp65 from crude cell lysates. GST-tagged PreScission™ protease was added to the samples and after digestion, cleaved tag and protease were removed from samples by adding GSH- and Strep-Tactin-beads. Aliquots were collected at all steps and subjected to Western blot analysis. (D) After tag removal, the final product was analyzed via SDS PAGE and silver staining with the indicated protein quantities loaded per lane.

Whereas IE-1 could be purified in the same manner as pp65 (Supplementary Figure S1), cleavage of the tag was unsuccessful in the case of BZLF1. This was unexpected since presence of the correct cleavage site could be confirmed on DNA level by Sanger sequencing. In addition, successful purification of the protein with Ni-IDA beads under native conditions indicated that the fusion protein was likely folded in a way that would allow the tag to be accessed (these findings are documented in detail in the master's thesis of Philipp Becker[265]). Nevertheless, quantitative cleavage of the tag could not be achieved for this protein. Hence, it was decided not to subject BZLF1 to protease digestion at all and instead work with the full-length fusion protein (Supplementary Figure S2).

The amount of pp65, IE-1 or BZLF1 required to elicit T cell restimulation was then determined using PBMCs from 3 CMV or EBV seropositive donors each and titrating the three proteins separately. IFNγ ELISpot analysis stimulated PBMCs revealed that robust reactivation was achieved using 0.5 µg/ml (pp65), 4.5 µg/ml (IE-1) and 3.3 µg/ml (BZLF1), respectively (data not shown). Hence, these concentrations were used for PBMC stimulation in all following experiments (VI.5.3).

Next, carbamoylation of these three proteins was induced using potassium cyanate (KOCN) instead of urea. The reaction kinetics for a given protein depend on a multitude of factors, with temperature, pH and the concentration of cyanic acid exerting the biggest influence. To avoid protein denaturation at higher temperatures, a previously published protocol where proteins are modified with 300 mM KOCN at 35 °C was adapted[266]. In order to quantify the amount of carbamoylation, an enzyme-linked immunosorbent assay (ELISA) was established using a polyclonal antibody mixture recognizing homocitrulline (carbamoylated lysine). The protocol was benchmarked to a commercial ELISA kit for the detection of protein carbamoylation, where it showed comparable sensitivity and specificity (data not shown). Using this method, the amount of carbamoylation was quantified over time for pp65, BZLF1 and IE-1 (Figure 13, section VI.3.10). After 6 hours of incubation with 300mM KOCN at pH 8.0 and 35 °C, ELISA signals appeared to reach a plateau for all proteins. For IE-1, saturation was reached the fastest, possibly because this protein contains a higher proportion of lysine residues (7.3%), compared to pp65 (3.9) and BZLF1 (3.3). However, it cannot be concluded from this data that protein carbamoylation has in fact reached saturation at this point, since steric hindrances might at some point preclude additional binding of the detection antibody. Moreover, due to the usage of homocitrulline-specific antibodies, possible arginine carbamoylation cannot be detected with this method at all. Therefore, the incubation period with KOCN was extended to 24 hours for all following experiments. Proteins modified according to this protocol are hereafter referred to as carb-pp65, carb-BZLF1 or carb-IE-1.

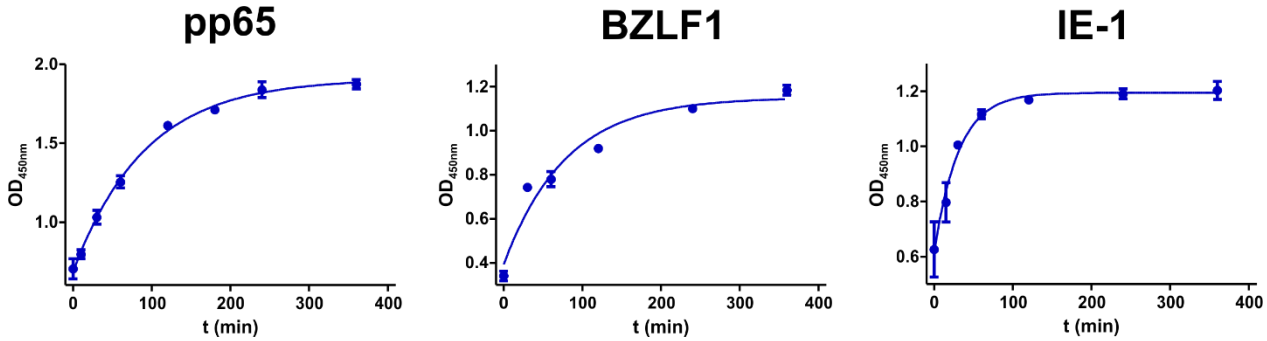

Figure 13 – Cyanate induces carbamoylation of lysine residues
pp65, BZLF1 or IE-1 were incubated at 35 °C with 300 mM potassium cyanate (KOCN) for up to 6 hours. At various time points, samples were collected and carbamoylation was analyzed via ELISA using antibodies that recognize carbamoylated lysine residues. The data displayed in this figure were collected in part during the master's thesis of Philipp Becker and Tobias Brunner under my experimental supervision[265,267].

Since IFNγ responses were completely suppressed if PBMCs were stimulated in the presence of millimolar amounts of KOCN (Supplementary Figure S3), it was always removed from protein samples via extensive dialysis after the carbamoylation reaction. To assess if carbamoylation has an influence on the restimulation of antigen-specific T cells, PBMCs from CMV or EBV seropositive donors were stimulated with equivalent amounts of unmodified or carbamoylated pp65, BZLF1 or IE-1 (Figure 14). For pp65 and BZLF1, stimulation with carbamoylated proteins led to a significant increase in IFNγ responses as compared to stimulation with the non-carbamoylated proteins. At the same time, background signals that were determined by stimulating PBMCs from CMV or EBV seronegative donors were not elevated as a result of protein modification. This indicates that the detected increase in T cell responses to carbamoylated pp65 and BZLF1 was indeed antigen-specific. The extent to which T cell responses were increased varied greatly from donor to donor and between the two proteins with carb-pp65 inducing a mean increase in spot forming units (SFU) of 39% (range 6 - 112%). Mean responses to carb-BZLF1 were increased by 80% (range 5 - 161%), not including one donor who reproducibly reacted to carb-BZLF1 with decreased T cell responses. In contrast to pp65 and BZLF1, T cell responses to IE-1 were significantly reduced for all donors when stimulated with the carbamoylated protein compared to its unmodified counterpart.

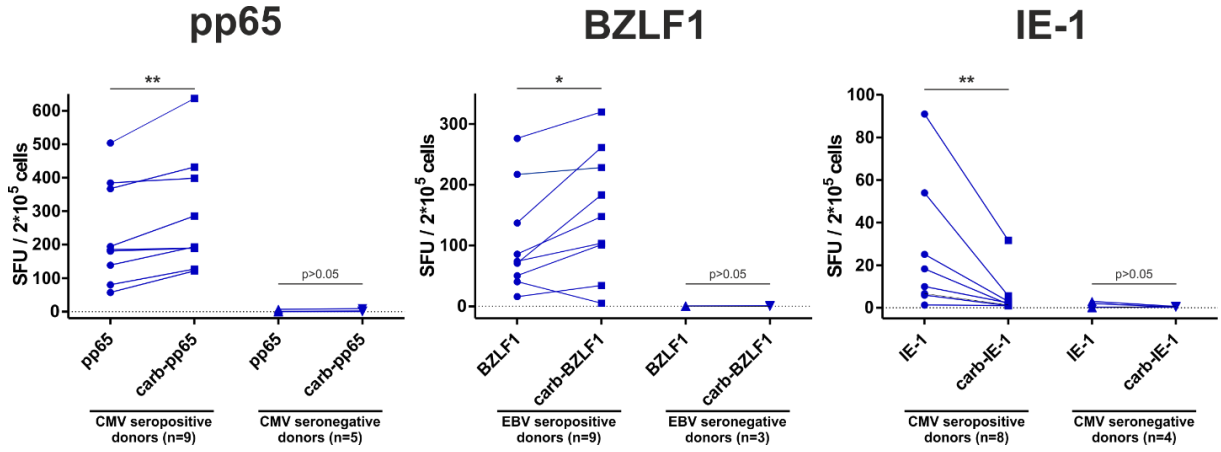

Figure 14 – Carbamoylation increases the restimulation of pp65- and BZLF1-specific T cells
PBMCS from the indicated number of donors were stimulated for 20 hours with unmodified or carbamoylated pp65 (0.5 µg/ml), IE-1 (4.5 µg/ml) or BZLF1 (3.3 µg/ml), respectively. T cell responses were quantified by IFNγ ELISpot assay. Values obtained with cells from a given donor are connected by lines. P values were calculated using the Wilcoxon signed rank test (two-tailed; one asterisk: $p<0.05$; two asterisks: $p<0.01$). The data displayed in this figure were collected in part during the master's thesis of Philipp Becker and Tobias Brunner under my experimental supervision[265,267].

Carbamoylation irreversibly modifies proteins and, as a result, also the epitopes recognized by T cells if they contain modified amino acids. Thus, shorter incubation periods with cyanate, concomitant with a lower degree of modification, might have an influence on T cell restimulation rates. However, using pp65 and testing 3 separate CMV positive donors, it was found that the impact of carbamoylation was greatest when the degree of carbamylation was highest, i.e. when this protein was incubated for 24 hours with potassium cyanate (Supplementary Figure S4).

Further it should be tested, whether the presence of UREA during stimulation might directly have an influence on IFNγ responses irrespective of the carbamoylation effect. To test this, urea was added separately to PBMCs for a final concentration of 50 mM. This is equivalent to the amount of UREA that would be present if the proteins were stored in 4 M solution, as it was done by Barabas *et al*. in the original paper describing increased T cell restimulation rates for UREA-treated BZLF1[249]. In contrast to carbamoylation, the presence of UREA during stimulation had no significant influence on T cell restimulation for pp65 (Figure 15). Other UREA concentrations, ranging from 25 mM to 150 mM, were also tested in the same manner for 2 individual CMV positive donors. Again, T cell responses were unaltered except for a trend towards reduced SFU numbers beyond a concentration of 100 mM, which is likely explained by UREA toxicity (data not shown).

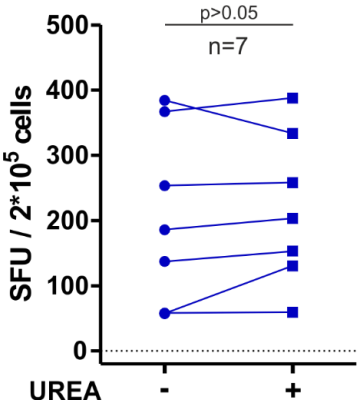

Figure 15 – The presence of urea has no impact on pp65-specific T cell responses
PBMCs from 7 CMV seropositive donors were stimulated for 20 hours with unmodified pp65 (0.5 µg/ml) in the presence (+) or absence (-) of urea (50 mM). T cell responses were quantified via IFNγ ELISpot assay. Values obtained with cells from a given donor are connected by lines. P values were calculated using the Wilcoxon signed rank test (two-tailed). The data displayed in this graph were collected during the master's thesis of Philipp Becker and Tobias Brunner under my experimental supervision[265,267].

In summary, carbamoylation has a positive impact on the restimulation of BZLF1- and pp65-specific T cells whereas for IE-1, this modification clearly reduces restimulation rates. At the same time, the presence of urea during stimulation has no significant impact on T cell responses, although a possible impact of protein denaturation should still be explored separately. It is therefore likely that the increased T cell responses reported by Barabas *et al.* for urea-treated BZLF1 are, at least in part, a result of protein carbamoylation. To further investigate the molecular details of this phenomenon, pp65 was mostly used as a model protein for the following experiments, since CMV positive blood donors with good pp65 responses dominated the cohort that was recruited for this work.

IV.1.2. Impact of negative protein charges on T cell restimulation

To further explore the mechanism by which carbamoylation alters T cell restimulation rates, it was next assessed if the observed effects are dependent on changes in the net charge of posttranslationally modified proteins. The ε-amino group of lysine and the guanidino-group of arginine residues are protonated at physiological pH, but carbamoylation leads to the loss of this positive charge[268]. As a result, it lowers the net charge of a given protein along with its isoelectric point (Figure 16).

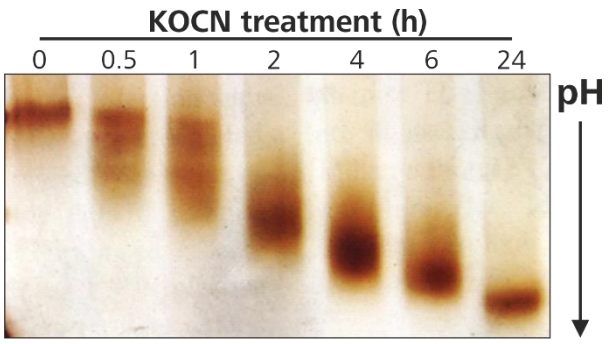

Figure 16 - Carbamoylation lowers the isoelectric point of pp65
pp65 was incubated for up to 24 hours with potassium cyanate (KOCN) and samples collected at the indicated time points were separated according to their net charge in isoelectric focusing (IEF) gel electrophoresis (section VI.3.9), followed by silver staining of the gel. This data was collected during the master's thesis of Tobias Brunner under my experimental supervision[267].

To estimate the extent to which charges are altered in the proteins used in this work, it was necessary to quantify the amount of lysine and arginine carbamoylation that takes place under the chosen conditions. The previously applied ELISA assay is an unsuitable method for addressing these questions, given that no quantitative evaluation of lysine carbamoylation is possible and arginine modifications are disregarded altogether (Figure 13). Hence, mass spectrometry was employed instead for analyzing the extent and pattern of carbamoylation. In order to quantify the amount of lysine carbamoylation, conversion of this amino acid to homocitrulline (HCit) was first measured (section VI.4.1). For this, carbamoylated pp65 was spiked with known quantities of isotopically labeled reference amino acids and hydrolyzed completely by boiling the sample in hydrochloric acid (HCl). The amino acid composition was then analyzed using a previously described method based on double isotope-dilution mass spectrometry[269,270]. For quantitative analysis of homocitrulline, it was critical to first determine hydrolysis conditions under which pp65 is completely disassembled into single amino acids while HCit remains (at least partially) intact. If partial homocitrulline degradation takes place during the incubation period with HCl, this can be corrected for by spiking the sample with a known amount of D_7-citrulline (D_7-Cit) before hydrolysis (there was no commercial source for isotopically labeled HCit). Compared do HCit, the side chain of citrulline is shortened by one CH_2-group, but the reactivity of both carbamoyl groups should be alike. Complete pp65 degradation with partially intact HCit/d_7-Cit levels was achieved by hydrolysis at 115 °C for 20 h: when the hydrolysis time was doubled or the temperature was increased to 150 °C, no intact HCit/d_7-Cit were left, but virtually identical normalized concentrations of phenylalanine, proline and valine were measured, indicating complete protein hydrolysis with the milder conditions (data not shown). After suitable conditions were established, the concentration of homocitrulline was measured and related to the total concentration of pp65, which was determined by quantifying phenylalanine, valine and proline (Figure 17). Using this technique, complete conversion of lysine to homocitrulline was found, demonstrating that this amino acid is quantitatively modified during a 24 hour incubation period with 300 mM KOCN at 35 °C.

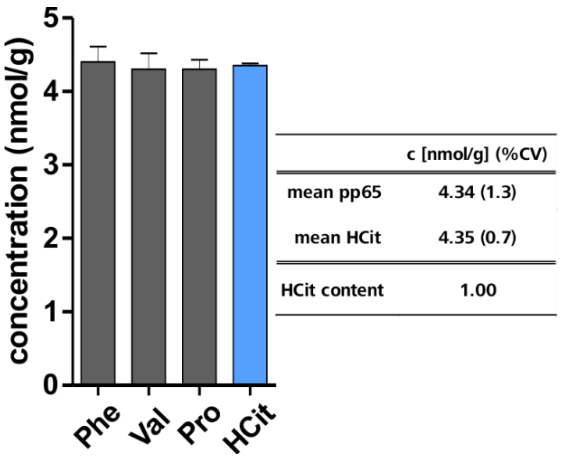

Figure 17 – Double isotope dilution mass spectrometry analysis of pp65-derived amino acids reveals complete conversion of lysine to homocitrulline

Carb-pp65 was spiked with known quantities of isotopically labeled reference amino acids, hydrolyzed and analyzed by LC-MS. The concentration of homocitrulline (HCit) was related to the total concentration of pp65 as determined by quantification of phenylalanine, valine and proline. Bars represent the mean concentration of the indicated amino acids derived from three independent hydrolysis experiments with error bars indicating the standard deviation (SD). The concentrations of pp65 (mean of Phe, Val and Pro quantification) and HCit along with the coefficient of variation (CV) are summarized next to the graph. The data was acquired in cooperation with Bernd Reisinger (PTB Braunschweig).

Whereas double isotope-dilution mass spectrometry allowed quantitative analysis of HCit formation, modification of arginine residues could not be assessed in the same manner, since there was no commercial source for isotopically labeled carbamoyl-arginine. To gain further insights into the degree of arginine modification, carb-pp65 was characterized at the peptide level (section VI.4.2). Although trypsin is the most frequently used protease for generating peptides to be analyzed by mass spectrometry, it cleaves after lysine residues and may therefore be inhibited by carbamoylation. Thus, pp65 was instead digested with a combination of Asp-N (cleaves N-terminally of aspartate) and Glu-C (cleaves C-terminally of glutamic acid) proteases. Peptides were desalted, separated by reversed-phase HPLC and analyzed via tandem mass spectrometry. The peptides that could be unambiguously identified covered 10 out of 22 individual lysine positions (45%) and 20 out of 36 individual arginine positions (55%) of pp65 in total (Figure 18A). At each lysine position, carbamoylation was detectable, albeit to a varying extent (ranging from 38-100%) with a cumulative modification degree of 90% (Figure 18B). By contrast, carbamoylation was only detected in one of the 20 arginine positions, where the degree of modification was 6% (0.3% in total). Higher susceptibility of lysine residues to carbamoylation has been reported before and can be explained by the roughly 100-fold higher nucleophilicity of this amino acid (pKa ≈ 10.5) compared to arginine (pKa ≈ 12.5)[253]. Even though the N-terminal amino group of pp65 was not covered by this analysis, it is very likely modified in a quantitative manner as well, considering that the pKa value is even lower (9.2) than that of lysine. Taken together, the chosen conditions for KOCN treatment likely induce near complete carbamoylation of the N-terminus as well as lysine residues, whereas arginine modifications seem negligible.

A

B

sequence of carbamoylated peptide	identification of modified amino acid	degree of carbamoylation
DVPSGKLFMHVTLGS	unambiguous	0.38
DQYVKVYLE	unambiguous	1.00
DVYYTSAFVFPTK	unambiguous	0.90
HPTFTSQYRIQGKLE	unambiguous, CID-MSMS	0.83
MISVLGPISGHVLKAVFSRG	unambiguous, CID-MSMS	0.97
GVWQPAAQPKRRRHRQ	unambiguous, ETD-MSMS	1.00
NTRATKMQVIG	unambiguous, ETD-MSMS	1.00
RKHRHLPVA	unambiguous, ETD-MSMS	1.00
DALPGPCIASTPKKHRGLE	unclear; KKHR or KKHR	1.00 / 0.95
NTRATKMQVIG	unambiguous, R and K modified	0.06

Figure 18 –Arginine residues are hardly carbamoylated according to MS/MS analysis of pp65 peptides

(A) Peptide map of carbamoylated pp65 after Glu-C/Asp-N digestion. All detected peptides containing lysine or arginine residues are highlighted in blue. Amino acids that showed carbamoylation are marked in orange while those that were always detected without the posttranslational modification are highlighted in violet. Black lines ("|") indicate theoretical cleavage sites. 10 lysine (45%) and 20 arginine (55%) residues could be evaluated in total. (B) Degree of carbamoylation per position. All peptide sequences in which modification was detected are listed with the degree of carbamoylation referring to the position highlighted in blue. If the collision-induced dissociation (CID)-based MSMS spectrum was not sufficient to unambiguously determine the position of carbamoylation for peptides containing lysine and arginine, the precursor of interest was subjected to an additional LC-MSMS run using electron transfer dissociation (ETD). An example of CID- and ETD-spectra of the same peptide is shown in supplementary Figure S5. The data was acquired in cooperation with Bernd Reisinger (PTB Braunschweig).

Assuming that these results are transferable to BZLF1 and IE-1, it becomes evident that quantitative deprotonation of lysine residues as a result of carbamoylation impacts the net charge of the chosen model proteins to a varying degree (Figure 19). While it shifts the sum of all charges from close to neutral to distinctly negative for pp65 (-3 to -25) and BZLF1 (-7 to -15), IE-1 already has a net charge of -34 even without any modifications. Since IE-1 has the highest number of lysine residues out of the three model proteins, this value can be shifted to a maximum of -70.

	net charge at physiological pH	
	unmodified	all lysines modified
pp65	-3	-25
BZLF1	-7	-15
IE-1	-34	-70

Figure 19 - Carbamoylation lowers the net charge of pp65, BZLF1 and IE-1 to a varying degree

Net charge of the indicated model proteins in their unmodified state or assuming complete carbamoylation of lysine residues.

By removing a sufficient number of positive charges from a given protein, it essentially becomes a polyanionic molecule. Many cell types, including antigen-presenting cells, express a variety of surface molecules belonging to the heterogeneous group of scavenger receptors[271]. Given that these receptors have been described to bind polyanionic macromolecules before[272], it was explored if the increased T cell restimulation rates of carb-pp65 and carb-BZLF1 are a result of enhanced receptor-mediated uptake into APCs. Interaction of scavenger receptors with their ligands can be inhibited by adding competing molecules such as

the negatively charged polysaccharide fucoidan[273,274]. To test if antigen-specific T cell responses are modified by this substance, PBMCs from 3 different CMV seropositive donors were stimulated in the presence of fucoidan with carb-pp65 or its unmodified counterpart (Figure 20). For donors 1 and 3, SFU numbers were not impacted by the addition of fucoidan when stimulating with unmodified pp65 while for donor 2, responses were increased. By contrast, T cell responses were noticeably reduced to a level that was comparable to the unmodified protein for all donors when stimulating fucoidan-pretreated cells with carb-pp65. This selective reduction in IFNγ positive cells indicates that negative charges might indeed be critical for the effects mediated by protein carbamoylation.

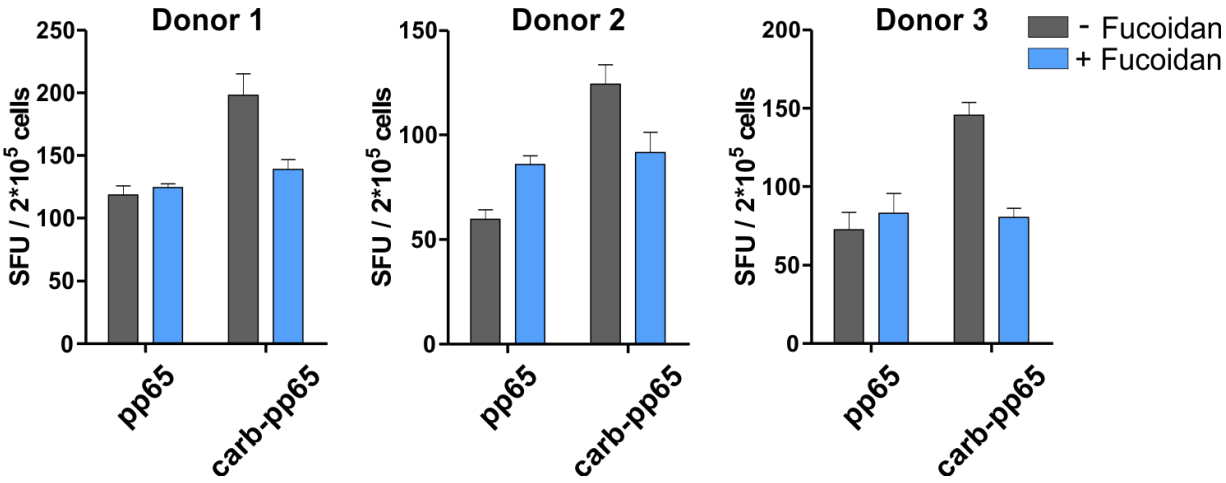

Figure 20 – Fucoidan treatment inhibits increased T cell stimulation by carbamyolated pp65
PBMCs from 3 CMV seropositive donors were pretreated with fucoidan (100 µg/ml) for 30 minutes or left untreated before stimulation with unmodified or carbamoylated pp65 (carb-pp65, 0.5 µg/ml). T cell responses were quantified by IFNγ ELISpot assay. The data shown in this figure were collected during the master's thesis of Tobias Brunner under my experimental supervision[267].

While negative charges seem to play an important role in the uptake of carbamoylated proteins into APCs, the added carbamoyl groups themselves might also contribute to this. To further explore the structural requirements for this phenomenon, another posttranslational modification was compared to carbamoylation with regard to T cell restimulation. Maleylation, the reaction of maleic anhydride with primary amino groups at basic pH, was chosen for this purpose (section VI.3.7)[275,276]. This reaction also modifies the ε-amino group of lysine residues with high specificity but in contrast to carbamoylation, one negative charge is added per reaction (Figure 21A). To compare the influence of carbamoylation and maleylation side-by-side, PBMCs from 3 CMV seropositive donors were stimulated in parallel with unmodified, carbamoylated or maleylated pp65 (Figure 21B). Compared to native pp65, both modifications increased IFNγ responses to a similar extent for all donors. Thus, in contrast to the removal of positive charges, the presence of carbamoyl groups is presumably not critical for the increased T cell stimulation observed for carb-pp65.

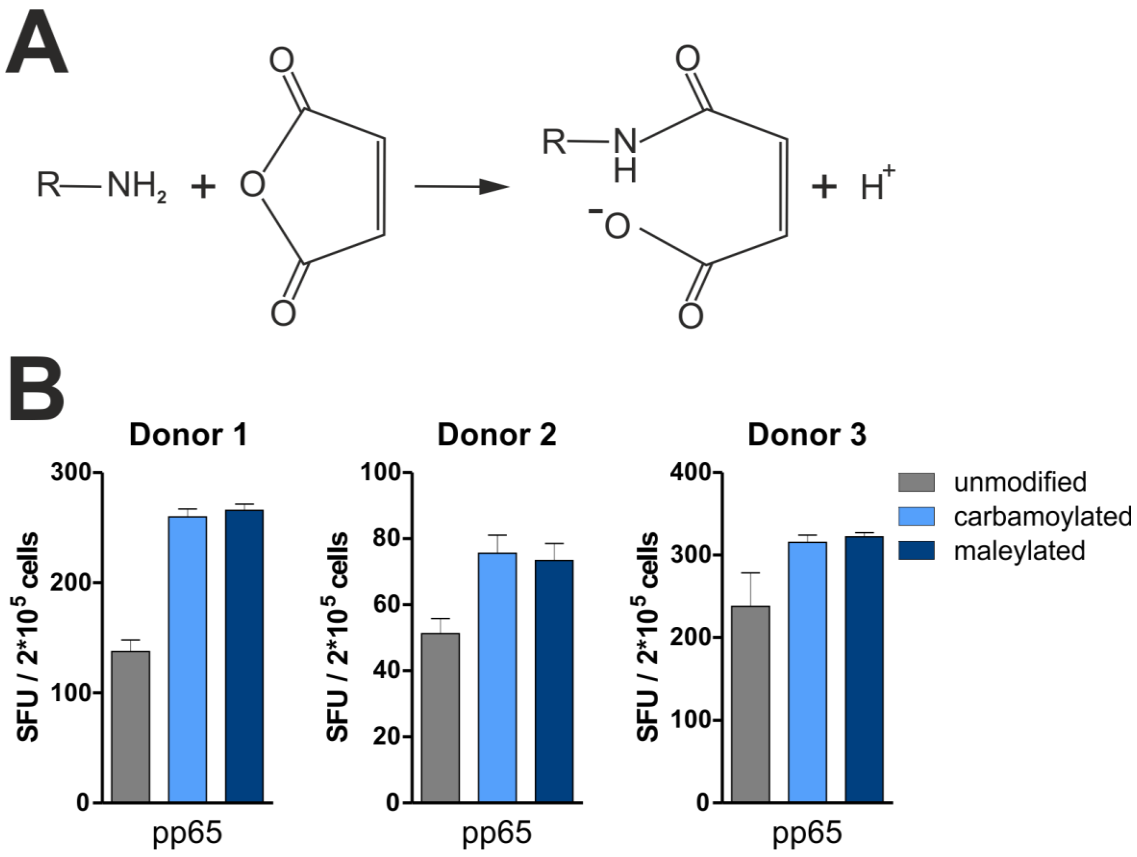

Figure 21 – Maleylation increases the restimulation of pp65-specific T cells similarly to carbamoylation
(A) Reaction of maleic anhydride with amino groups at basic pH. (B) pp65 was incubated for 24 hours with 30 mM maleic anhydride at pH 8.0 and 35 °C. PBMCs from 3 CMV seropositive donors were stimulated for 20 hours with unmodified, carbamoylated or maleylated pp65 (0.5 µg/ml each) and T cell restimulation was quantified via IFNγ ELISpot.

Because the removal of positive charges appears to be crucial for the increased T cell restimulation of carbamoylated proteins, it was explored if a similar effect can be mediated by adding negative charges instead of removing positive ones through the modification of lysine residues. To explore this possibility, amino acids carrying a negative charge at physiological pH were added to pp65. A sequence of 6 alternating aspartate and glutamate amino acids each was fused to the 3′ end of the pp65 gene, thereby shifting the protein net charge from -3 to -15 (Figure 22A). As for wild-type pp65, a recombinant baculovirus strain containing the gene-of interest was generated for protein production. The protein, hereafter referred to as pp65-6xDE, was purified from baculovirus-infected insect cells in analogous manner to the wild-type protein (Figure 22B-D). PBMCs from 6 CMV seropositive donors were then stimulated with equivalent amounts of either wild-type pp65 or pp65-6xDE, none of which were chemically modified (Figure 22E). However, the presence of 12 additional negative charges had no detectable influence on T cell restimulation rates.

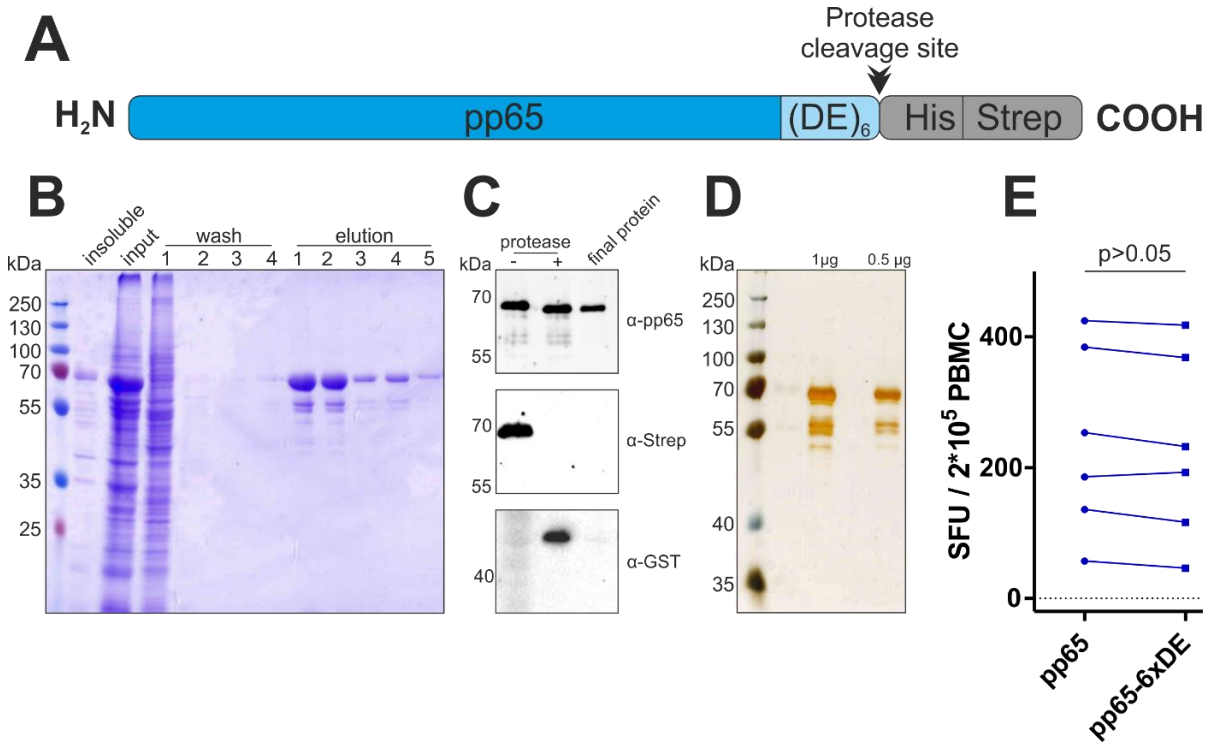

Figure 22 – C-terminal addition of 6 Glu and Asp residues does not increase the restimulation of pp65-specific T cells
(A) pp65 was fused C-terminally with 6 glutamic acid (Glu) and 6 aspartate (Asp) residues (designated pp65-6xDE). (B) pp65-6xDE was purified from Baculovirus-infected High Five cells using Ni-IDA beads. During purification, aliquots were collected from the insoluble fraction that was pelletized after cell lysis, the cell lysate (input), the washing steps as well as the elution fractions. Samples were subjected to SDS-PAGE and Coomassie-staining. (C) Proteolytic cleavage was performed for removing the His/Strep tandem affinity tag after purification of pp65-6xDE from crude cell lysates. GST-tagged PreScisson™ protease was added to the samples and after digestion, cleaved tag and protease were removed from samples by adding GSH- and Strep-Tactin-beads. Aliquots were collected at all steps and subjected to Western blot analysis. (D) After tag removal, the final product was analyzed via SDS PAGE and silver staining with the indicated protein quantities loaded per lane. (E) PBMCs from 6 CMV seropositive donors were stimulated for 20 hours with unmodified pp65 or pp65-6xDE (0.5 µg/ml each) and T cell restimulation was quantified via IFNγ ELISpot. Values obtained with cells from a given donor are connected by lines. The P value was calculated using the Wilcoxon signed rank test (two-tailed). The data shown in this figure was collected during the master's thesis of Philipp Becker under my experimental supervision[265].

Summarizing these results, carbamoylation removes positive charges, thereby lowering the isoelectric point of a given protein. Under the chosen reaction conditions, lysine residues are quantitatively modified, while arginine carbamoylation hardly occurs at all. Due to the amino acid composition of the 3 model proteins IE-1, BZLF1 and pp65, carbamoylation has a strongly varying influence on the degree to which their isoelectric point is altered. The lowered net charge, rather than the presence of carbamoyl groups, seems to be a critical requirement for the increased restimulation of pp65-specific T cells. Yet, a comparable result cannot be achieved by adding 12 negatively charged amino acids to pp65, implying that the net charge was either not sufficiently lowered, or that there are additional structural requirements with regard to the topological localization of the negative charges contributing to the increased restimulation of antigen-specific T cells.

IV.1.3. Uptake of carbamoylated proteins into antigen-presenting cells

Various steps that take place in antigen-presenting cells like protein uptake, processing and presentation precede T cell recognition and are therefore presumably rate-limiting. Thus, it is conceivable that carbamoylation impacts one or several of these steps. For instance, carbamoylation might i) increase protein uptake into APCs, ii) redirect modified proteins into a different APC subset, iii) enhance degradation and peptide loading on MHC complexes or iv) mediate increased cross presentation, concomitant with improved restimulation of $CD8^+$ T cells. To explore these possibilities, the fate of carbamoylated proteins in professional antigen presenting cells was analyzed.

Since professional APCs comprise a multitude of functionally distinct cell subsets, it was important to first identify cells capable of taking up unmodified or carbamoylated proteins. In peripheral blood, monocytes and B cells are the most abundant APC subsets, whereas dendritic cells and macrophages are present only in very small numbers[277]. To test which APC population contributes most to the restimulation of antigen-specific T cells during the stimulation of PBMCs, cells from a CMV seropositive donor were depleted of monocytes by removing CD14 positive cells via magnetic-activated cell sorting (MACS, section VI.5.4). After negative MACS selection, monocytes were hardly detectable in flow cytometry analysis, but the frequency of B cells was largely unaltered (Figure 23A). By contrast, after subjecting cells to the control treatment, both populations were still present. IFNγ responses were readily detectable when stimulating control-treated PBMCs with unmodified or carbamoylated pp65 (Figure 23B). As expected, carb-pp65 elicited higher restimulation rates than the unmodified protein. However, IFNγ secretion was completely abrogated after removal of monocytes and irrespective of pp65 modification. At the same time, neither CD14 negative selection, nor control treatment had a significant influence on the frequencies of IFNγ-producing effector cells (NK cells, $CD4^+$ and $CD8^+$ T cells, Supplementary Figure S6). This finding indicates that during the stimulation of PBMCs, monocytes are the main APC population responsible for the restimulation of antigen-specific T cells.

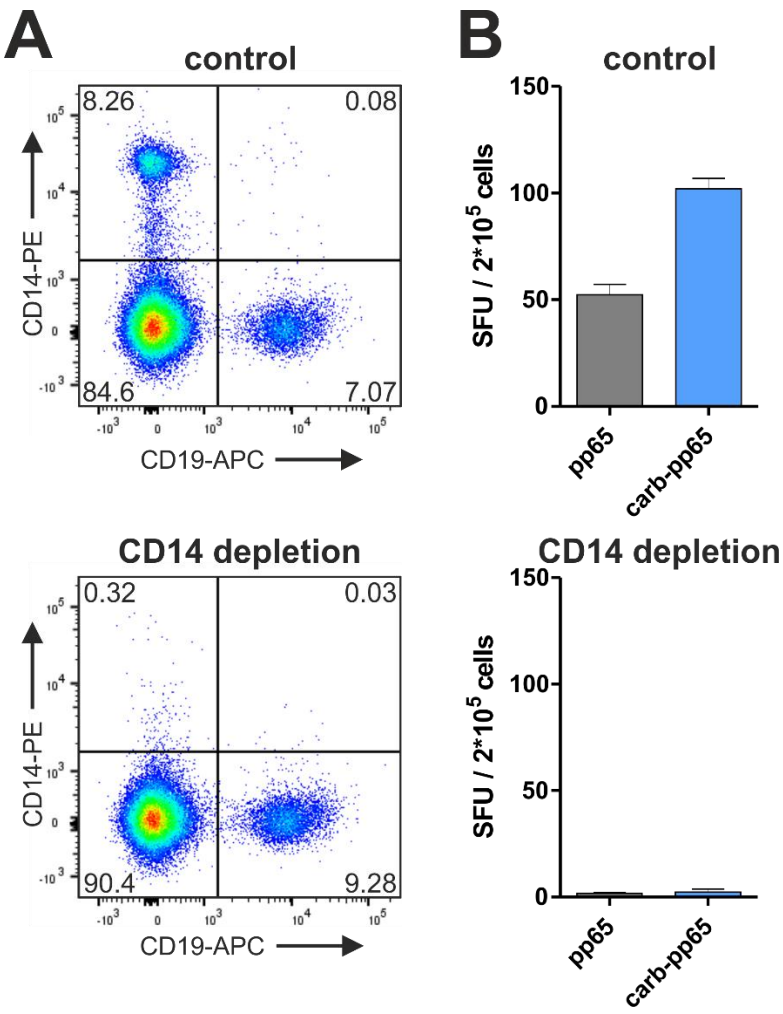

Figure 23 – Monocytes are the main population of antigen-presenting cells during PBMC stimulation
(A) PBMCs from a CMV seropositive donor were depleted of CD14 positive cells via magnetic-activated cell sorting (MACS, lower plot) or subjected to control treatment (omission of the CD14 antibody/bead conjugate; upper plot). An aliquot from both samples was stained each for CD14 and CD19 with fluorescently labeled antibodies and subjected to flow cytometry analysis. The pseudocolor plots show CD19- (X axis) and CD14-positive cells (Y axis) with the respective population frequencies (%) displayed in each corner. (B) The PBMC samples described in (A) were stimulated for 20 hours with pp65 or carb-pp65 (0.5 µg/ml each) and T cell responses were quantified by IFNγ ELISpot. Bars represent the mean with SEM (standard error of the mean) of 3 individual stimulations.

To confirm that monocytes are indeed capable of taking up and presenting pp65-derived peptides to T cells, they were separated from other PBMCs and stimulated in the presence of a pp65-specific T cell clone. CD14+ cells were isolated via positive MACS selection from PBMCs of a CMV seronegative donor. After 24 hours of cultivation, at which point expression of the monocyte marker CD14 was still very high (Figure 24A), cells were either pretreated with fucoidan or left untreated, followed by stimulation with unmodified or carbamoylated pp65 for two hours. Next, an HLA-matched, pp65-specific T cell clone was added along with Brefeldin A (BFA) to inhibit cytokine secretion. After 4 hours, cells were stained for CD8 and intracellular IFNγ, followed by flow cytometry analysis (Figure 24B). The percentage of IFNγ positive T cells was higher after stimulation with carb-pp65 (approx. 60%), compared to the unmodified protein (approx. 40%). In accordance with the results obtained using PBMC samples (Figure 20), fucoidan treatment had no influence on T cell responses when stimulating with pp65 whereas for carb-pp65, responses were markedly reduced and comparable to those obtained with the unmodified protein. In conclusion, monocytes seem to be the main APC population in PBMCs taking up pp65 and carb-pp65.

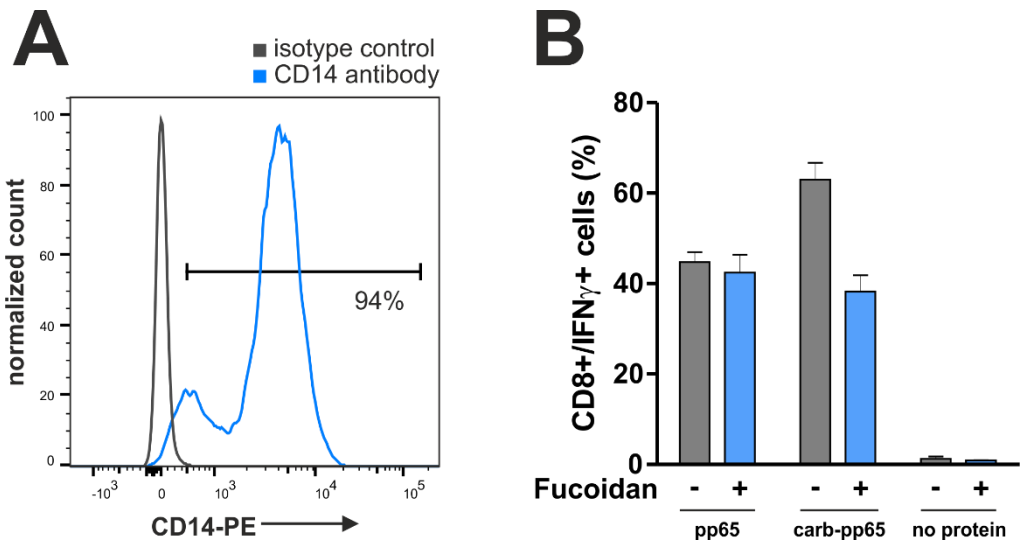

Figure 24 - pp65 carbamoylation enhances T cell restimulation with monocytes as antigen-presenting cells

(A) Monocytes were isolated from a CMV seronegative donor via MACS sorting using anti-CD14 beads and cultivated overnight. The next day, CD14 expression was assessed by flow cytometry after staining of samples with CD14- or isotype control antibody. (B) Samples described in (A) were pretreated with fucoidan (100 µg/ml) for 30 minutes or left untreated before stimulation with pp65, carb-pp65 (0.5 µg/ml each) or PBS only (no protein) for 2 hours. An HLA-matched, pp65-specific T cell clone was added along with Brefeldin A (BFA, 1 µg/ml) at an effector/target ratio of 1:1 and co-incubation lasted for 4 hours. Samples were then stained for CD8 and intracellular IFNγ and analyzed via flow cytometry. Bars display the mean (with SEM) percentage of CD8/IFNγ double positive cells from 3 individual stimulations. The data shown in this figure was collected during the master's thesis of Tobias Brunner under my experimental supervision[267].

Although during the stimulation of PBMCs, antigen-derived peptides seem to be presented mainly by monocytes, it was intriguing to assess whether protein carbamoylation has a similar effect when using other APC populations instead. To test this, monocytes were isolated from PBMCs of a CMV seronegative donor via MACS selection and either differentiated to monocyte-derived dendritic cells (moDCs) or monocyte-derived macrophages (moMϕs) over a period of 5 days. After this time, expression of the dendritic cell marker CD1a was strongly upregulated in moDCs and virtually undetectable on macrophages (Figure 25A). At the same time, in accordance with previously published literature, expression of scavenger receptor A1 (SR-A1), was high on macrophages, but also detectable on the surface of dendritic cells, albeit to a lower degree[278,279]. These data demonstrate that two distinct APC subsets were generated from monocytes over a period of five days. To assess their capacity to restimulate antigen-specific T cells, dendritic cells or macrophages were incubated with equivalent amounts of pp65 or carb-pp65 for two hours. Next, the HLA-matched, pp65-specific T cell clone was added along with BFA and cells were co-incubated for another 4 hours. T cell restimulation was again assessed by staining cells for CD8 and intracellular IFNγ, followed by flow cytometry analysis. After stimulation with pp65, 24% of T cells were IFNγ-positive when using moDCs compared to 27% for macrophages. For both APC populations, T cell restimulation rates were considerably increased as a result of stimulation with carb-pp65 (58% and 62% for DCs and macrophages, respectively). This

shows that the previously observed effects are not confined to monocytes, but can be transferred to other subsets of professional APCs as well.

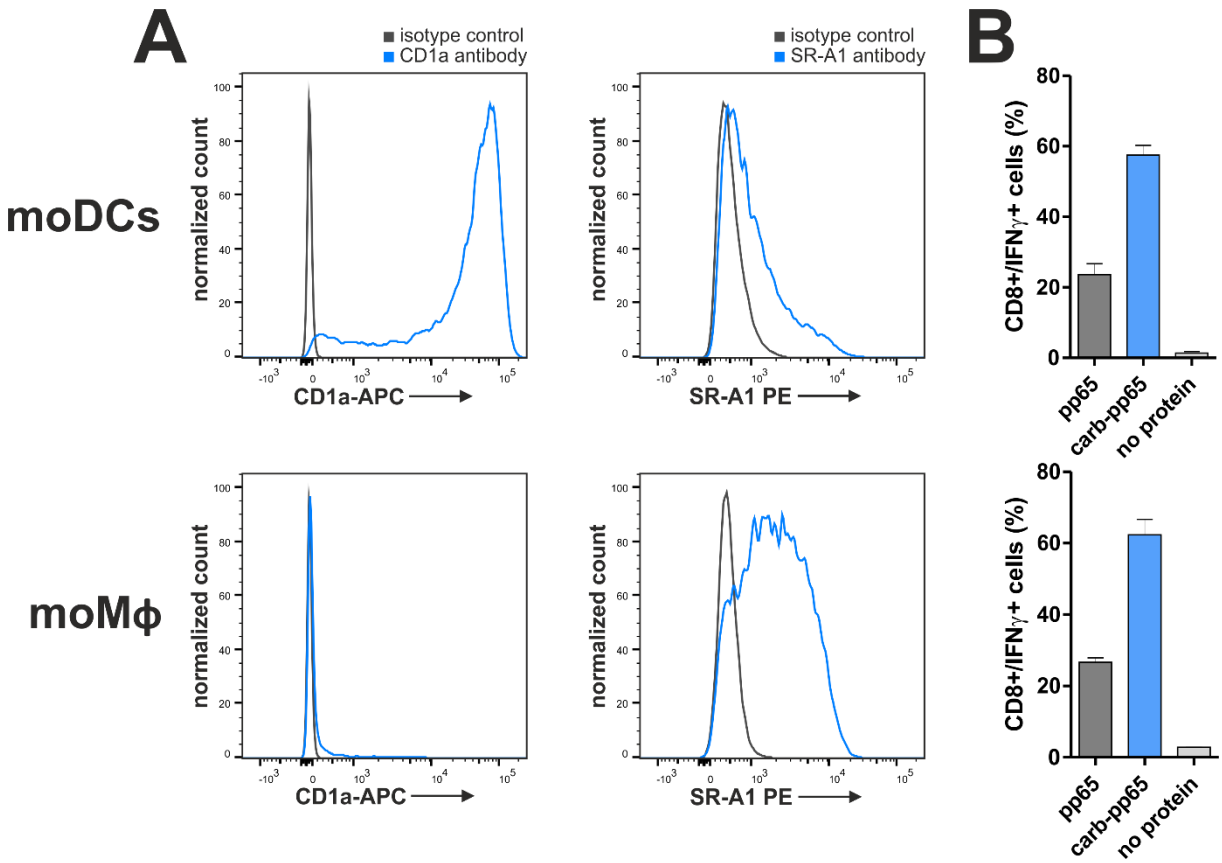

Figure 25 – pp65 carbamoylation enhances T cell restimulation also with dendritic cells and macrophages as antigen-presenting cells
(A) Monocytes were isolated from a CMV seronegative donor via MACS sorting using anti-CD14 beads and cultivated for 5 days with GM-CSF and IL-4 (1000 U/ml each) for differentiation to monocyte-derived dendritic cells (moDCs, upper panel) or with 50 U/ml GM-CSF for differentiation to monocyte-derived macrophages (moMϕs, lower panel). After differentiation, samples were stained for CD1a and scavenger receptor A1 (SR-A1), followed by flow cytometry analysis. Displayed histograms are representative of results from 3 different donors. (B) moDCs (upper graph) or moMϕs (lower graph) were stimulated with pp65, carb-pp65 (0.5 µg/ml each) or PBS only (no protein) for 2 hours. An HLA-matched, pp65-specific T cell clone was added along with Brefeldin A (BFA, 1 µg/ml) at an effector/target ratio of 1:1 and co-incubation lasted for 4 hours. Samples were then stained for CD8 and intracellular IFNγ and analyzed via flow cytometry. Bars display the mean (with SEM) percentage of CD8/IFNγ double positive cells from 3 individual stimulations. The data shown in this figure were collected during the master's thesis of Tobias Brunner under my experimental supervision[267].

Increased uptake of carbamoylated proteins into APCs could be one possible explanation for the increased restimulation of pp65- and BZLF1-specific T cells. To test this hypothesis, a reporter system was established for the quantification of cellular pp65 uptake. Enhanced green fluorescent protein (eGFP) was fused in-frame to the 5′ end of the pp65 gene (Figure 26A). As for wild-type pp65 and pp65-6xDE, a recombinant baculovirus strain containing the gene-of-interest was generated for protein production. The protein, referred to as GFP-pp65, was purified similarly to wild-type pp65 from baculovirus-infected insect cells using Ni-IDA beads (Figure 26B). However, in contrast to pp65 and pp65-6xDE, the tandem affinity tag was not removed after purification (Figure 26C), because higher fluorescence in-

tensity values were reproducibly obtained when cleavage and subsequent removal of protease and tag were omitted (data not shown). Uptake of the purified protein into human foreskin fibroblast (HFF) cells could be readily detected via confocal microscopy (Figure 26D).

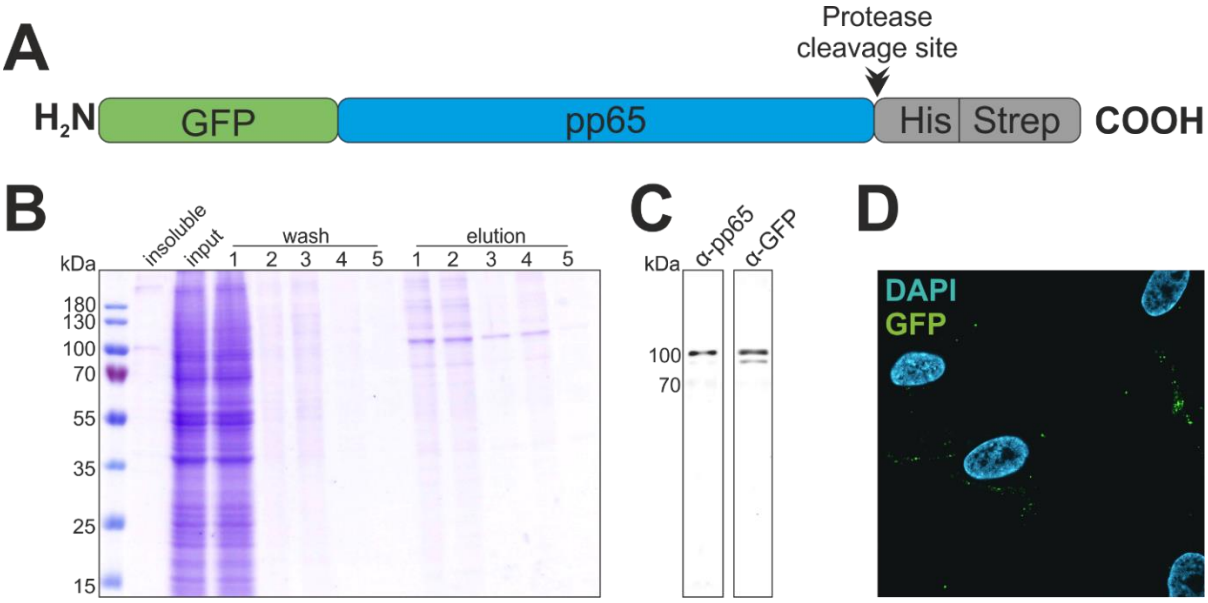

Figure 26 – Purification of GFP-pp65 from insect cells
(A) pp65 was fused N-terminally with enhanced green fluorescent protein (eGFP) and C-terminally with a His/Strep tandem tag. (B) GFP-pp65 was purified from Baculovirus-infected High Five cells using Ni-IDA beads. During purification, aliquots were collected from the insoluble fraction that was pelletized after cell lysis, the cleared cell lysate (input), the washing steps as well as the elution fractions. Samples were subjected to SDS-PAGE and Coomassie-staining. (C) GFP-pp65 was analyzed by Western blot analysis using anti-pp65- or anti-GFP-antibodies. (D) Human foreskin fibroblast (HFF) cells were incubated for 24 hours with GFP-pp65 (2.5 µg/ml). Cells were fixed with paraformaldehyde (PFA), stained with DAPI and analyzed via fluorescence microscopy. The data shown in (C) was acquired during the master's thesis of Tobias Brunner under my experimental supervision[267] while confocal microscopy was performed in cooperation with Manfred Marschall (Friedrich-Alexander University Erlangen-Nürnberg).

Next, GFP-pp65 was carbamoylated with potassium cyanate using the same conditions as for wild-type pp65. After 24 hours of incubation, carbamoylation was detectable via isoelectric focusing gel electrophoresis. As compared to unmodified GFP-pp65, the isoelectric point was clearly shifted (Figure 27A). At the same time, carbamoylation had no significant influence on the fluorescence intensity of GFP-pp65, which is an important prerequisite for quantitative comparison of protein uptake (Figure 27B and C). To test if carbamoylation has an influence on the uptake of pp65 into APCs, THP-1 macrophages were chosen as a well-established APC model[280]. THP-1 cells were differentiated to macrophages by incubation with phorbol myristate acetate (PMA) over a period of 6 days. To enhance the intracellular detection sensitivity of GFP-pp65, cells were pre-incubated with MG-132, an inhibitor of proteasomal degradation. Equivalent amounts of GFP-pp65 or carb-GFP-pp65 were added to the cells and after 4 hours, they were washed 5 times to remove proteins that were not taken up within this time frame. GFP fluorescence was then quantified by flow cytometry analysis (Figure 27D and E). Compared to unmodified GFP-pp65, protein uptake was clearly higher after carbamoylation, which might in turn also explain increased T cell restimulation when using carbamoylated proteins.

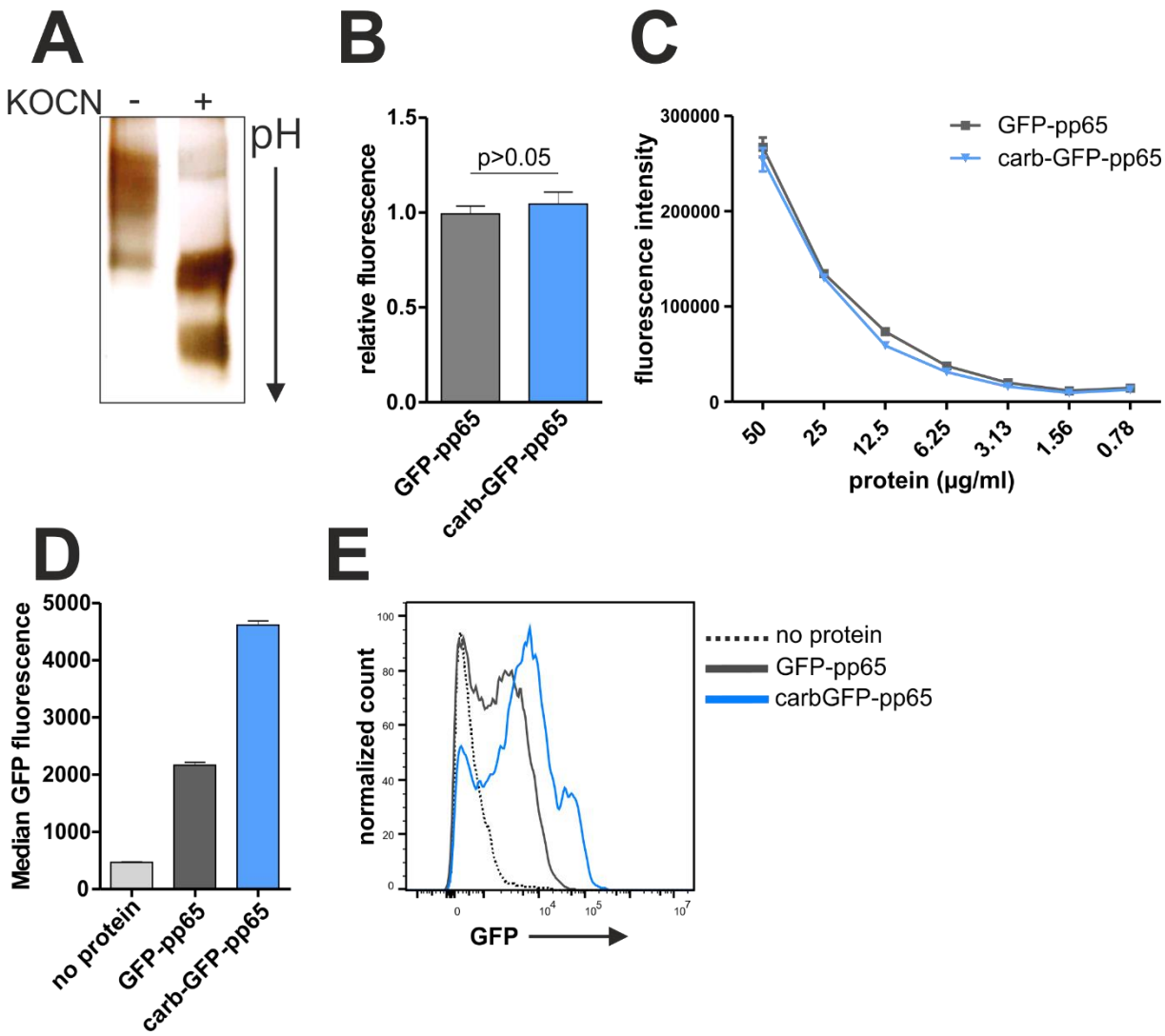

Figure 27 – Carbamoylated GFP-pp65 is taken up more efficiently into THP-1 cells
(A) GFP-pp65 was incubated for 24 hours with potassium cyanate or left untreated and samples were separated according to their net charge in isoelectric focusing (IEF) gel electrophoresis. (B) GFP-pp65 was incubated for 24 hours with 300 mM KOCN at 35 °C (carb-GFP-pp65) or in buffer lacking potassium cyanate (GFP-pp65). Aliquots were collected before and after the incubation period and fluorescence intensities of all samples were measured on a VICTOR multiplate reader. Values obtained after 24 hours were normalized to those before the incubation period to account for chromophore maturation[281]. Bars represent the mean (with SD) of all samples (n=9). (C) Unmodified or carbamoylated GFP-pp65 were adjusted to 50 µg/ml and diluted in 1:1 steps. Fluorescence intensities were measured on a VICTOR multiplate reader. Obtained values are presented as mean (with SEM) of 3 separate dilutions. (D) THP cells were incubated for 6 days with phorbol myristate acetate (PMA, 100 µg/ml) and pretreated for 30 minutes with MG-132 (10 µM) before addition of GFP-pp65 or carb-GFP-pp65 (2 µg/ml). After 4 hours, cells were analyzed via flow cytometry. Bars represent the mean (with SEM) of 3 individual samples. (E) Representative histogram of samples presented in (D). The data shown in this figure was collected in part during the master's thesis of Tobias Brunner under my experimental supervision[267].

Although increased uptake of carbamoylated pp65, concomitant with enhanced MHC presentation of pp65-derived peptides, is a plausible explanation for improved T cell restimulation, other steps in the antigen presentation process could be affected as well. Proteins that are taken up from the extracellular space, for example by clathrin-mediated endocytosis, are mostly degraded in phagolysosomes, followed by loading of peptides onto

MHC class II molecules and stimulation of $CD4^+$ T cells. However, by a mechanism known as cross-presentation, stimulation of $CD8^+$ T cells can also occur if peptides are instead loaded onto MHC class I complexes (for example as a result of protein leakage into the cytoplasm)[282]. It is therefore conceivable that carbamoylation selectively enhances cross presentation and that the increased T cell stimulation rates are mainly attributable to the additional reactivation of $CD8^+$ cells.

To investigate this, PBMCs from a CMV seropositive donor were depleted of $CD8^+$ T cells by negative MACS selection (Figure 28A). Cells were then stimulated with unmodified or carbamoylated pp65 and T cell responses were quantified by IFNγ ELISpot (Figure 28B). Irrespective of the presence of $CD8^+$ cells during stimulation, carb-pp65 elicited higher T cell response rates than unmodified protein. As observed before, the presence of fucoidan reduced the number of spot forming units only for the carbamoylated protein. However, compared to the control treatment, the overall responses were lower as a result of MACS depletion, demonstrating that the contribution of $CD8^+$ T cells was missing. These results show that carbamoylation does not exclusively enhance cross-presentation and that both class I and class II presentation benefit from the increased uptake of carb-pp65.

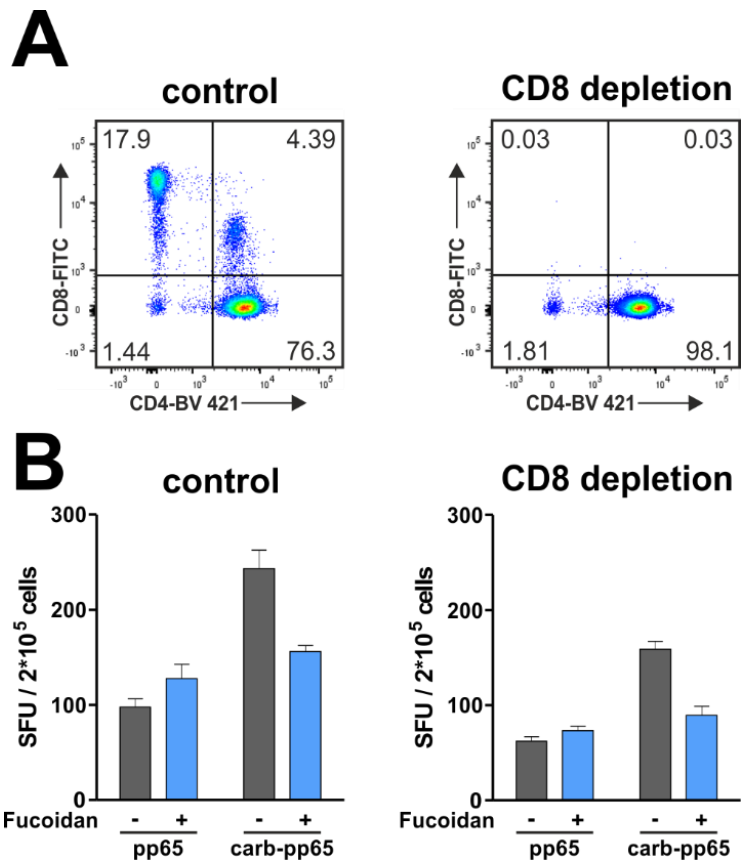

Figure 28 – Enhanced pp65 uptake benefits both MHC-I and MHC-II presentation
(A) PBMCs from a CMV seropositive donor were depleted of CD8 positive cells via MACS sorting or subjected to control treatment (omission of the CD8 antibody/bead conjugate). An aliquot from both samples was stained each for CD3, CD4 and CD8 with fluorescently labeled antibodies and subjected to flow cytometry analysis. Cells were first gated for CD3 positive events (data not shown). The pseudocolor plots show CD4- (X axis) and CD8-positive cells (Y axis) with the respective population frequencies (%) displayed in each corner. (B) PBMC samples were pretreated with fucoidan (100 µg/ml) for 30 minutes or left untreated before stimulation with pp65 or carb-pp65 (0.5 µg/ml each) for 20 hours. T cell responses were quantified via IFNγ ELISpot. Bars represent the mean with SEM (standard error of the mean) of 3 individual stimulations. The data shown in this figure was collected during the master's thesis of Tobias Brunner under my experimental supervision[267].

In summary, monocytes are the main APC population presenting antigen-derived peptides during the stimulation of PBMC samples. However, enhanced T cell reactivation as a result of protein carbamoylation can also be achieved when dendritic cells or macrophages act as

APCs. The enhanced restimulation appears to be a direct result of elevated protein uptake into antigen-presenting cells and both MHC class I and class II presentation benefit from this.

IV.1.4. Impact of protein carbamoylation on T cell priming *in vivo*

So far, the impact of posttranslational lysine modifications was only assessed for the reactivation of previously primed T cells, but enhanced protein uptake into APCs might also be beneficial for the priming of naïve T cells *in vivo*. Hence, it was interesting to investigate if protein carbamoylation could be used as a method for enhancing the immunogenicity of a given protein with potential implications for the design of novel vaccines or the improvement of existing ones.

To address this question, female Balb/c mice were immunized twice at week 0 and week 2 in a homologous prime/boost regimen with either unmodified or carbamoylated pp65 (Figure 29A and B, section VI.7). Both proteins were injected intramuscularly (i.m.), together with the adjuvant poly-IC (a synthetic dsRNA that acts as a TLR3 agonist, thereby boosting APC functions and T cell responses[283]). As positive control, a separate group of mice was immunized twice with a mammalian expression plasmid containing the pp65 gene (pcDNA3.1-pp65) and as negative control, another group received PBS mixed with poly-IC only. Four weeks after the initial priming immunization, splenocytes were isolated and stimulated over a period of 6 hours with a pp65 peptide pool in the presence of BFA. Cells were then stained for CD4, CD8 and intracellular IFNγ as well as interleukin 2 (IL-2), followed by flow cytometry analysis (Figure 29C).

For both IFNγ and IL-2, cytokine positive cells were hardly detectable at all in the group immunized with PBS and poly-IC only. In mice immunized with plasmid DNA, the number of IFNγ positive cells was significantly above background levels with a median of 2.2% for $CD8^+$ cells and 0.3% for $CD4^+$ cells, respectively. In the same group, the percentage of IL-2 producing cells seemed elevated as well (0.1% for $CD8^+$ and 0.2% for $CD4^+$ cells), but the difference to the control group was not statistically significant. However, neither pp65, nor carb-pp65 induced T cell responses that were significantly above the background, irrespective of the T cell subset or marker cytokine adressed. At the same time, antigen-independent stimulation of splenocytes from all groups with PMA and Ionomycin strongly induced cytokine responses, demonstrating that the isolated splenocytes were viable and capable of producing IFNγ and IL-2 at the time of stimulation (Supplementary Figure S7A). Thus, no conclusions can be drawn from this experiment with respect to potential differences in immunogenicity between pp65 and carb-pp65. Further optimization of the immunization conditions, for example regarding protein dosage, number of injections and formulation, will be required to elicit detectable T cell responses *in vivo*.

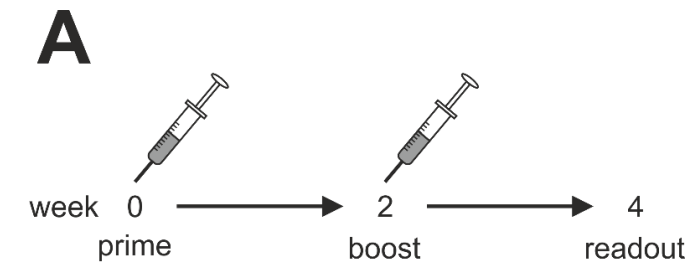

B

Group	Immunization	Adjuvant
1	2x PBS *(control)*	poly(I:C)
2	2x pp65 *(protein)*	poly(I:C)
3	2x carb-pp65 *(protein)*	poly(I:C)
4	2x pcDNA3.1-pp65 *(plasmid)*	none

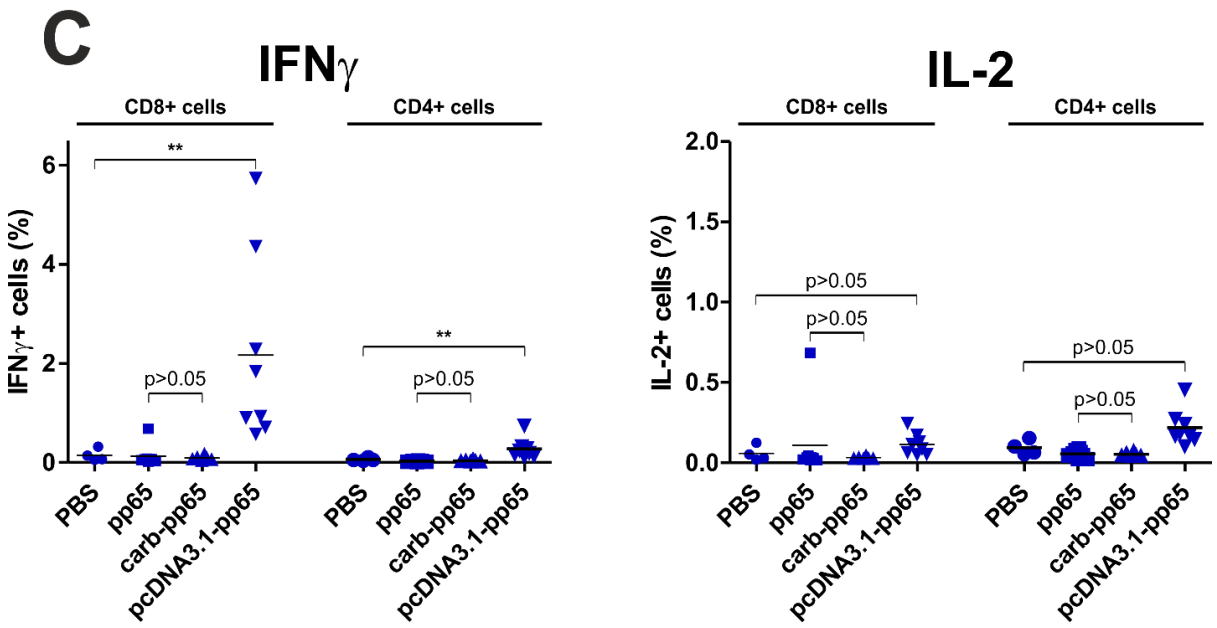

Figure 29 – Neither unmodified nor carbamoylated pp65 induce detectable T cell responses in mice (A) Female Balb/c mice were immunized intramuscularly at weeks 0 and 2 in a homologous prime/boost regimen. Animals were subdivided into four groups that received the reagents specified in table (B). Group 1 (n=4) received only PBS and poly(I:C) while groups 2 and 3 (n=8 mice each) were immunized with 4 µg pp65 or carb-pp65 per animal and injection (both proteins were admixed with poly(I:C)). Group 4 (n=8) received 50 µg plasmid-DNA encoding pp65 per immunization. (C) After 4 weeks, splenocytes were isolated and stimulated for 6 hours with a pp65 peptide pool in the presence of BFA. Cells were stained for CD4, CD8, intracellular IFNγ and IL-2, followed by flow cytometry analysis. The gating strategy for discriminating various subpopulations is illustrated in Supplementary Figure S7B. Graphs show IFNγ or IL-2 positive cells that are further subdivided into $CD4^+$ or $CD8^+$ T cells. Horizontal lines represent the mean and blue symbols the individual values of each animal. P values were calculated using the Mann Whitney test (two-tailed; two asterisks: $p<0.01$).

IV.2. Delivery of CMV antigens by viral vectors

Although immunomonitoring of CMV-specific T cells is a promising approach for identifying patients in need for antiviral therapy, it is clear that the development of a prophylactic or therapeutic vaccine would represent the most powerful strategy for limiting CMV-associated morbidities[229]. As it is well established that T cell responses are critical in controlling latent CMV infection, inducing or expanding T cell responses is a major goal of most vaccine concepts[99,284]. CMV vaccine candidates delivering T cell immunogens like IE-1 and pp65 might be applied as part of a prophylactic vaccine in combination with B cell immunogens to confine viral replication if sterile immunity cannot be achieved through the induction of antibody responses alone. At the same time, T cell vaccines could also be used in therapeutic concepts to boost immune responses in patients at risk for CMV reactivation.

Viral vectors are a favored tool for the delivery of heterologous antigens, in part owing to their strong stimulation of innate immunity and their capability to efficiently prime T cell responses during vaccination[191] (see also section III.6). Several vectors like the poxvirus strain Modified Vaccinia Ankara (MVA) are currently being evaluated as therapeutic vaccine candidates in clinical trials, but their efficacy has yet to be demonstrated[192,193]. Moreover, repeated administration of an antigen by a given vector is often impeded by the development of immunity to its backbone, which can be avoided by heterologous prime/boost immunizations. This underlines that novel vectors should still be developed and assessed for their capacity to deliver CMV immunogens.

Therefore, the second part of this this thesis addresses the generation as well as the virological and immunological characterization of viral vectors delivering the T cell immunogens IE-1 and pp65. Two emerging vector platforms that have so far not been tested in the context of a CMV vaccine are based on human Adenovirus 19a/64 (Ad19a/64, see III.6.2) and Sendai virus (SeV, see III.6.3), a murine paramyxovirus. In this work, these novel vectors were first characterized in a series of *ex vivo* assays, in order to identify promising candidates that are suitable for further *in vivo* testing. Hence, they were compared side-by-side to the well-established vectors Adenovirus 5 (Ad5) and Modified Vaccinia Ankara (MVA) carrying the same antigens. A major focus in the characterization of these vectors lay on the impact that transduction with these new vectors has on dendritic cells (DCs), because they are the main initiators of adaptive T cell immunity *in vivo*. Moreover, DCs that are manipulated *ex vivo* to present CMV antigens might be readily applied as a therapeutic vaccine. In this work, dendritic cells were generated by *in vitro* differentiation of monocytes to monocyte-derived dendritic cells (moDCs, section 0). This was achieved by MACS isolation of CD14 positive cells from PBMC samples, followed by cultivation in the presence of GM-CSF and IL-4 over a period of 5 to 6 days. During differentiation to dendritic cells, expression of the monocyte marker CD14 is reduced while CD1a expression is upregulated[285]. In order to confirm differentiation, expression of CD14 and CD1a was routinely measured by flow cytometry prior to usage of moDCs in any of the experiments (this quality

test is shown representatively for one donor in Supplementary Figure S8). Because monocytes are a suspected site of CMV latency[59,64], they were always isolated from blood samples of CMV seronegative donors to exclude possible expression of antigens like IE-1 or pp65.
For the generation of vectors expressing IE-1 or pp65, the corresponding genes first had to be inserted into the respective viral genomes. In the case of MVA, this was achieved by cloning the genes encoding IE-1 or pp65 into a transfer vector called pLZAW1[286]. This plasmid contains DNA sequences (termed left and right arm) that are homologous to regions up- and downstream of the poxviral gene locus J2R. This region encodes the viral thymidine kinase (TK) in wild-type virus strains, but it is deleted in MVA. The gene-of-interest was placed between these homologous sequences and Baby Hamster Kidney (BHK) cells, which are permissive for MVA replication[204], were transfected with the newly generated plasmids. Cells were then infected with the strain MVA-GFP that contains an eGFP gene in the J2R locus (Figure 30A). In cells that are simultaneously transfected and infected, homologous recombination can occur during the *de novo* synthesis of viral genomes[196], thereby replacing GFP with the gene-of-interest (Figure 30B). Since recombination occurs with low frequency[196], recombinant viruses then have to be separated from the parental strain MVA-GFP. This was achieved through a procedure termed plaque purification, where BHK cells are infected with different dilutions of newly harvested MVA suspensions. After infection, cells are overlaid with agarose to limit diffusion of viral particles within the cell culture dish and confine viral replication to a given area. After a period of three to four days, during which several rounds of viral replication can occur, holes in the BHK cell monolayer become visible. These plaques are a result of the cytopathic effect of MVA, thus indicating viral replication. Along with the gene-of-interest, the reporter gene LacZ (encoding the *E. coli* enzyme β-Galactosidase) is also inserted from the pLZAW1 plasmid into the genome of recombinant MVA particles. Hence, single plaques can then be picked at a suitable dilution that form blue spots after staining with Bluo-Gal (5-bromo-3-indolyl β-D-galactopyranoside). This process is then repeated over several rounds, until presence of the parental strain is no longer detectable via PCR. At this stage, the reporter gene LacZ is not required any more. In the integration cassette that is inserted into the MVA genome during homologous recombination, LacZ is flanked by the so-called »left arm« (≈ 500 bp of DNA that is found upstream of J2R) as well as a shorter version (≈ 300 bp) of this sequence. Thus, in a second recombination event, LacZ can be removed by homologous recombination during viral replication and white plaques are picked instead of blue ones during later stages of plaque purification (Figure 30B, see also section VI.6.1).

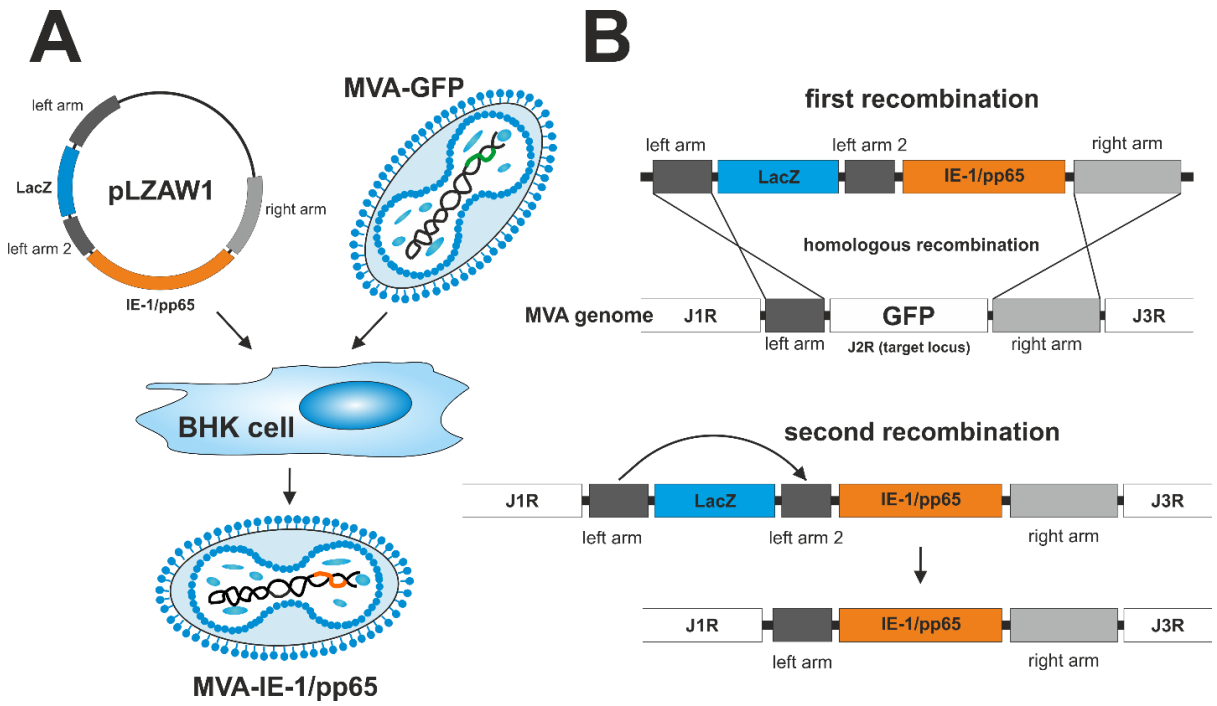

Figure 30 – Generation of recombinant MVA-IE1 and MVA-pp65 via homologous recombination
(A) In BHK cells that are transfected with pLZAW1 (containing IE-1 or pp65) and infected with MVA-GFP at the same time, homologous recombination can occur. During this process, GFP is replaced with the integration cassette containing IE-1 or pp65, as well as LacZ. (B) Site-specific integration of the desired genes is achieved by placing them between two sequences that are found upstream and downstream of the poxviral locus J2R (termed left or right arm, respectively). The entire integration cassette consists of the reporter gene LacZ, which is flanked by the left arm and a shortened repeat of that same sequence (termed left arm 2), the gene-of-interest (in this case IE-1 or pp65) and the right arm. In an event referred to as second recombination, LacZ can be removed from the viral genome by intragenomic recombination.

Plaque purification of MVA-IE-1 and MVA-pp65 was completed in a total of 5 rounds each (documented in detail in the master's thesis of Christiane Schwegler[287]). After this, high titer virus stocks were generated by large scale infection of BHK cells, followed by purification and concentration of MVA particles via two subsequent rounds of ultracentrifugation over a 30% sucrose cushion. The MVA strains were then subjected to a final quality control experiment: An aliquot from both of the newly produced master stocks was used to infect BHK cells and 10 single plaques were picked for each strain. The virus particles from each plaque were then used once more to infect BHK cells, followed by isolation of DNA and proteins from those cells. PCR screening reactions amplifying short fragments (≈ 400 bp) of IE-1 or pp65, as well as LacZ and GFP demonstrated that the transgenes were present in all plaques (Figure 31A). At the same time, LacZ and GFP were undetectable, showing that both the parental strain and the reporter gene were completely absent. Additionally, the complete open-reading frames of the IE-1 and pp65 were subjected to Sanger sequencing for each plaque with no detectable mutations. These results indicate that IE-1 and pp65 were stably integrated into the MVA genome. This finding was further confirmed on protein level, since Western blot analysis demonstrated that IE-1 and pp65 were expressed in each case without detectable truncations (Figure 31B). In conclusion, all quality criteria were met

and the newly generated strains MVA-IE-1 and MVA-pp65 were deemed suitable for further experiments.

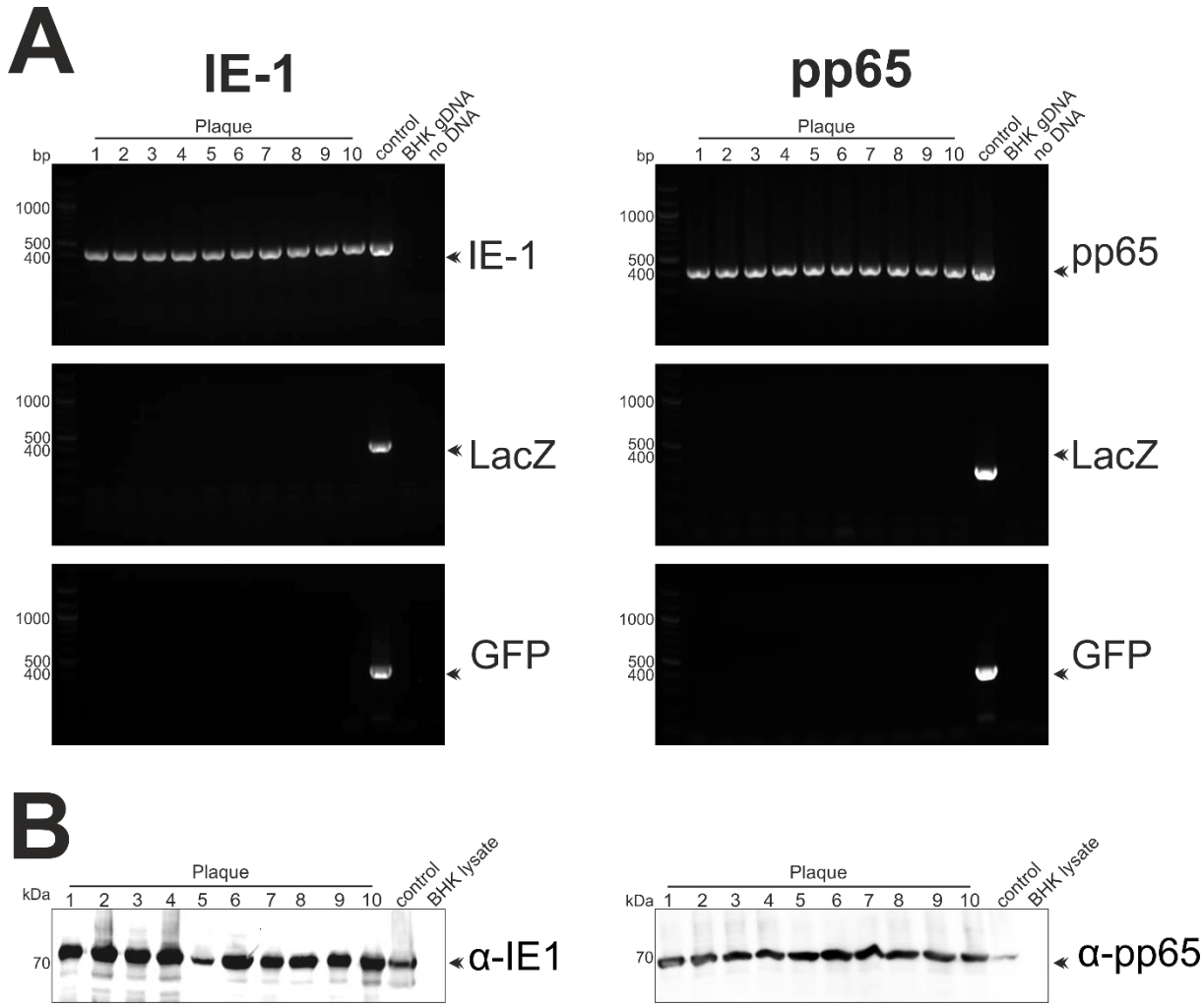

Figure 31 – Final quality control of MVA-IE-1

(A) BHK cells were separately infected with virions isolated from ten single plaques that were picked after infection of cells with the master stocks of MVA-IE-1 (left) or MVA-pp65 (right). Genomic DNA was isolated and different PCR reactions were performed with primer pairs amplifying short fragments (~400bp, expected sizes shown next to the gels) of IE-1, pp65, LacZ or GFP. As positive control, DNA plasmids containing the respective target genes were used as template DNA in separate reactions. Genomic DNA isolated from uninfected BHK cells as well as PCR reactions without template DNA served as negative controls. (B) Protein extracts from the same cells were subjected to SDS-PAGE and Western blot analysis using IE-1- (left) or pp65-specific (right) detection antibodies. Cells transiently transfected with pcDNA3.1-IE-1 or pcDNA3.1-pp65 were used as positive control, while cell lysates from uninfected BHK cells served as negative controls. The data displayed in this graph was collected during the master's thesis of Christiane Schwegler under my experimental supervision[287].

Recombinant Adenovirus or Sendai virus strains expressing IE-1, pp65 or GFP were generated by our cooperation partners Christian Thirion (Sirion Biotech GmbH) and Marian Wiegand (RSV Genius GmbH) with details on the respective procedures specified in sections VI.6.2 and VI.6.3. The immunological and virological characterization of all vectors is described in the following sections.

IV.2.1. Delivery of IE-1 and pp65 by Adenovirus vectors

One major limitation for application of subgroup C vectors like Ad5 is the requirement for CAR expression on the surface of a given cell subset for efficient transduction (see III.6.2). This is a particular obstacle for the direct delivery of genetic material to immune cells, where CAR expression is mostly low or entirely lacking[288–290]. By contrast, the tropism of adenoviruses from subgroup D is much broader since they interact with sialic acids that are found on virtually every cell type. Hence, in order to be capable of delivering IE-1 and pp65 directly to antigen-presenting cells (APCs), the CMV vaccine candidates were based on the subgroup D adenovirus Ad19a/64. The transgenes IE-1, pp65 or GFP were inserted into a E1/E3-deleted vector[234] at the position of the viral E1-region under the control of the CMV immediate/early promoter[291]. For comparison, the same ORFs were likewise inserted into the E1 region of a BAC-derived Ad5 vector under the identical promoter, or the Thymidin kinase locus of MVA under control of synthetic poxviral early/late promoter. AdV-mediated expression of all transgenes with the expected molecular weight was detectable by Western Blot after infection of permissive HEK293T cells (Figure 32A).

In a first step, the capacity of Ad19a/64 and Ad5 to transduce different leukocyte populations was investigated. To identify susceptible cell types, freshly isolated human peripheral blood mononuclear cells (PBMCs) were first infected directly with Ad19a/64-GFP or Ad5-GFP. Then, 24 hours post infection (hpi), the amount of GFP positive cells in various PBMC sub-populations that was defined via staining of the surface markers CD14, CD19, CD3, CD4, CD8 and CD56, followed by flow cytometry analysis (Figure 32B and C). After transduction with Ad5, GFP expression was only detectable in monocytes, with approximately 30% of cells being positive at a multiplicity of infection (MOI) of 1000. In contrast to this, all populations tested were GFP positive when transduced by Ad19a/64. The highest transduction rates were observed in monocytes (80% positive at MOI 100), followed by NK cells, $CD8^+$ T cells (30% each at MOI 1000) and $CD4^+$ T cells (20% at MOI 1000). Even B cells were transduced with an efficiency of 10% at MOI 100, which however, did not increase upon further increasing the vector load, suggesting that only a fraction of the CD19 positive cell population is susceptible to Ad19a/64 transduction. While there was considerable variation between the efficacy of transduction within different cell populations, this data confirms that Ad19a/64 is indeed more efficient at delivering genes to leukocytes than Ad5.

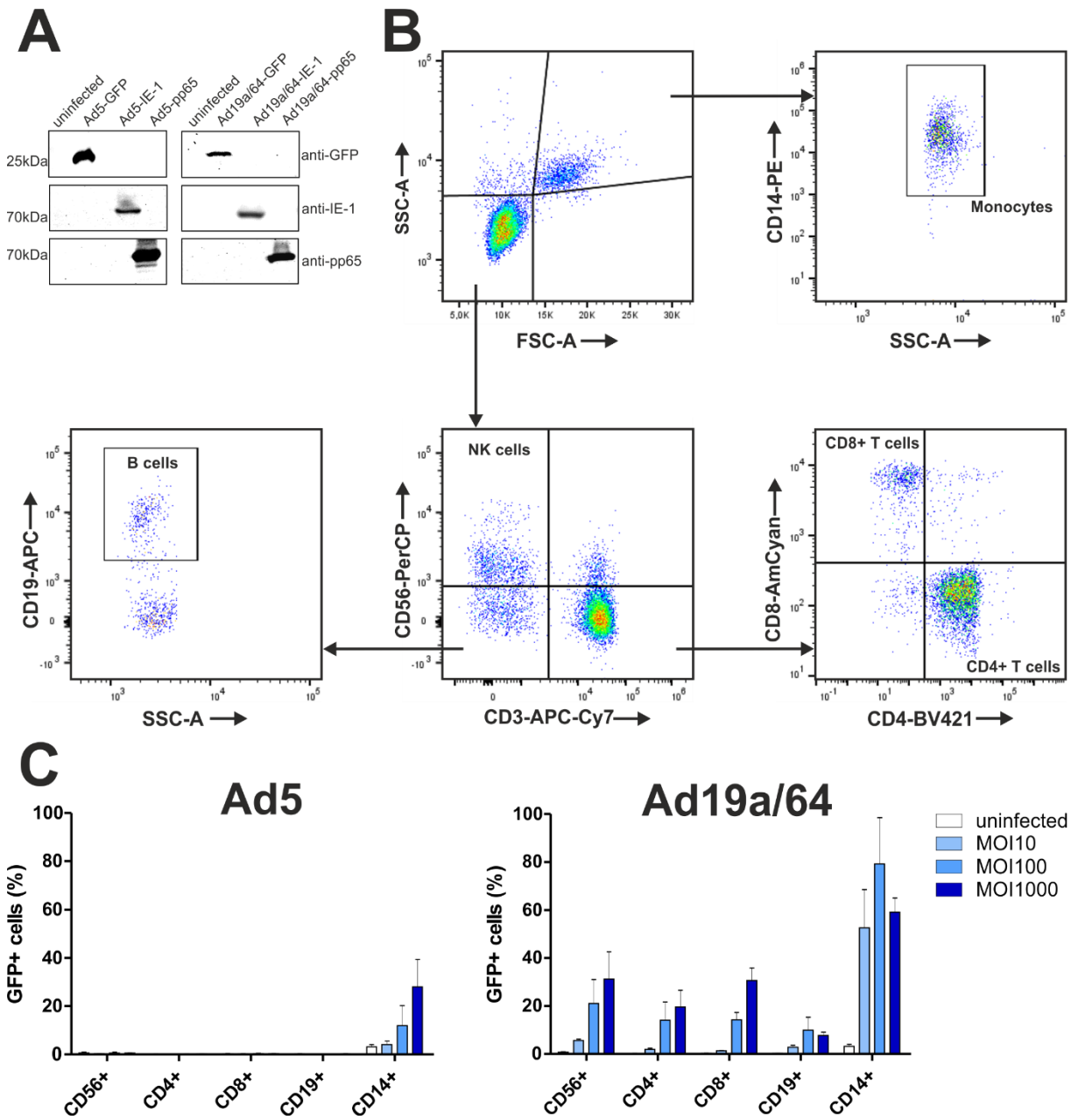

Figure 32 - Ad19a/64 vectors are capable of transducing a broad panel of human blood cells
(A) Western Blot analysis of transgene expression 48 hours post infection (hpi). HEK293T cells were infected at a multiplicity of infection (MOI) of 10 with Ad5 or Ad19a/64 vectors expressing the genes IE-1, pp65, or GFP as indicated. (B) Gating strategy to discriminate monocytes ($CD14^+$), B cells ($CD19^+$), NK cells ($CD3^-/CD56^+$) and T cells ($CD4^+$ or $CD8^+$). (C) Human peripheral blood mononuclear cells (PBMCs) from 3 different donors were transduced at the indicated MOIs with Ad5-GFP or Ad19a/64-GFP. The amount of GFP positive cells in the indicated populations was determined by flow cytometry at 24 hpi. Bars represent the mean and standard deviation (SD) of values from all donors.

Since various leukocyte populations were generally found to be susceptible to Ad19a/64 transduction, it was then tested whether this vector is capable of delivering CMV antigens to dendritic cells (DCs). Inducing antigen expression directly in this cell type by use of a suitable vector system might increase the magnitude of adaptive immune responses following vaccination as DCs are the most potent initiators of adaptive immune responses *in vivo*. Moreover, *ex vivo* generated and virally transduced DCs expressing CMV antigens might be readily reapplied to patients for priming or expansion of T cell responses. Of the multiple

DC subsets with distinct properties that are found in humans, monocyte-derived dendritic cells (moDCs) are commonly used for such approaches, since they can be easily obtained in large quantities[292–294]. To assess transduction rates, moDCs were generated *ex vivo* as described above, and were subsequently infected at different MOIs with viral vectors expressing IE-1, pp65 or GFP. Antigen expression was assessed via flow cytometry after 24 and 48 hours, respectively (Figure 33). Both MVA and Ad19a/64 efficiently transduced moDCs and mediated GFP expression with the maximum (approximately 80% of cells GFP positive) reached at MOI 10. Whereas MVA was slightly superior to Ad19a/64 in mediating GFP expression at low MOIs (MFI at MOI of 0.1 and 1; Figure 33B and D), the median fluorescence intensity (MFI) values at MOI 10 were higher when Ad19a/64 was used, indicating greater protein levels per transduced cell. Using Ad5, similar transduction rates were observed only at 100-1000-fold higher MOIs of 10,000, demonstrating that, compared to Ad19a/64, this vector is clearly limited in the transduction of moDCs. Due to the limited sensitivity of the monoclonal antibodies used in flow cytometry, the intracellular detection of IE-1 and pp65 was altogether less sensitive compared to GFP, but Ad19a/64 was again clearly superior to Ad5 in mediating antigen expression. At low MOIs, the percentage of antigen positive cells was higher for IE-1 and pp65 when MVA was used compared to Ad19a/64, although the corresponding values were very similar for GFP. Since the MFI values at low MOIs indicate higher protein quantities per cell for MVA, more events are probably capable of surpassing the signal threshold during the flow cytometric analysis under these conditions, which might explain these discrepancies.

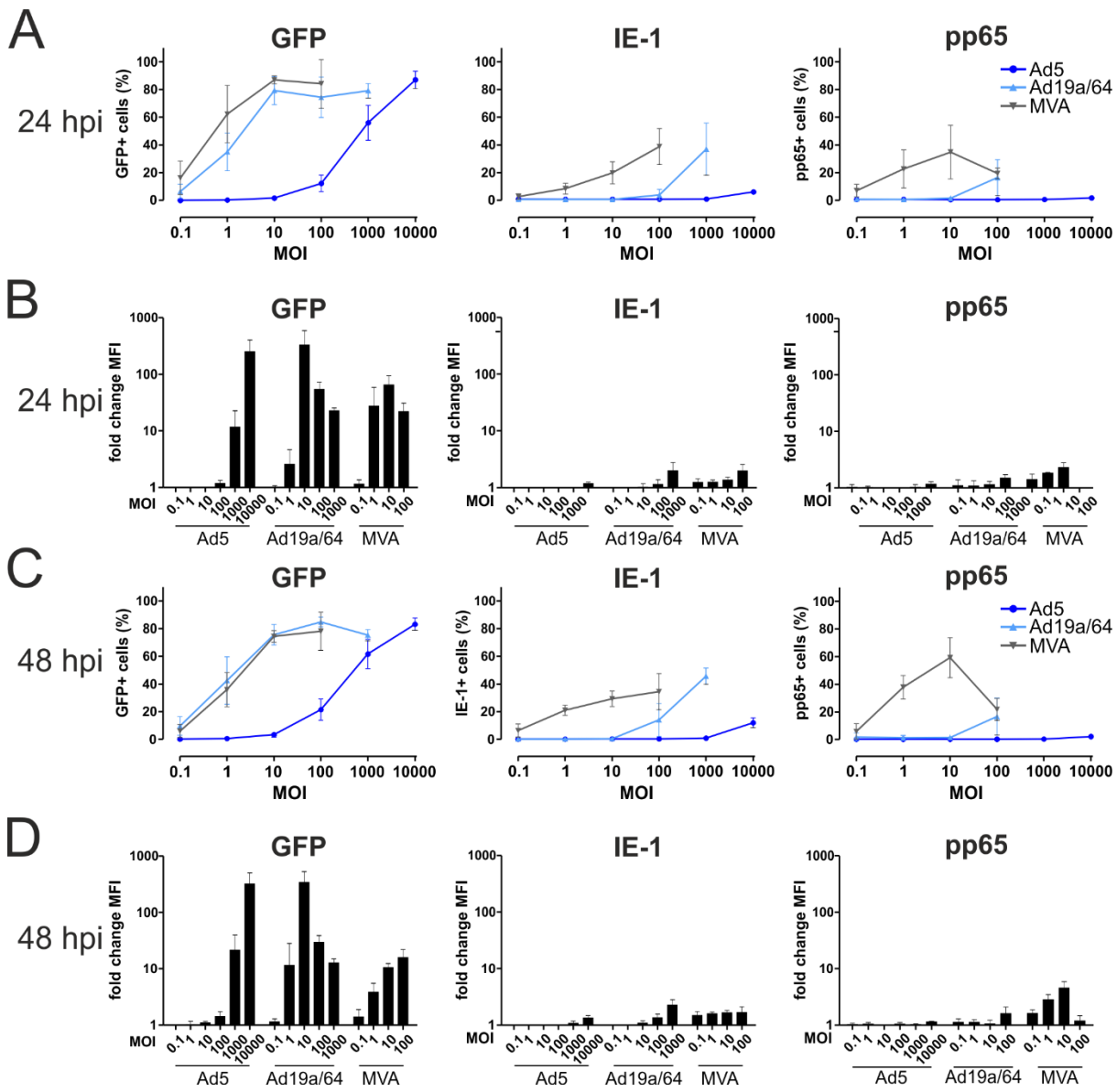

Figure 33 - MVA and Ad19a/64 efficiently transduce dendritic cells
MoDCs from 3 different CMV seronegative blood donors were infected at varying MOIs with the indicated vectors and intracellular presence of the transgenes GFP, IE-1, and pp65 was quantified via flow cytometry after 24 (A, B) and 48 hours (C, D). Results are given as the median percentage of cells positive for each antigen (A, C) with error bars representing the standard deviation. Median fluorescence intensity (MFI) values were normalized to the signals obtained from uninfected cells with bars representing the mean and standard deviation of values from all donors (B, D).

Recognition of pathogen-derived peptides by T cells requires antigen processing and presentation on major histocompatibility complex (MHC) molecules. Thus, for *in* vivo priming of naïve T cells, MHC presentation of a given peptide is a critical prerequisite. During natural adenovirus infection, the viral protein E3/19K disrupts export of newly synthesized MHC-class I complexes to the cell surface in order to evade T cell-mediated immune responses[295]. Although the corresponding gene is deleted along with the entire E3 region from both AdV vectors used in this study, it should be ensured that there is no major Ad19a/64-mediated interference with MHC-class I presentation. To explore this, virally

transduced moDCs were co-cultivated with CD8 positive, HLA-matched T cell clones recognizing IE-1- or pp65-derived peptides. As an indirect measure for antigen-presentation, T cell restimulation was quantified by intracellular staining of IFNγ, followed by flow cytometry analysis (Figure 34). MVA was most efficient at mediating T cell restimulation, inducing a maximum of 80% IFNγ positive T cells at MOI 1 for both antigens, although at MOI 100, T cell responses began to recede. Following Ad19a/64 transduction, a comparable amount of T cell restimulation was observed at MOI 10 (Ad19a/64-pp65) or 100 (Ad19a/64-IE-1), respectively. Using Ad5 vectors, similar levels were reached only at MOI 10,000, thus turning out to be 10 to 100-fold less potent in restimulating pp65 or IE-1 specific T cell clones. Since the T cell restimulation rates were largely reflective of the transduction rates, we conclude that none of the AdV vectors tested here detectably inhibits MHC-class I presentation.

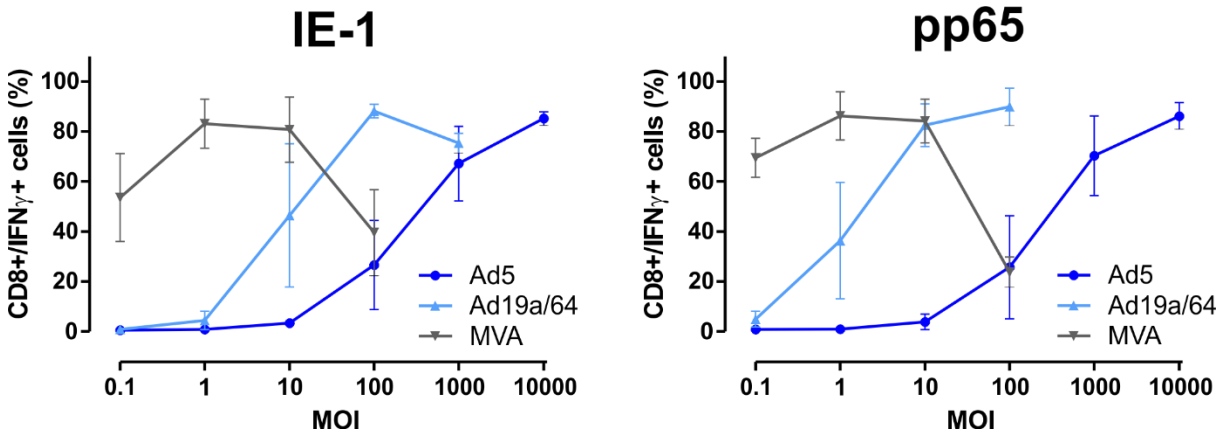

Figure 34 - T cell stimulation by virally transduced DCs correlates with transduction rates
MoDCs from 3 different CMV seronegative blood donors were infected at varying MOIs with the indicated vectors expressing IE-1 or pp65. 24 hpi, antigen-specific, HLA-matched T cell clones were added at an effector/target ratio of 1:1. After 6 hours of co-cultivation in the presence of Brefeldin A (BFA), cells were stained for CD8 and intracellular IFNγ and subjected to flow cytometry analysis. The fraction of cells co-expressing CD8 and IFNγ is displayed as the mean and standard deviation of values from all donors.

It is well established that priming of naïve T cells by dendritic cells requires the latter to be in a fully mature state and that immature or only partially matured DCs are likely to induce tolerance or anergy *in vivo*[296]. Phenotypically, maturation coincides with increased expression of surface molecules such as CD80, CD83, CD86 and MHC-II. Hence, it was tested if any of these markers are upregulated in moDCs by measuring their expression levels 24 and 48 hours after transduction (Figure 35). Transduction with both AdV vectors led to a dose-dependent upregulation of HLA-DR and CD86, except for Ad19 at MOI 1000, where a slight downregulation of CD80 and CD86 was detected. When MVA was used, HLA-DR and CD86 were also upregulated at MOI 0.1, whereas there was a pronounced downregulation of all four markers at higher MOIs with CD86 being affected the most. These data imply that additional inflammatory stimuli will be needed to induce full maturation of dendritic cells, but AdV vectors interfere to a lesser extent with this process than MVA.

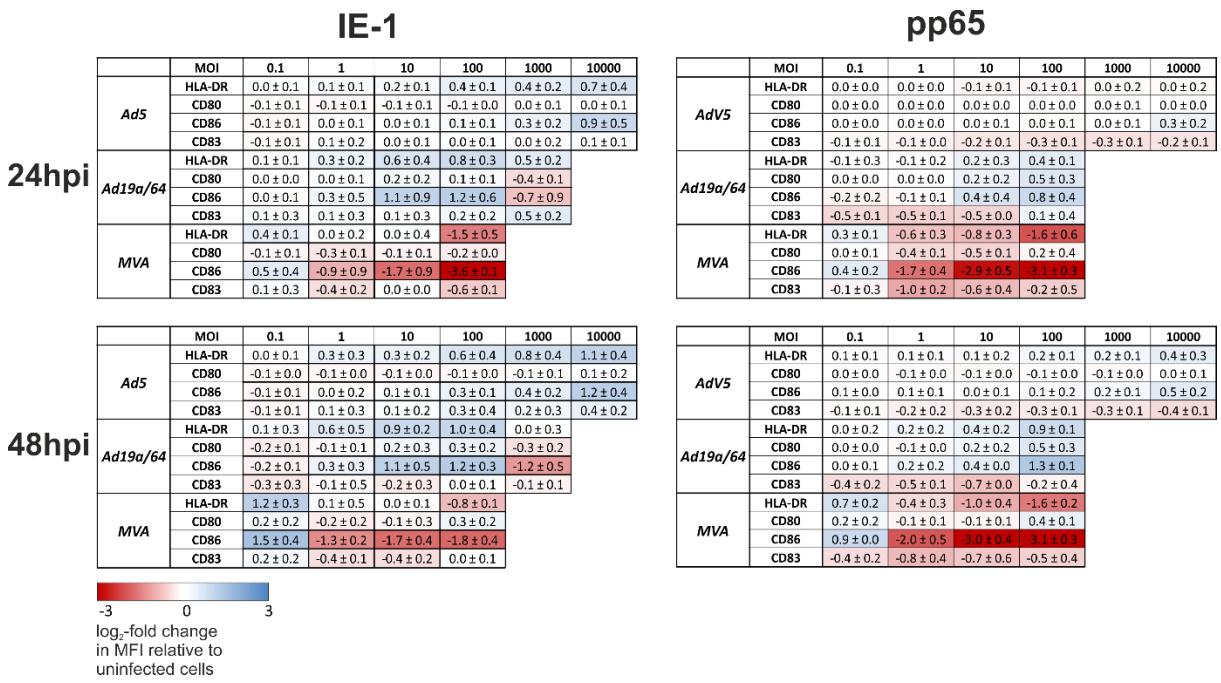

Figure 35 - None of the tested vectors mediate full maturation of dendritic cells
MoDCs from 3 different CMV seronegative donors were infected at various MOIs with IE-1 or pp65-expressing vectors. 24 and 48 hpi, samples were stained for HLA-DR, CD80, CD83 or CD86 and analyzed via flow cytometry. Obtained median fluorescence intensity (MFI) values were normalized to those of uninfected cells. Log_2 values which represent the mean (± standard deviation) from all experiments are displayed in a heatmap indicating up-regulation (blue) or down-regulation (red) of a given marker.

Many viruses induce apoptosis upon infection of dendritic cells, which can in turn impede T cell stimulation when using *ex vivo* transduced DCs as a therapeutic vaccine. Since premature death of virally transduced dendritic cells would limit their therapeutic potential or compromise their ability to elicit vaccine responses, the impact of MVA and AdV transduction on DC survival was investigated. moDCs were treated with IE-1- or pp65-expressing vectors and performed AnnexinV/7AAD staining after 24 and 48 hours (Figure 36). MVA infection induced the highest amount of cytotoxicity which was already evident at MOI 0.1. At higher virus concentrations, more than 90% of cells were positive for one or both cell death markers after 48 hours. Ad19a/64-mediated toxicity was detectable only starting from MOI 100 with almost all cells undergoing apoptosis at MOI 1000 over a period of 48 hours. Thus, in contrast to MVA, DC transduction and antigen expression take place at MOI 1 and 10 without apparent cytotoxicity when using Ad19a/64. By contrast, Ad5 transduction hardly induced cytotoxic effects at all over the observed time period although MOIs of up to 10,000 were tested. Although IE-1 was previously described to inhibit apoptosis by activating the phosphatidylinositide 3′-OH kinase (PI3K) pro-survival pathway[297], the amount of toxicity mediated by IE-1 and pp65 expressing vectors was comparable.

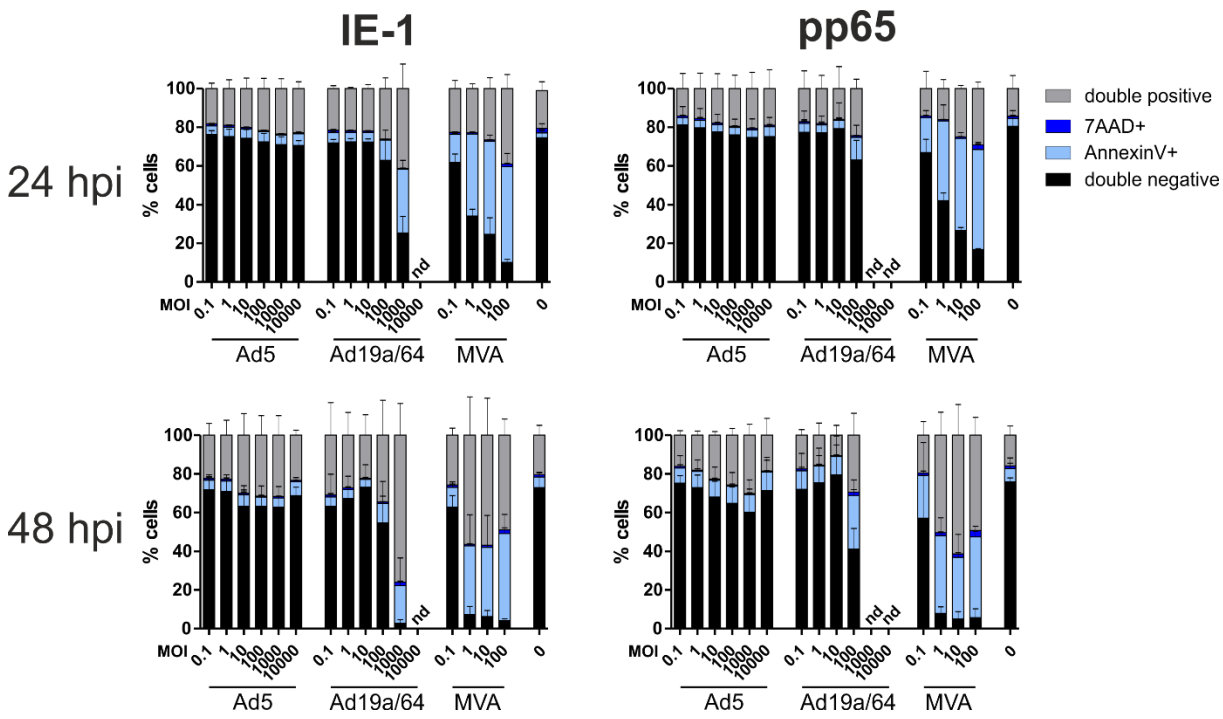

Figure 36 - MVA causes the highest amount of cell death in dendritic cells
MoDCs from 3 different CMV seronegative blood donors were transduced at varying MOIs with the indicated vectors. 24 or 48 hpi, cells were stained with AnnexinV-APC and 7AAD before flow cytometric analysis. Bars show the mean and standard deviation (SD) of values from all donors (nd: not determined).

The majority of currently approved vaccines is administered via intramuscular injection, a scenario in which viral vectors are likely to induce antigen expression predominantly in muscle cells and only to a lower extent directly in tissue-resident dendritic cells. In this scenario, antigen has to be acquired by DCs from the extracellular space and loaded onto MHC-class I molecules via cross-presentation for the priming of $CD8^+$ T cells. To test if AdV-transduced cells or fragments thereof are taken up secondarily by DCs and if MHC-class I presentation takes place, an *in vitro* cross-presentation assay was employed. HeLa cells were transduced with AdV vectors expressing IE-1 or pp65 and 24 hpi, they were added to moDCs. After 24 hours of co-culture, antigen-specific T cell clones were added and the intracellular presence of IFNγ was quantified after 6 hours by flow cytometry. Direct antigen presentation by HeLa cells can be excluded due to an HLA mismatch with the T cell clones used in this experiment. Prior to the addition of HeLa cells to DCs, they were washed multiple times to ensure that no residual extracellular virus particles were left that might infect DCs directly. To test if these washing steps sufficiently removed the inoculum, the supernatant of each washing step was added separately to moDCs. After 24 hours, antigen-specific T cell clones were added and restimulation was assessed as before. Four washing steps were sufficient to reduce T cell activation to background levels, indicating that no detectable amount of free virus remained in the culture (shown representatively for pp65 vectors in Figure 37A). Using GFP-expressing vectors, it was found that HeLa cells are susceptible to infection with both AdV vectors, although Ad19a/64 was again superior to Ad5 in mediating GFP expression (Figure 37B). Nonetheless, at MOI 1000, almost all HeLa cells were GFP positive irrespective

of the vector used with comparable MFI values. Accordingly, the degree of cross-presentation induced by Ad5 or Ad19a/64 transduced cells was generally very similar (Figure 37C). This finding also implies that many of the differences between Ad5 and Ad19a/64 that were observed in this study are a direct result of their distinct cell tropism.

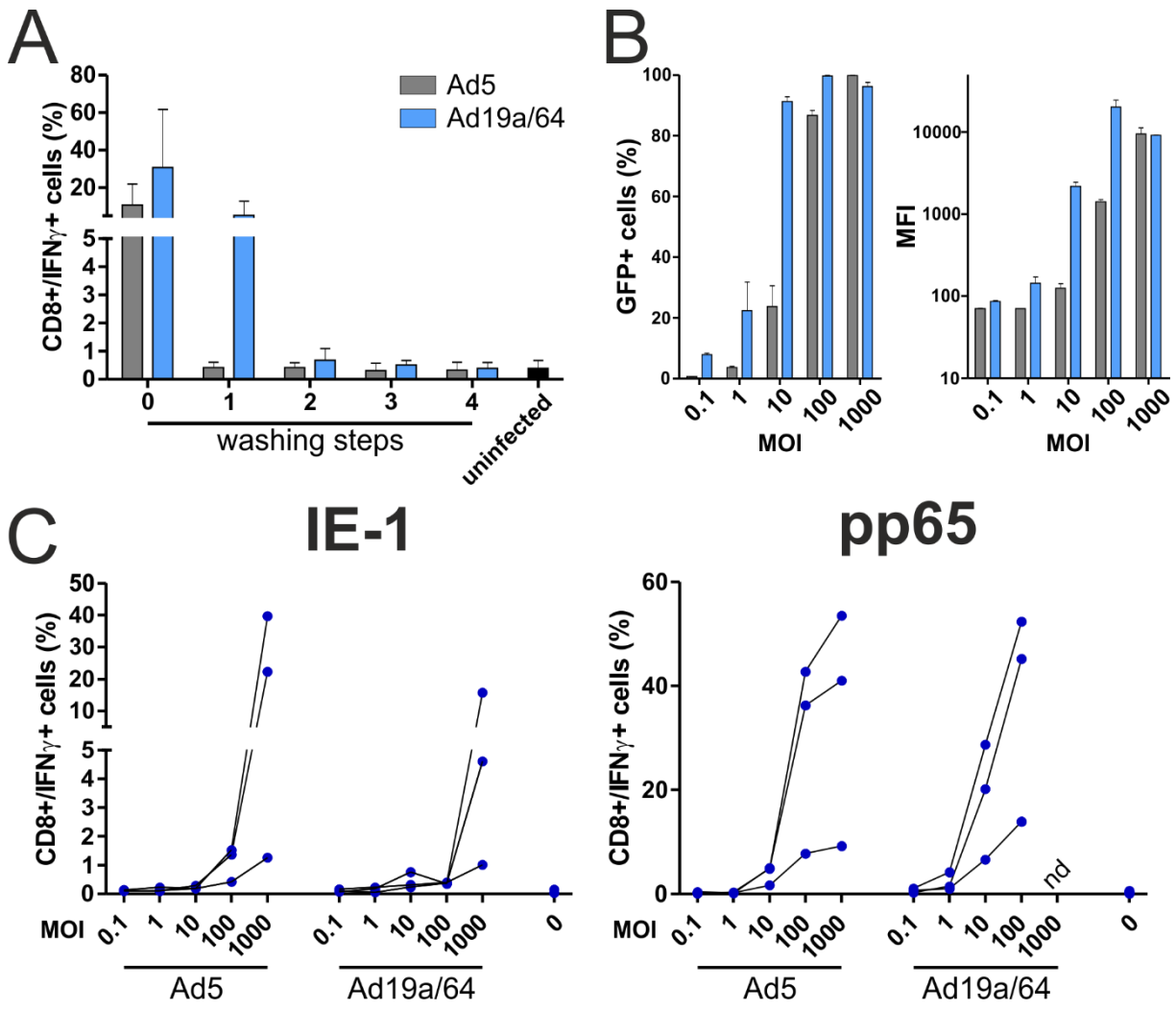

Figure 37 – Cross-presentation of IE-1 and pp65 by Ad5 and Ad19a/64-infected cells
(A) HeLa cells were transduced at MOI 1000 with Ad5- or Ad19a/64-pp65. 24 hpi, the supernatant from overnight culture (0) as well as from 4 subsequent washing steps with cell culture medium (1-4) was collected and added to moDCs. After 24 hours, a pp65-specific, HLA-matched T cell clone was added to moDCs at an effector/target ratio of 1:1. Co-culture lasted for another 6 hours in the presence of BFA, followed by CD8/IFNγ staining and flow cytometry analysis. Bars represent the mean and SD from 3 experiments with different blood donors. (B) HeLa cells were transduced at the indicated MOIs with Ad5-GFP or Ad19a/64-GFP and GFP expression was quantified 24 hpi via flow cytometry. (C) HeLa cells were transduced at the indicated MOIs with IE-1 or pp65 expressing AdV vectors. 24 hpi, cells were washed 4 times and added to moDCs at a 1:1 ratio. After 24 hours of co-cultivation, antigen-specific T cell clones were added for a HeLa/DC/T cell ratio of 1:1:1. T cell restimulation was measured after 6 hours as described in A. Connected lines indicate values that were obtained using moDCs from an individual donor (MFI: median fluorescence intensity; nd: not determined).

IV.2.2. Delivery of IE-1 and pp65 by Sendai virus vectors

No case of symptomatic SeV infection in humans has been reported to date. Nevertheless, we wanted to achieve further vector attenuation, since next to CMV negative young women, possible target groups for a CMV vaccine also include immunocompromised patients such as transplant recipients. We chose a previously described SeV strain in which the amino acids 2-77 of the viral P gene were deleted. Partial deletion of this gene prevents switching of the viral RNA-dependent RNA polymerase (vRdRp) from mRNA synthesis to genome replication, ultimately inhibiting the generation of progeny virus[298]. This strain, hereafter referred to as replication-deficient SeV (rdSeV) served as the backbone for the insertion of the CMV antigens IE-1, pp65 or, as control, GFP (Figure 38A). For comparison, the same transgenes were inserted into the parental strain containing the full-length P-gene, hence termed replication-competent SeV (rcSeV). MVA-IE-1 and MVA-pp65 again served as control/benchmark/reference. Expression of all transgenes could be readily detected by western blot analysis after successful transduction of Vero cells (Figure 38B). To test if partial deletion of the viral P gene in rdSeV is sufficient to prevent replication in human moDCs, viral titers in the cell culture supernatant were determined over a period of 48 hours after infection. Whereas rcSeV was capable of replicating to high titers in moDCs, the number of infectious particles was considerably below the baseline level after 24 hours and undetectable after 48 hours for rdSeV, indicating that no virus was produced *de novo* (Figure 38C). When a functional P gene was provided *in trans* by a Vero cell-based helper cell line (V3-10), rdSeV replication was restored and similar to that of rcSeV in moDCs.

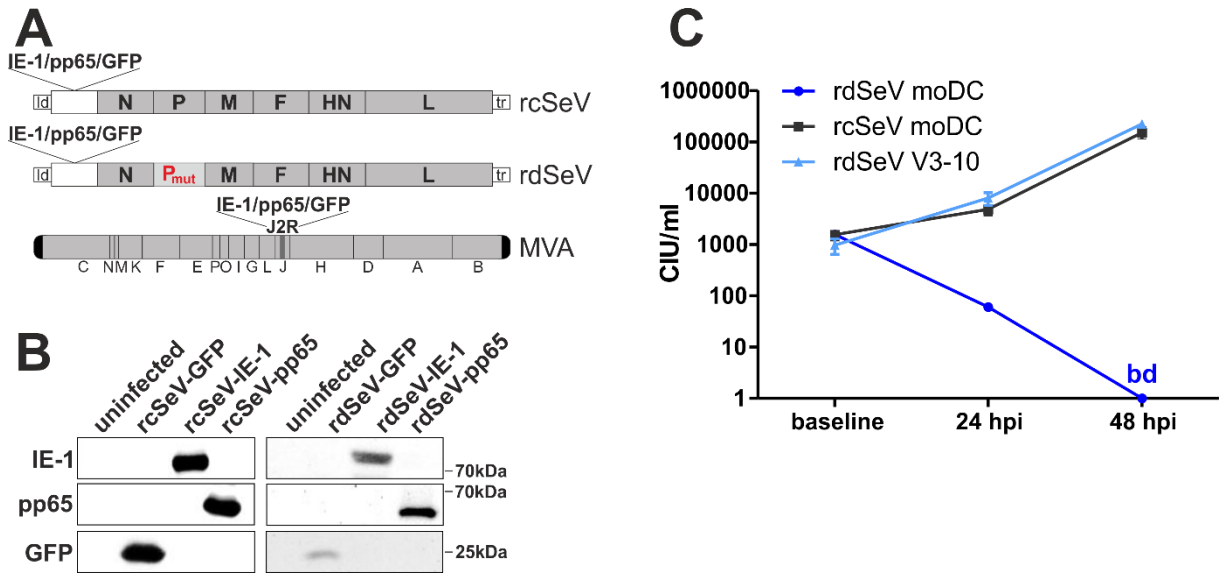

Figure 38 - Sendai virus is capable of replicating in moDCs

(A) Schematic representation of viral genomes highlighting transgene insertion sites (not to scale). SeV genes and MVA genome segments are indicated by their common labels[299,300]. The modified SeV P gene is highlighted as Pmut. (B) Western Blot analysis of transgene expression 48 hours post infection (hpi) of Vero cells at MOI 1 with replication-competent (rcSeV) or replication-deficient (rdSeV) Sendai virus strains expressing the indicated genes IE-1, pp65 or GFP. (C) Titration of cell culture supernatants at different time points after infection of human monocyte-derived dendritic cells (moDCs) with rcSeV-GFP or rdSeV-GFP at MOI 1. rdSeV was also used to infect the Vero cell line V3-10 (trans-complementing a full-length version of the viral P gene) at the same MOI. 3 hours post infection, cells were washed once with medium and an aliquot was collected

to determine baseline virus levels (residual virions that did not enter target cells and were not removed by washing). Viral titers are given as cell infectious units (CIU) per ml (bd: below detection limit).

Next, it was tested if expression of the heterologous antigens IE-1, pp65 or GFP is induced in dendritic cells upon transduction with the different SeV strains. MoDCs were generated by *ex vivo* differentiation of monocytes and transduced at different MOIs with each vector. The percentage of antigen positive cells was determined 24 and 48 hours after transduction by flow cytometry (Figure 39). In contrast to GFP, IE-1 and pp65 were stained intracellularly using labelled antibodies prior to the measurement. In accordance with previously published data, rcSeV was found to be capable of efficiently transducing moDCs[301]. For the GFP-carrying vectors, antigen expression was generally MOI-dependent and at a similar level for rcSeV and MVA. Whereas MFI levels were slightly higher for MVA at low MOIs, peak expression levels were highest with rcSeV at MOI 10 and 100, respectively. The percentage of GFP-positive cells as well as the monitored MFI was, however, clearly lowest when using rdSeV, showing that partial deletion of the P gene has a negative influence on overall transgene production. Nevertheless, the capacity to transduce dendritic cells and mediate transgene expression are preserved. Compared to GFP, intracellular detection of IE-1 and pp65 was altogether less sensitive for want of suitable flow cytometry antibodies. Consequently, expression of both IE-1 and pp65 was below the limit of detection for rdSeV and signals were significantly lower than those obtained after transduction with the corresponding rcSeV or MVA vectors carrying GFP.

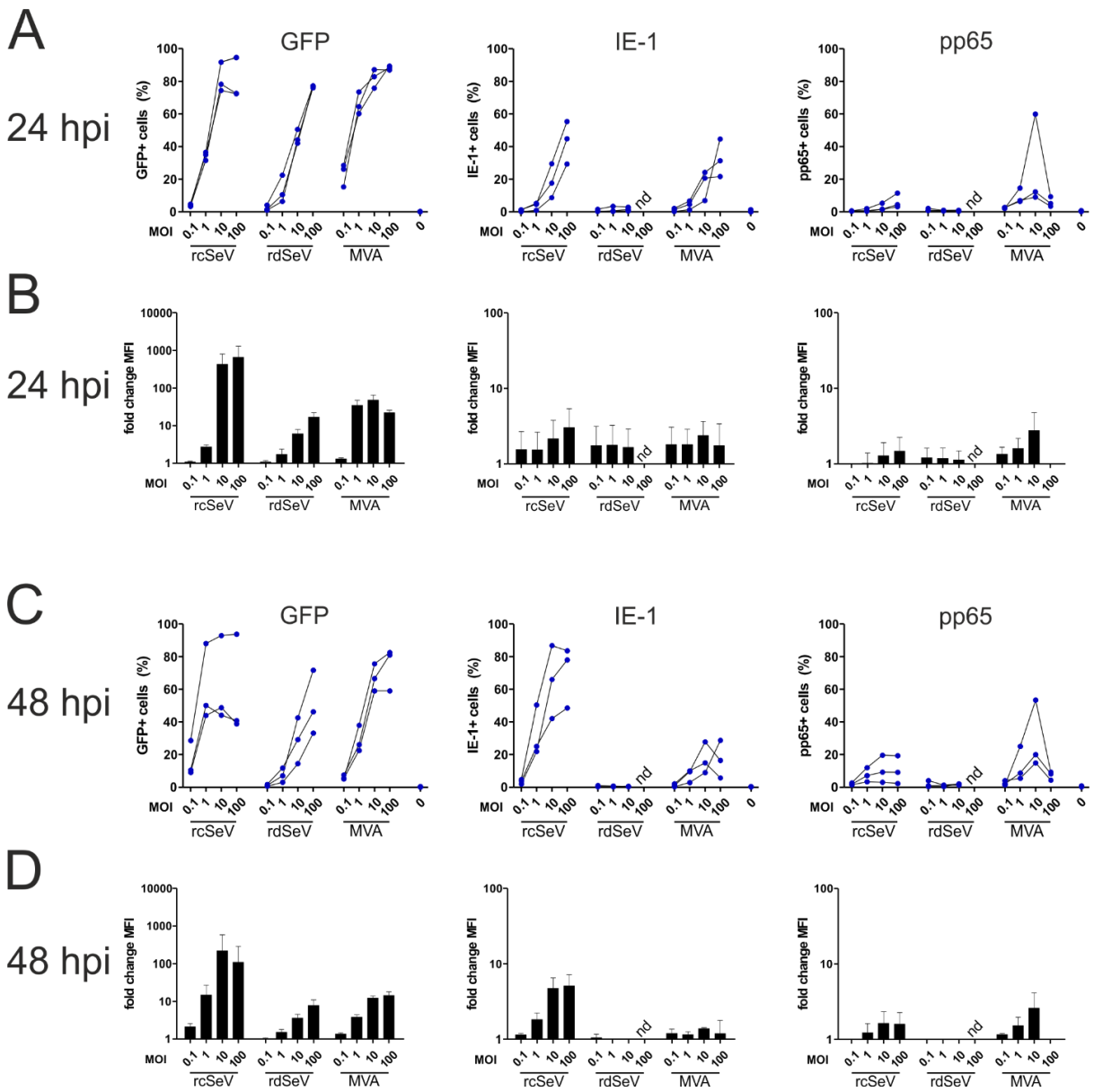

Figure 39 - SeV efficiently transduces moDCs with rcSeV eliciting higher transgene expression than rdSeV

MoDCs from 3 different CMV seronegative blood donors were infected at the indicated MOIs and intracellular presence of the transgenes GFP, IE-1 and pp65 was quantified via flow cytometry after 24 (A, B) and 48 hours (C, D), respectively (nd: not determined). Results are presented as the percentage of cells positive for a given antigen (A, C), with connected lines indicating values that were obtained using cells from a given donor. Median fluorescence intensity (MFI) values were normalized to the signals obtained from uninfected cells with bars representing the mean and standard deviation of values from all donors (B, D).

In addition to the vector-mediated expression of IE-1 and pp65 in dendritic cells, processing of the antigen and MHC-presentation are other critical prerequisites for the initiation or expansion of adaptive immune responses. As a surrogate marker for this process, the vectors were tested for their capacity to restimulate antigen-specific T cell clones after transduction of dendritic cells. 24 hours after infection at various MOIs, moDCs were co-cultivated with HLA-matched IE-1- or pp65-specific T cell clones and measured T cell reactivation by determining the intracellular presence of IFNγ after another 6 hours. To verify that the responses were antigen-specific, GFP-expressing vectors of each type were also tested in

the same manner, none of which induced IFNγ-secretion even at high MOIs (data not shown). All vectors efficiently restimulated T cells with the maximum (approximately 80% of cells IFNγ positive) reached at MOI 1 for MVA and MOI 10 for both Sendai vectors (Figure 40). Whereas T cell responses were decreasing at higher MOIs when MVA was used, no such decrease in T cell restimulation was observed for the SeV vectors. Interestingly, rdSeV was equally capable of eliciting moDC-driven T cell restimulation as rcSeV despite hardly detectable antigen levels in moDCs in flow cytometry (Figure 39). Apart from minor differences, presumably reflecting differences in T cell receptor avidity of the clones used, the same trends were observable for IE-1 and pp65.

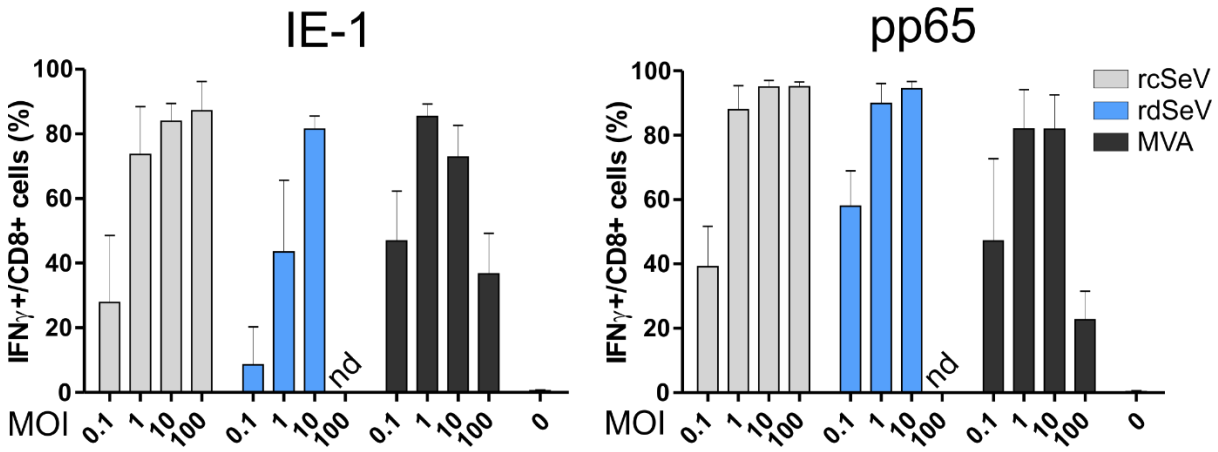

Figure 40 - Infection with both Sendai vectors leads to efficient restimulation of T cells by transduced moDCs
MoDCs from 3 different CMV seronegative blood donors were infected at the indicated MOIs with IE-1- or pp65-expressing vectors. 24 hpi, antigen-specific T cell clones were added at an effector/target ratio of 1:1. After 6 hours of co-cultivation in the presence of BFA, cells were stained for CD8 and intracellular IFNγ and analyzed via flow cytometry. Bars represent the mean and standard deviation of values from all donors (nd: not determined).

For efficient priming or expansion of T cell responses, SeV-transduced DCs should exhibit a certain degree of longevity *in vivo*, which would otherwise hamper possible applications as a therapeutic vaccine. Sendai virus has long been known to cause strong cytopathic effects upon infection and was recently identified as a mediator of necroptotic cell death[302,303]. Thus, it was assessed if the attenuation of rdSeV might reduce undesired induction of cell death in dendritic cells. To test this, moDCs were transduced at various MOIs with IE-1- or pp65-expressing virus strains and performed AnnexinV/7AAD staining after 24 and 48 hours, respectively. All tested vectors caused cell death in an MOI-dependent manner and irrespective of the transgene, with MVA evidently being the most toxic variant (Figure 41). 24 hours after infection, the percentage of AnnexinV/7AAD positive cells for a given MOI was comparable between both Sendai vectors. However after 48 hours, the proportion of healthy cells was further decreased when rcSeV was used while it remained constant for rdSeV, confirming that this vector is clearly less toxic than the original strain or MVA. Generally, the inserted transgene had again no obvious influence on cell death induction in this assay (compare Figure 36).

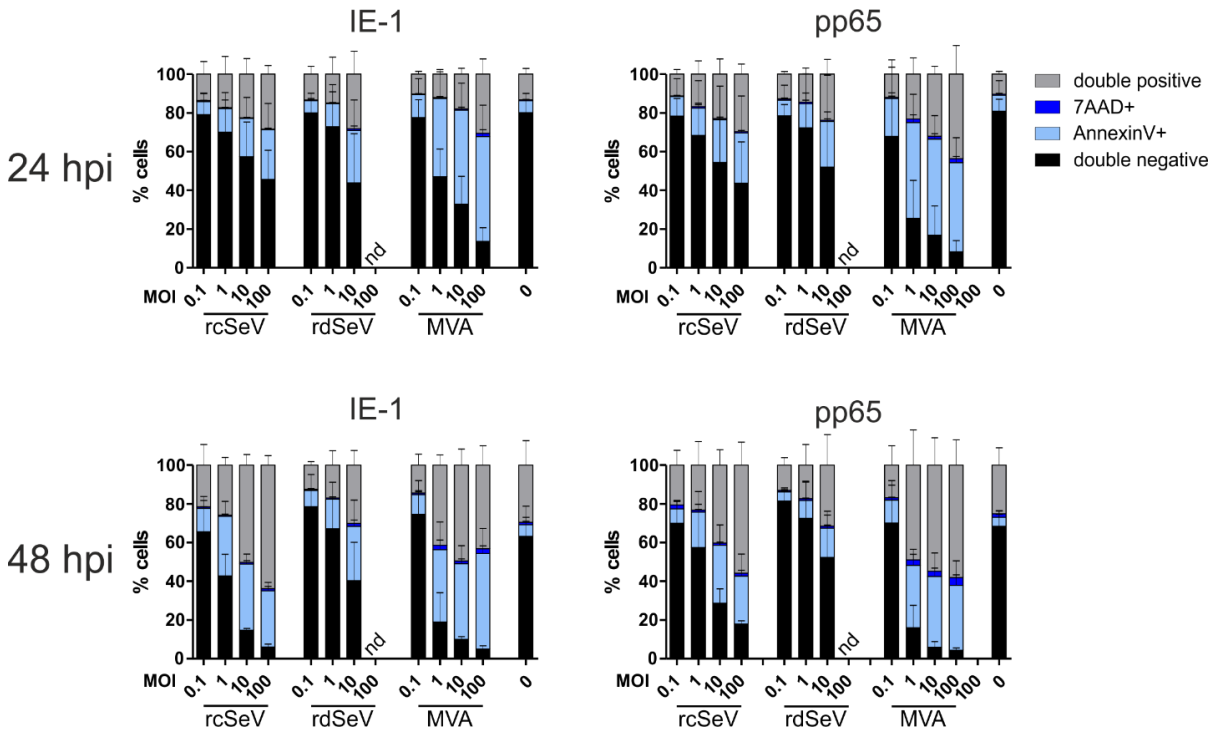

Figure 41 - Attenuated rdSeV is less cytotoxic than rcSeV
moDCs from 3 different CMV seronegative blood donors were infected at the indicated MOIs with IE-1 or pp65-expressing vectors. After 24 or 48 hours, samples were co-stained with AnnexinV/7AAD and cells positive for one or both markers were quantified by flow cytometry. Bars represent the mean and standard deviation (SD) of values from all donors (nd: not determined).

As mentioned above (section IV.2.1, Figure 35), *in vivo* T cell priming requires DCs to be in a fully mature state, which results in the upregulation of CD80, CD83, CD86 and HLA-DR. To assess whether any of these markers are upregulated in response to transduction with SeV or MVA vectors, the surface expression was measured via flow cytometry after 24 and 48 hours (Figure 42). MVA-IE-1 and MVA-pp65 induced upregulation of CD80, CD86 and HLA-DR at MOI 0.1, while the expression of CD83 was largely unaltered. At higher MOIs, marker expression was generally lower than that of uninfected cells with CD86 and HLA-DR being affected the most. In contrast, after transduction with the SeV vectors, markers were upregulated in a time- and MOI-dependent manner, except for some downregulation of CD80 and CD83 when rcSeV-IE-1 was used. Especially at higher MOIs, SeV vectors were clearly superior to MVA in mediating maturation with rdSeV inducing the highest overall upregulation. It is worth noting that SeV induced maturation seemed less pronounced for IE-1 carrying vectors which possibly reflects immunomodulatory properties of this protein. The observed tendencies were mostly more pronounced after 48 hours than after 24 hours.

IE-1

24hpi

	MOI	0.1	1	10	100
rcSeV	HLA-DR	0.1 ± 0.0	0.0 ± 0.0	0.2 ± 0.1	0.1 ± 0.2
	CD80	0.0 ± 0.1	0.0 ± 0.2	-0.1 ± 0.3	0.0 ± 0.3
	CD86	0.0 ± 0.1	0.0 ± 0.1	0.4 ± 0.4	0.6 ± 0.5
	CD83	0.1 ± 0.1	0.4 ± 0.2	0.9 ± 0.1	0.4 ± 0.1
rdSeV	HLA-DR	0.2 ± 0.1	0.5 ± 0.2	0.3 ± 0.2	*nd*
	CD80	0.2 ± 0.1	0.2 ± 0.2	0.2 ± 0.3	*nd*
	CD86	0.3 ± 0.1	0.7 ± 0.2	0.4 ± 0.3	*nd*
	CD83	-0.3 ± 0.2	0.1 ± 0.3	0.4 ± 0.4	*nd*
MVA	HLA-DR	0.3 ± 0.1	0.0 ± 0.1	-0.5 ± 0.1	-1.5 ± 0.7
	CD80	0.1 ± 0.1	-0.2 ± 0.1	-0.5 ± 0.0	-0.6 ± 0.0
	CD86	0.6 ± 0.2	-0.2 ± 0.6	-1.7 ± 0.6	-2.8 ± 1.0
	CD83	0.1 ± 0.1	-0.2 ± 0.2	-0.1 ± 0.2	-0.6 ± 0.4

pp65

	MOI	0.1	1	10	100
rcSeV	HLA-DR	0.1 ± 0.1	0.2 ± 0.2	0.4 ± 0.2	0.4 ± 0.1
	CD80	0.1 ± 0.0	0.1 ± 0.0	0.2 ± 0.0	0.3 ± 0.0
	CD86	0.1 ± 0.0	0.0 ± 0.0	0.3 ± 0.2	0.6 ± 0.2
	CD83	0.0 ± 0.1	0.3 ± 0.3	0.9 ± 0.3	1.2 ± 0.3
rdSeV	HLA-DR	0.8 ± 0.4	1.2 ± 0.4	0.8 ± 0.2	*nd*
	CD80	0.2 ± 0.1	0.3 ± 0.2	0.6 ± 0.2	*nd*
	CD86	1.4 ± 0.5	1.8 ± 0.4	1.4 ± 0.2	*nd*
	CD83	0.0 ± 0.3	0.5 ± 0.4	0.7 ± 0.2	*nd*
MVA	HLA-DR	0.6 ± 0.1	-0.2 ± 0.4	-0.5 ± 0.4	-1.3 ± 0.3
	CD80	-0.1 ± 0.1	-0.6 ± 0.0	-0.6 ± 0.2	-0.3 ± 0.2
	CD86	1.1 ± 0.2	-0.8 ± 0.8	-1.6 ± 0.6	-2.1 ± 0.4
	CD83	0.0 ± 0.1	-0.7 ± 0.3	-0.4 ± 0.3	-0.1 ± 0.2

-3 0 3

log_2-fold change in MFI relative to uninfected cells

48hpi

	MOI	0.1	1	10	100
rcSeV	HLA-DR	0.6 ± 0.2	0.7 ± 0.1	0.5 ± 0.3	0.4 ± 0.5
	CD80	0.1 ± 0.4	0.0 ± 0.4	-0.3 ± 0.4	-0.2 ± 0.4
	CD86	1.0 ± 0.4	1.1 ± 0.2	0.4 ± 0.1	0.2 ± 0.3
	CD83	0.3 ± 0.2	-0.2 ± 0.5	-0.6 ± 0.3	-0.8 ± 0.4
rdSeV	HLA-DR	0.8 ± 0.4	1.0 ± 0.4	0.8 ± 0.4	*nd*
	CD80	0.2 ± 0.1	0.4 ± 0.3	0.4 ± 0.4	*nd*
	CD86	0.6 ± 0.2	0.9 ± 0.2	0.6 ± 0.2	*nd*
	CD83	-0.6 ± 0.1	-0.4 ± 0.2	-0.1 ± 0.2	*nd*
MVA	HLA-DR	1.1 ± 0.0	0.5 ± 0.7	-1.7 ± 0.4	-1.5 ± 0.2
	CD80	0.6 ± 0.4	0.4 ± 0.5	-0.2 ± 0.1	0.1 ± 0.2
	CD86	1.3 ± 0.3	0.4 ± 2.4	-2.2 ± 0.9	-2.2 ± 0.8
	CD83	0.2 ± 0.4	-0.2 ± 0.8	-0.8 ± 0.5	-0.5 ± 0.3

	MOI	0.1	1	10	100
rcSeV	HLA-DR	0.5 ± 0.1	0.7 ± 0.3	0.6 ± 0.6	0.6 ± 0.6
	CD80	0.2 ± 0.2	0.3 ± 0.2	0.2 ± 0.1	0.4 ± 0.1
	CD86	1.0 ± 0.1	1.2 ± 0.3	0.8 ± 0.6	0.3 ± 0.6
	CD83	0.4 ± 0.1	0.6 ± 0.2	0.4 ± 0.3	0.4 ± 0.3
rdSeV	HLA-DR	0.8 ± 0.4	1.1 ± 0.5	1.3 ± 0.5	*nd*
	CD80	0.4 ± 0.0	0.8 ± 0.2	0.9 ± 0.2	*nd*
	CD86	1.2 ± 0.4	1.6 ± 0.5	1.7 ± 0.3	*nd*
	CD83	0.0 ± 0.6	0.8 ± 0.7	1.0 ± 0.3	*nd*
MVA	HLA-DR	1.1 ± 0.7	-1.2 ± 0.3	-1.3 ± 0.6	-1.3 ± 0.6
	CD80	0.7 ± 0.2	0.0 ± 0.1	0.0 ± 0.3	0.4 ± 0.4
	CD86	2.0 ± 0.7	-1.1 ± 0.6	-1.4 ± 0.7	-1.1 ± 0.7
	CD83	0.3 ± 0.3	-0.3 ± 0.3	-0.2 ± 0.4	0.2 ± 0.3

Figure 42 - SeV induces maturation of dendritic cells
moDCs from 3 different CMV seronegative blood donors were infected at the indicated MOIs with IE-1 or pp65-expressing vectors. After 24 or 48 hours, samples were stained for CD80, CD83, CD86 or HLA-DR and analyzed via flow cytometry. Obtained median fluorescence intensity (MFI) values were normalized to those of uninfected cells. Log_2 values which represent the mean (± standard deviation) from all donors are displayed in a heatmap indicating up-regulation (blue) or down-regulation (red) of a given marker (nd: not determined).

Along with the upregulation of costimulatory molecules on the surface of dendritic cells, secretion of distinct cytokines is also critical for T cell priming and definition of the induced effector phenotype. To explore the cytokine release profile of moDCs in response to transduction with SeV or MVA, the secretion of various cytokines was measured in a cytometric bead multiplex assay. All vectors induced production of IL-6, while presence of the anti-inflammatory cytokine IL-10 was hardly detectable and did not surpass the level produced by uninfected cells (Figure 43). IFNα responses were above background for all vectors at MOI 1 and, at MOI 10, only detectable when rdSeV was used. By contrast, TNF secretion was lowest for rdSeV, and IL-18 release was only detectable after MVA infection. The observed trends were similar irrespective of the transgenes carried by the respective vectors, indicating that insertion of IE-1 or pp65 has no major influence on the cytokine profile of transduced moDCs. Combined with the pronounced upregulation of maturation markers, these data indicate that transduction with Sendai vectors alone might be sufficient to induce full maturation of dendritic cells.

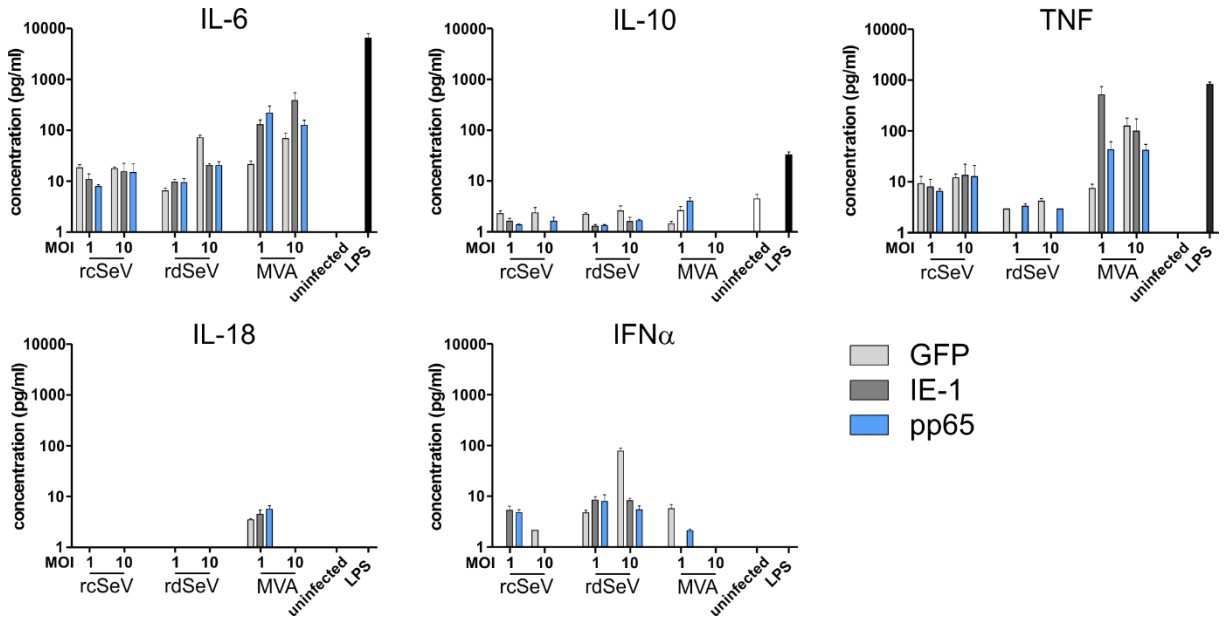

Figure 43 - SeV transduction induces secretion of IL-6 and IFN**α**
moDCs from 3 different, CMV seronegative blood donors were infected with either GFP, IE-1 or pp65 expressing vectors. 48 hours after infection, the presence of 13 different cytokines in the conditioned cell culture medium was assessed by a bead-based multiplex immunoassay. Uninfected cells that were untreated or stimulated with LPS (1 µg/ml) served as controls. Selected cytokine concentrations are depicted with bars representing the mean and standard error of the mean (SEM) of 3 measurements from the same donor (performed in one experiment). Levels were not reproducibly above the limit of detection for IL-1β, IFNγ, IL-12p70, IL-17A, IL-23 and IL-33, and no significant differences in secretion were detected for MCP-1 and IL-8 (data not shown).

Finally, it was tested if other immune cells besides DCs can be transduced by Sendai vectors for other potential gene delivery applications. Hence, rcSeV-GFP was used to infect human peripheral blood mononuclear cells (PBMCs) as a whole and the amount of GFP positive cells in different leukocyte populations was determined after 24 hours to identify permissive cell types (Figure 44). Except for B cells, all addressed subpopulations (NK cells, monocytes, $CD4^+$ and $CD8^+$ T cells) exhibited GFP expression, though to varying degrees. Since partial deletion of the P gene likely has no influence on target cell tropism, rdSeV is presumably capable of transducing these cells as well. Monocytes were transduced most efficiently, with approximately 80% of cells being GFP positive, followed by NK cells (50%) and T cells (20%) at MOI 10. Similar trends were observed at MOI 1 albeit with lower overall transduction rates. Since partial deletion of the P gene presumably has no influence on the cellular tropism of rdSeV, the obtained results are likely transferrable to this vector as well. These results suggest that Sendai virus could be a useful tool for transduction of a variety of immune cells.

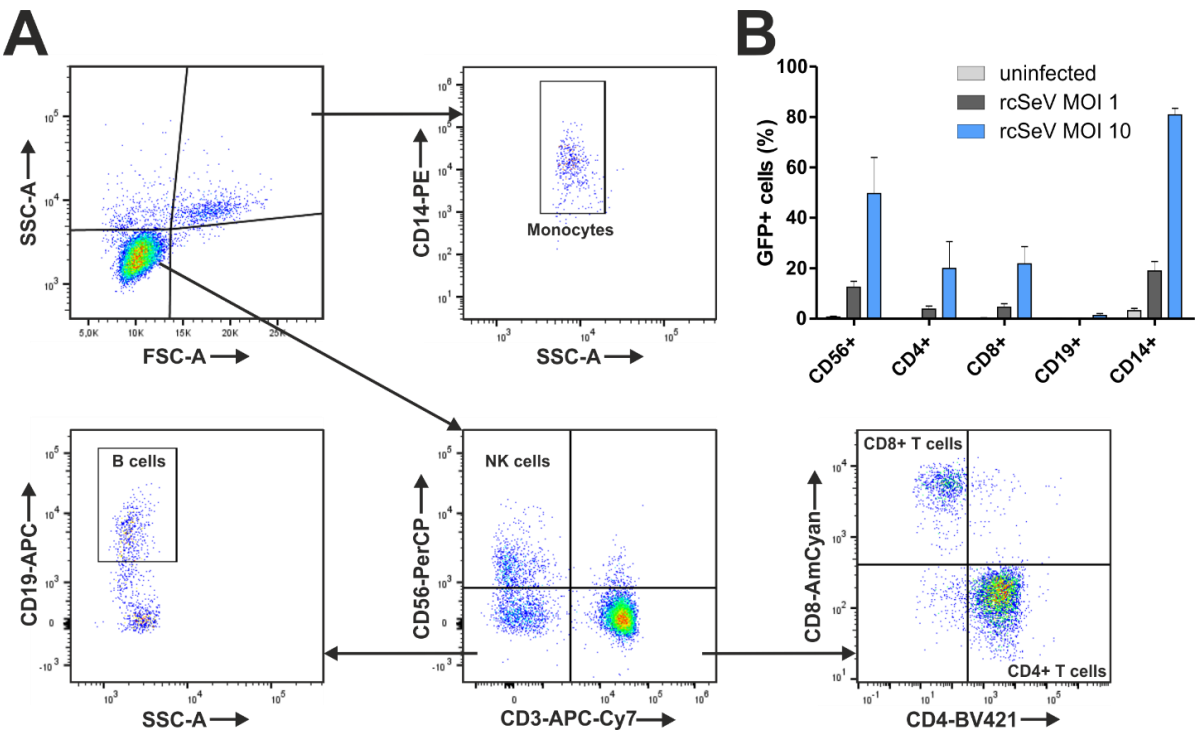

Figure 44 - SeV is capable of transducing T cells, NK cells and monocytes
(A) Gating strategy for discriminating different leukocyte populations. PBMCs from 3 different CMV seronegative blood donors were infected at MOI 1 or 10 with rcSeV-GFP. (B) 24 hpi, the amount of GFP positive cells in the indicated populations was determined by flow cytometry. Bars represent the mean and standard deviation (SD) of values from all donors.

V. Discussion

V.1. Carbamoylation enhances protein uptake into antigen-presenting cells

Quantification of CMV-specific T cells is considered a promising approach for identifying immunosuppressed patients at risk for CMV disease that would ideally allow very early initiation of antiviral therapy before the onset of viremia while avoiding unnecessary drug administration. Various methods are currently available for quantifying pathogen-specific T cells, all of which have advantages and drawbacks. Visualization of pathogen-specific T cells via fluorescently labeled MHC multimers (e.g. MHC-I tetramers, pentamers or streptamers[304]) allows fast detection of T cells, but their use in routine diagnostics is limited because i) the MHC complexes have to be matched with the HLA background of a given patient that is usually not known, ii) only pre-selected peptides can be assessed and iii) there is no information on the functionality of the detected T cells. Other methods trying to circumvent such limitations rely mainly on the stimulation of autologous cells (e.g. from whole blood or PBMC samples) with pathogen-derived antigens, followed by indirect detection of antigen-specific T cells via reactivation markers such as IFNγ. Reactivation can be measured for example via intracellular cytokine staining (ICS) and flow cytometry analysis[167], ELISpot[305] or ELISA based methods[306]. ICS allows co-staining with various additional markers and advanced phenotyping on a single cell level, but may be more difficult to implement in routine diagnostics since it requires costly flow cytometry devices along with the expertise to operate them. By contrast, ELISpot and ELISA based methods often require overnight culture of cells, but they can be used more easily in a diagnostic setting since the devices used for evaluating the results are less expensive and hardly require any special training. In addition, both ELISA and ELISpot methods offer very high sensitivity, compared to ICS and multimer staining[164,307,308]. Although, in contrast to ICS, the subset of cells producing IFNγ (e.g. $CD4^+$ cells, $CD8^+$ cells, NK cells) cannot be distinguished with these methods, ELISpot analysis permits quantification of IFNγ-producing cells. Moreover, the amount of marker released per cell can be estimated from the spot diameters. When using ELISA-based interferon-γ release assays (IGRAs) instead, only the total amount of IFNγ can be determined. Therefore, out of the currently available methods for T cell immune monitoring, ELISpot-based assays might offer the best balance between technical requirements, sensitivity and obtainable information.

In addition to the read-out assay, a suitable reagent for T cell stimulation has to be selected as well. The majority of assays that measure antigen-specific reactivation of memory T cells use either overlapping peptide pools (e.g. 15-mers) or recombinant proteins for stimulation[305,309,310]. Peptide pools allow sensitive restimulation of both $CD4^+$ and $CD8^+$ T cells, in part because they can simply replace peptides that are presented on the cell surface by

MHC complexes, thereby making cellular uptake, processing and MHC-loading unnecessary. However, the manufacturing process of peptide pools is costly and individual peptides differ with regard to solubility in aqueous solutions and long-term stability. As a result, it is difficult to predict if a given peptide within the pool is capable of being loaded onto MHC complexes. By contrast, recombinant proteins have to be taken up by APCs and subjected to the cellular antigen processing and presentation machinery, thus mimicking the natural antigen presentation process during CMV infection more closely. Moreover, in some cases, two distant parts of a protein can be excised and ligated together to form a novel peptide during processing of antigens by the proteasome[311]. This process is termed proteasomal peptide splicing and can generate unique MHC class I-restricted responses[312]. Although it was long presumed that proteasomal peptide splicing occurs only rarely, more recent work showed that it accounts for one-third of the entire HLA class I immunopeptidome in terms of diversity and one-fourth in terms of abundance[313]. Since spliced peptides are not accounted for in the design of peptide pools, the corresponding T cells are not addressed. Thus, using full-length proteins instead of peptide pools and allowing proteasomal processing might increase the sensitivity of T cell immune monitoring. *In vivo,* monocytes are a suspected site of CMV latency and therefore likely an important APC subset during viral reactivation[64]. Since monocytes are also the major APC population responsible for presenting pp65-derived peptides in PBMCs (Figure 23), antigen processing and presentation during CMV reactivation might be closely mimicked by the stimulation of PBMCs with recombinant proteins. In turn, this could increase the prognostic value of the detected responses. However, efficient protein uptake into APCs is critical for the sensitivity with which antigen-specific T cells are detected and the amount of cross presentation (i.e. MHC-I presentation of proteins taken up from the extracellular space) is likely rate limiting for the restimulation of $CD8^+$ T cells. Therefore, methods for enhanced antigen delivery to APCs are needed. To this end, protein carbamoylation might be a simple and cost-effective method for improving protein uptake into APCs and increasing both MHC-I and MHC-II presentation.

Out of the three proteins that were analyzed in this work, pp65 and BZLF1 showed increased restimulation of antigen-specific T cells as a result of carbamoylation (Figure 14). In addition, enhanced protein uptake (Figure 27), concomitant with increased MHC-I and MHC-II presentation (Figure 28) could be demonstrated for carb-pp65. The extent to which T cell restimulation was increased varied strongly from donor to donor, possibly because the maximum amount of T cells was already restimulated in some donors. However, this might also be the result of a tradeoff between increased protein uptake into APCs and impaired recognition of T cell epitopes due to the modification of lysines. Given that this modification not only results in the addition of a carbamoyl group, but also in the removal of positive charges from the ε-amino group of lysines, profound changes are introduced into affected epitopes that likely impair binding to MHC molecules or recognition by T cells specific for such peptides. According to this hypothesis, donors that hardly recognize any lysine-containing T cell epitopes would benefit most from carbamoylation, since antigen

uptake and presentation would be increased without T cell recognition being impaired. If, on the other hand, many lysine-containing epitopes elicit a dominant response within the T cell pool of a given donor, increased protein uptake into APCs would be less beneficial, since T cell recognition would be hampered at the same time. For instance, PBMCs from one donor reproducibly displayed reduced T cell reactivation rates when carbamoylated BZLF-1 was used for stimulation (Figure 14). It is possible that for this donor, BZLF1 recognition was dominated by epitopes containing lysine residues and that T cell recognition was impaired as a result of carbamoylation. Recent work from Rist *et al.* showed that T cell responses to BZLF1 tend to cluster at specific regions of the protein and that the lysine-containing peptide CRAKFKQLL (aa189-197) was recognized by numerous subjects despite expression of different HLA-alleles[314]. Although the HLA-background of the donor in question was not determined, immunodominant T cell responses to epitopes that are modified as a result of carbamoylation might explain the reduced restimulation rates. This could be investigated by mapping the BZLF-1 T cell response of this donor with a pool of overlapping peptides spanning the entire protein. If strong responses to a lysine-containing epitope are found, a modified version of the peptide with homocitrulline instead of lysine could be compared to the wild-type peptide with regard to T cell restimulation.

For IE-1, T cell responses were strongly reduced after carbamoylation. Again, this could be explained by carbamoylation-induced changes in the recognized epitopes, resulting in impaired T cell restimulation. Carbamoylation might have a more profound impact on IE-1 than on the other model proteins, because it contains a higher proportion of lysines (7.3%) compared to pp65 (3.9%) or BZLF1 (3.3%). Hence, alterations might have a higher chance of affecting critical T cell epitopes. It should also be pointed out that IE-1 displays a remarkably negative net charge even without any modifications (-34), compared to pp65 (-3) and BZLF1 (-7). Because for pp65, the carbamoylation-mediated increase in T cell stimulation can be reversed by the addition of fucoidan (Figure 20) and maleylation has a similar impact as carbamoylation (Figure 21), negative charges might play a critical role for the increased uptake of this protein into APCs. Thus, given its already very low isoelectric point, it is possible that cellular uptake of IE-1 cannot be increased significantly by the carbamoylation-mediated removal of positive charges. It is therefore possible that a negative impact of alterations in critical T cell epitopes outweighs increased protein uptake. *In silico* analysis of the electrostatic surface potential of IE-1 confirms that the surface of this protein is indeed dominated by negatively charged areas even without any modifications (Figure 45). To investigate if negative charges are also important for the uptake of unmodified IE-1 into APCs, fucoidan could be added to PBMCs prior to stimulation as previously performed for pp65 (Figure 20). Carbamoylation could also have other detrimental influences on IE-1 that might explain reduced T cell stimulation. For example, protein stability might be affected by the shift in net charge from -34 to -70 (assuming complete modification of lysines). However, storage of carbamoylated IE-1 over a period of several weeks at 4 °C was not associated

with reduced protein concentrations (data not shown), indicating that precipitation of IE-1 is an unlikely explanation for reduced T cell restimulation.

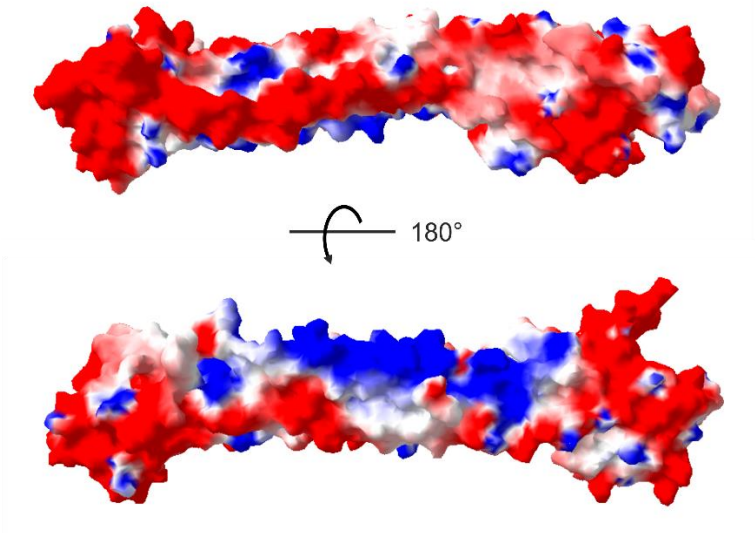

Figure 45 – The electrostatic surface of IE-1 is dominated by negative charges
The structure of the core domain of human IE-1 (amino acids 25-383 of 491 in total) was predicted with HHPred[315] using the recently published structure of rhesus cytomegalovirus IE-1[47] as a template. The electrostatic surface potential was calculated with the Poisson-Boltzmann Solvent Area method[316] using the program Swiss Pdb Viewer and mapped to the surface of human IE-1. Red patches indicate regions with negative electrostatic potential, blue patches display regions with positive electrostatic potential.

Whereas carbamoylation clearly altered the reactivation of antigen-specific T cells, the mere presence of urea during stimulation did not seem to have an impact on this (Figure 15). However, protein denaturation might also have an influence on protein uptake and presentation and should still be assessed separately. To detach a possible influence of denaturation from carbamoylation effects, other chaotropic reagents such as guanidine hydrochloride could be used instead of urea for inducing protein denaturation without eliciting carbamoylation at the same time.

Mass spectrometry measurements allowed quantitative analysis of the extent and localization of carbamoylation. Two separate methods were employed to address this, namely isotope dilution mass spectrometry (IDMS) and tandem mass spectrometry (MS/MS) analysis of pp65-derived peptides after GluC and AspN digestion. Results from both analysis techniques indicate a high degree of lysine carbamoylation. According to IDMS, KOCN treatment led to complete conversion of lysine residues to homocitrulline (Figure 17), whereas MS/MS analysis of peptides indicated that only 90% of lysines were carbamoylated (Figure 18). During IDMS, hydrolysis conditions first had to be determined under which pp65 was completely disassembled into single amino acids while carbamoyl groups were still present, a least to some extent. Isotopically labeled D_7-citrulline was spiked in for quantifying carbamoylated lysines and to measure the extent to which carbamoyl groups would be removed under given hydrolysis conditions. After incubation with 6M HCl at 115 °C for 20 h, total hydrolysis was achieved while at the same time, 20% of the initially added amount of D_7-citrulline was still detectable. From this, a factor was calculated to correct for homocitrulline (HCit) degradation during hydrolysis. Since compared to HCit, citrulline is shortened by one CH_2-group, the reactivity of the two carbamoyl groups is presumably similar, but not identical. Thus, it is possible that the amount of HCit hydrolysis was overestimated and that the true extent of carbamoylation is in fact lower. Still, from the obtained data it

can be concluded that the extent to which lysines are modified is at least 90%, and that arginine modification hardly occurs at all (0.3%) under the chosen KOCN treatment conditions. By extension, the N-terminus is very likely modified in a quantitative manner, since the α-amino group has an even higher nucleophilicity (pKa ≈ 9.2) than the ε-amino group of lysines (pKa ≈ 10.5). Although these results were obtained with pp65, the observed trends most likely hold true for the other model proteins as well.

The removal of positive charges lowers the net charge of a given protein, an effect that could be visualized by isoelectric focusing (Figure 16). Since for the majority of proteins, charged amino acids are mostly surface-exposed[317,318], removal of positive charges presumably enlarges areas which exhibit a negative electrostatic surface potential. Such clusters of negatively charged amino acids might be critical for the increased restimulation of antigen-specific T cells by carb-pp65. This is supported by the observation that addition of fucoidan as a negatively charged competitor reduced T cell restimulation rates when carb-pp65 was used for stimulation (Figure 20). At the same time, fucoidan had no impact on T cell reactivation when unmodified pp65 was used. This indicates that there might be two separate uptake mechanisms, one of which is largely independent of the electrostatic surface potential (e.g. macropinocytosis, phagocytosis, etc.) and another one which requires negative surface areas. Interestingly, one donor (#2) showed a trend for increased T cell restimulation for unmodified pp65 when fucoidan was added (Figure 20). Various immune-modulation effects have been described for fucoidan before, including promotion of antigen uptake into macrophages *in vitro*[274] and adjuvant properties like enhancement of DC maturation *in vivo*[319], possibly explaining increased T cell restimulation rates when using unmodified pp65. However, it is unclear why not all donors react to this reagent in the same manner. The finding that maleylation induces an increase in T cell restimulation that is similar to carbamoylation further shows that i) the added carbamoyl groups themselves are no structural requirement for increased uptake and that ii) removal of positive charges seems to be more important than the addition of negative ones. In line with this interpretation, the addition of 6 Asp and 6 Glu residues (6xDE) to the C-terminal end of pp65 did not result in increased T cell restimulation, compared to the wild-type protein (Figure 22). This indicates that the mere lowering of the isoelectric point is not sufficient for inducing increased protein uptake, but that further structural requirements, for example concerning the distribution of charges on the surface of a given protein have to be fulfilled as well. It is possible that the 6xDE-tag was folded in such a way that sterical hindrances precluded access by components mediating cellular uptake (e.g. receptors). Moreover, despite the exclusive presence of negative charges in this short sequence, the surface area of the tag could be too small for binding to a postulated interaction partner. It might be worthwhile to use model proteins where 3D structures are available for further attempts at inserting negatively charged amino acids in order to better predict the impact of such mutations on the electrostatic surface potential.

Using defined APC subsets instead of an inhomogeneous mixture of antigen-presenting cells as it is found in PBMCs, it was observed that carbamoylated pp65 is superior to its

unmodified counterpart in mediating restimulation of a pp65-specific T cell clone, irrespective of whether monocytes, macrophages or dendritic cells (Figure 25) were pulsed with the protein. Increased uptake of carbamoylated proteins is therefore not just confined to monocytes, which are the main APC population when stimulating PBMCs (Figure 23), but can be extended to other cell types as well. This implies a common uptake mechanism for carbamoylated pp65 into various APC subsets. Antigen presenting cells express a variety of membrane-bound scavenger receptors (SRs) belonging to the group of pattern recognition receptors (PRRs)[278]. Scavenger receptors recognize numerous modified-self- and non-self-ligands and carry out a remarkably wide range of functions including ligand uptake, transport of cargo within the cell, pathogen clearance and lipid transport[271]. This striking breadth in ligand interaction is not just attributable to the mere size of this family (more than 30 human SRs are currently known[320]), but also a result of promiscuous interactions with other co-receptors and recognition of structurally independent features such as negative charges. Although scavenger receptors are subdivided into various structurally unrelated subfamilies (termed A-L, not all of which are present in humans[320]), they often share very similar charge distributions within their binding domains. This is exemplified in Figure 46 for the class A member »macrophage receptor with collagenous structure« (MARCO) and class E member »lectin-like oxidized LDL receptor 1« (Lox-1). Cationic patches that are present in both domains despite no similarity in their primary sequence could explain why some scavenger receptors preferentially bind negatively charged ligands[271].

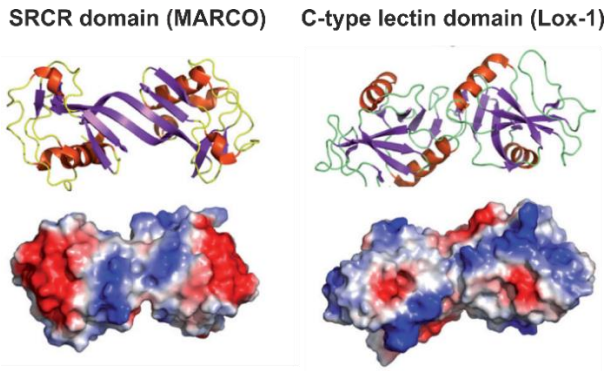

Figure 46 - Structural features of the ligand-binding sites of MARCO and Lox-1
Shown are the cartoon representation (top) and the electrostatic potential (bottom) of the scavenger receptor cysteine-rich (SRCR) domain (dimerized) of macrophage receptor with collagenous structure (MARCO) and the C-type lectin domain of lectin-like oxidized LDL receptor 1 (Lox-11). Red patches indicate regions of negative electrostatic potential, blue patches show regions of positive electrostatic potential. Figure from Canton et al.[271] adapted with permission from Nature Publishing Group (license number 4211240999780).

Indeed, the capacity of scavenger receptors to bind polyanionic ligands is well-established and has been described for various members, including SR-A1, CD36, MARCO and Lox-1[321–325]. In addition, the negatively charged polysaccharide fucoidan, which was used in this work as a competitor for the uptake of carb-pp65, binds scavenger receptors with high affinity as well[326]. It is therefore conceivable that the carbamoylation-mediated enlargement of negatively charged surface areas enables protein interaction with scavenger receptors, thus inducing increased cellular uptake and improved restimulation of antigen-specific T cells (Figure 47).

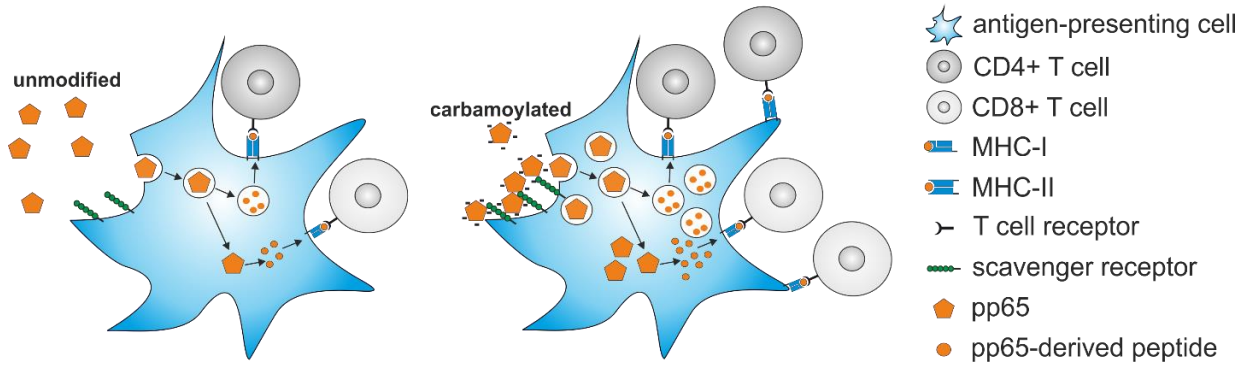

Figure 47 – Possible uptake of carb-pp65 via scavenger receptors
Unmodified pp65 can be taken up from the extracellular space via mechanisms such as phagocytosis or macropinocytosis. The removal of positive charges by carbamoylation presumably increases negatively charged areas on the surface of pp65. This might enable interaction with scavenger receptors, thereby enhancing protein uptake into APCs through additional receptor-mediated endocytosis.

Finally, neither immunization of mice with unmodified, nor with carbamoylated pp65 resulted in the induction of detectable T cell responses at all (Figure 29). As a result, no conclusions can be drawn from this experiment regarding the capability of carb-pp65 to induce T cell responses *in vivo*. To address this question in the future, a dose-escalation study should first be performed to identify the amount of pp65 required for induction of detectable T cell responses. Other model proteins that are commonly used and available in large quantities such as ovalbumin could also be tested instead of pp65. Further booster immunizations, different adjuvants or a heterologous prime/boost regimen (for example with DNA or the viral vectors described in IV.2) might be warranted as well to surpass the detection threshold. It is also possible that carb-pp65 induced T cell responses to homocitrulline-containing peptides that could not be quantified with sufficient sensitivity, since carbamoylated lysines were not present in the peptide pool that was used for restimulation of splenocytes. Moreover, it should also be assessed in further experiments if carbamoylation alters the quality or quantity of the elicited antibody response.

In summary, the data from this work lead to a model in which carbamoylation alters protein uptake into antigen-presenting cells due to the removal of positive charges. Although carbamoylation is therefore a simple method for increasing the sensitivity with which antigen-specific T cells are detected, this has further implications in other areas beyond T cell immune monitoring. For example, manipulation of the electrostatic surface potential of a given protein could also be used to enhance immunogenicity of protein-based vaccines *in vivo*. Instead of carbamoylation, other chemical modifications could be used to remove positive charges as well. Reversible modifications that are reverted at acidic pH could also be used to enhance protein uptake into APCs. Once endocytic vesicles containing modified proteins are acidified, the primary amino acid sequence would be restored and no immune responses would be induced to modified epitopes. Collectively, the data from this work indicates that it might be meaningful to take the electrostatic surface potential of a given protein into consideration when designing novel immunogens.

V.2. Ad19a/64 is an interesting alternative to Ad5 for Adenovirus-mediated gene delivery

Although Ad5 was repeatedly demonstrated to induce strong T cell responses in various animal models, it has so far proven difficult to overcome preexisting vector immune responses in humans[327]. Furthermore, results from a prophylactic HIV vaccine phase IIb efficacy trial (STEP trial), where the HIV antigens gag, pol and nef were delivered by Ad5 vectors, even showed increased side effects and higher susceptibility to HIV infection in individuals with high preexisting Ad5 antibody titers[328]. Moreover, subgroup C strains are also inefficient at transducing cells that lack CAR expression. These limitations have spurred the search for alternative AdV vectors in recent years. The subgroup D strain Ad19a/64 that was used as the vector backbone in this study could be a useful alternative to Ad5 due to considerably lower preexisting immunity to this virus in humans (>90% vs. 16 – 19%)[231,232] and because of its known receptor usage suggesting a broader target cell tropism. Ad19a/64 entry was previously described to be dependent on the presence of common sialic acids as well as the viral knob protein, although the exact binding motif has not been elucidated yet[236].

The broad tropism of Ad19a/64 was demonstrated by transgene expression in various leukocyte populations (Figure 32), with the highest transduction rates for monocytes and monocyte-derived dendritic cells[234]. By contrast, transduction of the tested leukocyte subpopulations with Ad5 was either unsuccessful or only achievable at very high MOIs for monocytes and moDCs. This is in accordance with poor or lacking CAR expression on most leukocytes[290]. CAR-independent infection of moDCs by Ad5 has also been reported previously and was suggested to rely on lactoferrin and DC-SIGN[329]. Nevertheless, compared to Ad19a/64, such alternative Ad5 entry pathways appear to be orders of magnitude less efficient in mediating the transduction of moDCs.

Compared to Ad5, both Ad19a/64 and MVA were rather efficient at inducing antigen expression in moDCs (Figure 33). While at low MOIs, MFI values were highest for MVA, peak values were higher for the AdV vectors. This might be explained in part by different promoters controlling transcription of GFP, IE-1 and pp65 since in both AdV vectors, the immediate/early promoter of CMV is used whereas for the MVA vectors, a poxviral synthetic early/late promoter was chosen[291]. At the same time, when using Ad5, much higher MOIs (100-1000-fold) were required for reaching MFI values that were comparable to Ad19a/64. Consistent with the observed DC transduction rates determined for IE-1- and pp65-expressing vectors, MVA was best at mediating T cell restimulation (particularly at low MOIs), followed by Ad19a/64 and, with some distance, by Ad5 (Figure 34). The same trends were observed for both antigens and minor variances between IE-1 and pp65 are likely explained by differences in peptide processing and presentation kinetics or T cell receptor avidities of the clones used. At MOI 100, the T cell restimulation rates were declining for MVA, a phenomenon that was hardly observed even at higher MOIs for the AdV vectors.

This reduction in T cell restimulation is probably a direct result of cytotoxicity, since the poxvirus strain was found to induce the highest amount of cell death (evident already at MOI 0.1, Figure 36). Since Ad19a/64 induced detectable cytotoxic effects only starting from MOI 100, the window in which transduction and antigen presentation take place without the induction of cell death appears to be larger for this vector than for MVA. Interestingly, cell death was not above background levels for the tested MOIs using Ad5, though this is likely not a feature of Ad5 in general, but rather due to inefficient entry into moDCs.

In accordance with previously published data, there was pronounced downregulation of maturation markers following MVA transduction starting from MOI 1 (Figure 35)[330]. At the same time, it was surprising that CD86 and HLA-DR were upregulated at MOI 0.1. Previous work by Pascutti *et al*. demonstrated that instead of MVA-infected DCs, uninfected bystander cells are increasing the expression of CD86 and HLA-DR, which could explain why upregulation was only observed at MOI 0.1[331]. The same markers were upregulated as a result of AdV transduction in a dose-dependent manner although the expression of CD80 and CD83 was largely unaltered. Thus, during *ex vivo* transduction of dendritic cells, it might be necessary to add additional activation stimuli such as IFNγ or a TLR agonist to induce full maturation of moDCs and boost their stimulatory capacity.

Finally, both Ad5 and Ad19a/64 were capable of transducing HeLa cells (which do express the CAR receptor[332]) at similar rates, with comparable protein levels being obtained at MOI 1000 (Figure 37B). Accordingly, cross-presentation by DCs co-cultivated with transduced HeLa cells did not differ significantly between the two AdV vectors (Figure 37C). In this experimental setting, the amount of antigen produced in HeLa cells seems to be the major determinant of subsequent T cell restimulation rates.

Taking these results together, Ad19a/64 could be a useful vector for the *ex vivo* delivery of immunogens to dendritic cells, since transduction, antigen expression and -presentation are superior to Ad5 while at the same time there is no interference with DC maturation, and cytotoxicity is clearly less pronounced than for MVA. The ability to transduce moDCs without inhibiting maturation or inducing apoptosis is a particularly beneficial vector characteristic, since dendritic cells presenting CMV antigens have great therapeutic potential for immunosuppressed patients such as transplant recipients. Currently, DCs pulsed with pp65 mRNA are even tested in clinical studies for the treatment of glioblastoma[190], where expression of CMV antigens is frequently detectable[188,189].

For more classical vaccination concepts, where intramuscular immunization is the most frequently used delivery route, muscle cells are presumably the main producers of antigen. Since it was previously demonstrated that in contrast to Ad5, Ad19a/64 is also capable of transducing myocytes with high efficiency, it is likely that secondary antigen uptake by dendritic cells will be higher *in vivo* when this vector is used[236]. At the same time, direct *in vivo* transduction of dendritic cells is also a feasible route for antigen delivery when using Ad19a/64 or MVA.

These results provide evidence that vectors based on Ad19a/64 are promising tools for the delivery of CMV antigens and that further in vivo testing of the described immunogens as vaccine candidates in appropriate animal models is warranted. Beyond that, the favorable vector characteristics of Ad19a/64 could also be exploited for other applications such as prophylaxis or treatment of other chronic infections associated e.g. with various tumor diseases as well as the delivery of tumor antigens for immunotherapy of cancer.

V.3. Attenuated SeV is a promising vector system for the delivery of antigens to dendritic cells

In recent years, four different vaccine concepts utilizing viral vectors for the delivery of CMV antigens have made it into clinical trials (reviewed in[192]): Of those, a vector based on MVA containing pp65, as well as an exon of IE-1 and IE-2 each (HCMV-MVA Triplex), is the only one currently being tested in phase II. The results from phase I, investigating safety and immunogenicity in a small cohort of healthy adults in a homologous prime/boost regimen, were recently published[193]. While strong and durable T cell responses were induced upon priming, the booster immunization hardly showed an additional benefit. At the same time, anti-MVA immunity was detectable. In a different setting, however, it was previously reported that immune responses elicited by the closely related vaccinia strain NYVAC could be increased in a heterologous prime/boost regimen employing a DNA prime, as compared to the NYVAC alone group[333]. Thus, it is likely that the immunogenicity of MVA could be improved upon by likewise combining it in a heterologous prime/boost regimen with secondary delivery modalities, such as the Sendai virus vectors described here.

Live attenuated virus vectors often pose residual health risks when administered as a vaccine, but usually exhibit superior immunogenicity compared to inactivated virions. Although SeV has as yet not been reported to cause disease in humans, clinical trials have so far only been conducted with healthy individuals. Thus, for immunocompromised individuals, which are the main target group for therapeutic CMV vaccines, higher safety measures might have to be implemented. In order to increase the safety of Sendai virus-based CMV vaccine candidates, a replication-deficient SeV strain with a partial deletion of the P gene was chosen. This deletion interrupts the interaction between the viral P- and N proteins and, as a consequence, renders the viral RNA-dependent RNA polymerase (vRdRp) incapable of switching from mRNA synthesis (using the negative-strand viral RNA genome as template) to the *de novo* production of (-)-strand viral genomes from viral (+)-mRNAs[298]. It was demonstrated in the present study that human dendritic cells are permissive for replication of SeV (Figure 38), which underlines the requirement for further attenuation to limit proliferation during a state of immunosuppression *in vivo.* In this regard, the N-terminal truncation of the phosphoprotein already proved to be sufficient to inhibit the generation of viral progeny upon infection of DCs (Figure 38). Yet, after entry of rdSeV into a cell, mRNA synthesis (boosting RNA copy numbers in the cell) as well as protein translation still take place, thus preserving the advantages of live attenuated vectors to some extent.

Although transgene expression is initiated in moDCs after SeV infection, the overall amount of protein was markedly reduced when using rdSeV compared to the parental strain (Figure 39). Although reduced mRNA synthesis as a result of partial P deletion has been observed before, the underlying molecular mechanism has not been elucidated yet[334]. This might be explained by the inability of the vRdRp complex from rdSeV to switch to genome replication. During infection with wild-type SeV strains, newly generated genome copies could serve as

additional templates for subsequent rounds of mRNA synthesis, thereby amplifying overall gene expression. Importantly, despite decreased transgene levels, restimulation of antigen-specific T cells was hardly affected, which is in accordance with previously published data suggesting that the intracellular quantity of a given immunogen is not connected to the amount of MHC-presentation on the cell surface[335].

All vectors that were compared in this study caused cell death in an MOI- and, with the exception of rdSeV, time-dependent manner (Figure 41). It is possible that cells which were negative for cell death markers after 24 hours initially remained uninfected and that secondary infections by newly released virions, concomitant with induction of apoptosis, account for the increase in dying cells between 24 and 48 hours. Because MVA was previously reported not to produce viral progeny in moDCs[336], such an effect is only conceivable for replication-competent SeV, which might explain why the proportion of dead cells remained constant over the observed time period for rdSeV. Information on the duration of Paramyxovirus replication in cell culture is scarce[1], but viral titers were above the baseline level already at 24 hours after infection of moDCs with rcSeV (Figure 38C), showing that the replication cycle can be completed in this time frame. Thus, one or more rounds of infection would be possible within 48 hours. Nevertheless, an increase in dead cells over time was also evident for the replication-competent vectors at higher MOIs (10 and 100). Under these conditions, few cells should initially remain uninfected, which indicates that replication-deficiency alone is an unlikely explanation for the reduced cytotoxicity of rdSeV. The discrepancy might also be explained by the different patterns of cytokines released after infection with the different vectors. For instance, secretion of TNF, a potent inducer of cell death[337], could be the cause of the toxicity observed here. In fact, the amounts of TNF produced upon infection mirror the degree of toxicity of the three vectors.

Priming of T cells *in vivo* requires a finely tuned combination of signals from dendritic cells, the main constituents of which are (i) MHC-presentation of a given peptide, (ii) presence of co-stimulatory molecules on the DC surface and (iii) cytokine secretion[338]. Already at low MOIs, $CD8^+$ T cell clones were efficiently restimulated by moDCs after transduction with all vectors tested, indicating no major viral interference with the antigen processing- and presentation-machinery. However, the restimulatory capacity of MVA-transduced DCs was diminished at higher MOIs, a phenomenon that was not observed for the SeV vectors and which may be linked to the higher cytotoxicity of the poxvirus strain. Reduced T cell stimulation by MVA may also be the result of a noticeable downregulation of costimulatory receptors from MOIs 1 to 100 as part of a previously described immune evasion mechanism[330]. By contrast, maturation markers tended to be upregulated in an MOI-dependent manner by both SeV vectors with only few exceptions, which is in accordance with findings by other groups describing Sendai virus as a potent inducer of DC maturation[339,340]. However, it was striking that upregulation of maturation markers after SeV infection was gen-

erally less pronounced for IE-1-expressing vectors compared to their pp65-containing counterparts, with CD83 even being downregulated to some extent. During CMV infection, IE-1 plays a central role in suppressing various innate immune response pathways (reviewed in[39]) and may therefore also counteract DC maturation when expressed by heterologous vectors. The immediate-early protein IE-2 of CMV was recently found to induce proteasomal degradation of CD83[341], an immune evasion strategy that is similarly employed by other Herpesviruses such as HSV-1[342]. Since IE-1 and IE-2 are alternative splicing products from the same gene locus with the first 85 amino acids being identical due to the shared usage of two exons, it is conceivable that IE-1 could likewise be capable of inducing CD83 degradation. Such detrimental influences on DC maturation and function may be avoided by using a functionally inactivated IE-1 protein as previously proposed by Tang and colleagues[343]. Irrespective of a given transgene, SeV-transduced DCs might indeed be capable of priming T cell responses without the need for further components (like adjuvants) when taking into account that in addition to antigen presentation and DC maturation, the Sendai vectors are also capable of inducing secretion of proinflammatory cytokines such as IL-6 and IFNα.

Finally, SeV was also found to exhibit a broad target cell tropism. In addition to human moDCs, T cells, NK cells and monocytes are efficiently transduced by Sendai virus as well. This opens up a variety of possible gene delivery applications in basic research and gene therapy.

In conclusion, the favorable immunological characteristics of Sendai virus in combination with the enhanced safety profile of rdSeV, emphasize the potential of this vector system, thus warranting further testing of SeV as vaccine platform in general and as a CMV vaccine candidate in particular.

VI. Materials and methods

Unless noted otherwise, all chemicals were purchased from Sigma and Merck, cell culture flasks and general plastic material from BD Falcon, Sarstedt and Eppendorf.

VI.1. Cell culture techniques

Insect cell lines were cultivated at 26 °C, mammalian cells were cultured at 37 °C and 5 % CO_2. Handling of cells was performed under sterile conditions in class II laminar flow hoods. Before reaching full confluence, adherent cells were split 1:10 by washing them with PBS, incubation with Trypsin-EDTA for 3 minutes and resuspension in culture medium. Suspension cells were kept within the desired density range by replacing a suitable volume of the culture with fresh medium. Once a week, suspension cells were centrifuged at 100 xg for 10 minutes. The supernatant was discarded and the cell pellet was resuspended in a suitable amount of fresh culture medium. Cells concentrations were determined by mixing an aliquot of the cell suspension 1:1 with trypan blue (for visualizing dead cells) and counting living cells in a hemocytometer.

Medium/Reagent	Supplier	Additives
Phosphate buffered saline (PBS)	Sigma-Aldrich	none
Penicillin/Streptomycin (Pen/Strep)	Pan Biotech	none
Fetal calf serum (FCS)	Sigma-Aldrich	none
TC-100 insect medium	Thermo Fisher	10% FCS, 1% Pen/Strep
RPMI	Pan Biotech	10% FCS, 1% Pen/Strep
Ultraculture	Lonza	1% Pen/Strep
DMEM	Thermo Fisher	10% FCS, 1% Pen/Strep
Insect Xpress	Lonza	1% Pen/Strep

Cell line	ATCC#	Growth	Culture medium
BHK-21	C-13	adherent	DMEM
Hek293T	CRL-3216	adherent	DMEM
HeLa	CCl-2	adherent	DMEM
High Five	n.a.	suspension	Insect Xpress
Peripheral blood mononuclear cells (PBMCs)	n.a.	semiadherent	UltraCulture
Primary monocytes	n.a.	adherent	RPMI
SF9	PTA-3099	adherent	TC-100
THP-1	TIB-202	adherent	RPMI
T cell clones	n.a.	suspension	RPMI

VI.2. Baculovirus expression system

The proteins pp65, IE-1, BZLF1, pp65-6xDE, and GFP-pp65 were produced in insect cells after infection with recombinant baculovirus strains. Bacmids containing the respective genes were first generated by site-specific recombination in *E. coli* cells, followed by generation of recombinant baculovirus strains via transfection of SF9 cells with the purified viral genomes. For large-scale protein production, High-Five cells were infected with the newly generated baculovirus strains and proteins were purified via affinity chromatography.

VI.2.1. Bacmid generation

Recombinant baculovirus strains were generated using the bac-to-bac baculovirus expression system from Thermo Fisher[344]. First, the gene of interest (IE-1, pp65, BZLF1, pp65-6xDE or GFP-pp65) was inserted into the multiple cloning site (MCS) of the transfervector pFAST-Bac-T1 by standard molecular cloning techniques[345] via the EcoRI and KpnI restriction sites. Correct insertion of the gene-of-interest and absence of mutations was confirmed by Sanger sequencing. Plasmid DNA from sequence-verified clones was prepared via alkaline extraction, followed by isopropanol precipitation[346]. Chemically competent DH10Bac cells (200 µl) were thawed on ice and 15 ng of plasmid DNA were added, followed by 30 min of incubation on ice. Cells were heat-shocked by incubation in a 42 °C water bath for 45 seconds. Next, cells were cooled on ice for 2 min, followed by addition of 1 ml of lysogeny broth (LB) medium and incubation at 37 °C for 4 hours while constantly shaking the suspension at 220 rpm. 100 µl of the suspension were then plated on LB agar plates containing kanamycin (50 µg/ml), gentamycin (10 µg/ml), tetracycline (10 µg/ml), IPTG (40 µg/ml) and Bluo-Gal (100 µg/ml). Plates were incubated for 48 h at 37 °C, after which time white colonies were picked and streaked onto new LB agar plates containing the same additives. After incubating these plates for 48 h at 37 °C, several white colonies were again picked and subjected to colony PCR analysis using the primers M13fwd and M13rev as well as the GoTaq Green Master Mix kit according to the manufacturer's instruction. Clones that were positive for bacmids with a transgene insertion could be distinguished from parental bacmids via the amplified DNA sequence (2300 bp + the transgene size vs. 300 bp). Bacmid DNA was again isolated by alkaline extraction, followed by isopropanol precipitation.

Reagent	Supplier
pFastBac-T1 (plasmid)	Thermo Fisher
E. coli DH10Bac cells (chemically competent)	Thermo Fisher
Ampicillin	Sigma–Aldrich
Kanamycin	Sigma–Aldrich
Gentamycin	Sigma–Aldrich
Tetracycline	Sigma–Aldrich
Isopropyl-β-D-thiogalactopyranosid (IPTG)	Sigma–Aldrich

5-bromo-3-indolyl β-D-galactopyranoside (Bluo-Gal)	Biomol
GoTaq Green Master Mix	Promega

Primer	Sequence (5'-3')
M13fwd	GTTTTCCCAGTCACGAC
M13rev	CAGGAAACAGCTATGAC

Medium	Composition
Lysogeny broth (LB)	0.5% (w/v) yeast extract, 1% (w/v) tryptone, 1% (w/v) NaCl

VI.2.2. Transfection of insect cells with recombinant bacmids

$9x10^5$ SF-9 cells were seeded in a volume of 1.4 ml into each well of a 6-well plate, followed by+ incubation at 26 °C for 2 hours. For transfection of insect cells, the Effectene transfection kit (Qiagen) was used according to the manufacturer's instructions: 0.8 µg of bacmid DNA were diluted in 100 µl buffer EC. After addition of 6.4 µl enhancer, the suspension was briefly vortexed and incubated at room temperature (RT) for 5 min. Next, 20 µl of Effectene were added and after thorough vortexing (≥ 10 sec), the mixture was incubated at RT for 10 min. 600 µl of TC-100 medium were mixed with the suspension and added to the cells by evenly distributing small droplets over the plate area. Cells were incubated at 26 °C until they showed signs of viral infection as determined by visual inspection (3-6 days), including cell and nuclear enlargement or the formation of polyhedra. Baculoviruses were then harvested by transferring cells and culture medium into a new tube and centrifuging the suspension at 500 xg for 5 min. The supernatant, representing the P1 virus stock, was transferred into a new tube and stored at 4 °C until further use.

For generation of high titer virus stocks, $1x10^7$ SF9 cells in 30 ml TC-100 medium were seeded into a T175 cell culture flask and after 2 hours of incubation at 26°C, 500 µl of the P1 stock were added. When cells appeared thoroughly infected (3-4 days post infection), cells and medium were transferred into a 50 ml conical tube and centrifuged for 10 minutes at 500 xg and the supernatant (P2-stock) was stored at 4 °C until further use (up to 3 months).

VI.2.3. Infection of High Five cells

High Five cells were held in suspension culture at a density between $3x10^5$ and $2.5x10^6$ cells per ml. For small scale cultures (40 ml), cells were cultivated in 125 ml Corning Erlenmeyer plastic flasks (Sigma-Aldrich) whereas for large scale cultures (300 ml), 1 l flasks were used. Cultures were constantly rotated on horizontal shakers at 140 rpm (40 ml cultures) or 100 rpm (300 ml cultures). For infection with recombinant baculoviruses, an exponentially growing culture (viability ≥ 90% as determined by trypan blue staining) was set to a density of $1x10^6$ per ml and after 2 hours, the desired amount of virus suspension was added. The

added volume of virus suspension (P2 stock) was chosen in such a way that infected cells would stop dividing after 48 hours. The required amount of virus to reach the day of proliferation arrest (dpa) after 48 hours was determined separately for the P2 stock of each baculovirus strain: in preceding experiments, various small scale cultures were infected with different dilutions of the P2 stocks and cell growth was assessed by daily counting of cells on a hemocytometer. After 3 days, cells were harvested by transferring cultures to 50 ml conical tubes that centrifuged for 5 min at 1000 xg and 4 °C. The supernatant was discarded and cell pellets were stored at -20 °C until protein purification (section VI.3.2).

VI.3. Protein biochemistry techniques

VI.3.1. Bradford assay

Protein concentrations were determined via the Bradford assay[347]. Proteins solutions were stained using Bradford reagent (Biorad) according to the manufacturer's instructions. Samples were measured in triplicates and mean values were calculated. Dilutions of a bovine serum albumin (BSA) stock solution with known concentration were used for generating a calibration line, thus allowing protein quantification. Data acquisition was performed with a 680 microplate reader (Bio-Rad) and the endpoint of the colorimetric reaction was measured at 595 nm.

VI.3.2. Protein purification from insect cells

During purification of recombinant proteins via affinity chromatography, all solutions and buffers were precooled on ice. Likewise, samples were handled on ice and centrifuged at 4 °C. At relevant steps during purification, aliquots were collected and stored at -20 °C until further analysis.

The frozen pellets (each one corresponding to 50 ml of initial cell culture volume) of baculovirus-infected High Five cells (section VI.2.3) were thawed and resuspended in 40 ml PBS, followed by centrifugation at 1000 xg for 5 min. The supernatant was discarded and cells were resuspended in 20 ml lysis buffer supplemented with 1 tablet cOmplete™ ULTRA Mini Protease inhibitor. The suspension was then incubated on an end-over-end shaker for 30 min at 4 °C. Next, cells were subjected to ultrasound treatment by dipping the suspension into the macrotip of a Branson Sonifier 450 device (output control: 5.5, duty cycle: 80%, converter 102-C, 1/8) in 6 one-minute intervals with 1 minute of incubation on ice between pulses. The suspension was then incubated for another 15 min on an end-over-end shaker at 4 °C, followed by centrifugation at 4.000 xg for 30 min. The supernatant was transferred into a new 50 ml conical tube, 2 ml of resuspended Ni-IDA-beads (50% suspension) were added to each sample and the suspension was mixed on an end-over-end shaker for 2 h at 4 °C. Cells were then centrifuged for 5 min at 1000 xg and the supernatant was replaced with 40 ml wash buffer. After one repetition of this washing step, the suspension was

transferred to a disposable 5 ml column. The beads were then washed on the column by adding a total of 40 ml wash buffer, with the flow-through being discarded.
For BZLF1 and GFP-pp65 (where the His/Strep tandem tag was not cleaved), the protein was eluted after this step by adding 2 ml elution buffer, followed by 1 ml and then 3x 500 µl of the same buffer (the flow through was collected at each step). Fractions with sufficient protein concentrations were pooled, sterile-filtered (filter pore size 0.45 µm), frozen in liquid nitrogen and stored at -80 °C until further use.
For the remaining proteins (pp65, IE-1 and pp65-6xDE), the column was locked after the washing steps and 2 ml elution buffer were added along with 60 U Prescission Protease. The column was then incubated overnight on an end-over-end shaker at 4 °C. The next day, the columns were opened and the flow through was collected. Additionally, 1 ml and then 3x 500 µl elution buffer were added to the beads with the flow through being collected at each step. Fractions with sufficient protein concentrations were pooled. 800 µl glutathione Sepharose and 1200µl Strep-Tactin Sepharose were added to a new disposable 5 ml column and washed with 10 ml wash buffer. The pooled elution fractions were then added to the column (which was locked) and the bead suspension was incubated on an end-over-end shaker for 4 h at 4 °C. The columns were opened and the flow through was collected. Additionally, 1 ml and then 3x 500 µl elution buffer were added to the beads with the flow through again being collected at each step. Suitable fractions were pooled, sterile-filtered (filter pore size 0.45 µm), frozen in liquid nitrogen and stored at -80 °C until further use.

Reagent/Consumable	Supplier
cOmplete™ ULTRA Mini Protease inhibitor	Roche
dithiothreitol (DTT)	Sigma-Aldrich
Ni-IDA beads	Carl Roth
Glutathione Sepharose	GE Healthcare
Strep-Tactin Sepharose	IBA Lifesciences
Pierce™ Disposable Columns, 5 mL	Thermo Fisher
Pierce™ Prescission Protease	Thermo Fisher

Buffer	Composition
Lysis buffer	50 mM NaH_2PO_4, 300 mM NaCl, 10 mM imidazole, 0.5% (v/v) Tween-20, 1 mM DTT, pH to 8.0 with NaOH
Wash buffer	50 mM NaH_2PO_4, 300 mM NaCl, 20 mM imidazole, 0.05% (v/v) Tween-20, pH to 8.0 with NaOH
Elution buffer	50 mM NaH_2PO_4, 300 mM NaCl, 250 mM imidazole, 0.05% (v/v) Tween-20, pH to 8.0 with NaOH

VI.3.3. SDS-PAGE

Proteins were separated according to their size in sodiumdodecylsulfate-polyacrylamide gel electrophoresis (SDS-PAGE)[348]. Protein solutions were mixed with 5x Laemmli buffer and incubated at 95 °C for 5 minutes. Samples were then loaded onto a 10% or 12.5% SDS gel

and electrophoresis was performed. PageRuler™ Prestained Protein Ladder served as a standard for estimating the size of the proteins assessed.

Reagent	Supplier
PageRuler™ Prestained Protein Ladder	Thermo Fisher

Buffer	Composition
1x Laemmli buffer	62.5 mM Tris; 1% (w/v) SDS; 5% (v/v) β-Mercaptoethanol; 0.5 mM EDTA; 5% (v/v) glycerol; 0.005% (w/v) bromophenol blue; pH 6.8

VI.3.4. Coomassie staining

After electrophoresis, SDS gels were incubated for 15 minutes in Coomassie staining solution. Gels were then destained by incubation with 5% acetic acid until protein bands were clearly visible.

Reagent	Supplier
Coomassie Brilliant Blue R-250	AppliChem

Buffer	Composition
Coomassie staining solution	1.25% (w/v) Coomassie Brilliant Blue R-250, 50% (v/v) ethanol, 7% (v/v) acetic acid

VI.3.5. Western blot analysis

Proteins separated by SDS-PAGE were transferred to a nitrocellulose membrane (pore size: 0.45 µm) via Western blot using a semi-dry blotting device (Serva Electrophoresis) according to the manufacturer's instructions (1.5 mA/cm² membrane for 1 hour). For saturating all protein binding spots on the membrane after blotting, it was incubated with 5% MTBS for at least one hour or overnight. Immunostaining was performed by washing the membrane 3 times with TTBS before incubation with the primary antibody (which was diluted in TBS) for 1 hour. After another 3 washing steps with TTBS, the membrane was incubated for 1 hour with the HRP-conjugated secondary antibody. Last, the membrane was subjected to 3 more washing steps and substrate solution was added. After 5 minutes, the substrate solution was removed and signals were detected with a ChemiluxPro device (Intas).

Buffer	Composition
TBS	50 mM Tris/HCl pH 7.5; 150 mM NaCl
MTBS	50 mM Tris/HCl pH 7.5; 150 mM NaCl; 5% (w/v) non-fat dried milk powder
TTBS	50 mM Tris/HCl pH 7.5; 150 mM NaCl; 0.05% (v/v) Tween-20
Substrate solution	100 mM Tris/HCl pH 8.5; 12.5 mM luminol; 1.98 mM coumaric acid; 610 µl/l 30% H_2O_2

Primary antibody	Supplier	Cat-#	Dilution
goat anti GST	Biomol	100-101-200	1:1000
mouse anti His	Thermo Fisher	MA1-21315	1:1000
mouse anti Strep	Qiagen	34850	1:1000
mouse anti pp65	Abcam	ab53489	1:1000
mouse anti IE-1	Abcam	ab30924	1:1000
mouse anti BZLF1	Santa Cruz	sc-53904	1:500
rabbit anti GFP	Santa Cruz	sc-8334	1:2000

Secondary antibody	Supplier	Cat-#	Dilution
anti mouse HRP	Dianova	115-036-003	1:5000
anti goat HRP	Dako	P0449	1:1000
anti rabbit HRP	Dako	P0448	1:5000

VI.3.6. Silver staining

After electrophoresis, the SDS gel was incubated for 1 h in fixation solution (the amount of each solution added was sufficient to cover the gel completely). The gel was then incubated for 10 min with 50% EtOH and afterwards for another 10 min with 30%. Next, the gel was incubated for 1 minute with sodium thiosulphate solution (0.2 g/l) and then washed three times with H_2O. The gel was then incubated for 20 min with staining solution, followed by another three washing steps with H_2O. After removal of H_2O, developing solution was added and when bands were sufficiently distinct (5-10 min), the reaction was stopped by incubating the gel for 5 min with 5% acetic acid. Finally, the gel was washed twice with H_2O.

Buffer	Composition
fixation solution	50% methanol, 12% acetic acid, 50 µl formaldehyde (37% stock)/100 ml
staining solution	0.1% (w/w) $AgNO_3$, 75 µl formaldehyde (37% stock)/100 ml
developing solution	6% (w/w) Na_2CO_3, 50 µl formaldehyde (37% stock)/100 ml, 0.4 mg/l sodium thiosulfate

VI.3.7. Posttranslational modification

Protein samples (stored in elution buffer, see section VI.3.2) were diluted 1:10 with a 3 M stock solution of KOCN (for inducing carbamoylation) or a 300 mM stock solution of maleic anhydride (for inducing maleylation; both chemicals were dissolved in sodium phosphate buffer). Samples were then incubated at 35 °C for 24 hours. Afterwards, residual KOCN or maleic anhydride were removed via extensive dialysis to sodium phosphate buffer at 4 °C using the Pur-A-Lyzer™ Midi Dialysis Kit according to the manufacturer's instructions.

Reagent/Consumable	Supplier
KOCN	Sigma-Aldrich

Maleic anhydride (99%)	Sigma-Aldrich
Pur-A-Lyzer™ Midi Dialysis Kit MWCO 6-8kDa	Sigma-Aldrich

Buffer	Composition
sodium phosphate buffer	50 mM NaH_2PO_4, 300 mM NaCl, 1 mM DTT, pH 8.0

VI.3.8. Fluorescence analysis

For measuring the fluorescence intensities of GFP-pp65 and carb-GFP-pp65, the protein solutions were diluted to the desired concentration in PBS and transferred into an uncoated 96 well plate. Data was acquired at room temperature on a Victor3 multilabel plate reader (Perkin Elmer) with the following settings: excitation at 485 nm (CW lamp energy 12600), emission filter F535, measurement time 1 s.

VI.3.9. Isoelectric focusing

Isoelectric focusing was performed with the SERVAGel IEF 3-10 starter kit (Serva): 1-3 µg of protein were diluted with 2x loading buffer and loaded onto a precasted gel that was included in the kit. Electrophoresis was performed for 60 min at 50 V, followed by 2 h at 200 V. Afterwards, silver staining (section VI.3.6) was performed for visualizing bands.

VI.3.10. Carbamoyl-ELISA

Protein samples with varying concentrations (ranging from 100 ng/µl to 1 µg/µl) were diluted 1:100, 1:1.000 and 1:10.000. 100 µl per sample and dilution were added to a Nunc MaxiSorp flat-bottom 96 well plate. To determine the linear range of the assay, a BSA sample (1 µg/µl) that was carbamoylated according to the procedure described in section VI.3.10 was diluted in 1:10 steps from 100 ng/µl to 0.001 ng/µl and 100 µl of each dilution were added to the plate as well. The samples were then incubated overnight at 4 °C. Next, the plate was washed three times with 200 µl PBS-T and the supernatant was discarded. All washing steps were performed with a HydroFlex plate washer device (Tecan). 150 µl of blocking buffer were added to each well and the plate was incubated at RT on an orbital shaker (100 rpm) for 2 hours. Again, the plate was washed three times with 200 µl PBS-T and the supernatant was discarded. 100 µl of primary antibody solution were added to each well and the plate was incubated at RT on an orbital shaker (100 rpm) for 1 hour. The plate was then washed six times with 200 µl PBS-T, the supernatant was discarded and 100 µl of secondary antibody solution were added, followed by incubation on an orbital shaker (100 rpm) for 1 hour at RT. Finally, the plate was washed 10 times with 200 µl PBS-T, the supernatant was discarded and 100 µl of TMB substrate (TMB A and TMB B were mixed shortly before), were added to each well. After 90 sec of incubation, the reaction was stopped by adding 50 µl of 1 M H_2SO_4 to each well and mixing thoroughly. Data acquisition was performed with a 680 microplate reader (Bio-Rad) and the colorimetric reaction was

measured at 450 nm. Only dilutions that were within the linear range of the assay were used for further analysis (Figure 13).

Consumable	Supplier
Nunc MaxiSorp® flat-bottom 96 well plate	Thermo Fisher

Buffer	Composition
Blocking buffer	5 % (w/w) BSA in PBS, 1mg/ml NaN_3
PBS-T	0.05% (v/v) Tween-20 in PBS
TMB A	30 mM tri-potassium citrate-monohydrate, pH 4.1 with 10% (w/v) citric acid
TMB B	0.24% (w/v) TMB, 10% (v/v) acetone, 90% (v/v) ethanol, 80 mM H_2O_2
TMB substrate	TMB A and TMB B mixed in a 20:1 ratio

Antibody	Supplier	Cat#	dilution
Anti Carbamyl-lysine antibody	Abcam	ab175135	1:1000
Anti goat HRP secondary antibody	Abcam	ab6741	1:1000

VI.4. Mass spectrometry analysis

VI.4.1. LC-MS analysis of amino acid composition

The carbamylated pp65 protein was subjected to amino acid analysis and the extent of HCit formation was determined by comparing the HCit concentration with the concentrations of Phe, Val, and Pro (as surrogates for the total protein concentration). The method was based on double isotope dilution mass spectrometry as described previously[349–351]. In short, the same amounts of isotopically labeled Phe, Pro, Val as well as D_7-Cit[269] were added to the protein sample and to a reference solution containing the pure amino acids in their natural isotope forms as well as HCit. Sample and reference were treated equally and the peak area ratios of natural to labeled amino acids were determined in both solutions und used for amino acid quantification. After adjusting the peak area ratios to unity in a pre-experiment, three protein samples (12 µg in 5 mM ammonium acetate) and one reference were processed as follows: Each solution was transferred to a 5 mL vacuum hydrolysis tube (Pierce) and dried in a stream of nitrogen. Subsequently, 400 µl 6 mol/l hydrochloric acid supplemented with 0.1 % (w/v) phenol were added, the liquid was frozen in liquid nitrogen and the tubes were evacuated. Hydrolysis was performed at 115 °C for 20 h. After drying in a stream of nitrogen, reconstitution was performed in 1 ml 80 % acetonitrile/5 mM ammonium acetate pH 3.6 (v/v). LC-MS analyses were performed using a HP series 1100 HPLC interfaced with a HP Series 1100MSD G1946A mass spectrometer (G1314A binary pump, G1313A autosampler, both Agilent Technologies). Amino acids were separated on a Thermo Accucore HILIC column (150 x 2.1 mm, 2.6 µm) (Thermo Fisher) at 25 °C with a flow rate of 0.4 ml/min. 2 µl were injected to quantify natural and labeled Phe (m/z

166.1/176.1), Pro (m/z 116.1/122.1), and Val (m/z 118.1/124.1), whereas 10 µL were injected to quantify HCit/D_7-Cit (m/z 190.1/183.2) (ion traces given in parentheses). Isocratic elution was performed with 80 % acetonitrile/5 mM ammonium acetate pH 3.6 (v/v) over 10 min. Detection was performed in positive-ion mode, and the electrospray ionization (ESI) source parameters were as follows: 4.0 kV spray voltage, 350 °C drying gas temperature, 13 l/min drying gas flow, and 30 psig nebulizer pressure.

Reagent	Supplier
L-phenylalanine-$^{13}C_9/^{15}N$ (≥ 98 %)	Fluka
L-proline-$^{13}C_5/^{15}N$ (≥ 98 %)	Fluka
L-valine-$^{13}C_5/^{15}N$ (≥ 98 %)	Fluka
L-phenylalanine-$^{13}C_9/^{15}N$ (≥ 98 %)	Cambridge Isotope Laboratories, Inc.
L-proline-$^{13}C_5/^{15}N$ (≥ 98 %)	Cambridge Isotope Laboratories, Inc.
L-valine-$^{13}C_5/^{15}N$ (≥ 98 %)	Cambridge Isotope Laboratories, Inc.
homocitrulline (≥ 98.7 %)	Bachem
2,3,3,4,4,5,5-D_7-L-citrulline (D_7-Cit) (≥ 98%)	CDN Isotopes
ammonium acetate (p.a.)	Fluka

VI.4.2. MS/MS analysis of pp65-derived peptides

0.16 % Rapigest SF (w/v) was added to 16 µg carbamylated pp65 protein in 100 mM sodium phosphate pH 7.8 yielding a final Rapigest SF concentration of 0.1 % (w/v) for enzymatic digestion. The sample was reduced by 5 mM TCEP at 37 °C for 45 min and alkylated with 15 mM IAA at 25 °C for 30 min in the dark. After quenching the remaining IAA with 20 mM DTT for 30 min in the dark, enzymatic digestion was performed as follows: Carbamoylated pp65 was incubated with 1/10 Glu-C (w/w) at 37 °C for 4 h, 1/20 Asp-N (w/w) was added, and incubation at 37 °C was continued overnight. After adding 5 % acetonitrile (v/v), the sample was acidified to pH 2 with TFA and incubated at 37 °C for 40 min to cleave Rapigest SF. The supernatant was removed and desalted using a CHROMABOND® C18ec cartridge (500 mg, Macherey-Nagel) according to the manufacturer´s protocol. After lyophilization, the sample was reconstituted in 50 µL 5 % acetonitrile/0.1 % formic acid (v/v) and 6 µL were injected into an Agilent series 1200 LC system (G1312B binary pump, G1367C autosampler) (Agilent Technologies) coupled to a LTQ Orbitrap Elite hybrid mass spectrometer (Thermo Fisher). Peptides were separated on a Phenomenex Aeris PEPTIDE XB-C18 column (250 x 2.1 mm, 3.6 µm) (Torrance) at 25 °C with a flow rate of 0.2 ml/min. Two-step gradient elution was performed from 2.5 % to 40 % acetonitrile/0.1 % formic acid (v/v) over 100 min as well as from 40 % to 80 % acetonitrile/0.1 % formic acid (v/v) over 50 min. The HESI-II probe was operated at the following conditions: 4.2 kV spray voltage, 300 °C/320 °C heater/capillary temperature, and 36/17 sheath/auxiliary gas flow rate. Using a data-dependent top 5 method with a minimum signal threshold of 1000 counts, MS survey scans were acquired in the Orbitrap from m/z 200 to 2100 at a resolution of 120000.

The five most intense signals were subjected to collision induced dissociation (CID) in the ion trap with an isolation width of m/z 2, a normalized collision energy of 35 %, and an activation time of 10 ms. Dynamic exclusion of 14 s (1 repeat count, 12 s repeat duration) was applied. The AGC target was set to 1E6 for MS scans (200 ms maximum injection time) and to 1E4 for MSMS scans (50 ms maximum injection time). The settings *predict ion injection time* and *enable monoisotopic precursor selection* were enabled. Data were analyzed with the Proteome Discoverer 1.3 (Thermo Fisher) using the pp65 protein sequence as a database in combination with the SEQUEST search algorithm. MS and MS/MS tolerances were set to 10 ppm and 0.8 Da, respectively, and carbamidomethylation of cysteine was set as static modification, whereas carbamoylation of lysine and arginine was set as dynamic modification. As combined cutting of Asp-N and Glu-C cannot be specified in the program, no enzyme specificity was selected and only peptides with expected cleavages were selected for further analysis[352]. To determine the degree of carbamoylation at a specific position, all identified peptides containing the position of interest were processed with Thermo Xcalibur 2.2. For each peptide, the sum of intensities of all contributing charge states and isotopomers was extracted from the MS data and integrated over the respective chromatographic peak. The degree of carbamoylation was calculated by dividing the sum of all peptides carbamoylated at a specific position by the sum of the areas of all peptides containing the position of interest (the calculation is based on the assumption that unmodified and carbamoylated peptides as well as peptides of different length arising from missed cleavages exhibit the same mass spectrometric response factor). If the CID-based MSMS spectrum was not sufficient to unambiguously determine the position of carbamoylation for peptides containing lysine and arginine, the precursor of interest was subjected to an additional LC-MSMS run using electron transfer dissociation (ETD). The following fragmentation parameters were applied: 3E5 AGC target (100 ms maximum injection time), 50 µA emission current, -70 V electron energy, 16 psi CI gas pressure, and 160 °C source temperature.

Reagent	Supplier
Rapigest SF	Waters
Pierce™ Glu-C protease (MS grade)	Thermo Fisher
Endoproteinase Asp-N (sequencing grade)	Sigma-Aldrich
Pierce™ tris(2-carboxyethyl)phosphine (TCEP)-HCl (premium grade)	Thermo Fisher
6 M hydrochloric acid (sequanal grade)	Thermo Fisher
formic acid (98–100%, p. a.)	Merck
iodoacetamide (IAA)	Sigma-Aldrich
acetonitrile (Chromasolv grade	Sigma-Aldrich
trifluoroacetic acid (TFA)	Sigma-Aldrich
ammonium acetate (p.a.)	Fluka

VI.5. Isolation, cultivation and differentiation of primary cells

VI.5.1. Ethics

Blood donations were collected from healthy, adult volunteers who gave written informed consent beforehand. Sample collections and experiments were approved by the ethics committee of the University of Regensburg (file reference 16-101-0347).

VI.5.2. Isolation of PBMCs

Heparinized blood samples (15 – 60 ml of blood were mixed with one droplet of Na-Heparin) were added to an equivalent volume of PBS and the suspension was carefully layered over 15 ml Ficoll in a 50 ml conical tube. Samples were centrifuged for 15 minutes at 1000 xg with the centrifuge brake turned off. The upper plasma layer was carefully aspirated and discarded, leaving the mononuclear cell layer (lymphocytes, monocytes, and thrombocytes) undisturbed at the interphase. Next, the mononuclear cell layer was transferred to a new 50 ml conical tube, which was subsequently filled to 50 ml with PBS and centrifuged for 10 min at 350 xg with the brake turned back on. Afterwards, the supernatant was discarded and the pellet was resuspended in the desired medium or buffer (sections VI.5.3 and VI.5.4).

Reagent	Supplier
Na-Heparin	Ratiopharm
Ficoll-Paque Plus	GE Healthcare

VI.5.3. ELISpot assay

For this assay, the T track basic ELISpot kit (Lophius Biosciences) was used: After PBMC isolation (section VI.5.2), the cell pellet was resuspended in 1 ml of Ultraculture (UC) medium and living cells were counted with a hemocytometer. Next, UC medium was added for a concentration of $2x10^6$ cells/ml and 100 µl aliquots were distributed to the desired number of wells in an ELISpot plate that was pre-coated with an IFNγ-antibody by the manufacturer. 50 µl of stimulation mixture were then added consisting of 35 µl UC medium and the stimulator protein that was diluted to 15 µl with sodium phosphate buffer (section VI.3.7). In some cases, fucoidan from *Fucus vesiculosus* (Sigma-Aldrich; final concentration 100 µg/ml) was added to PBMCs 30 minutes before addition of the stimulation mixture. The plate was incubated for 20 h in a humidified incubator at 37 °C and 5% CO_2. Afterwards, the supernatant was discarded and the plate was washed 6 times with 200 µl of buffer WB1. 100 µl of antibody solution (mAB-AP was diluted 1:180 in buffer DB) was added to each well and the plate was incubated for 2 h at RT in the dark. After this incubation period, the supernatant was again discarded and the plate was washed 3 times with 200 µl of WB1, followed by 3 washing steps with 200 µl of WB 2 each. After removing the supernatant, 50 µl of stain solution were added per well and the plate was incubated at RT and protected from light until spots were clearly visible (10-15 min). The plate was then

washed 3 times with H_2O and after drying, spots were counted on an AID robotic EliSpot Reader (Autoimmune Diagnostica GmbH).

VI.5.4. MACS sorting

After PBMC isolation (section VI.5.2), the cell pellet was resuspended in 50 ml P2 buffer and centrifuged for 10 min at 350 xg. The supernatant was discarded and the pellet was resuspended in 800 µl MACS buffer. Next, 100 µl of CD14 (Figure 23 and Figure 24) or CD8 (Figure 28) microbeads were added and the suspension was incubated for 15 min at 4 °C. Afterwards, 10 ml of MACS buffer were added and the mixture was transferred to a 15 ml conical tube, followed by centrifugation at 600 xg for 10 min. During centrifugation, a MACS separation column was placed into a magnetic multistand and equilibrated with 1 ml MACS buffer. After centrifugation, the supernatant was discarded and the bead/cell pellet was resuspended in 1 ml MACS buffer and added to the MACS column, allowing the liquid to pass through the column by gravity flow. For negative selection experiments (Figure 23 and Figure 28), the flow-through was collected and cells that were depleted of monocytes or $CD8^+$ T cells were used for further experiments.

For positive selection experiments (Figure 24) or for further differentiation of monocytes (Figure 25, sections IV.2.1 and IV.2.2), the flow-through was discarded and 1 ml of MACS buffer was added to the column. After all liquid had passed through the column, it was removed from the multistand and placed into a 15 ml conical tube. Again, 1 ml of MACS buffer was added to the column and the cells were flushed into the tube by pushing the plunger into the column. Cells were then counted and resuspended in the desired volume of medium (sections VI.5.5 and VI.5.6).

Reagent/Consumable	Supplier
EDTA (cell culture grade)	Invitrogen
CD14 MicroBeads, human	Miltenyi
CD8 MicroBeads, human	Miltenyi
MACS Separation MS Columns	Miltenyi
MACS Multistand	Miltenyi

Buffer	Composition
P2 buffer	1% (v/v) FCS in PBS
MACS buffer	1% (v/v) FCS, 20mM EDTA in PBS

VI.5.5. Monocyte differentiation to moDCs or moMΦs

After monocyte isolation via MACS sorting (section VI.5.4), cells were diluted to 10 ml in MACS buffer and centrifuged for 10 min at 350 xg. Next, the pellet was resuspended for a cell density of $1x10^6$/ml either in DC-medium containing 1000 U IL-4 and GM-CSF each (for

differentiation to moDCs) or in macrophage medium containing 50 U/ml GM-CSF only. The suspension was incubated in T25 cell culture flasks at 37 °C and 5% CO_2 for 5-6 days. After two days, half the medium was transferred to a 15 ml conical tube, centrifuged 10 min at 500 xg and cells were resuspended in 5 ml of the respective medium containing all aforementioned supplements. The fresh medium was then transferred back to the cell culture flask along with the resuspended cells.

At different time points, aliquots (100 - 500 µl) were collected from the flasks and the expression of surface markers was analyzed to assess differentiation: Cells were centrifuged for 5 min at 500 xg and 4 °C, the supernatant was removed and the cell pellet was resuspended in 500 µl of FACS buffer (which was precooled on ice). After repetition of this washing step, the supernatant was discarded and cells were resuspended in 30 µl of antibody- or isotype control antibody solutions (diluted in PBS) and incubated for 30 min in the dark at 4 °C. Afterwards, cells were again washed two times with 500 µl of FACS buffer. For CD14- or CD1a-stained cells (as well as their respective isotype control samples), cells were resuspended in 200 µl of FACS buffer and analyzed by flow cytometry.

For SR-A1 (or the corresponding isotype control sample), cells were resuspended with 30 µl of secondary antibody solution (likewise diluted in PBS). After another 30 min incubation period at 4 °C in the dark, cells were again washed two times as described above and resuspended in 200 µl of FACS buffer, followed by flow cytometry analysis.

Reagent/Consumable	Supplier
FCS, lot# 123M3398	Sigma-Aldrich
Penicillin/Streptomycin (Pen/Strep)	Pan Biotech
RPMI 1640 with Glutamine and Pen/Strep	Pan Biotech
MEM non-essential amino acids (NE-AA), 100x stock solution	Gibco
MEM Vitamins, 100x stock solution	Gibco
L-Glutamine, 200 mM Stock solution	Pan Biotech
Sodium Pyruvate, 100x stock solution	Gibco
β-Mercapto-EtOH, 50 mM stock solution	Gibco
IL-4, premium grade	Miltenyi
GM-CSF, premium grade	Miltenyi

Buffer	Composition
DC-Medium	425 ml RPMI 1640, 50 ml FCS, 5ml Pen/Strep, 5 ml NE-AA, 5 ml Vitamins, 5 ml Glutamine, 5 ml Sodium Pyruvate, 100 µl β-Mercaptoethanol
Macrophage Medium	RPMI 1640, 10% FCS, 1% Pen/Strep
FACS buffer	PBS with 1% FCS, 1mg/ml NaN_3

Primary antibody	Isotype	Conjugate	Supplier	Cat#	dilution
mouse anti human CD14	IgG1κ	PE	Biolegend	367104	1:50
mouse anti human CD1a	IgG1κ	APC	Biolegend	300110	1:50
mouse anti human SR-A1	IgG1κ	none	R&D Systems	mab27081	1:50

Isotype control	Conjugate	Supplier	Cat#	dilution
MOPC-21-IgG1κ	PE	Biolegend	400114	1:50
MOPC-21-IgG1κ	APC	Biolegend	400120	1:50
LEAF™ Mouse IgG1κ	none	Biolegend	401405	1:50

Secondary antibody	Conjugate	Supplier	Cat#	dilution
Goat anti mouse IgG	PE	Biolegend	405307	1:50

VI.5.6. Expansion of T cell clones

The CD8+ T cell clones 4G6 (recognizing the pp65-derived peptide TPRVTGGGAM on HLA-B7) and 1C3 (recognizing the IE-1-derived peptide QIKVRVDMV on HLA-B8) were a kind gift from Dirk Busch (TU Munich). For usage in multiple experiments, they first had to be expanded with suitable feeder cells (consisting of a mixture of PBMCs and LCL cells). $25x10^6$ HLA-matched PBMCs (γ-irradiated at 35 Gy), $5x10^6$ HLA-matched LCL cells (γ-irradiated at 50 Gy) and $2x10^5$ cells of the clone to be expanded were transferred in a total of 20 ml CTL medium into a T25 cell culture flask. The stimulatory anti-CD3 antibody OKT3 was added for a final concentration of 30 ng/ml. After 24 hours, human IL-2 was added (100 U/ml) and at day 4 of the co-culture, the suspension was centrifuged for 8 min at 200 xg. The supernatant was discarded and cells were resuspended in 20 fresh CTL medium containing IL-2 only (not the CD3 antibody). At day 8, half the medium was replenished by removing 10 ml from the flask, centrifuging the suspension as described before and returning the cell pellet, resuspended in 10 ml fresh medium with IL-2 (100 /ml), to the flask. From day 9-12, cells were counted daily and split if necessary to keep the cell density between $1x10^6$ and $2x10^6$/ml. At day 12, cells were counted, centrifuged and resuspended in freezing medium for a density of $2x10^6$ cells/ml. Cells were then distributed to the desired number of cryotubes and slowly frozen to -80 °C. Finally, cells were stored in liquid nitrogen until further use.

Reagent/Consumable	Supplier
human serum "odd the clot"	Biochrom
Ultra-LEAF anti-human CD3 Antibody OKT3	Biolegend
human IL-2, premium grade	Miltenyi

Medium	Composition
CTL medium	RPMI 1640, 10% human serum, 4 mM L-glutamine, 25 µM β-mercaptoethanol, 1% Pen/Strep

T cell clone	Cognate epitope	HLA restriction
4G6	TPRVTGGGAM	HLA-B7
1C3	QIKVRVDMV	HLA-B8

VI.5.7. Mixed leukocyte reaction (MLR)

After five days of differentiation, the culture medium of moDCs or moMϕs Figure 25, section VI.5.5) was changed to RPMI with 10 % FCS and 1 % Pen/Strep. $5x10^4$ cells in 100 µl were seeded each into the desired number of wells from a 96-well flat-bottom plate. For monocytes (Figure 24, section VI.5.4), the same number of cells per well (also diluted in RPMI) was seeded into 96 well plates directly after MACS isolation. Cells were then incubated overnight at 37 °C and 5% CO_2.

The next day, pp65 or carb-pp65 (diluted to 15 µl with sodium phosphate buffer) were added along with $5x10^4$ cells of an antigen-specific, HLA-matched T cell clone (in 35 µl RPMI medium) for a final volume of 150 µl. For monocytes, fucoidan (final concentration 100 µg/ml) was added to some wells 30 minutes before addition of the stimulation mixture. After 2 h, BFA was added (1 µg/ml) and cells were co-cultivated for another 4 hours.

The plates were then centrifuged for 5 min at 350 xg and 4 °C and the supernatant was discarded. Cells were washed two times with 200 µl of precooled FACS buffer with centrifugation for 5 min at 350 xg and 4 °C after each step. After the second washing step, the supernatant was removed and the cell pellet was resuspended in 100 µl Cytofix/Cytoperm. Fixation lasted for 30 min at 4 °C, after which cells were washed twice with 200 µl Perm/Wash with centrifugation for 5 min at 500 xg and 4 °C after each step. Cells were then resuspended in 50 µl staining solution, consisting of anti-CD8-FITC and anti-IFNγ-APC antibodies (diluted in Perm/Wash) and incubated for 30 min at 4 °C in the dark. Finally, cells were washed twice with 200 µl Perm/Wash with centrifugation for 5 min at 500 xg and 4 °C after each step and cells were resuspended in 100 µl FACS buffer, followed by flow cytometry analysis.

Reagent/Consumable	Supplier
paraformaldehyde (PFA)	Merck Millipore
Saponin from Quillaja bark (Lot 1310498)	Sigma-Aldrich
Fucoidan from *Fucus vesiculosus*	Sigma-Aldrich
Brefeldin A (BFA)	Sigma-Aldrich

Buffer	Composition
FACS buffer	PBS with 1% FCS, 1mg/ml NaN_3
Cytofix/Cytoperm	PBS with 4 % (w/v) paraformaldehyde (PFA) and 1 % (w/v) saponin
Perm/Wash	PBS with 0.1 % (w/v) saponin

Antibody	Isotype	Conjugate	Supplier	Cat#	dilution
mouse anti human CD8a	IgG1κ	FITC	Biolegend	301006	1:60
mouse anti human IFN-γ	IgG1κ	APC	Biolegend	502512	1:60

T cell clone	Cognate epitope	HLA restriction
4G6	TPRVTGGGAM	HLA-B7

VI.6. Virological techniques

VI.6.1. Generation of recombinant MVA vectors

VI.6.1.1. *In vitro* recombination (IVR)

The genes encoding IE-1 or pp65 were inserted into the MCS of the transfer plasmid pLZAW1 via the BamHI and EcoRI restriction sites by standard molecular cloning techniques[345]. The newly generated plasmids pLZAW1-IE-1 and pLZAW1-pp65 were purified from *E. coli* cells with a plasmid midi kit (Qiagen) according to the manufacturer's instructions.

$1x10^6$ BHK-21 cells were seeded into each well of a 6 well plate in 2 ml medium and incubated overnight at 37 °C and 5% CO_2. The next day, the medium was removed and cells were infected with MVA-GFP at different MOIs (0.5, 0.167, 0.056, 0.019 and 0.006) in a total of 1 ml DMEM devoid of any supplements. Cells were then incubated for 2 h at 37 °C and 5% CO_2. Afterwards, cells were transfected with pLZAW1 vectors using the Effectene Kit from Qiagen: the medium was removed and 1.4 ml DMEM with 10% FCS and 1% Pen/Strep were added. 0.88 µg of DNA per plasmid and well were diluted to 100 µl with buffer EC. After addition of 6.4 µl enhancer, the suspension was briefly vortexed and incubated at room temperature (RT) for 5 min. Next, 20 µl of Effectene were added and after thorough vortexing (≥ 10 sec), the mixture was incubated at RT for 10 min. 600 µl of DMEM medium were mixed with the suspension and added to the cells by evenly distributing small droplets over the plate area. The cells were then incubated for 72 hours at 37 °C and 5% CO_2. Afterwards, cells were scraped off the bottom of the culture dish, transferred along with the medium to 2 ml reaction tubes and stored at -80 °C until further use.

VI.6.1.2. Plaque purification

$2x10^6$ BHK cells each were seeded into the desired number of 10 cm petri dishes in a total of 10 ml. Cell lysates from IVR were subjected to 3 freeze/thaw cycles by transferring the tubes to liquid nitrogen, followed by thawing at 37 °C. Then, the lysates were subjected to ultrasound treatment on the cup horn of a Branson Sonifier 450 device (output: 8.5; cycle: 80%; 1 minute pause between pulses). The culture medium of BHK cells was discarded and replaced with different dilutions (a total of four 1:3 dilution steps for each MOI in the IVR reaction, beginning with 1:20 for MOI 0.0006 and 0.019, 1:100 for MOI 0.056, 1:200 for MOI 167 and 1:500 for MOI 0.5) in a total of 4 ml DMEM without any supplements. After two hours of incubation at 37 °C and 5% CO_2, the viral inoculum was removed and cells were overlaid with 12 ml first overlay solution (which was freshly mixed shortly before). After 3 days of incubation at 37 °C and 5% CO_2, the dishes were overlaid with 5 ml each

of second overlay solution (which was again freshly mixed shortly before), followed by another incubation period for 6 hours at 37 °C and 5% CO_2. Blue plaques were then picked with glass Pasteur pipettes and transferred into 1.5 ml reaction tubes along with 500 µl DMEM devoid of any supplements. The picked plaques were stored at -80 °C until the next plaque round, when they were subjected to 3 freeze/thaw cycles and ultrasound treatment as described above.

The following plaque purification rounds were performed in an analogous manner to round one with slight modifications: 2 - 4 suitable plaque punches per construct were chosen from each preceding round for the next one. The plaque punches were always diluted 1:100, 1:400, 1:1600 and 1:6400 and each dilution was used to infect BHK cells. Blue plaques were picked at the dilutions that were best suited for obtaining single ones, until no parental virus was detectable via PCR any more (section VI.6.1.3). At this point, white plaques were picked in all following rounds instead of blue ones until the presence of LacZ was not detectable via PCR any longer.

Reagent/Consumable	Supplier
Bluo-Gal	Biomol
Neutral red	Sigma Aldrich
LMP-Agarose	Affymetrix

Buffer	Composition
2x DMEM (Roth)	2xDMEM, 0.74 % (w/v) $NaHCO_3$, 20% (v/v) FCS, 2% (v/v) Pen/Strep 0.7% (w/v) L-glucose
LMP solution	2.4% LMP agarose (w/v) in H_2O dest., kept at 42 °C
overlay solution A	2xDMEM with 20% FCS and 2% Pen/Strep, kept at 35 °C
overlay solution B	2xDMEM with 20% FCS, 2% Pen/Strep, 1.6 µg/µl Bluo-Gal, 210 µg/ml neutral red, kept at 35 °C
first overlay solution	1:1 mixture of LMP solution and overlay solution A
second overlay solution	1:1 mixture of LMP solution and overlay solution B

VI.6.1.3. PCR screening

DNA was isolated from MVA-infected BHK-21 cells using the QIAamp DNA mini Kit (Qiagen) according to the manufacturer's instructions. Screening for the genes IE-1, pp65, GFP or LacZ was performed with the GoTaq Green Master Mix kit (Promega) according to the manufacturer's instructions using the primers specified in the table below.

Primer	Sequence (5'-3')
IE-1 fwd	GCTTCTAGTCACCATAGGGTG
IE-1 rev	GCATTGAGGAGATCTGCATGAAG
pp65 fwd	GTAGATGTCGTTGGCGTCC
pp65 rev	CTTGAGTACCGACACACCTG
GFP fwd	GTGTTCTGCTGGTAGTGGTC

GFP rev	CCTGAAGTTCATCTGCACCAC
lacZ-Int-fwd	CCGCTGGATAACGACATTGG
lacZ-Int-rev	CTGACAATGGCAGATCCCAG

VI.6.2. Generation of recombinant AdV vectors

Ad5 and Ad19a/64 vectors were generated as previously described by Ruzsics *et al.*[353] and based on an Ad19a ME strain-derived BAC-cloned vector[234,354]. Briefly, the genes-of-interest (GOI) IE-1, pp65 or eGFP were cloned into shuttle vectors pO6-A5-CMV-gfp and pO6-19a-CMV-MCS, respectively, under the control of a CMV promoter. The CMV-GOI-SV40-pA was then transferred via Flp-recombination in *E. coli* into the respective BAC vectors containing the genome of E1/E3 deleted replication deficient Ad5 or Ad19a-based vectors. Recombinant viral DNA was released from the purified BAC-DNA by restriction digest with Pac-I. The obtained linear DNA was transfected into Hek293 cells for virus propagation. Viral vectors were released from cells via NaDeoxycholate extraction. Residual free DNA was digested by DNase I. Afterwards, vectors were purified by CsCl gradient ultracentrifugation followed by a buffer exchange to 10 mM Hepes pH 8.0, 2 mM $MgCl_2$, 4% Sucrose via PD10 columns (GE). Titration was performed based on the RapidTiter (Clontech) method by detection of infected HEK Hek293 cells via immunohistochemical staining with anti-hexon antibody (Ad5: Santa Cruz, Ad19a: Novus). Insert integrity was confirmed by PCR amplification of the GOI in DNA purified from the extracted vectors. Functionality of the insert was confirmed by qPCR and Western blot of infected NIH3T3 or Hek293 cells.

VI.6.3. Generation of recombinant SeV vectors

All recombinant Sendai virus variants were generated from a cDNA template encoded on plasmid DNA. cDNA templates of rcSeV-GFP and rdSeV-GFP were generated previously[334]. The new constructs rcSeV-IE-1, rcSeV-pp65, rdSeV-IE-1 and rdSeV-pp65 were cloned by exchanging the GFP transgene from the above named GFP expressing cDNA constructs against the respective transgenes (IE-1 and pp65) via NotI restriction digest.

Recombinant viruses were recovered through virus rescue experiments from transfected BSR-T7 cells as described before[298] with slight modifications. FuGENE6 (Roche) was used as transfection reagent at 2.0 µl/µg DNA. Virus was harvested from the supernatant and amplified in Vero cells (replication-competent SeV) or in the helper cell line V3-10[245] (replication-deficient SeV vector). Virus preparations were titrated as previously described[245] and titres are given as cell infectious units per millilitre (ciu/ml). The integrity of the various SeV vector genomes was confirmed by RT-PCR and sequencing.

VI.6.4. Viral infection

For infection of various cell types, cells were diluted in the suitable culture medium (DMEM or RPMI, see section VI.1) devoid of any supplement. $3x10^4 – 5x10^4$ cells in a volume of 30 µl were added to each well and the plate was incubated for 2 h at 37 °C and 5% CO_2. Virus suspensions were likewise diluted in RPMI or DMEM and added to the cells in a volume of 20 µl. After 3 hours, the plate was centrifuged for 5 min at 350 xg, followed by removal of the supernatant and infected cells were cultivated in RPMI or DMEM with 10% FCS and 1% Pen/Strep for the desired amount of time.

VI.6.5. Viral target cell tropism

PBMCs were infected with GFP-expressing vectors (Figure 32 and Figure 44) according to section VI.6.4. and 24 hours post infection (hpi), the plate was centrifuged for 5 min at 350 xg and 4 °C. The supernatant was removed and cells were washed with 200 µl precooled FACS buffer. After repetition of this washing step, cells were resuspended in 50 µl staining solution (all antibodies were diluted in PBS). After staining, cells were washed twice with 200 µl FACS buffer as described above and analyzed on a FACS Canto II device (Becton Dickinson).

Buffer	Composition
FACS buffer	PBS with 1% FCS, 1 mg/ml NaN_3

Antibody	Isotype	Conjugate	Supplier	Cat#	dilution
mouse anti human CD3	IgG1κ	APC-Cy7	Biolegend	344818	1:60
mouse anti human CD4	IgG1κ	BV421	Biolegend	300532	1:60
mouse anti human CD8	IgG1κ	AmCyan	Becton Dickinson	339199	1:60
mouse anti human CD14	IgG1κ	PE	Biolegend	367104	1:60
mouse anti human CD19	IgG1κ	APC	Biolegend	302211	1:60
mouse anti human CD56	IgG1κ	PerCP	Biolegend	318341	1:60

VI.6.6. Intracellular IE-1/pp65 staining

moDCs were infected with IE-1- or pp65-expressing vectors (Figure 33 and Figure 39) according to section VI.6.4. 24 or 48 hours after infection, the plate was centrifuged for 5 min at 350 xg and 4 °C. moDCs were then washed twice with 200 µl precooled FACS buffer with centrifugation at 350 xg and 4 °C for 5 min after each step. Next, cells were fixed by resuspending the pellet in 100 µl Cytofix/Cytoperm and incubating the plate for 30 min at 4 °C. The plate was centrifuged for 5 min at 350 xg and 4 °C and the supernatant was discarded. Cells were washed twice with 200 µl Perm/Wash with centrifugation at 350 xg and 4 °C for 5 min after each step. After removal of the supernatant, cells were resuspended in 50 µl primary antibody solution (IE-1- or pp65-antibody diluted in Perm/Wash) and incu-

bated for 30 min at 4 °C. Cells were washed twice with 200 µl Perm/Wash with centrifugation at 350 xg and 4 °C for 5 min after each step. Next, 50 µl of secondary antibody solution (diluted in Perm/Wash as well) were added to the cells, followed by incubation for 30 min at 4 °C in the dark. Cells were again washed twice with 200 µl Perm/Wash with centrifugation at 350 xg and 4 °C for 5 min after each step. Finally, cells were resuspended in 200 µl FACS buffer and flow cytometry analysis was performed using a FACS Canto II device (BD Biosciences).

Buffer	Composition
FACS buffer	PBS with 1% FCS, 1 mg/ml NaN_3
Cytofix/Cytoperm	PBS with 4 % (w/v) paraformaldehyde (PFA) and 1 % (w/v) saponin
Perm/Wash	PBS with 0.1 % (w/v) saponin

Primary antibody	Supplier	Cat#	Dilution
mouse anti IE-1	Abcam	ab30924	1:50
mouse anti pp65	Abcam	ab53489	1:50

Secondary antibody	Conjugate	Supplier	Cat#	dilution
Goat anti-mouse IgG	PE	Biolegend	405307	1:50

VI.6.7. T cell restimulation by virally transduced moDCs

moDCs were infected with IE-1- or pp65-expressing vectors (Figure 34 and Figure 40) according to section VI.6.4. 24 hpi, T cells were added at an effector/target cell ratio of 1:1 along with BFA (1 µg/ml). After 6 hours of co-incubation, cells were stained according to section VI.5.6.

Antibody	Isotype	Conjugate	Supplier	Cat#	dilution
mouse anti human CD8a	IgG1κ	FITC	Biolegend	301006	1:60
mouse anti human IFN-γ	IgG1κ	APC	Biolegend	502512	1:60

T cell clone	Cognate epitope	HLA restriction
4G6	TPRVTGGGAM	HLA-B7
1C3	QIKVRVDMV	HLA-B8

VI.6.8. Analysis of DC maturation

moDCs were infected with IE-1- or pp65-expressing vectors (Figure 35 and Figure 42) according to section VI.6.4. 24 hpi or 48 hpi, the plates were centrifuged for 5 min at 350 xg and 4 °C and the supernatant was discarded. moDCs were then washed twice with 200 µl precooled FACS buffer with centrifugation at 350 xg and 4 °C for 5 min after each step. Cells were fixed by resuspending the pellet in 100 µl PBS with 4% (w/v) PFA and incubating

the plate for 30 min at 4 °C. Afterwards, the plate was centrifuged for 5 min at 350 xg and 4 °C and the supernatant was discarded. moDCs were again washed twice with 200 µl precooled FACS buffer with centrifugation at 350 xg and 4 °C for 5 min after each step. Samples were then stained by adding 50 µl of antibody solution (diluted in PBS) and incubating the plate for 30 min at 4 °C in the dark. After two final washing steps with FACS buffer as described above, cells were diluted in 200 µl FACS buffer and analyzed on a FACS Canto II device (BD Biosciences).

Buffer	Composition
FACS buffer	PBS with 1% FCS, 1 mg/ml NaN_3

Antibody	Isotype	Conjugate	Supplier	Cat#	dilution
mouse anti human CD80	IgG1κ	FITC	Biolegend	557226	1:60
mouse anti human CD83	IgG1κ	PE/Cy7	Biolegend	305326	1:60
mouse anti human CD86	IgG1κ	V450	Becton Dickinson	560359	1:60
mouse anti human HLA-DR	IgG2aκ	APC	Biolegend	307610	1:60

VI.6.9. AnnexinV/7AAD assay

To determine the amount of viable cells 24 or 48 hours after infection, the APC Annexin V Apoptosis Detection Kit with 7-AAD (Biolegend) was used according to the manufacturer's instructions (Figure 36 and Figure 41). Flow cytometry analysis was performed using an Attune NxT flow cytometer (Life Technologies).

VI.6.10. Cytokine secretion analysis

48 hours after infection, cell culture supernatants were collected and stored at -20 °C until analysis. For cytokine quantification, the Legendplex Human Inflammation Panel (13-plex Kit, Bio-legend) was used according to the manufacturer's instructions. Data acquisition was performed using an Attune NxT device (Life Technologies) and cytokine concentrations were determined using the software provided with the kit (Figure 43).

VI.6.11. Cross presentation assay

HeLa cells were infected with IE-1- or pp65-expressing AdV vectors (Figure 37) according to section VI.6.4. 24 hpi, cells were washed 4 times with RPMI1640 medium, followed by detachment from cell culture plates with Trypsin/EDTA solution (Pan Biotech). HeLa cells were added to moDCs at a 1:1 ratio. After 24 hours of co-incubation, T cells were added along with Brefeldin A (BFA, 1 µg/ml) at a moDC/T cell ratio of 1:1. Co-incubation lasted for 6 hours after which cells were fixed and stained for CD8 and IFNγ as described in section VI.5.6.

VI.7. Animal experiments

All animal experiments were approved by the responsible veterinary department of the government of Lower Franconia (file number DMS-2532-2-69). 4 weeks old, female BALB/cAnNCrl mice were ordered from Charles River Laboratories and housed for two weeks at the animal facility D4 (University of Regensburg) in a pathogen-free environment. After this period, (week 0) and after two weeks (Figure 29), the animals were immunized after sedation with the inhalation anesthetic isoflurane (Baxter). pp65, carb-pp65 (4 µg each with 100 µg/ml poly(I:C)) or pcDNA3.1-pp65 (50 µg), dissolved in a total of 50 µl PBS, were injected into the *tibialis anterior* muscle of the left hind leg.

Two weeks after the booster immunization, each spleen was removed with surgical instruments in a sterile manner and transferred to 10 ml PBS in a 50 µl conical tube. The spleen was placed in a cell strainer, which was transferred to a petri dish along with 10 ml of PBS. The spleen was then mashed through the strainer with the plunger of a 5 ml syringe into the petri dish. The cell strainer was rinsed with 5 ml PBS and discarded. The splenocyte solution was transferred from the petri dish into a 50 ml conical tube and centrifuged for 5 min at 300 xg. The supernatant was removed and the pellet was resuspended in 5 ml lysis buffer, followed by centrifugation for 5 min at 300 xg. The supernatant was discarded and the pellet was resuspended in 10 ml wash medium, followed by another centrifugation step for 5 min at 300 xg. After repeating this washing step two more times, cells were resuspended in 1 ml splenocyte medium, counted and set to a density of $2x10^7$ cells/ml.

100 µl aliquots were then distributed to the desired number of wells in a 96 well round bottom plate. Next, 100 µl of stimulation mixture were added, consisting of a pp65 peptide pool (600 ng/peptide) and BFA (200 ng), diluted in splenocyte medium. For positive control, some wells were stimulated with 100 µl PMA (0.1 µg/ml), ionomycin (1 µg/ml) and BFA (200 ng), diluted in splenocyte medium. For negative control, BFA only (200 ng), likewise diluted in splenocyte medium, was added to some cells. The splenocyte cultures were then incubated at 37 °C and 5% CO_2 for six hours.

Afterwards, the plates were centrifuged at 4 °C for 5 min (350 xg) and the supernatant was discarded. Cells were then washed twice with 150 µl precooled FACS buffer with centrifugation at 350 xg and 4 °C after each step. After removal of the supernatant, CD4 and CD8 antibodies were added (diluted to 30 µl in PBS) and cells were incubated for 30 min at 4 °C in the dark. Cells were then washed twice with 150 µl precooled FACS buffer with centrifugation at 350 xg and 4 °C after each step. Next, 150 µl Cytofix/Cytoperm were added, followed by incubation for 30 min at 4 °C in the dark. After the incubation, cells were washed twice with 150 µl precooled Perm/Wash with centrifugation at 350 xg and 4 °C after each step. After the second washing steps, the supernatant was removed and cell pellets were resuspended in IFNγ and IL-2 antibody solution (diluted to 30 µl with Perm/Wash). Cells were then incubated for 30 min at 4 °C in the dark. Finally, cells were

again washed twice with 150 µl precooled Perm/Wash with centrifugation at 350 xg and 4 °C after each step. The cell pellets were resuspended in 200 µl FACS buffer and analyzed on an Attune NxT acoustic focusing cytometer (Thermo Fisher).

Reagent/Consumable	Supplier
Plastipack 1 ml syringe	Becton Dickinson
27G needle 0.4x19 mm	Becton Dickinson
Poly(I:C)	Sigma-Aldrich
Brefeldin A (BFA)	Sigma-Aldrich
pp65 Pepmix	Lophius Biosciences (138 15mers, spanning pp65 with 11 aa overlap)
PMA	Sigma-Aldrich
Ionomycin	Sigma-Aldrich
HEPES (1 M)	Gibco
β-Mercapto-EtOH	Gibco
cell strainer 100 µm	Thermo Fisher

Buffer	Composition
Lysis buffer	150 mM NH_4Cl, 1 mM $KHCO_3$, 0,1 mM Na_2EDTA, pH 7.2 with HCl
Splenocyte medium	Ultraculture medium with 1% L-Glutamine, 1% Pen/Strep, 20 mM HEPES, 50 µM β-Mercapto-EtOH
Wash buffer	PBS with 1% Splenocyte medium
FACS buffer	PBS with 1% FCS, 1 mg/ml NaN_3
Cytofix/Cytoperm	PBS with 4 % (w/v) paraformaldehyde (PFA) and 1 % (w/v) saponin
Perm/Wash	PBS with 0.1 % (w/v) saponin

Antibody	Isotype	Conjugate	Supplier	Cat#	dilution
rat anti-mouse IFN-γ	IgG1κ	PE	Biolegend	505808	1:60
rat anti-mouse IL-2	IgG2bκ	APC	Biolegend	503809	1:60
rat anti-mouse CD4	IgG2bκ	APC/Fire	Biolegend	100459	1:60
rat anti-mouse CD8a	IgG2aκ	PerCP/Cy5.5	Biolegend	100733	1:60

VI.8. Analysis of flow cytometry data

Flow cytometry analysis was performed using either a FACS Canto II device (Becton Dickinson) or an Attune Nxt Acoustic focusing cytometer (Thermo Fisher). If spectral overlap had to be compensated, singly stained samples for each color as well as an unstained sample were prepared and the automatic compensation function of the given cytometer's software (FACS DIVA or Attune™ NxT Software) was used. Raw data was analyzed using the software Flowjo (version 10). For gating cells, doublets were always excluded first in an FSC-A/FSC-H plot and cells debris was excluded according to FSC/SSC properties. Further gates were defined as required (e.g. Figure 23, Figure 28, Figure 32, Figure 44 and Figure S7).

VI.9. Statistics

Statistical analysis was performed with the software GraphPad Prism (Version 5.01).

VI.10. Homology modeling and electrostatic surface potential calculation

The structure of human IE-1 was modeled for the amino acids 25 - 383 with HHPred[315], using the structure of the *Macacine herpesvirus 3* IE-1 core domain (PDB: 4WID)[47] as a template (Figure 45). The electrostatic surface potential was calculated with the Poisson-Boltzmann solver of the software DeepView (Swiss-PdbViewer, Swiss Institute of Bioinfomatics) with the following settings: Dielectric constant (solvent): 80; dielectric constant (protein): 4; solvent ionic strength (mol/ml): 0; use charged residues only.

I. Appendix

I.1. Abbreviations

Ad5	Adenovirus type 5
Ad19a/	Adenovirus type 19a/64
AdV	Adenovirus
AIDS	Acquired immunodeficiency syndrome
APC	Antigen-presenting cell
ART	Antiretroviral therapy
BFA	Brefeldin A
BHK	Baby hamster kidney cells
Bluo-Gal	5-bromo-3-indolyl β-D-galactopyranoside
CID	Collision-induced dissociation
CIT	Citrulline
CMV	Cytomegalovirus
CV	Coefficient of variation
CVID	Common variable immunodeficiency
DC	Dendritic cell
dpa	Day of proliferation arrest
DTT	Dithiothreitol
EBV	Epstein-Barr virus
eGFP	Enhanced green fluorescent protein
ELISA	Enzyme-linked immunosorbent assay
ELISpot	Enzyme-linked immunospot assay
ETD	Electron transfer dissociation
FSC	Forward scatter
GC	Glycoprotein complex
GFP	Green fluorescent protein
GM-CSF	Granulocyte-macrophage colony-stimulating factor
GP	Glycoprotein
HBV	Hepatitis B virus
HCit	Homocitrulline
HCl	Hydrochloric acid
HCMV	Human Cytomegalovirus
HCV	Hepatitis C virus
HIV	Human immunodeficiency virus
HFF	Human foreskin fibroblast
HLA	Human leukocyte antigen
HPLC	High pressure liquid chromatography
IAA	Iodoacetamide
IE-1	Immediate-early 1
IEF	Isoelectric focussing
IFN	Interferon
IL	Interleukin
IVR	*In vitro* recombination
IPTG	Isopropyl-β-D-thiogalactopyranosid
IRL	Internal repeat long
kb	Kilobase
kDa	Kilodalton
KOCN	Potassium Cyanate
LB	Lysogeny broth
LC-MS	Liquid chromatography-mass spectrometry
LPS	Lipopolysaccharide
MACS	Magnetic-activated cell sorting
MARCO	macrophage receptor with collagenous structure
MCS	Multiple cloning site
MCMV	Murine cytomegalovirus
MHC	Major histocompability complex
MLR	Mixed leukocyte reaction
MOI	Multiplicity of infection
moMϕ	Monocyte-derived macrophages
moDCs	Monocyte-derived dendritic cells
MS	mass spectrometry
MVA	Modified Vaccinia Ankara
NK cell	Natural killer cell
ORF	Open-reading frame
PBMC	Peripheral blood mononuclear cells
PBS	Phosphate buffered saline
PC	Pentameric complex

PFA	Paraformaldehyde
PMA	Phorbol-12-myristate-13-acetat
poly(I:C)	Polyinosinic:polycytidylic acid
pp65	Phosphoprotein 65 kDa
PRR	Pattern recognitinon receptor
QALY	Quality-adjusted life year
qPCR	Quantitative polymerase chain reaction
rpm	Revolutions per minute
RT	Room temperature
SCID	Severe combined immunodeficiency
SD	Standard deviation
SDS-PAGE	Sodium dodecyl sulfate polyacrylamide gel electrophoresis
SEM	Standard error of the mean
SeV	Sendai Virus
SFU	Spot forming units
SR	Scavenger receptor
SR-A1	Scavenger receptor A1
SRCR	Scavenger receptorcysteine-rich domain
TCEP	tris(2-carboxyethyl)phosphine
TFA	Trifluoroacetic acid
TK	Thymidin kinase
TLR	Toll-like receptor
TRL	Terminal repeat long
TRS	Terminal repeat short
UL	Unique long
US	Unique short

I.2. Supplementary data

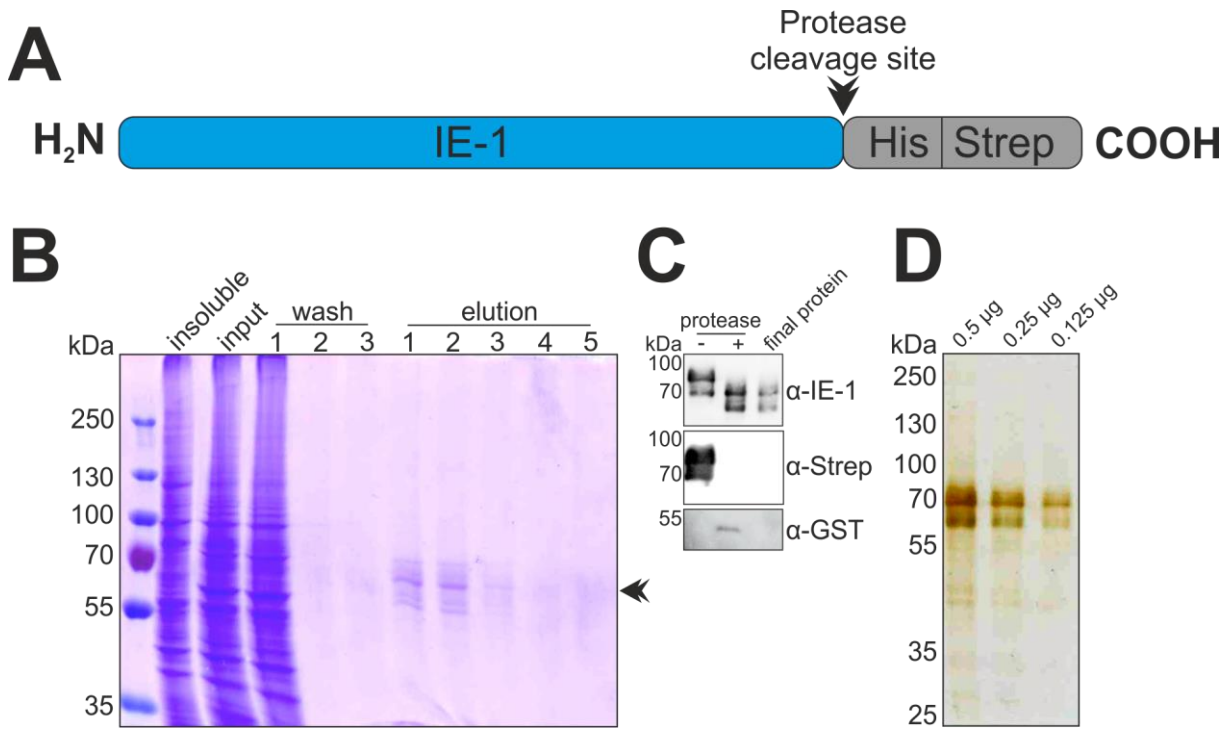

Figure S1 - Purification of IE-1 from insect cells
(A) IE-1 (55kDa, apparent molecular weight 72kDa[48]) was fused C-terminally with a His/Strep tandem tag for affinity purification. Tag and protein are separated by the recognition sequence of the 3C protease of human rhinovirus, allowing removal of the tag by proteolytic cleavage using PreScission™ protease after purification. (B) IE-1 was purified from Baculovirus-infected High Five cells using Ni-IDA beads. During purification, aliquots were collected from the insoluble fraction that was pelletized after cell lysis, the cell lysate (input), the washing steps as well as the elution fractions. Samples were subjected to SDS-PAGE and Coomassie-staining. (C) Proteolytic cleavage was performed for removing the His/Strep tandem affinity tag after purification of IE-1 from crude cell lysates. GST-tagged PreScission™ protease was added to the samples and after digestion, cleaved tag and protease were removed from samples by adding GSH- and Strep-Tactin-beads. Aliquots were collected at all steps and subjected to Western blot analysis. (D) After tag removal, the final product was analyzed via SDS PAGE and silver staining with the indicated protein quantities loaded per lane.

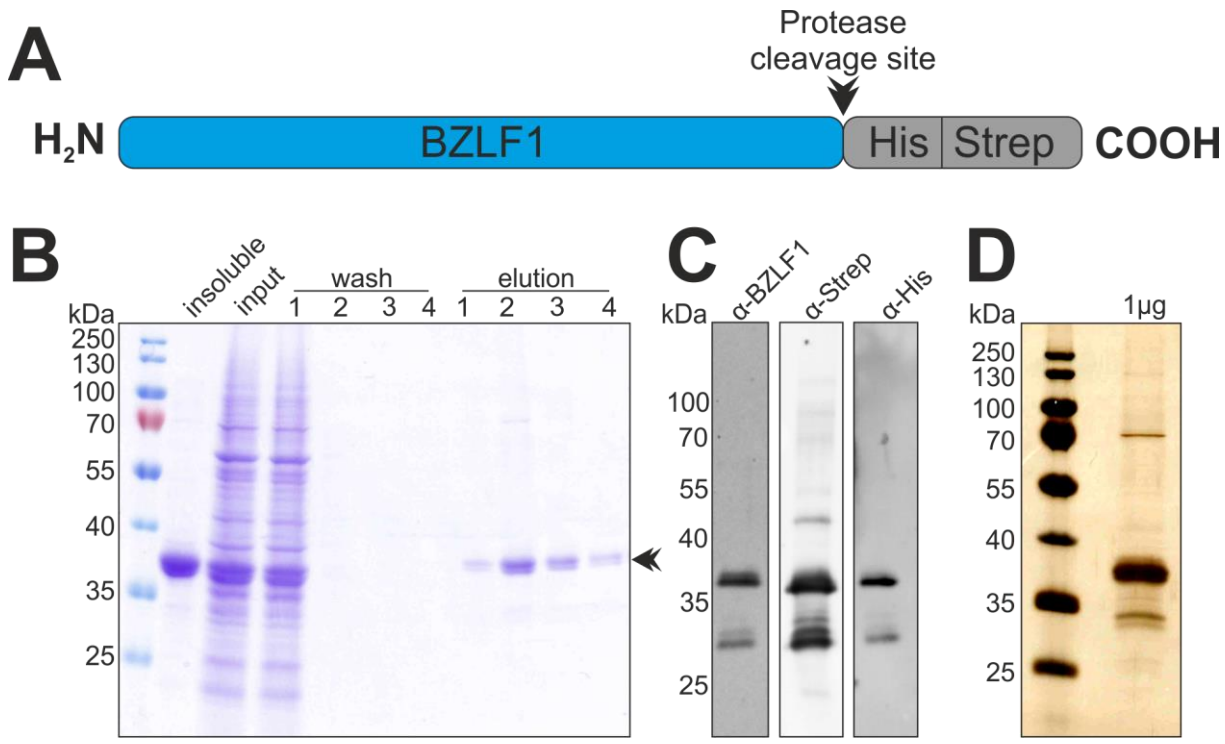

Figure S2 - Purification of BZLF1 from insect cells
(A) BZLF1 (29 kDa) was fused C-terminally with a His/Strep tandem tag for affinity purification. Tag and protein are separated by the recognition sequence of the 3C protease of human rhinovirus, allowing removal of the tag by proteolytic cleavage using PreScission™ protease after purification. (B) BZLF1 was purified from Baculovirus-infected High Five cells using Ni-IDA beads. During purification, Aliquots were collected from the insoluble fraction that was pelletized after cell lysis, the cell lysate (input), the washing steps as well as the elution fractions. Samples were subjected to SDS-PAGE and Coomassie-staining. (C) Western blot of pooled elution fractions after affinity chromatography. Tag cleavage was not performed for BZLF1. (D) The final product was analyzed via SDS PAGE and silver staining. The data was collected during the master thesis of Philipp Becker under my experimental supervision[265].

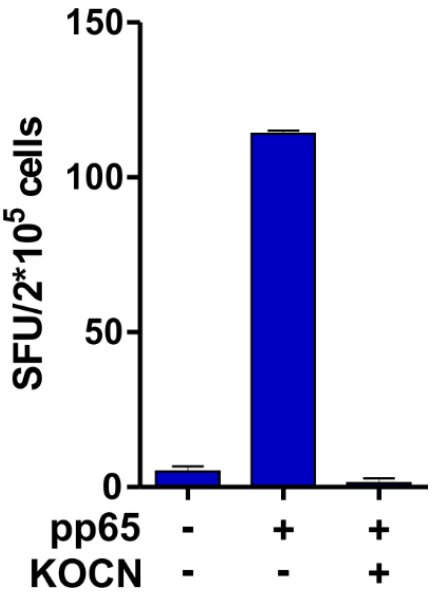

Figure S3 – **Potassium cyanate suppresses signals in IFNγ** ELISpot
$2x10^5$ PBMCs each from a CMV seropositive donor were cultivated for 20 hours in the presence (+) or absence (-) of pp65 or 20 mM potassium cyanate (KOCN). T cell responses were quantified by IFNγ ELISpot Assay.

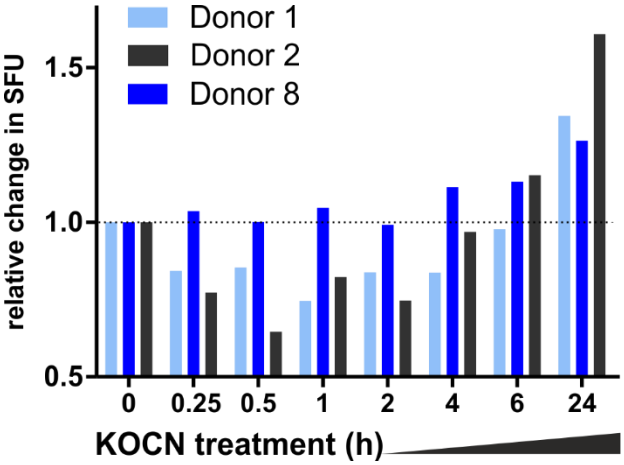

Figure S4 – 24 hours of KOCN treatment leads to the greatest increase in T cell restimulation rates
pp65 was incubated for up to 24 hours with 300 mM potassium cyanate. Aliquots were collected at the indicated time points and subjected to dialysis for removal of KOCN. PBMCs from 3 CMV seropositive donors were stimulated for 20 hours with the different pp65-isoforms and T cell responses were quantified via IFNγ-ELISpot. Obtained spot-forming unit (SFU) values were normalized to those of unmodified pp65.

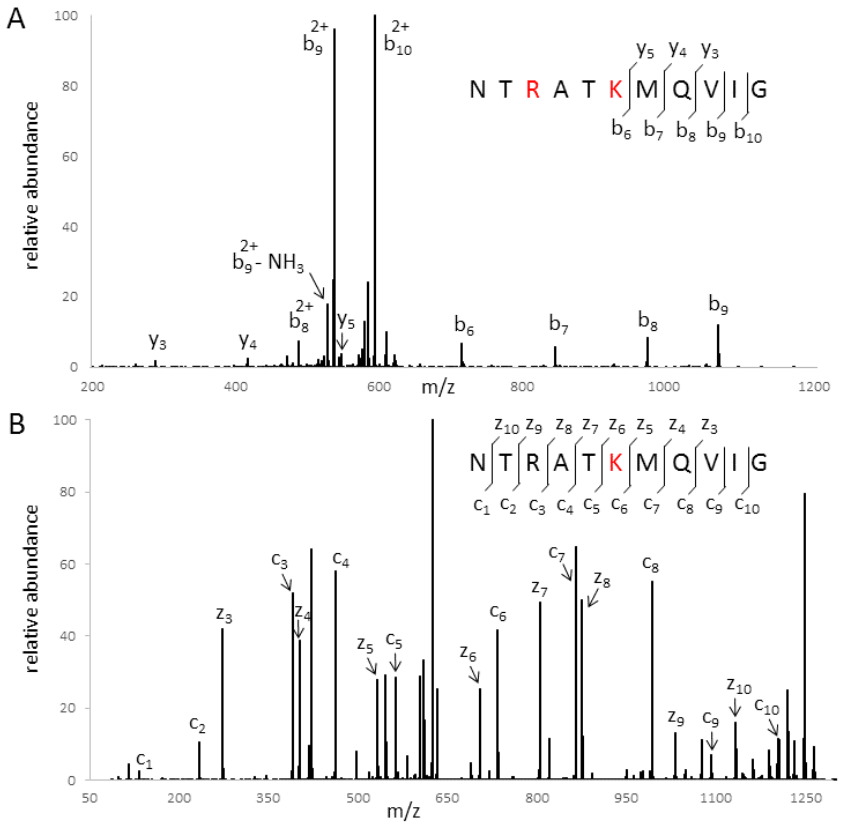

Figure S5 – ETD spectrum allows unambiguous identification of carbamoylation site
MSMS spectra of the single-carbamylated peptide NTRATKMQVIG generated by (A) collision-induced dissociation (CID; charge state 2) and (B) electron transfer dissociation (ETD; charge state 3). While in the case of CID fragmentation, carbamylation cannot unambiguously be assigned to lysine or arginine (both marked in red), ETD fragmentation clearly proofs the carbamylation of lysine (marked in red). The data was acquired in cooperation with Bernd Reisinger (PTB Braunschweig).

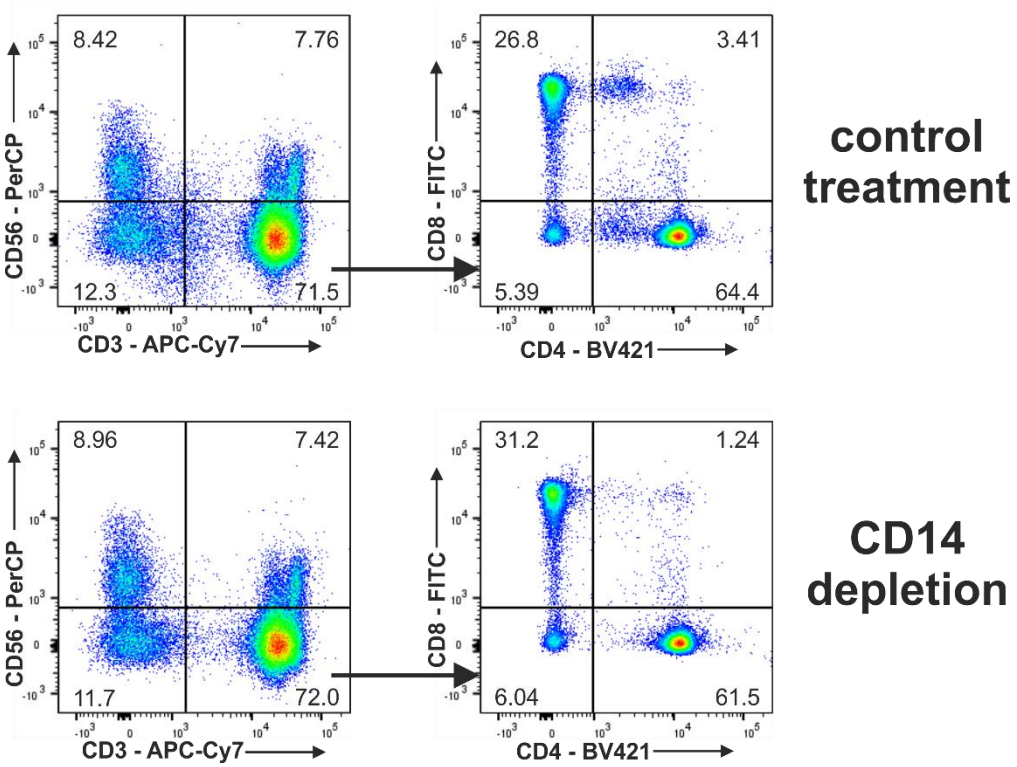

Figure S6 – CD14 depletion has no detectable impact on NK and T cell frequency

PBMCs from a CMV seropositive donor were depleted of CD14 positive cells via magnetic-activated cell sorting (MACS, lower panel) or subjected to control treatment (omission of the CD14 antibody/bead conjugate; upper panel). An aliquot from both samples was stained each for CD3, CD4, CD8 and CD56 with fluorescently labeled antibodies and subjected to flow cytometry analysis. The pseudocolor plots show NK cells ($CD3^-/CD56^+$) CD4 T cells ($CD3^+/CD4^+$) and CD8 T cells ($CD3^+/CD8^+$) with the respective population frequencies (%) displayed in each corner. The data shown in this figure was collected during the master's thesis of Tobias Brunner under my experimental supervision[267].

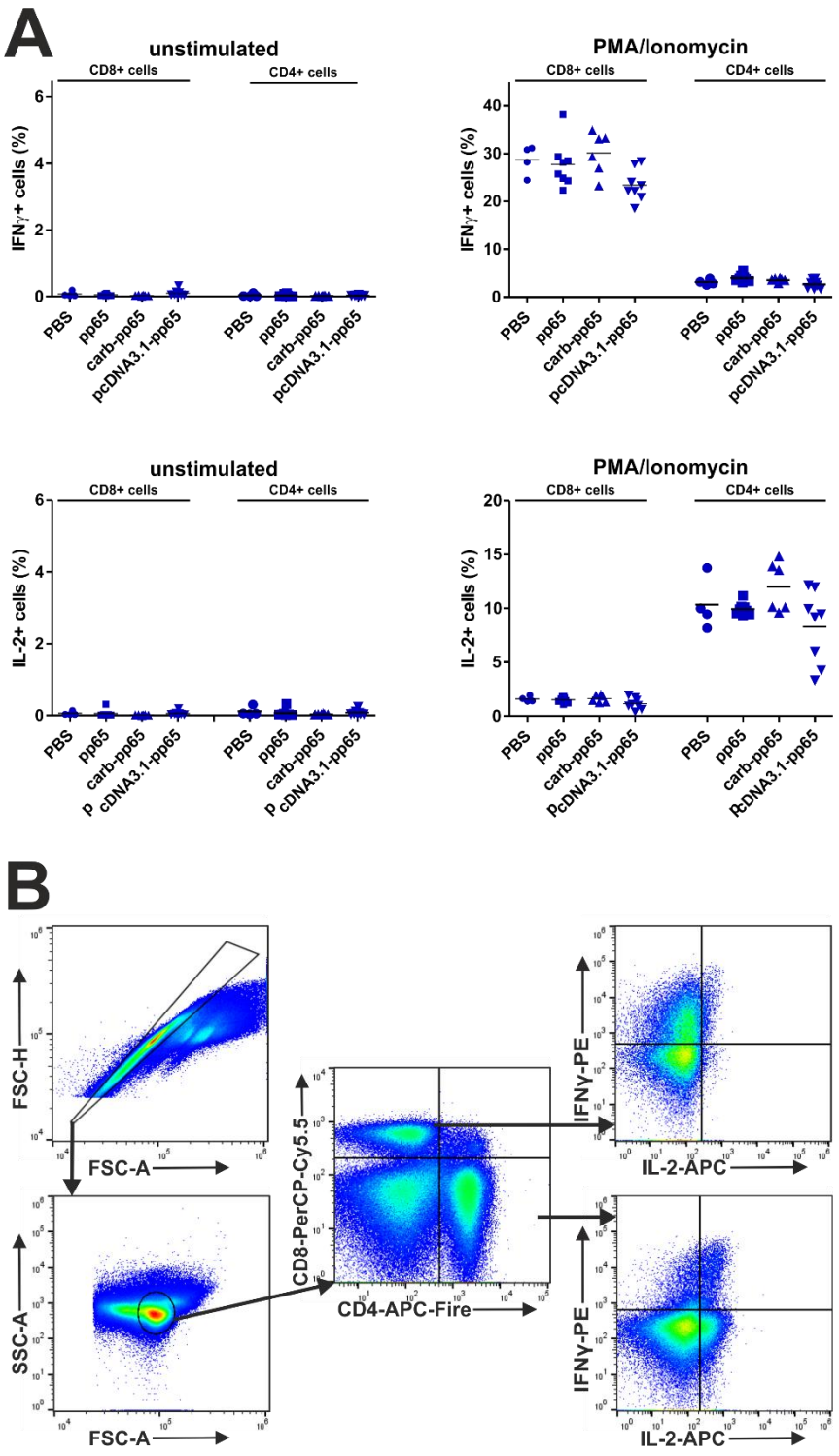

Figure S7 - Splenocyte stimulation with PMA/Ionomycin induces **IFNγ/IL**-2 synthesis

(A) Mice were immunized according to the regimen in Figure 29 and at week 4, splenocytes were isolated and stimulated for 6 hours with BFA only (as negative control) or BFA with PMA/Ionomycin (positive control). Cells were stained for CD4, CD8, intracellular IFNγ and IL-2, followed by flow cytometry analysis. Graphs show IFNγ or IL-2 positive cells that are further subdivided into $CD4^+$ or $CD8^+$ T cells. Horizontal lines represent the mean and blue symbols the individual values of each animal. (B) Gating strategy for identifying IFNγ and IL-2 positive T cells. Cell doublets and aggregates were first excluded in a forward scatter area (FSC-A) vs. forward scatter height (FSC-H) plot. Next, a gate was set around splenocytes according to FSC/SSC properties and T cells were identified by plotting CD4 signals against CD8. From CD4 and CD8 positive cells each, IFNγ signals were plotted against IL-2 signals and gates identifying cytokine-positive cells were defined according to the respective background values (determined using an unstimulated sample).

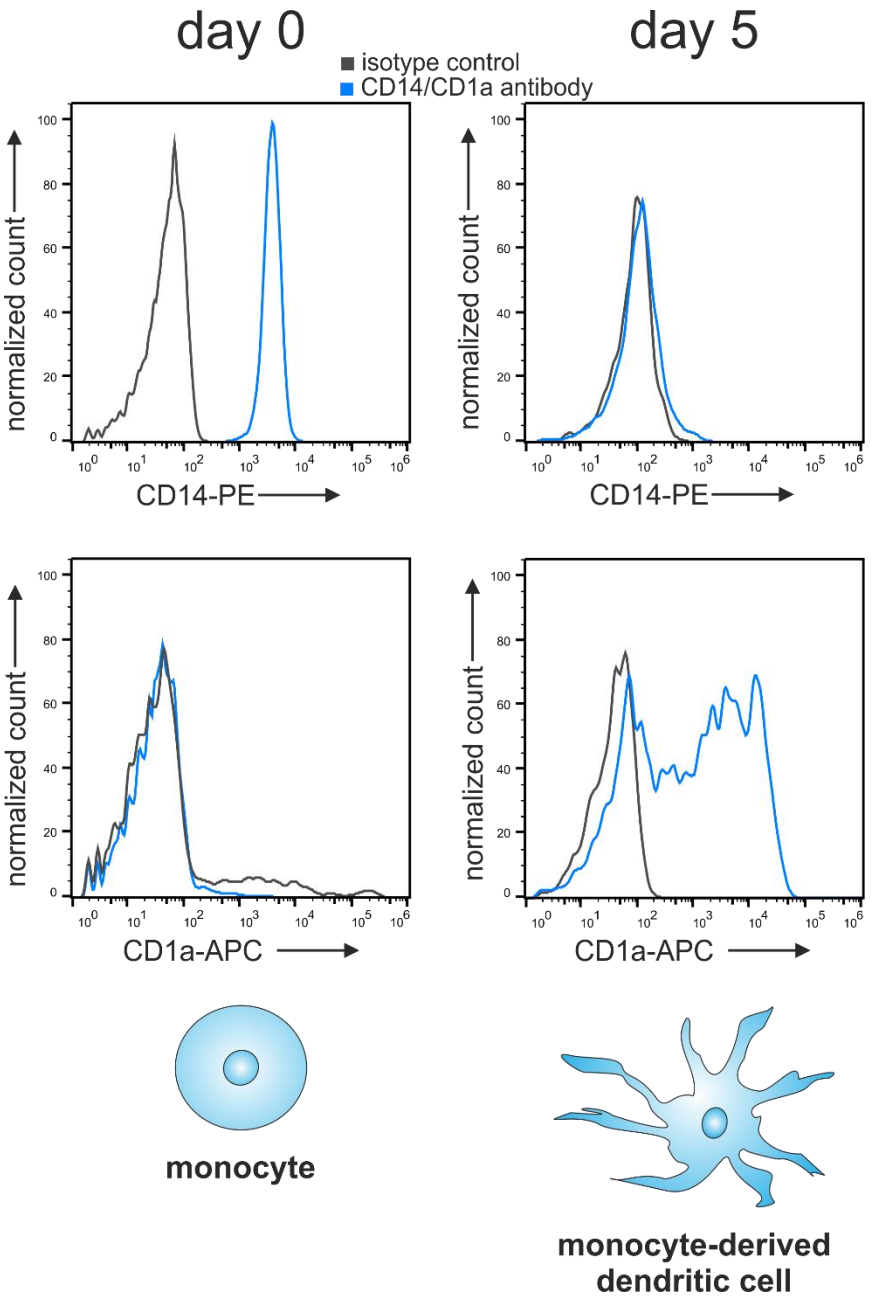

Figure S8– CD14/CD1a expression during monocyte differentiation to moDCs
Monocytes from a CMV seronegative donor were isolated via MACS sorting using CD14 antibody/bead conjugates and cultivated for 5 days in the presence of IL-4 and GM-CSF (1000 U/ml each). Directly after isolation and at day 5, samples were collected and stained for CD14 or CD1a, followed by flow cytometry analysis.

I.3. References

1. Knipe, D. M. & Howley, P. M. *Fields Virology*. (Lippincott Williams&Wilki, 2013).
2. Modrow, S., Falke, D., Truyen, U. & Schätzl, H. *Molekulare Virologie*. (Spektrum Akademischer Verlag, 2010).
3. Gardner, T. J. & Tortorella, D. Virion Glycoprotein-Mediated Immune Evasion by Human Cytomegalovirus: a Sticky Virus Makes a Slick Getaway. *Microbiol. Mol. Biol. Rev. MMBR* 80, 663–677 (2016).
4. Crowe, W. E., Maglova, L. M., Ponka, P. & Russell, J. M. Human cytomegalovirus-induced host cell enlargement is iron dependent. *Am. J. Physiol. Cell Physiol.* 287, C1023-1030 (2004).
5. Cannon, M. J., Schmid, D. S. & Hyde, T. B. Review of cytomegalovirus seroprevalence and demographic characteristics associated with infection. *Rev. Med. Virol.* 20, 202–213 (2010).
6. Staras, S. A. S. *et al.* Seroprevalence of cytomegalovirus infection in the United States, 1988-1994. *Clin. Infect. Dis. Off. Publ. Infect. Dis. Soc. Am.* 43, 1143–1151 (2006).
7. Ludwig, A. & Hengel, H. Epidemiological impact and disease burden of congenital cytomegalovirus infection in Europe. *Euro Surveill. Bull. Eur. Sur Mal. Transm. Eur. Commun. Dis. Bull.* 14, 26–32 (2009).
8. Cook, C. H. Cytomegalovirus reactivation in 'immunocompetent' patients: a call for scientific prophylaxis. *J. Infect. Dis.* 196, 1273–1275 (2007).
9. Sia, I. G. & Patel, R. New strategies for prevention and therapy of cytomegalovirus infection and disease in solid-organ transplant recipients. *Clin. Microbiol. Rev.* 13, 83–121 (2000).
10. Pass, R. F. & Anderson, B. Mother-to-Child Transmission of Cytomegalovirus and Prevention of Congenital Infection. *J. Pediatr. Infect. Dis. Soc.* 3, S2–S6 (2014).
11. Hansen, S. G. *et al.* Evasion of CD8+ T cells is critical for superinfection by cytomegalovirus. *Science* 328, 102–106 (2010).
12. Meyer-König, U., Ebert, K., Schrage, B., Pollak, S. & Hufert, F. T. Simultaneous infection of healthy people with multiple human cytomegalovirus strains. *Lancet Lond. Engl.* 352, 1280–1281 (1998).
13. Crough, T. & Khanna, R. Immunobiology of human cytomegalovirus: from bench to bedside. *Clin. Microbiol. Rev.* 22, 76–98, Table of Contents (2009).
14. Chee, M. S. *et al.* Analysis of the protein-coding content of the sequence of human cytomegalovirus strain AD169. *Curr. Top. Microbiol. Immunol.* 154, 125–169 (1990).
15. Varnum, S. M. *et al.* Identification of Proteins in Human Cytomegalovirus (HCMV) Particles: the HCMV Proteome. *J. Virol.* 78, 10960–10966 (2004).
16. Davison, A. J. Comparative analysis of the genomes. in *Human Herpesviruses: Biology, Therapy, and Immunoprophylaxis* (eds. Arvin, A. et al.) (Cambridge University Press, 2007).
17. Ng, K. R., Li, J. Y. Z. & Gleadle, J. M. Human cytomegalovirus encoded microRNAs: hitting targets. *Expert Rev. Anti Infect. Ther.* 13, 1469–1479 (2015).
18. Spaete, R. R., Gehrz, R. C. & Landini, M. P. Human cytomegalovirus structural proteins. *J. Gen. Virol.* 75 (Pt 12), 3287–3308 (1994).
19. Mocarski Jr., E. S. Comparative analysis of herpesvirus-common proteins. in *Human Herpesviruses: Biology, Therapy, and Immunoprophylaxis* (eds. Arvin, A. et al.) (Cambridge University Press, 2007).
20. Yu, X., Jih, J., Jiang, J. & Zhou, Z. H. Atomic structure of the human cytomegalovirus capsid with its securing tegument layer of pp150. *Science* 356, (2017).
21. Kalejta, R. F. Tegument proteins of human cytomegalovirus. *Microbiol. Mol. Biol. Rev. MMBR* 72, 249–265, table of contents (2008).
22. Liu, B. & Stinski, M. F. Human cytomegalovirus contains a tegument protein that enhances transcription from promoters with upstream ATF and AP-1 cis-acting elements. *J. Virol.* 66, 4434–4444 (1992).
23. Silva, M. C., Yu, Q.-C., Enquist, L. & Shenk, T. Human cytomegalovirus UL99-encoded pp28 is required for the cytoplasmic envelopment of tegument-associated capsids. *J. Virol.* 77, 10594–10605 (2003).
24. Arnon, T. I. *et al.* Inhibition of the NKp30 activating receptor by pp65 of human cytomegalovirus. *Nat. Immunol.* 6, 515–523 (2005).
25. Odeberg, J., Plachter, B., Brandén, L. & Söderberg-Nauclér, C. Human cytomegalovirus protein pp65 mediates accumulation of HLA-DR in lysosomes and destruction of the HLA-DR alpha-chain. *Blood* 101, 4870–4877 (2003).
26. Connolly, S. A., Jackson, J. O., Jardetzky, T. S. & Longnecker, R. Fusing structure and function: a structural view of the herpesvirus entry machinery. *Nat. Rev. Microbiol.* 9, 369–381 (2011).
27. Hetzenecker, S., Helenius, A. & Krzyzaniak, M. A. HCMV Induces Macropinocytosis for Host Cell Entry in Fibroblasts. *Traffic Cph. Den.* 17, 351–368 (2016).
28. Compton, T., Nepomuceno, R. R. & Nowlin, D. M. Human cytomegalovirus penetrates host cells by pH-independent fusion at the cell surface. *Virology* 191, 387–395 (1992).
29. Hahn, G. *et al.* Human cytomegalovirus UL131-128 genes are indispensable for virus growth in endothelial cells and virus transfer to leukocytes. *J. Virol.* 78, 10023–10033 (2004).
30. Wang, D. & Shenk, T. Human cytomegalovirus virion protein complex required for epithelial and endothelial cell tropism. *Proc. Natl. Acad. Sci. U. S. A.* 102, 18153–18158 (2005).
31. Nogalski, M. T., Chan, G. C. T., Stevenson, E. V., Collins-McMillen, D. K. & Yurochko, A. D. The HCMV gH/gL/UL128-131 complex triggers the specific cellular activation required for efficient viral internalization into target monocytes. *PLoS Pathog.* 9, e1003463 (2013).

32. Gerna, G. *et al.* Dendritic-cell infection by human cytomegalovirus is restricted to strains carrying functional UL131-128 genes and mediates efficient viral antigen presentation to CD8+ T cells. *J. Gen. Virol.* 86, 275–284 (2005).
33. Ryckman, B. J., Jarvis, M. A., Drummond, D. D., Nelson, J. A. & Johnson, D. C. Human cytomegalovirus entry into epithelial and endothelial cells depends on genes UL128 to UL150 and occurs by endocytosis and low-pH fusion. *J. Virol.* 80, 710–722 (2006).
34. Kari, B. & Gehrz, R. A human cytomegalovirus glycoprotein complex designated gC-II is a major heparin-binding component of the envelope. *J. Virol.* 66, 1761–1764 (1992).
35. Ogawa-Goto, K. *et al.* Microtubule network facilitates nuclear targeting of human cytomegalovirus capsid. *J. Virol.* 77, 8541–8547 (2003).
36. Stinski, M. F. & Meier, J. L. Immediate–early viral gene regulation and function. in *Human Herpesviruses: Biology, Therapy, and Immunoprophylaxis* (eds. Arvin, A. et al.) (Cambridge University Press, 2007).
37. White, E. A. & Spector, D. H. Early viral gene expression and function. in *Human Herpesviruses: Biology, Therapy, and Immunoprophylaxis* (eds. Arvin, A. et al.) (Cambridge University Press, 2007).
38. Anders, D. G., Kerry, J. A. & Pari, G. S. DNA synthesis and late viral gene expression. in *Human Herpesviruses: Biology, Therapy, and Immunoprophylaxis* (eds. Arvin, A. et al.) (Cambridge University Press, 2007).
39. Paulus, C. & Nevels, M. The human cytomegalovirus major immediate-early proteins as antagonists of intrinsic and innate antiviral host responses. *Viruses* 1, 760–779 (2009).
40. Marchini, A., Liu, H. & Zhu, H. Human cytomegalovirus with IE-2 (UL122) deleted fails to express early lytic genes. *J. Virol.* 75, 1870–1878 (2001).
41. Gawn, J. M. & Greaves, R. F. Absence of IE1 p72 protein function during low-multiplicity infection by human cytomegalovirus results in a broad block to viral delayed-early gene expression. *J. Virol.* 76, 4441–4455 (2002).
42. Zhu, H., Shen, Y. & Shenk, T. Human cytomegalovirus IE1 and IE2 proteins block apoptosis. *J. Virol.* 69, 7960–7970 (1995).
43. Huh, Y. H. *et al.* Binding STAT2 by the acidic domain of human cytomegalovirus IE1 promotes viral growth and is negatively regulated by SUMO. *J. Virol.* 82, 10444–10454 (2008).
44. Taylor, R. T. & Bresnahan, W. A. Human cytomegalovirus immediate-early 2 protein IE86 blocks virus-induced chemokine expression. *J. Virol.* 80, 920–928 (2006).
45. Amsler, L., Verweij, M. & DeFilippis, V. R. The tiers and dimensions of evasion of the type I interferon response by human cytomegalovirus. *J. Mol. Biol.* 425, 4857–4871 (2013).
46. Scherer, M. & Stamminger, T. Emerging Role of PML Nuclear Bodies in Innate Immune Signaling. *J. Virol.* 90, 5850–5854 (2016).
47. Scherer, M. *et al.* Crystal Structure of Cytomegalovirus IE1 Protein Reveals Targeting of TRIM Family Member PML via Coiled-Coil Interactions. *PLoS Pathog.* 10, (2014).
48. Wilkinson, G. W., Kelly, C., Sinclair, J. H. & Rickards, C. Disruption of PML-associated nuclear bodies mediated by the human cytomegalovirus major immediate early gene product. *J. Gen. Virol.* 79 (Pt 5), 1233–1245 (1998).
49. McMahon, T. P. & Anders, D. G. Interactions between human cytomegalovirus helicase-primase proteins. *Virus Res.* 86, 39–52 (2002).
50. Hamilton, S. T., Milbradt, J., Marschall, M. & Rawlinson, W. D. Human cytomegalovirus replication is strictly inhibited by siRNAs targeting UL54, UL97 or UL122/123 gene transcripts. *PloS One* 9, e97231 (2014).
51. Ertl, P. F. & Powell, K. L. Physical and functional interaction of human cytomegalovirus DNA polymerase and its accessory protein (ICP36) expressed in insect cells. *J. Virol.* 66, 4126–4133 (1992).
52. Anders, D. G. & Gibson, W. Location, transcript analysis, and partial nucleotide sequence of the cytomegalovirus gene encoding an early DNA-binding protein with similarities to ICP8 of herpes simplex virus type 1. *J. Virol.* 62, 1364–1372 (1988).
53. Marschall, M., Muller, Y. A., Diewald, B., Sticht, H. & Milbradt, J. The human cytomegalovirus nuclear egress complex unites multiple functions: Recruitment of effectors, nuclear envelope rearrangement, and docking to nuclear capsids. *Rev. Med. Virol.* 27, (2017).
54. Milbradt, J. *et al.* Proteomic analysis of the multimeric nuclear egress complex of human cytomegalovirus. *Mol. Cell. Proteomics MCP* 13, 2132–2146 (2014).
55. Schauflinger, M., Villinger, C., Mertens, T., Walther, P. & von Einem, J. Analysis of human cytomegalovirus secondary envelopment by advanced electron microscopy. *Cell. Microbiol.* 15, 305–314 (2013).
56. Villinger, C., Neusser, G., Kranz, C., Walther, P. & Mertens, T. 3D Analysis of HCMV Induced-Nuclear Membrane Structures by FIB/SEM Tomography: Insight into an Unprecedented Membrane Morphology. *Viruses* 7, 5686–5704 (2015).
57. Mettenleiter, T. C. Herpesvirus assembly and egress. *J. Virol.* 76, 1537–1547 (2002).
58. Mettenleiter, T. C. Budding events in herpesvirus morphogenesis. *Virus Res.* 106, 167–180 (2004).
59. Wills, M. R., Poole, E., Lau, B., Krishna, B. & Sinclair, J. H. The immunology of human cytomegalovirus latency: could latent infection be cleared by novel immunotherapeutic strategies? *Cell. Mol. Immunol.* 12, 128–138 (2015).
60. Goodrum, F., Reeves, M., Sinclair, J., High, K. & Shenk, T. Human cytomegalovirus sequences expressed in latently infected individuals promote a latent infection in vitro. *Blood* 110, 937–945 (2007).
61. Mendelson, M., Monard, S., Sissons, P. & Sinclair, J. Detection of endogenous human cytomegalovirus in CD34+ bone marrow progenitors. *J. Gen. Virol.* 77 (Pt 12), 3099–3102 (1996).

62. Kondo, K., Kaneshima, H. & Mocarski, E. S. Human cytomegalovirus latent infection of granulocyte-macrophage progenitors. *Proc. Natl. Acad. Sci. U. S. A.* 91, 11879–11883 (1994).
63. Hahn, G., Jores, R. & Mocarski, E. S. Cytomegalovirus remains latent in a common precursor of dendritic and myeloid cells. *Proc. Natl. Acad. Sci. U. S. A.* 95, 3937–3942 (1998).
64. Hargett, D. & Shenk, T. E. Experimental human cytomegalovirus latency in CD14+ monocytes. *Proc. Natl. Acad. Sci. U. S. A.* 107, 20039–20044 (2010).
65. Reeves, M. B., MacAry, P. A., Lehner, P. J., Sissons, J. G. P. & Sinclair, J. H. Latency, chromatin remodeling, and reactivation of human cytomegalovirus in the dendritic cells of healthy carriers. *Proc. Natl. Acad. Sci. U. S. A.* 102, 4140–4145 (2005).
66. Sinclair, J. Human cytomegalovirus: Latency and reactivation in the myeloid lineage. *J. Clin. Virol. Off. Publ. Pan Am. Soc. Clin. Virol.* 41, 180–185 (2008).
67. Delale, T. *et al.* MyD88-dependent and -independent murine cytomegalovirus sensing for IFN-alpha release and initiation of immune responses in vivo. *J. Immunol. Baltim. Md 1950* 175, 6723–6732 (2005).
68. Tabeta, K. *et al.* Toll-like receptors 9 and 3 as essential components of innate immune defense against mouse cytomegalovirus infection. *Proc. Natl. Acad. Sci. U. S. A.* 101, 3516–3521 (2004).
69. Boehme, K. W., Guerrero, M. & Compton, T. Human cytomegalovirus envelope glycoproteins B and H are necessary for TLR2 activation in permissive cells. *J. Immunol. Baltim. Md 1950* 177, 7094–7102 (2006).
70. Compton, T. *et al.* Human cytomegalovirus activates inflammatory cytokine responses via CD14 and Toll-like receptor 2. *J. Virol.* 77, 4588–4596 (2003).
71. Polić, B. *et al.* Hierarchical and redundant lymphocyte subset control precludes cytomegalovirus replication during latent infection. *J. Exp. Med.* 188, 1047–1054 (1998).
72. Bukowski, J. F., Woda, B. A., Habu, S., Okumura, K. & Welsh, R. M. Natural killer cell depletion enhances virus synthesis and virus-induced hepatitis in vivo. *J. Immunol. Baltim. Md 1950* 131, 1531–1538 (1983).
73. Bukowski, J. F., Warner, J. F., Dennert, G. & Welsh, R. M. Adoptive transfer studies demonstrating the antiviral effect of natural killer cells in vivo. *J. Exp. Med.* 161, 40–52 (1985).
74. Kuijpers, T. W. *et al.* Human NK cells can control CMV infection in the absence of T cells. *Blood* 112, 914–915 (2008).
75. Orange, J. S. Formation and function of the lytic NK-cell immunological synapse. *Nat. Rev. Immunol.* 8, 713–725 (2008).
76. Gumá, M. *et al.* Expansion of CD94/NKG2C+ NK cells in response to human cytomegalovirus-infected fibroblasts. *Blood* 107, 3624–3631 (2006).
77. Lopez-Vergès, S. *et al.* Expansion of a unique CD57^{+}NKG2Chi natural killer cell subset during acute human cytomegalovirus infection. *Proc. Natl. Acad. Sci. U. S. A.* 108, 14725–14732 (2011).
78. Rölle, A. & Brodin, P. Immune Adaptation to Environmental Influence: The Case of NK Cells and HCMV. *Trends Immunol.* 37, 233–243 (2016).
79. Rölle, A. *et al.* IL-12-producing monocytes and HLA-E control HCMV-driven NKG2C+ NK cell expansion. *J. Clin. Invest.* 124, 5305–5316 (2014).
80. Foley, B. *et al.* Human cytomegalovirus (CMV)-induced memory-like NKG2C(+) NK cells are transplantable and expand in vivo in response to recipient CMV antigen. *J. Immunol. Baltim. Md 1950* 189, 5082–5088 (2012).
81. Schlums, H. *et al.* Cytomegalovirus infection drives adaptive epigenetic diversification of NK cells with altered signaling and effector function. *Immunity* 42, 443–456 (2015).
82. Peng, H. & Tian, Z. Natural Killer Cell Memory: Progress and Implications. *Front. Immunol.* 8, 1143 (2017).
83. Chandramouli, S. *et al.* Structural basis for potent antibody-mediated neutralization of human cytomegalovirus. *Sci. Immunol.* 2, (2017).
84. Jonjić, S. *et al.* Antibodies are not essential for the resolution of primary cytomegalovirus infection but limit dissemination of recurrent virus. *J. Exp. Med.* 179, 1713–1717 (1994).
85. Boppana, S. B. & Britt, W. J. Antiviral antibody responses and intrauterine transmission after primary maternal cytomegalovirus infection. *J. Infect. Dis.* 171, 1115–1121 (1995).
86. Fornara, C. *et al.* Primary human cytomegalovirus infections: kinetics of ELISA-IgG and neutralizing antibody in pauci/asymptomatic pregnant women vs symptomatic non-pregnant subjects. *J. Clin. Virol. Off. Publ. Pan Am. Soc. Clin. Virol.* 64, 45–51 (2015).
87. Gerna, G. *et al.* Differential kinetics of human cytomegalovirus load and antibody responses in primary infection of the immunocompetent and immunocompromised host. *J. Gen. Virol.* 96, 360–369 (2015).
88. Kabanova, A. *et al.* Antibody-driven design of a human cytomegalovirus gHgLpUL128L subunit vaccine that selectively elicits potent neutralizing antibodies. *Proc. Natl. Acad. Sci. U. S. A.* 111, 17965–17970 (2014).
89. Wang, D. *et al.* A replication-defective human cytomegalovirus vaccine for prevention of congenital infection. *Sci. Transl. Med.* 8, 362ra145 (2016).
90. Wen, Y. *et al.* Human cytomegalovirus gH/gL/UL128/UL130/UL131A complex elicits potently neutralizing antibodies in mice. *Vaccine* 32, 3796–3804 (2014).
91. Wussow, F. *et al.* A vaccine based on the rhesus cytomegalovirus UL128 complex induces broadly neutralizing antibodies in rhesus macaques. *J. Virol.* 87, 1322–1332 (2013).
92. Macagno, A. *et al.* Isolation of human monoclonal antibodies that potently neutralize human cytomegalovirus infection by targeting different epitopes on the gH/gL/UL128-131A complex. *J. Virol.* 84, 1005–1013 (2010).

93. Pereira, L., Maidji, E., McDonagh, S. & Tabata, T. Insights into viral transmission at the uterine-placental interface. *Trends Microbiol.* 13, 164–174 (2005).
94. Tabata, T., McDonagh, S., Kawakatsu, H. & Pereira, L. Cytotrophoblasts infected with a pathogenic human cytomegalovirus strain dysregulate cell-matrix and cell-cell adhesion molecules: a quantitative analysis. *Placenta* 28, 527–537 (2007).
95. Lilleri, D. *et al.* Fetal human cytomegalovirus transmission correlates with delayed maternal antibodies to gH/gL/pUL128-130-131 complex during primary infection. *PloS One* 8, e59863 (2013).
96. Lilleri, D., Kabanova, A., Lanzavecchia, A. & Gerna, G. Antibodies against neutralization epitopes of human cytomegalovirus gH/gL/pUL128-130-131 complex and virus spreading may correlate with virus control in vivo. *J. Clin. Immunol.* 32, 1324–1331 (2012).
97. Schleiss, M. R., Permar, S. R. & Plotkin, S. A. Progress Toward Development of a Vaccine Against Congenital Cytomegalovirus Infection. *Clin. Vaccine Immunol. CVI* (2017). doi:10.1128/CVI.00268-17
98. Sylwester, A. W. *et al.* Broadly targeted human cytomegalovirus-specific CD4+ and CD8+ T cells dominate the memory compartments of exposed subjects. *J. Exp. Med.* 202, 673–685 (2005).
99. Klenerman, P. & Oxenius, A. T cell responses to cytomegalovirus. *Nat. Rev. Immunol.* 16, 367–377 (2016).
100. Jackson, S. E., Mason, G. M., Okecha, G., Sissons, J. G. P. & Wills, M. R. Diverse specificities, phenotypes, and antiviral activities of cytomegalovirus-specific CD8+ T cells. *J. Virol.* 88, 10894–10908 (2014).
101. Lilleri, D., Fornara, C., Revello, M. G. & Gerna, G. Human cytomegalovirus-specific memory CD8+ and CD4+ T cell differentiation after primary infection. *J. Infect. Dis.* 198, 536–543 (2008).
102. Appay, V. *et al.* Memory CD8+ T cells vary in differentiation phenotype in different persistent virus infections. *Nat. Med.* 8, 379–385 (2002).
103. Karrer, U. *et al.* Memory inflation: continuous accumulation of antiviral CD8+ T cells over time. *J. Immunol. Baltim. Md 1950* 170, 2022–2029 (2003).
104. Wherry, E. J. & Kurachi, M. Molecular and cellular insights into T cell exhaustion. *Nat. Rev. Immunol.* 15, 486–499 (2015).
105. Frebel, H., Richter, K. & Oxenius, A. How chronic viral infections impact on antigen-specific T-cell responses. *Eur. J. Immunol.* 40, 654–663 (2010).
106. Seckert, C. K. *et al.* Viral latency drives 'memory inflation': a unifying hypothesis linking two hallmarks of cytomegalovirus infection. *Med. Microbiol. Immunol. (Berl.)* 201, 551–566 (2012).
107. Liu, X. *et al.* Epigenetic control of cytomegalovirus latency and reactivation. *Viruses* 5, 1325–1345 (2013).
108. Sylwester, A. *et al.* A new perspective of the structural complexity of HCMV-specific T-cell responses. *Mech. Ageing Dev.* 158, 14–22 (2016).
109. Whiting, C. C. *et al.* Large-Scale and Comprehensive Immune Profiling and Functional Analysis of Normal Human Aging. *PloS One* 10, e0133627 (2015).
110. Tu, W. & Rao, S. Mechanisms Underlying T Cell Immunosenescence: Aging and Cytomegalovirus Infection. *Front. Microbiol.* 7, (2016).
111. Barry, A. P. *et al.* Depletion of CD8+ cells in sooty mangabey monkeys naturally infected with simian immunodeficiency virus reveals limited role for immune control of virus replication in a natural host species. *J. Immunol. Baltim. Md 1950* 178, 8002–8012 (2007).
112. Mutter, W., Reddehase, M. J., Busch, F. W., Bühring, H. J. & Koszinowski, U. H. Failure in generating hemopoietic stem cells is the primary cause of death from cytomegalovirus disease in the immunocompromised host. *J. Exp. Med.* 167, 1645–1658 (1988).
113. Reddehase, M. J. *et al.* Interstitial murine cytomegalovirus pneumonia after irradiation: characterization of cells that limit viral replication during established infection of the lungs. *J. Virol.* 55, 264–273 (1985).
114. Riddell, S. R. *et al.* Restoration of viral immunity in immunodeficient humans by the adoptive transfer of T cell clones. *Science* 257, 238–241 (1992).
115. Einsele, H. *et al.* Infusion of cytomegalovirus (CMV)-specific T cells for the treatment of CMV infection not responding to antiviral chemotherapy. *Blood* 99, 3916–3922 (2002).
116. Walter, E. A. *et al.* Reconstitution of cellular immunity against cytomegalovirus in recipients of allogeneic bone marrow by transfer of T-cell clones from the donor. *N. Engl. J. Med.* 333, 1038–1044 (1995).
117. Lancini, D., Faddy, H. M., Flower, R. & Hogan, C. Cytomegalovirus disease in immunocompetent adults. *Med. J. Aust.* 201, 578–580 (2014).
118. Kotton, C. N. Management of cytomegalovirus infection in solid organ transplantation. *Nat. Rev. Nephrol.* 6, 711–721 (2010).
119. Ljungman, P., Hakki, M. & Boeckh, M. Cytomegalovirus in Hematopoietic Stem Cell Transplant Recipients. *Hematol. Oncol. Clin. North Am.* 25, 151–169 (2011).
120. Drew, W. L. Cytomegalovirus Infection in Patients with AIDS. *Clin. Infect. Dis.* 14, 608–615 (1992).
121. Sinzger, C., Digel, M. & Jahn, G. Cytomegalovirus cell tropism. *Curr. Top. Microbiol. Immunol.* 325, 63–83 (2008).
122. Steininger, C. Clinical relevance of cytomegalovirus infection in patients with disorders of the immune system. *Clin. Microbiol. Infect. Off. Publ. Eur. Soc. Clin. Microbiol. Infect. Dis.* 13, 953–963 (2007).
123. Boeckh, M. & Geballe, A. P. Cytomegalovirus: pathogen, paradigm, and puzzle. *J. Clin. Invest.* 121, 1673–1680 (2011).
124. Manicklal, S., Emery, V. C., Lazzarotto, T., Boppana, S. B. & Gupta, R. K. The "Silent" Global Burden of Congenital Cytomegalovirus. *Clin. Microbiol. Rev.* 26, 86–102 (2013).

125. Kenneson, A. & Cannon, M. J. Review and meta-analysis of the epidemiology of congenital cytomegalovirus (CMV) infection. *Rev. Med. Virol.* 17, 253–276 (2007).
126. Stagno, S. *et al.* Congenital cytomegalovirus infection: The relative importance of primary and recurrent maternal infection. *N. Engl. J. Med.* 306, 945–949 (1982).
127. Ornoy, A. & Diav-Citrin, O. Fetal effects of primary and secondary cytomegalovirus infection in pregnancy. *Reprod. Toxicol. Elmsford N* 21, 399–409 (2006).
128. Yow, M. D. *et al.* Epidemiologic characteristics of cytomegalovirus infection in mothers and their infants. *Am. J. Obstet. Gynecol.* 158, 1189–1195 (1988).
129. Demmler, G. J. Infectious Diseases Society of America and Centers for Disease Control. Summary of a workshop on surveillance for congenital cytomegalovirus disease. *Rev. Infect. Dis.* 13, 315–329 (1991).
130. Fowler, K. B. *et al.* The outcome of congenital cytomegalovirus infection in relation to maternal antibody status. *N. Engl. J. Med.* 326, 663–667 (1992).
131. Nigro, G. Maternal-fetal cytomegalovirus infection: from diagnosis to therapy. *J. Matern.-Fetal Neonatal Med. Off. J. Eur. Assoc. Perinat. Med. Fed. Asia Ocean. Perinat. Soc. Int. Soc. Perinat. Obstet.* 22, 169–174 (2009).
132. Emery, V. C. & Lazzarotto, T. Cytomegalovirus in pregnancy and the neonate. *F1000Research* 6, 138 (2017).
133. Kralickova, P. *et al.* Cytomegalovirus disease in patients with common variable immunodeficiency: three case reports. *Int. Arch. Allergy Immunol.* 163, 69–74 (2014).
134. Hanley, P. J. *et al.* CMV-specific T cells generated from naïve T cells recognize atypical epitopes and may be protective in vivo. *Sci. Transl. Med.* 7, 285ra63 (2015).
135. Dropulic, L. K. & Cohen, J. I. Severe Viral Infections and Primary Immunodeficiencies. *Clin. Infect. Dis. Off. Publ. Infect. Dis. Soc. Am.* 53, 897–909 (2011).
136. Rieder, F. & Steininger, C. Cytomegalovirus vaccine: phase II clinical trial results. *Clin. Microbiol. Infect. Off. Publ. Eur. Soc. Clin. Microbiol. Infect. Dis.* 20 Suppl 5, 95–102 (2014).
137. Bowen, E. F., Griffiths, P. D., Davey, C. C., Emery, V. C. & Johnson, M. A. Lessons from the natural history of cytomegalovirus. *AIDS Lond. Engl.* 10 Suppl 1, S37-41 (1996).
138. Squifflet, J.-P. & Legendre, C. The economic value of valacyclovir prophylaxis in transplantation. *J. Infect. Dis.* 186 Suppl 1, S116-122 (2002).
139. Razonable, R. R., Emery, V. C. & 11th Annual Meeting of the IHMF (International Herpes Management Forum). Management of CMV infection and disease in transplant patients. 27-29 February 2004. *Herpes J. IHMF* 11, 77–86 (2004).
140. Hernandez, M. D. P., Martin, P. & Simkins, J. Infectious Complications After Liver Transplantation. *Gastroenterol. Hepatol.* 11, 741–753 (2015).
141. Splendiani, G. *et al.* Infectious complications in renal transplant recipients. *Transplant. Proc.* 37, 2497–2499 (2005).
142. Haidar, G. & Singh, N. Viral infections in solid organ transplant recipients: novel updates and a review of the classics. *Curr. Opin. Infect. Dis.* (2017). doi:10.1097/QCO.0000000000000409
143. Azevedo, L. S. *et al.* Cytomegalovirus infection in transplant recipients. *Clinics* 70, 515–523 (2015).
144. Ohata, K. *et al.* Cytomegalovirus infection in living-donor and cadaveric lung transplantations. *Interact. Cardiovasc. Thorac. Surg.* (2017). doi:10.1093/icvts/ivx226
145. Khan, S., Fischman, C. & Huprikar, S. Low-dose valganciclovir prophylaxis for cytomegalovirus in intermediate-risk (R+) renal transplant recipients: single center experience. *Transpl. Infect. Dis. Off. J. Transplant. Soc.* (2017). doi:10.1111/tid.12780
146. Kalil, A. C., Levitsky, J., Lyden, E., Stoner, J. & Freifeld, A. G. Meta-analysis: the efficacy of strategies to prevent organ disease by cytomegalovirus in solid organ transplant recipients. *Ann. Intern. Med.* 143, 870–880 (2005).
147. Hammerstrom, A. E. *et al.* Prevention of CMV Reactivation in Haploidentical Stem Cell Transplantation. *Biol. Blood Marrow Transplant. J. Am. Soc. Blood Marrow Transplant.* (2017). doi:10.1016/j.bbmt.2017.09.018
148. Kwan, L. P., Mok, M. M., Choy, B. Y. & Chan, T. M. Acute kidney injury in a renal transplant recipient due to concomitant use of vancomycin and foscarnet. *Nephrol. Carlton Vic* 22, 821–822 (2017).
149. Bonatti, H. *et al.* Use of Cidofovir for Cytomegalovirus Disease Refractory to Ganciclovir in Solid Organ Recipients. *Surg. Infect.* 18, 128–136 (2017).
150. Aslani, H. R. *et al.* Incidence of Ganciclovir Resistance in CMV-positive Renal Transplant Recipients and its Association with UL97 Gene Mutations. *Iran. J. Pharm. Res. IJPR* 16, 805–810 (2017).
151. Boeckh, M. *et al.* Valganciclovir for the prevention of complications of late cytomegalovirus infection after allogeneic hematopoietic cell transplantation: a randomized trial. *Ann. Intern. Med.* 162, 1–10 (2015).
152. Kotton, C. N. CMV: Prevention, Diagnosis and Therapy. *Am. J. Transplant. Off. J. Am. Soc. Transplant. Am. Soc. Transpl. Surg.* 13 Suppl 3, 24–40; quiz 40 (2013).
153. Natori, Y. *et al.* Can Viral Load be used as a Surrogate Marker in Clinical Studies of Cytomegalovirus in Solid Organ Transplantation: A Systematic Review and Meta-analysis. *Clin. Infect. Dis. Off. Publ. Infect. Dis. Soc. Am.* (2017). doi:10.1093/cid/cix793
154. Hasegawa, J. *et al.* Preemptive anti-cytomegalovirus therapy in high-risk (donor positive, recipient negative cytomegalovirus serostatus) kidney transplant recipients. *Int. J. Infect. Dis. IJID Off. Publ. Int. Soc. Infect. Dis.* (2017). doi:10.1016/j.ijid.2017.09.023

155. Eiz-Vesper, B., Maecker-Kolhoff, B. & Blasczyk, R. Adoptive T-cell immunotherapy from third-party donors: characterization of donors and set up of a T-cell donor registry. *Front. Immunol.* 3, 410 (2012).
156. Forcina, A., Noviello, M., Carbone, M. R., Bonini, C. & Bondanza, A. Predicting the Clinical Outcome of Allogeneic Hematopoietic Stem Cell Transplantation: The Long and Winding Road toward Validated Immune Biomarkers. *Front. Immunol.* 4, 71 (2013).
157. Pei, X.-Y. *et al.* Cytomegalovirus-Specific T-Cell Transfer for Refractory Cytomegalovirus Infection After Haploidentical Stem Cell Transplantation: The Quantitative and Qualitative Immune Recovery for Cytomegalovirus. *J. Infect. Dis.* (2017). doi:10.1093/infdis/jix357
158. Reusser, P., Riddell, S. R., Meyers, J. D. & Greenberg, P. D. Cytotoxic T-lymphocyte response to cytomegalovirus after human allogeneic bone marrow transplantation: pattern of recovery and correlation with cytomegalovirus infection and disease. *Blood* 78, 1373–1380 (1991).
159. Lilleri, D. *et al.* Prospective simultaneous quantification of human cytomegalovirus-specific CD4+ and CD8+ T-cell reconstitution in young recipients of allogeneic hematopoietic stem cell transplants. *Blood* 108, 1406–1412 (2006).
160. Gratama, J. W. *et al.* Monitoring cytomegalovirus IE-1 and pp65-specific CD4+ and CD8+ T-cell responses after allogeneic stem cell transplantation may identify patients at risk for recurrent CMV reactivations. *Cytometry B Clin. Cytom.* 74, 211–220 (2008).
161. Boeckh, M. *et al.* Late cytomegalovirus disease and mortality in recipients of allogeneic hematopoietic stem cell transplants: importance of viral load and T-cell immunity. *Blood* 101, 407–414 (2003).
162. Krause, H., Hebart, H., Jahn, G., Müller, C. A. & Einsele, H. Screening for CMV-specific T cell proliferation to identify patients at risk of developing late onset CMV disease. *Bone Marrow Transplant.* 19, 1111–1116 (1997).
163. Espigado, I. *et al.* Timing of CMV-specific effector memory T cells predicts viral replication and survival after allogeneic hematopoietic stem cell transplantation. *Transpl. Int. Off. J. Eur. Soc. Organ Transplant.* 27, 1253–1262 (2014).
164. Fuji, S., Kapp, M. & Einsele, H. Monitoring of pathogen-specific T-cell immune reconstitution after allogeneic hematopoietic stem cell transplantation. *Front. Immunol.* 4, 276 (2013).
165. Cwynarski, K. *et al.* Direct visualization of cytomegalovirus-specific T-cell reconstitution after allogeneic stem cell transplantation. *Blood* 97, 1232–1240 (2001).
166. Pourgheysari, B. *et al.* Early reconstitution of effector memory CD4+ CMV-specific T cells protects against CMV reactivation following allogeneic SCT. *Bone Marrow Transplant.* 43, 853–861 (2009).
167. Tormo, N. *et al.* Reconstitution of CMV pp65 and IE-1-specific IFN-γ CD8(+) and CD4(+) T-cell responses affording protection from CMV DNAemia following allogeneic hematopoietic SCT. *Bone Marrow Transplant.* 46, 1437–1443 (2011).
168. Institute of Medicine (US) Committee to Study Priorities for Vaccine Development. *Vaccines for the 21st Century: A Tool for Decisionmaking*. (National Academies Press (US), 2000).
169. Xia, L., Su, R., An, Z., Fu, T.-M. & Luo, W. Human Cytomegalovirus vaccine development: Immune responses to look into vaccine strategy. *Hum. Vaccines Immunother.* 0 (2017). doi:10.1080/21645515.2017.1391433
170. Kimberlin, D. W. *et al.* Effect of ganciclovir therapy on hearing in symptomatic congenital cytomegalovirus disease involving the central nervous system: a randomized, controlled trial. *J. Pediatr.* 143, 16–25 (2003).
171. Drew, W. L. *et al.* Prevalence of resistance in patients receiving ganciclovir for serious cytomegalovirus infection. *J. Infect. Dis.* 163, 716–719 (1991).
172. Limaye, A. P. Ganciclovir-resistant cytomegalovirus in organ transplant recipients. *Clin. Infect. Dis. Off. Publ. Infect. Dis. Soc. Am.* 35, 866–872 (2002).
173. Blázquez-Gamero, D. *et al.* Prevention and treatment of fetal cytomegalovirus infection with cytomegalovirus hyperimmune globulin: a multicenter study in Madrid. *J. Matern.-Fetal Neonatal Med. Off. J. Eur. Assoc. Perinat. Med. Fed. Asia Ocean. Perinat. Soc. Int. Soc. Perinat. Obstet.* 1–211 (2017). doi:10.1080/14767058.2017.1387890
174. Jacobson, M. A. *et al.* Antigen-specific T cell responses induced by Towne cytomegalovirus (CMV) vaccine in CMV-seronegative vaccine recipients. *J. Clin. Virol.* 35, 332–337 (2006).
175. Bernstein, D. I. *et al.* Randomized, double-blind, Phase 1 trial of an alphavirus replicon vaccine for cytomegalovirus in CMV seronegative adult volunteers. *Vaccine* 28, 484–493 (2009).
176. Zhong, J. & Khanna, R. Ad-gBCMVpoly: A novel chimeric vaccine strategy for human cytomegalovirus-associated diseases. *J. Clin. Virol. Off. Publ. Pan Am. Soc. Clin. Virol.* 46 Suppl 4, S68-72 (2009).
177. Wloch, M. K. *et al.* Safety and immunogenicity of a bivalent cytomegalovirus DNA vaccine in healthy adult subjects. *J. Infect. Dis.* 197, 1634–1642 (2008).
178. Pepperl, S., Münster, J., Mach, M., Harris, J. R. & Plachter, B. Dense Bodies of Human Cytomegalovirus Induce both Humoral and Cellular Immune Responses in the Absence of Viral Gene Expression. *J. Virol.* 74, 6132–6146 (2000).
179. Drulak, M. W. *et al.* Vaccination of seropositive subjects with CHIRON CMV gB subunit vaccine combined with MF59 adjuvant for production of CMV immune globulin. *Viral Immunol.* 13, 49–56 (2000).
180. Dasari, V., Smith, C. & Khanna, R. Recent advances in designing an effective vaccine to prevent cytomegalovirus-associated clinical diseases. *Expert Rev. Vaccines* 12, 661–676 (2013).
181. Pass, R. F. *et al.* Vaccine prevention of maternal cytomegalovirus infection. *N. Engl. J. Med.* 360, 1191–1199 (2009).

182. Kharfan-Dabaja, M. A. *et al.* A novel therapeutic cytomegalovirus DNA vaccine in allogeneic haemopoietic stem-cell transplantation: a randomised, double-blind, placebo-controlled, phase 2 trial. *Lancet Infect. Dis.* 12, 290–299 (2012).
183. Wu, S. J., Villarreal, D. O., Shedlock, D. J. & Weiner, D. B. Synthetic DNA Approach to Cytomegalovirus Vaccine/Immune Therapy. *Adv. Exp. Med. Biol.* 848, 131–148 (2015).
184. Wang, D. & Shenk, T. Human cytomegalovirus UL131 open reading frame is required for epithelial cell tropism. *J. Virol.* 79, 10330–10338 (2005).
185. Wussow, F. *et al.* Human Cytomegalovirus Vaccine Based on the Envelope gH/gL Pentamer Complex. *PLOS Pathog* 10, e1004524 (2014).
186. Fu, T.-M. *et al.* Restoration of viral epithelial tropism improves immunogenicity in rabbits and rhesus macaques for a whole virion vaccine of human cytomegalovirus. *Vaccine* 30, 7469–7474 (2012).
187. Slezak, S. L. *et al.* CMV pp65 and IE-1 T cell epitopes recognized by healthy subjects. *J. Transl. Med.* 5, 17 (2007).
188. Prins, R. M., Cloughesy, T. F. & Liau, L. M. Cytomegalovirus immunity after vaccination with autologous glioblastoma lysate. *N. Engl. J. Med.* 359, 539–541 (2008).
189. Mitchell, D. A. *et al.* Sensitive detection of human cytomegalovirus in tumors and peripheral blood of patients diagnosed with glioblastoma. *Neuro-Oncol.* 10, 10–18 (2008).
190. Batich, K. A. *et al.* Long-term Survival in Glioblastoma with Cytomegalovirus pp65-Targeted Vaccination. *Clin. Cancer Res. Off. J. Am. Assoc. Cancer Res.* 23, 1898–1909 (2017).
191. Ura, T., Okuda, K. & Shimada, M. Developments in Viral Vector-Based Vaccines. *Vaccines* 2, 624–641 (2014).
192. Schleiss, M. R. Cytomegalovirus vaccines under clinical development. *J. Virus Erad.* 2, 198–207 (2016).
193. La Rosa, C. *et al.* MVA vaccine encoding CMV antigens safely induces durable expansion of CMV-specific T cells in healthy adults. *Blood* 129, 114–125 (2017).
194. Volz, A. & Sutter, G. Modified Vaccinia Virus Ankara: History, Value in Basic Research, and Current Perspectives for Vaccine Development. *Adv. Virus Res.* 97, 187–243 (2017).
195. Schramm, B. & Locker, J. K. Cytoplasmic organization of POXvirus DNA replication. *Traffic Cph. Den.* 6, 839–846 (2005).
196. Stuart N. Isaacs. *Vaccinia Virus and Poxvirology - Methods and Protocols (1st edition)*. (Springer).
197. Huygelen, C. [Jenner's cowpox vaccine in light of current vaccinology]. *Verh. - K. Acad. Voor Geneeskd. Van Belg.* 58, 479-536; discussion 537-538 (1996).
198. Haim, M., Gdalevich, M., Mimouni, D., Ashkenazi, I. & Shemer, J. Adverse reactions to smallpox vaccine: the Israel Defense Force experience, 1991 to 1996. A comparison with previous surveys. *Mil. Med.* 165, 287–289 (2000).
199. Moussatché, N. *et al.* Accidental infection of laboratory worker with vaccinia virus. *Emerg. Infect. Dis.* 9, 724–726 (2003).
200. Tartaglia, J. *et al.* NYVAC: a highly attenuated strain of vaccinia virus. *Virology* 188, 217–232 (1992).
201. Mayr, A., Stickl, H., Müller, H. K., Danner, K. & Singer, H. [The smallpox vaccination strain MVA: marker, genetic structure, experience gained with the parenteral vaccination and behavior in organisms with a debilitated defence mechanism (author's transl)]. *Zentralbl. Bakteriol. [B]* 167, 375–390 (1978).
202. Antoine, G., Scheiflinger, F., Dorner, F. & Falkner, F. G. The complete genomic sequence of the modified vaccinia Ankara strain: comparison with other orthopoxviruses. *Virology* 244, 365–396 (1998).
203. Mayr, A. & Munz, E. [Changes in the vaccinia virus through continuing passages in chick embryo fibroblast cultures]. *Zentralblatt Bakteriol. Parasitenkd. Infekt. Hyg. 1 Abt Med.-Hyg. Bakteriol. Virusforsch. Parasitol. Orig.* 195, 24–35 (1964).
204. Carroll, M. W. & Moss, B. Host range and cytopathogenicity of the highly attenuated MVA strain of vaccinia virus: propagation and generation of recombinant viruses in a nonhuman mammalian cell line. *Virology* 238, 198–211 (1997).
205. Hage, E., Gerd Liebert, U., Bergs, S., Ganzenmueller, T. & Heim, A. Human mastadenovirus type 70: a novel, multiple recombinant species D mastadenovirus isolated from diarrhoeal faeces of a haematopoietic stem cell transplantation recipient. *J. Gen. Virol.* 96, 2734–2742 (2015).
206. Yoshitomi, H., Sera, N., Gonzalez, G., Hanaoka, N. & Fujimoto, T. First isolation of a new type of human adenovirus (genotype 79), species Human mastadenovirus B (B2) from sewage water in Japan. *J. Med. Virol.* 89, 1192–1200 (2017).
207. Wold, W. S. M. & Toth, K. Adenovirus vectors for gene therapy, vaccination and cancer gene therapy. *Curr. Gene Ther.* 13, 421–433 (2013).
208. Liu, J. *et al.* Magnitude and phenotype of cellular immune responses elicited by recombinant adenovirus vectors and heterologous prime-boost regimens in rhesus monkeys. *J. Virol.* 82, 4844–4852 (2008).
209. Hillgenberg, M., Schnieders, F., Löser, P. & Strauss, M. System for efficient helper-dependent minimal adenovirus construction and rescue. *Hum. Gene Ther.* 12, 643–657 (2001).
210. Harvey, B.-G. *et al.* Safety of local delivery of low- and intermediate-dose adenovirus gene transfer vectors to individuals with a spectrum of morbid conditions. *Hum. Gene Ther.* 13, 15–63 (2002).
211. Zheng, C., Baum, B. J., Iadarola, M. J. & O'Connell, B. C. Genomic integration and gene expression by a modified adenoviral vector. *Nat. Biotechnol.* 18, 176–180 (2000).
212. Benihoud, K., Yeh, P. & Perricaudet, M. Adenovirus vectors for gene delivery. *Curr. Opin. Biotechnol.* 10, 440–447 (1999).

213. Mast, T. C. *et al.* International epidemiology of human pre-existing adenovirus (Ad) type-5, type-6, type-26 and type-36 neutralizing antibodies: correlates of high Ad5 titers and implications for potential HIV vaccine trials. *Vaccine* 28, 950–957 (2010).
214. Bergelson, J. M. *et al.* Isolation of a common receptor for Coxsackie B viruses and adenoviruses 2 and 5. *Science* 275, 1320–1323 (1997).
215. Lyons, M. *et al.* Adenovirus type 5 interactions with human blood cells may compromise systemic delivery. *Mol. Ther. J. Am. Soc. Gene Ther.* 14, 118–128 (2006).
216. Green, N. K. *et al.* Extended plasma circulation time and decreased toxicity of polymer-coated adenovirus. *Gene Ther.* 11, 1256–1263 (2004).
217. Khare, R., Chen, C. Y., Weaver, E. A. & Barry, M. A. Advances and future challenges in adenoviral vector pharmacology and targeting. *Curr. Gene Ther.* 11, 241–258 (2011).
218. Alonso-Padilla, J. *et al.* Development of Novel Adenoviral Vectors to Overcome Challenges Observed With HAdV-5-based Constructs. *Mol. Ther. J. Am. Soc. Gene Ther.* 24, 6–16 (2016).
219. Barouch, D. H. *et al.* International Seroepidemiology of Adenovirus Serotypes 5, 26, 35, and 48 in Pediatric and Adult Populations. *Vaccine* 29, 5203–5209 (2011).
220. Milligan, I. D. *et al.* Safety and Immunogenicity of Novel Adenovirus Type 26- and Modified Vaccinia Ankara-Vectored Ebola Vaccines: A Randomized Clinical Trial. *JAMA* 315, 1610–1623 (2016).
221. Kelly, C. *et al.* Chronic hepatitis C viral infection subverts vaccine-induced T-cell immunity in humans. *Hepatol. Baltim. Md* 63, 1455–1470 (2016).
222. Nyombayire, J. *et al.* First-in-Human Evaluation of the Safety and Immunogenicity of an Intranasally Administered Replication-Competent Sendai Virus–Vectored HIV Type 1 Gag Vaccine: Induction of Potent T-Cell or Antibody Responses in Prime-Boost Regimens. *J. Infect. Dis.* 215, 95–104 (2017).
223. Penaloza-MacMaster, P. *et al.* Alternative serotype adenovirus vaccine vectors elicit memory T cells with enhanced anamnestic capacity compared to Ad5 vectors. *J. Virol.* 87, 1373–1384 (2013).
224. Nébié, I. *et al.* Assessment of Chimpanzee Adenovirus Serotype 63 Neutralizing Antibodies Prior to Evaluation of a Candidate Malaria Vaccine Regimen Based on Viral Vectors. *Clin. Vaccine Immunol. CVI* 21, 901–903 (2014).
225. Hayton, E.-J. *et al.* Safety and tolerability of conserved region vaccines vectored by plasmid DNA, simian adenovirus and modified vaccinia virus ankara administered to human immunodeficiency virus type 1-uninfected adults in a randomized, single-blind phase I trial. *PloS One* 9, e101591 (2014).
226. Ersching, J. *et al.* Neutralizing antibodies to human and simian adenoviruses in humans and New-World monkeys. *Virology* 407, 1–6 (2010).
227. Ledgerwood, J. E. *et al.* Chimpanzee Adenovirus Vector Ebola Vaccine. *N. Engl. J. Med.* 376, 928–938 (2017).
228. Mastrangeli, A. *et al.* 'Sero-switch' adenovirus-mediated in vivo gene transfer: circumvention of anti-adenovirus humoral immune defenses against repeat adenovirus vector administration by changing the adenovirus serotype. *Hum. Gene Ther.* 7, 79–87 (1996).
229. Delany, I., Rappuoli, R. & De Gregorio, E. Vaccines for the 21st century. *EMBO Mol. Med.* 6, 708–720 (2014).
230. Zhou, X. *et al.* Analysis of human adenovirus type 19 associated with epidemic keratoconjunctivitis and its reclassification as adenovirus type 64. *Invest. Ophthalmol. Vis. Sci.* 53, 2804–2811 (2012).
231. Vogels, R. *et al.* Replication-deficient human adenovirus type 35 vectors for gene transfer and vaccination: efficient human cell infection and bypass of preexisting adenovirus immunity. *J. Virol.* 77, 8263–8271 (2003).
232. Aoki, K. & Tagawa, Y. A twenty-one year surveillance of adenoviral conjunctivitis in Sapporo, Japan. *Int. Ophthalmol. Clin.* 42, 49–54 (2002).
233. Laibson, P. R. Adenoviral keratoconjunctivitis. *Int. Ophthalmol. Clin.* 15, 187–201 (1975).
234. Ruzsics, Z. *et al.* Transposon-assisted cloning and traceless mutagenesis of adenoviruses: Development of a novel vector based on species D. *J. Virol.* 80, 8100–8113 (2006).
235. Arnberg, N., Kidd, A. H., Edlund, K., Olfat, F. & Wadell, G. Initial interactions of subgenus D adenoviruses with A549 cellular receptors: sialic acid versus alpha(v) integrins. *J. Virol.* 74, 7691–7693 (2000).
236. Thirion, C. *et al.* Adenovirus vectors based on human adenovirus type 19a have high potential for human muscle-directed gene therapy. *Hum. Gene Ther.* 17, 193–205 (2006).
237. Parker, J. C., Whiteman, M. D. & Richter, C. B. Susceptibility of inbred and outbred mouse strains to Sendai virus and prevalence of infection in laboratory rodents. *Infect. Immun.* 19, 123–130 (1978).
238. Whelan, S. P. J., Barr, J. N. & Wertz, G. W. Transcription and replication of nonsegmented negative-strand RNA viruses. *Curr. Top. Microbiol. Immunol.* 283, 61–119 (2004).
239. Armeanu, S. *et al.* Cell cycle independent infection and gene transfer by recombinant Sendai viruses. *J. Virol. Methods* 108, 229–233 (2003).
240. Markwell, M. A. & Paulson, J. C. Sendai virus utilizes specific sialyloligosaccharides as host cell receptor determinants. *Proc. Natl. Acad. Sci. U. S. A.* 77, 5693–5697 (1980).
241. Yonemitsu, Y. *et al.* Efficient gene transfer to airway epithelium using recombinant Sendai virus. *Nat. Biotechnol.* 18, 970–973 (2000).
242. Iida, A. & Inoue, M. Concept and Technology Underlying Sendai Virus (SeV) Vector Development. in *Sendai Virus Vector* (ed. Nagai, Y.) 69–89 (Springer Japan, 2013). doi:10.1007/978-4-431-54556-9_3

243. Nagai, Y. Paramyxovirus replication and pathogenesis. Reverse genetics transforms understanding. *Rev. Med. Virol.* 9, 83–99 (1999).
244. Slobod, K. S. *et al.* Safety and immunogenicity of intranasal murine parainfluenza virus type 1 (Sendai virus) in healthy human adults. *Vaccine* 22, 3182–3186 (2004).
245. Wiegand, M. A. *et al.* A Respiratory Syncytial Virus Vaccine Vectored by a Stable Chimeric and Replication-Deficient Sendai Virus Protects Mice without Inducing Enhanced Disease. *J. Virol.* 91, (2017).
246. Adderson, E. *et al.* Safety and immunogenicity of an intranasal Sendai virus-based human parainfluenza virus type 1 vaccine in 3- to 6-year-old children. *Clin. Vaccine Immunol. CVI* 22, 298–303 (2015).
247. Jones, B. G. *et al.* Sendai virus-based RSV vaccine protects African green monkeys from RSV infection. *Vaccine* 30, 959–968 (2012).
248. Ishii, H. & Matano, T. Development of an AIDS vaccine using Sendai virus vectors. *Vaccine* 33, 6061–6065 (2015).
249. Barabas, S. *et al.* Urea-mediated cross-presentation of soluble Epstein-Barr virus BZLF1 protein. *PLoS Pathog.* 4, e1000198 (2008).
250. Mitchell, D. A. *et al.* Tetanus toxoid and CCL3 improve dendritic cell vaccines in mice and glioblastoma patients. *Nature* 519, 366–369 (2015).
251. Lau, W. L. & Vaziri, N. D. Urea, a true uremic toxin: the empire strikes back. *Clin. Sci. Lond. Engl. 1979* 131, 3–12 (2017).
252. Verbrugge, F. H., Tang, W. H. W. & Hazen, S. L. Protein carbamylation and cardiovascular disease. *Kidney Int.* 88, 474–478 (2015).
253. Kollipara, L. & Zahedi, R. P. Protein carbamylation: in vivo modification or in vitro artefact? *Proteomics* 13, 941–944 (2013).
254. Gorisse, L. *et al.* Protein carbamylation is a hallmark of aging. *Proc. Natl. Acad. Sci. U. S. A.* 113, 1191–1196 (2016).
255. Nilsson, L., Lundquist, P., Kågedal, B. & Larsson, R. Plasma cyanate concentrations in chronic renal failure. *Clin. Chem.* 42, 482–483 (1996).
256. Flückiger, R., Harmon, W., Meier, W., Loo, S. & Gabbay, K. H. Hemoglobin carbamylation in uremia. *N. Engl. J. Med.* 304, 823–827 (1981).
257. Taga, Y. *et al.* Hydroxyhomocitrulline Is a Collagen-Specific Carbamylation Mark that Affects Cross-link Formation. *Cell Chem. Biol.* (2017). doi:10.1016/j.chembiol.2017.08.010
258. Delanghe, S., Delanghe, J. R., Speeckaert, R., Van Biesen, W. & Speeckaert, M. M. Mechanisms and consequences of carbamoylation. *Nat. Rev. Nephrol.* (2017). doi:10.1038/nrneph.2017.103
259. Loria, V., Dato, I., Graziani, F. & Biasucci, L. M. Myeloperoxidase: a new biomarker of inflammation in ischemic heart disease and acute coronary syndromes. *Mediators Inflamm.* 2008, 135625 (2008).
260. Apostolov, E. O., Shah, S. V., Ray, D. & Basnakian, A. G. Scavenger receptors of endothelial cells mediate the uptake and cellular pro-atherogenic effects of carbamylated LDL. *Arterioscler. Thromb. Vasc. Biol.* 29, 1622–1630 (2009).
261. Schmidt, T. G. M. & Skerra, A. The Strep-tag system for one-step purification and high-affinity detection or capturing of proteins. *Nat. Protoc.* 2, 1528–1535 (2007).
262. Waugh, D. S. An Overview of Enzymatic Reagents for the Removal of Affinity Tags. *Protein Expr. Purif.* 80, 283–293 (2011).
263. Kost, T. A., Condreay, J. P. & Jarvis, D. L. Baculovirus as versatile vectors for protein expression in insect and mammalian cells. *Nat. Biotechnol.* 23, 567–575 (2005).
264. Luckow, V. A., Lee, S. C., Barry, G. F. & Olins, P. O. Efficient generation of infectious recombinant baculoviruses by site-specific transposon-mediated insertion of foreign genes into a baculovirus genome propagated in Escherichia coli. *J. Virol.* 67, 4566–4579 (1993).
265. Phlipp Becker. *Influence of Posttranslational Protein Modifications on the Restimulation of Antigen-specific T cells (Master's Thesis)*. (University of Regensburg, 2017).
266. Weisgraber, K. H., Innerarity, T. L. & Mahley, R. W. Role of lysine residues of plasma lipoproteins in high affinity binding to cell surface receptors on human fibroblasts. *J. Biol. Chem.* 253, 9053–9062 (1978).
267. Tobias Brunner. *The Influence of in vitro Carbamylation on the Restimulation of pp65-specific T cells (Master's Thesis)*. (University of Regensburg, 2016).
268. Beswick, H. T. & Harding, J. J. Conformational changes induced in bovine lens alpha-crystallin by carbamylation. Relevance to cataract. *Biochem. J.* 223, 221–227 (1984).
269. Jaisson, S., Gorisse, L., Pietrement, C. & Gillery, P. Quantification of plasma homocitrulline using hydrophilic interaction liquid chromatography (HILIC) coupled to tandem mass spectrometry. *Anal. Bioanal. Chem.* 402, 1635–1641 (2012).
270. Kato, M., Kato, H., Eyama, S. & Takatsu, A. Application of amino acid analysis using hydrophilic interaction liquid chromatography coupled with isotope dilution mass spectrometry for peptide and protein quantification. *J. Chromatogr. B Analyt. Technol. Biomed. Life. Sci.* 877, 3059–3064 (2009).
271. Canton, J., Neculai, D. & Grinstein, S. Scavenger receptors in homeostasis and immunity. *Nat. Rev. Immunol.* 13, 621–634 (2013).
272. Platt, N. & Gordon, S. Scavenger receptors: diverse activities and promiscuous binding of polyanionic ligands. *Chem. Biol.* 5, R193-203 (1998).
273. Kwak, J.-Y. Fucoidan as a Marine Anticancer Agent in Preclinical Development. *Mar. Drugs* 12, 851–870 (2014).
274. Thelen, T. *et al.* The class A scavenger receptor, macrophage receptor with collagenous structure, is the major phagocytic receptor for Clostridium sordellii expressed by human decidual macrophages. *J. Immunol. Baltim. Md 1950* 185, 4328–4335 (2010).
275. Das Purkayastha, M. *et al.* Effect of maleylation on physicochemical and functional properties of

rapeseed protein isolate. *J. Food Sci. Technol.* 53, 1784–1797 (2016).
276. Qasim, M. A. & Salahuddin, A. The Conformational Consequences of Maleylation of Amino Groups in Ovalbumin. *J. Biochem. (Tokyo)* 85, 1029–1035 (1979).
277. Nair, S., Archer, G. E. & Tedder, T. F. ISOLATION AND GENERATION OF HUMAN DENDRITIC CELLS. *Curr. Protoc. Immunol. Ed. John E Coligan Al* 0 7, Unit7.32 (2012).
278. Abdul Zani, I. *et al.* Scavenger Receptor Structure and Function in Health and Disease. *Cells* 4, 178–201 (2015).
279. Ben, J., Zhu, X., Zhang, H. & Chen, Q. Class A1 scavenger receptors in cardiovascular diseases. *Br. J. Pharmacol.* 172, 5523–5530 (2015).
280. Qin, Z. The use of THP-1 cells as a model for mimicking the function and regulation of monocytes and macrophages in the vasculature. *Atherosclerosis* 221, 2–11 (2012).
281. Macdonald, P. J., Chen, Y. & Mueller, J. D. Chromophore maturation and fluorescence fluctuation spectroscopy of fluorescent proteins in a cell-free expression system. *Anal. Biochem.* 421, 291–298 (2012).
282. Joffre, O. P., Segura, E., Savina, A. & Amigorena, S. Cross-presentation by dendritic cells. *Nat. Rev. Immunol.* 12, 557–569 (2012).
283. Martins, K. A. O., Bavari, S. & Salazar, A. M. Vaccine adjuvant uses of poly-IC and derivatives. *Expert Rev. Vaccines* 14, 447–459 (2015).
284. Schleiss, M. R. Cytomegalovirus vaccines under clinical development. *J. Virus Erad.* 2, 198–207 (2016).
285. Ohradanova-Repic, A., Machacek, C., Fischer, M. B. & Stockinger, H. Differentiation of human monocytes and derived subsets of macrophages and dendritic cells by the HLDA10 monoclonal antibody panel. *Clin. Transl. Immunol.* 5, e55 (2016).
286. Perdiguero, B. *et al.* Virological and immunological characterization of novel NYVAC-based HIV/AIDS vaccine candidates expressing clade C trimeric soluble gp140(ZM96) and Gag(ZM96)-Pol-Nef(CN54) as virus-like particles. *J. Virol.* 89, 970–988 (2015).
287. Christiane Schwegler. *Ex vivo evaluation of viral vectors for delivery of CMV IE-1 and pp65 (Master's Thesis)*. (University of Regensburg, 2015).
288. Rebel, V. I. *et al.* Maturation and lineage-specific expression of the coxsackie and adenovirus receptor in hematopoietic cells. *Stem Cells Dayt. Ohio* 18, 176–182 (2000).
289. Philipson, L. & Pettersson, R. F. The coxsackie-adenovirus receptor--a new receptor in the immunoglobulin family involved in cell adhesion. *Curr. Top. Microbiol. Immunol.* 273, 87–111 (2004).
290. Horvath, J. & Weber, J. M. Nonpermissivity of human peripheral blood lymphocytes to adenovirus type 2 infection. *J. Virol.* 62, 341–345 (1988).
291. Chakrabarti, S., Sisler, J. R. & Moss, B. Compact, synthetic, vaccinia virus early/late promoter for protein expression. *BioTechniques* 23, 1094–1097 (1997).
292. K K Ma, C. *et al.* Adjuvant Peptide Pulsed Dendritic Cell Vaccination in Addition to T Cell Adoptive Immunotherapy for Cytomegalovirus Infection in Allogeneic Hematopoietic Stem Cell Transplant (HSCT) Recipients. *Biol. Blood Marrow Transplant. J. Am. Soc. Blood Marrow Transplant.* (2017). doi:10.1016/j.bbmt.2017.08.028
293. Schuler-Thurner, B. *et al.* Rapid induction of tumor-specific type 1 T helper cells in metastatic melanoma patients by vaccination with mature, cryopreserved, peptide-loaded monocyte-derived dendritic cells. *J. Exp. Med.* 195, 1279–1288 (2002).
294. Bol, K. F. *et al.* Prophylactic vaccines are potent activators of monocyte-derived dendritic cells and drive effective anti-tumor responses in melanoma patients at the cost of toxicity. *Cancer Immunol. Immunother. CII* 65, 327–339 (2016).
295. Windheim, M., Hilgendorf, A. & Burgert, H. G. Immune evasion by adenovirus E3 proteins: exploitation of intracellular trafficking pathways. *Curr. Top. Microbiol. Immunol.* 273, 29–85 (2004).
296. Dudek, A. M., Martin, S., Garg, A. D. & Agostinis, P. Immature, Semi-Mature, and Fully Mature Dendritic Cells: Toward a DC-Cancer Cells Interface That Augments Anticancer Immunity. *Front. Immunol.* 4, 438 (2013).
297. Yu, Y. & Alwine, J. C. Human cytomegalovirus major immediate-early proteins and simian virus 40 large T antigen can inhibit apoptosis through activation of the phosphatidylinositide 3′-OH kinase pathway and the cellular kinase Akt. *J. Virol.* 76, 3731–3738 (2002).
298. Wiegand, M. A., Bossow, S., Schlecht, S. & Neubert, W. J. De novo synthesis of N and P proteins as a key step in Sendai virus gene expression. *J. Virol.* 81, 13835–13844 (2007).
299. Longhi, S., Bloyet, L.-M., Gianni, S. & Gerlier, D. How order and disorder within paramyxoviral nucleoproteins and phosphoproteins orchestrate the molecular interplay of transcription and replication. *Cell. Mol. Life Sci. CMLS* (2017). doi:10.1007/s00018-017-2556-3
300. Gómez, C. E., Nájera, J. L., Krupa, M., Perdiguero, B. & Esteban, M. MVA and NYVAC as vaccines against emergent infectious diseases and cancer. *Curr. Gene Ther.* 11, 189–217 (2011).
301. Armeanu, S. *et al.* Severe impairment of dendritic cell allostimulatory activity by Sendai virus vectors is overcome by matrix protein gene deletion. *J. Immunol. Baltim. Md 1950* 175, 4971–4980 (2005).
302. Bitzer, M. *et al.* Sendai virus infection induces apoptosis through activation of caspase-8 (FLICE) and caspase-3 (CPP32). *J. Virol.* 73, 702–708 (1999).
303. Schock, S. N. *et al.* Induction of necroptotic cell death by viral activation of the RIG-I or STING pathway. *Cell Death Differ.* 24, 615–625 (2017).
304. Schmidt, J., Dojcinovic, D., Guillaume, P. & Luescher, I. Analysis, Isolation, and Activation of

Antigen-Specific CD4+ and CD8+ T Cells by Soluble MHC-Peptide Complexes. *Front. Immunol.* 4, (2013).
305. Banas, B. *et al.* Validation of T-Track® CMV to assess the functionality of cytomegalovirus-reactive cell-mediated immunity in hemodialysis patients. *BMC Immunol.* 18, 15 (2017).
306. Yong, M. K. *et al.* Identifying Cytomegalovirus Complications Using the Quantiferon-CMV Assay After Allogeneic Hematopoietic Stem Cell Transplantation. *J. Infect. Dis.* 215, 1684–1694 (2017).
307. Barabas, S. *et al.* An optimized IFN-γ ELISpot assay for the sensitive and standardized monitoring of CMV protein-reactive effector cells of cell-mediated immunity. *BMC Immunol.* 18, 14 (2017).
308. Abate, D. *et al.* Comparison of Cytomegalovirus (CMV) Enzyme-Linked Immunosorbent Spot and CMV Quantiferon Gamma Interferon-Releasing Assays in Assessing Risk of CMV Infection in Kidney Transplant Recipients. *J. Clin. Microbiol.* 51, 2501–2507 (2013).
309. Godard, B. *et al.* Optimization of an elispot assay to detect cytomegalovirus-specific CD8+ T lymphocytes. *Hum. Immunol.* 65, 1307–1318 (2004).
310. Manuel, O. *et al.* Assessment of cytomegalovirus-specific cell-mediated immunity for the prediction of cytomegalovirus disease in high-risk solid-organ transplant recipients: a multicenter cohort study. *Clin. Infect. Dis. Off. Publ. Infect. Dis. Soc. Am.* 56, 817–824 (2013).
311. Berkers, C. R. *et al.* Peptide Splicing in the Proteasome Creates a Novel Type of Antigen with an Isopeptide Linkage. *J. Immunol. Baltim. Md 1950* 195, 4075–4084 (2015).
312. Berkers, C. R. *et al.* Definition of Proteasomal Peptide Splicing Rules for High-Efficiency Spliced Peptide Presentation by MHC Class I Molecules. *J. Immunol. Baltim. Md 1950* 195, 4085–4095 (2015).
313. Liepe, J. *et al.* A large fraction of HLA class I ligands are proteasome-generated spliced peptides. *Science* 354, 354–358 (2016).
314. Rist, M. J., Neller, M. A., Burrows, J. M. & Burrows, S. R. T cell epitope clustering in the highly immunogenic BZLF1 antigen of Epstein-Barr virus. *J. Virol.* 89, 703–712 (2015).
315. Söding, J., Biegert, A. & Lupas, A. N. The HHpred interactive server for protein homology detection and structure prediction. *Nucleic Acids Res.* 33, W244-248 (2005).
316. Adar, R. M., Andelman, D. & Diamant, H. Electrostatics of patchy surfaces. *Adv. Colloid Interface Sci.* 247, 198–207 (2017).
317. Miller, S., Janin, J., Lesk, A. M. & Chothia, C. Interior and surface of monomeric proteins. *J. Mol. Biol.* 196, 641–656 (1987).
318. Kajander, T. *et al.* Buried charged surface in proteins. *Struct. Lond. Engl. 1993* 8, 1203–1214 (2000).
319. Jin, J.-O. *et al.* Fucoidan can function as an adjuvant in vivo to enhance dendritic cell maturation and function and promote antigen-specific T cell immune responses. *PloS One* 9, e99396 (2014).
320. PrabhuDas, M. R. *et al.* A Consensus Definitive Classification of Scavenger Receptors and Their Roles in Health and Disease. *J. Immunol. Baltim. Md 1950* 198, 3775–3789 (2017).
321. Brown, M. S. & Goldstein, J. L. Lipoprotein metabolism in the macrophage: implications for cholesterol deposition in atherosclerosis. *Annu. Rev. Biochem.* 52, 223–261 (1983).
322. Gu, X. *et al.* The efficient cellular uptake of high density lipoprotein lipids via scavenger receptor class B type I requires not only receptor-mediated surface binding but also receptor-specific lipid transfer mediated by its extracellular domain. *J. Biol. Chem.* 273, 26338–26348 (1998).
323. Acton, S. *et al.* The collagenous domains of macrophage scavenger receptors and complement component C1q mediate their similar, but not identical, binding specificities for polyanionic ligands. *J. Biol. Chem.* 268, 3530–3537 (1993).
324. Ojala, J. R. M., Pikkarainen, T., Tuuttila, A., Sandalova, T. & Tryggvason, K. Crystal structure of the cysteine-rich domain of scavenger receptor MARCO reveals the presence of a basic and an acidic cluster that both contribute to ligand recognition. *J. Biol. Chem.* 282, 16654–16666 (2007).
325. Park, H., Adsit, F. G. & Boyington, J. C. The 1.4 angstrom crystal structure of the human oxidized low density lipoprotein receptor lox-1. *J. Biol. Chem.* 280, 13593–13599 (2005).
326. Iesaki, T. *et al.* Fucoidan, a ligand of scavenger receptor class a, causes vascular relaxation through a nitric oxide/cGMP-mediated pathway in rat aorta. *Atherosclerosis* 235, e36 (2014).
327. Zaiss, A. K., Machado, H. B. & Herschman, H. R. The influence of innate and pre-existing immunity on adenovirus therapy. *J. Cell. Biochem.* 108, 778–790 (2009).
328. Buchbinder, S. P. *et al.* Efficacy assessment of a cell-mediated immunity HIV-1 vaccine (the Step Study): a double-blind, randomised, placebo-controlled, test-of-concept trial. *Lancet* 372, 1881–1893 (2008).
329. Adams, W. C. *et al.* Adenovirus serotype 5 infects human dendritic cells via a coxsackievirus-adenovirus receptor-independent receptor pathway mediated by lactoferrin and DC-SIGN. *J. Gen. Virol.* 90, 1600–1610 (2009).
330. Engelmayer, J. *et al.* Vaccinia virus inhibits the maturation of human dendritic cells: a novel mechanism of immune evasion. *J. Immunol. Baltim. Md 1950* 163, 6762–6768 (1999).
331. Pascutti, M. F. *et al.* Interplay between modified vaccinia virus Ankara and dendritic cells: phenotypic and functional maturation of bystander dendritic cells. *J. Virol.* 85, 5532–5545 (2011).
332. Brüning, A. & Runnebaum, I. B. CAR is a cell-cell adhesion protein in human cancer cells and is expressionally modulated by dexamethasone, TNFalpha, and TGFbeta. *Gene Ther.* 10, 198–205 (2003).
333. McCormack, S. *et al.* EV02: a Phase I trial to compare the safety and immunogenicity of HIV DNA-C prime-NYVAC-C boost to NYVAC-C alone. *Vaccine* 26, 3162–3174 (2008).

334. Bossow, S. *et al.* Evaluation of Nucleocapsid and Phosphoprotein P Functionality as Critical Factors During the Early Phase of Paramyxoviral Infection. *Open Virol. J.* 6, 73–81 (2012).
335. Croft, N. P. *et al.* Kinetics of antigen expression and epitope presentation during virus infection. *PLoS Pathog.* 9, e1003129 (2013).
336. Chahroudi, A. *et al.* Differences and similarities in viral life cycle progression and host cell physiology after infection of human dendritic cells with modified vaccinia virus Ankara and vaccinia virus. *J. Virol.* 80, 8469–8481 (2006).
337. Wajant, H., Pfizenmaier, K. & Scheurich, P. Tumor necrosis factor signaling. *Cell Death Differ.* 10, 45–65 (2003).
338. Reis e Sousa, C. Dendritic cells in a mature age. *Nat. Rev. Immunol.* 6, 476–483 (2006).
339. Hosoya, N. *et al.* Comparison between Sendai virus and adenovirus vectors to transduce HIV-1 genes into human dendritic cells. *J. Med. Virol.* 80, 373–382 (2008).
340. López, C. B. *et al.* TLR-independent induction of dendritic cell maturation and adaptive immunity by negative-strand RNA viruses. *J. Immunol. Baltim. Md 1950* 173, 6882–6889 (2004).
341. Heilingloh, C. S. *et al.* The Major Immediate-Early Protein IE2 of Human Cytomegalovirus Is Sufficient to Induce Proteasomal Degradation of CD83 on Mature Dendritic Cells. *Front. Microbiol.* 8, (2017).
342. Heilingloh, C. S., Mühl-Zürbes, P., Steinkasserer, A. & Kummer, M. Herpes simplex virus type 1 ICP0 induces CD83 degradation in mature dendritic cells independent of its E3 ubiquitin ligase function. *J. Gen. Virol.* 95, 1366–1375 (2014).
343. Tang, A. *et al.* Functionally inactivated dominant viral antigens of human cytomegalovirus delivered in replication incompetent adenovirus type 6 vectors as vaccine candidates. *Hum. Vaccines Immunother.* 1–9 (2017). doi:10.1080/21645515.2017.1308988
344. Lin, B., Meng, H., Bing, H., Zhangsun, D. & Luo, S. Efficient expression of acetylcholine-binding protein from Aplysia californica in Bac-to-Bac system. *BioMed Res. Int.* 2014, 691480 (2014).
345. Green, M. R. & Sambrook, J. *Molecular Cloning: A Laboratory Manual (Fourth Edition): Three-volume set*. (Cold Spring Harbor Laboratory Press, 2012).
346. Birnboim, H. C. & Doly, J. A rapid alkaline extraction procedure for screening recombinant plasmid DNA. *Nucleic Acids Res.* 7, 1513–1523 (1979).
347. Bradford, M. M. A rapid and sensitive method for the quantitation of microgram quantities of protein utilizing the principle of protein-dye binding. *Anal. Biochem.* 72, 248–254 (1976).
348. Laemmli, U. K. Cleavage of structural proteins during the assembly of the head of bacteriophage T4. *Nature* 227, 680–685 (1970).
349. Henrion, A. Reduction of systematic errors in quantitative analysis by isotope dilution mass spectrometry (IDMS): an iterative method. *Fresenius J. Anal. Chem.* 350, 657–658 (1994).
350. Burkitt, W. I. *et al.* Toward Système International d'Unité-traceable protein quantification: From amino acids to proteins. *Anal. Biochem.* 376, 242–251 (2008).
351. Milton, M J T & Wielgosz, R I. Uncertainty in SI-traceable measurements of amount of substance by isotope dilution mass spectrometry. : Publications : National Physical Laboratory. *Metrologia 2000, 37, 199-206*
352. Anderson, D. C., Green, G. R., Smith, K. & Selker, E. U. Extensive and varied modifications in histone H2B of wild-type and histone deacetylase 1 mutant Neurospora crassa. *Biochemistry (Mosc.)* 49, 5244–5257 (2010).
353. Ruzsics, Z., Lemnitzer, F. & Thirion, C. Engineering adenovirus genome by bacterial artificial chromosome (BAC) technology. *Methods Mol. Biol. Clifton NJ* 1089, 143–158 (2014).
354. Wadell, G. & de Jong, J. C. Restriction endonucleases in identification of a genome type of adenovirus 19 associated with keratoconjunctivitis. *Infect. Immun.* 27, 292–296 (1980).

I.4. Danksagung

Im Laufe der letzten Jahre wurde ich von zahlreichen Menschen tatkräftig unterstützt, sodass es mir eine große Freude ist, mich an dieser Stelle auch schriftlich bedanken zu dürfen.
An erster Stelle möchte ich mich herzlich bei meinem Doktorvater Prof. Dr. Ralf Wagner bedanken. Danke, dass du immer ein offenes Ohr für meine Anliegen und Probleme hattest und dass ich mich auf deine Unterstützung absolut verlassen konnte. Danke auch dafür, dass du mich konsequent gefördert und mir gleichzeitig an einigen Stellen auch kreative Freiheiten überlassen hast, wodurch ich viel dazulernen konnte.
Ein ganz großes Dankeschön gilt auch Dr. Benedikt Asbach, der meistens meine erste Anlaufstelle bei Fragen und Problemen war. Lieber Benedikt, im Laufe meines Studiums und meiner Promotion hab ich von dir sicherlich am meisten über die Arbeit im Labor gelernt. Nicht nur dafür möchte ich mich bedanken, sondern auch für die stets nette und geduldige Art und Weise, mit der du mir die vielen Methoden beigebracht hast und für deine zahllosen Ratschläge, mit denen du meine Arbeit in vielerlei Hinsicht bereichert hast.
Zudem möchte ich mich bei den Mitarbeitern von Lophius Biosciences PD Dr. Ludwig Deml, Dr. Sascha Barabas, Dr. Harald Guldan und Dr. Alexandra Asbach-Nitzsche bedanken, die mich besonders zu Beginn meiner Promotion mit zahlreichen Ratschlägen, Protokollen und Tipps unterstützt haben.
Des Weiteren möchte ich mich bei meinen Masterstudenten Christiane Schwegler, Tobias Brunner, Markus Fleischmann und Philipp Becker bedanken, die sich tatkräftig im Rahmen meines Projekts engagiert haben und viele wertvolle Impulse geliefert haben.
Außerdem möchte ich mich herzlich bei vielen Mitarbeitern der AG Wagner bedanken, mit denen ich sowohl im Labor, als auch privat sehr gerne meine Zeit verbracht habe. Besonders hervorheben möchte ich dabei meinen Laborkollegen und Golden-State Fan Thomas Schuster, der wesentlich zu unserer guten Stimmung im 64er Labor beigetragen hat. Danke auch an (Dr.) Jogi Meier, sowohl für die bioinformatische Unterstützung und sonstigen Anmerkungen zu meiner Arbeit, als auch für die schöne Zeit, die wir nach Feierabend miteinander verbracht haben! In diesem Zusammenhang möchte ich außerdem Basti, Benny, Anja, Julia, Krystina, Tanja, Kristina, Vroni, David, Christina, Alex und Meli nicht unerwähnt lassen. Nicht zuletzt wegen eurer freundlichen und kollegialen Art hab ich mich in unserer Arbeitsgruppe immer sehr wohl gefühlt.
Meiner Familie, insbesondere meinen Eltern, möchte ich zutiefst für die bedingungslose Unterstützung danken, die meine lange Ausbildung überhaupt erst ermöglicht hat.
Zu guter Letzt möchte ich dir, liebe Miriam, für alles danken. Danke, dass du immer für mich da bist, dass du meine schlechte Laune, mit der ich an stressigen Tagen manchmal aus der Arbeit gekommen bin, immer in gute Laune umgewandelt hast, uns vor allem danke dafür, dass du deine Zeit mit mir verbringst.